

An investigation of casing structural integrity in shale gas horizontal wells during hydraulic fracturing using FEA and machine learning algorithms.

MOHAMMED, A.I.

2021

The author of this thesis retains the right to be identified as such on any occasion in which content from this thesis is referenced or re-used. The licence under which this thesis is distributed applies to the text and any original images only – re-use of any third-party content must still be cleared with the original copyright holder.



**An Investigation of Casing Structural Integrity in Shale Gas Horizontal
Wells During Hydraulic Fracturing Using FEA and Machine Learning
Algorithms**

Mohammed, A.I

2021



An Investigation of Casing Structural Integrity in Shale Gas Horizontal Wells
During Hydraulic Fracturing Using FEA and Machine Learning Algorithms

Auwalu Inuwa Mohammed

A thesis submitted in partial fulfilment of the
requirements of
Robert Gordon University
for the degree of Doctor of Philosophy

September 2021



School of Engineering

PhD THESIS

Auwalu Inuwa Mohammed

An Investigation of Casing Structural Integrity in Shale Gas Horizontal Wells During Hydraulic Fracturing Using FEA and Machine Learning Algorithms

Supervisors: Professor James Njuguna
Professor Babs Oyeneyin
Dr Mark Bartlett

September 2021

Robert Gordon University, Aberdeen, 2021. All right reserved. No part of this publication may be produced without the written permission of the copyright owner

This thesis is submitted in partial fulfilment of the requirements for the degree of Doctor of Philosophy

Declaration

I hereby declare that the research report in this thesis is original and have been completed independently by myself (Auwalu Inuwa Mohammed), under the supervision of Professor James Njuguna, Professor Babs Oyeneyin and Dr Mark Bartlett. This PhD thesis has not been submitted for the award of any other degree or professional qualification elsewhere.

Where other sources are quoted full references are given.

Auwalu Inuwa Mohammed

September 2021

Dedication

This thesis is dedicated to all humankind with particular emphasis on my late father, my mother and my beloved family, and all those promoting justice, care, and peace globally.

Acknowledgement

In the name of Allah, Most Gracious, Most Merciful. All praise is due to Allah, the Lord of the Worlds, for His favour and blessing on me.

I particularly want to thank Professor James Njuguna for his patience, helpful suggestions and guidance throughout my PhD journey. I personally benefitted from his wealth of skills and expertise during this training for my PhD – thank you. I also want to thank Professor Babs Oyeneyin and Dr Mark Bartlett for their contributions in making this research a success.

I must not forget to thank the Federal Republic of Nigeria for given me the opportunity to study for my Doctorate through the Petroleum Technology Development Fund (PTDF). I also want to thank Professor Kambiz Kayvantash of CADLM France, for access to their commercial software.

A big thank you to my Mother, Uncles, Brothers and Sisters for all your prayers and encouragement during this challenging period of research in COVID -19 pandemic. I also want to thank my loving wife (Majida) for her support throughout this research journey. A special thanks to my friends Dr Shohel Ahmed Siddique, Dr Azeem Islam, Dr Kristof Starost, Dr Mansur Hamma – Adama and Dr Adamu Ali-Gombe, MARYAM HEIDARIAN, Engr Zahrah Zanna Ibrahim, Muhammad Said Atiku, Mutiu Adegboye, Bola Adewoye and Haval Hawez.

I must also thank Dr Rosslyn Shanks, Mrs Audrey McIvor, Mrs Kirsty Stevenson and Mrs Petrena Morrison. My appreciation to the lecturers specifically Dr Nadimul Faisal and Dr Gbenga Oluyemi, technicians, friends and colleagues (N436) in the School of Engineering, the Graduate School, and the library staff.

Abstract:

Unconventional oil and gas operators are currently facing the challenge of casing lateral buckling and/or deformation during shale gas wells stimulation through hydraulic fracturing. Failure of the casing during this process can lead to huge financial loss, catastrophic consequences and even fatalities depending on the magnitude and circumstance of the incident.

An in-depth literature review was conducted focusing on casing lateral buckling /deformation, factors attributing to casing failure, failure mechanism, and the resulting failure mode in shale gas horizontal wells is carried out. The study covered casing types, failure modes and mechanism, and impact of material selection on casing failure with the viewpoint of casing failure mechanism, cement, and rock as an integrated system. In the follow up, the casing material selection using ANSYS Granta Edupack (CES) and multicriteria decision making (MCDM) for three different scenarios of buckling tendencies were investigated. A finite element analysis (FEA) using two simulation scenarios for casing structural integrity was then investigated in both radial and axial configurations under the mechanics of a combine system - casing, cement and formation rock.

Next, a detailed novel study on casing structural integrity using both FEA and machine learning is accomplished. In this research, the effect of combined loading using multiple parameters to establish the relationship and effect of each on stress, displacement and ultimately casing safety factor is revealed. Finally, real time parametric prediction and optimisation using Lunar and Quasar (ODYSSEE software package) enabled the examination of the casing structural responses based on the pertinent parameters. In effect, a similar trend was found between “KNN” and Lunar predictions on parameters influencing casing buckling phenomena and the corresponding Mises stress.

In conclusion, FEA study showed that time dependent rock slippage - creep during stimulation lead to an increase transverse displacement and corresponding stresses on the casing. This new understanding is a major breakthrough in establishing casing health status during shale gas well stimulation. The optimised design shows 89% reduction in total deformation and 87% reduction in von Mises in comparison to unoptimised simulation result. Also, the optimised design gives a safety factor of 3.3 against the previous 0.8129 without optimisation. The Lunar optimisation provided the ideal parameter values for the attainment of pre-define von Mises stress as a function of other factors during design phase. This quick approach shows both accuracy and validation of the two independents procedures arriving at the same conclusion. We found that concurrent investigation of the casing buckling attributing factors and optimisation using FEA and ODYSSEE package is sufficient to maintain casing structural integrity during shale gas extraction process. The study also revealed alternative and better suited materials choices than the currently commercially preference (P110 & Q125).

Key Words: FEA, MCDM, Machine learning, Casing Integrity, Optimisation, Prediction, Buckling, Material Selection, Failure Modes

Achievements

Journal articles:

1. Mohammed, A.I., Oyeneyin, B., Atchison, B. and Njuguna, J., 2019. Casing structural integrity and failure modes in a range of well types-a review. *Journal of natural gas science and engineering*, 68, p.102898
2. Mohammed, A.I., Oyeneyin, B., Bartlett, M. and Njuguna, J., 2020. Prediction of casing critical buckling during shale gas hydraulic fracturing. *Journal of petroleum science and engineering*, 185, p.106655.
3. Mohammed, A.I., Bartlett, M., Oyeneyin, B., Kayvantash, K. and Njuguna, J., 2021. An application of FEA and machine learning for the prediction and optimisation of casing buckling and deformation responses in shale gas wells in an in-situ operation. *Journal of natural gas science and engineering*, p.104221.)
4. Multicriteria material selection for casing pipe in shale gas wells application. (Submitted Journal of Petroleum Exploration and Production Technology- Accepted Under review)
5. Data Driven Pipe Structural Evaluations, Correlations and Strength Analysis For TOPSIS, AHP and Non-Weighted. A manuscript under preparation

Conference proceedings:

- Njuguna, J. and Mohammed, A.I. (2020) Combined Approach on FEA & Machine Learning for the Prediction and Optimisation of Casing Buckling and Deformation Responses in Shale Gas Wells in an In-situ Operation. 8th Pipeline Maintenance and Integrity Management Virtual Conference 29 -30 October 2020.
- Auwalu I Mohammed, Mark Bartlett, Babs Oyeneyin, Kambiz Kayvantash, James Njuguna (23 – 25 February 2021) Harnessing MCDM and Machine

Learning for in Casing Selection and Optimisation for Oil and Gas Wells
Application: An abstract Submitted to Subsea Expo Conference 2020
(Event reschedule to 22 to 24 February 2022 due to COVID 19)

Posters:

- Auwalu Inuwa Mohammed (2018) Casing Structural Integrity and Performance Prediction in Unconventional Wells 2018. Presented at Society of Petroleum Engineers Technical Session Organised by Robert Gordon University Students Chapter.
- Auwalu Inuwa Mohammed (2020) Application of Finite Element Analysis and Machine Learning for the Prediction and Optimisation of Casing Structural Responses in Shale Gas Wells. Elevator Pitch, Graduate School Robert Gordon University 2020

Technical Presentations/Sessions:

- Auwalu Inuwa Mohammed (2018) 'Casing Structural Integrity and Performance Verification in Unconventional Wells'. Presented at Petroleum Engineering Research Group Monthly Seminar on the 10th October 2018.
- Auwalu Inuwa Mohammed (2019) Investigation of Casing Lateral Buckling in Horizontal Wells. Presented at Petroleum Engineering Research Group Monthly Seminar 9th October 2019.
- Auwalu Inuwa Mohammed (2019) Simulation of Casing structural responses during shale gas hydraulic fracturing. Presented at School of Engineering Seminar, Robert Gordon University 2019.

Industry Projects:

1. Benchmarking Study for Innovative Milling Technology for (P&A During Decommissioning) - Product Design
2. GRP Grating Panels Testing, Sparrow Offshore Engineering Ltd
3. Thermal conductivity testing of insulation samples before and after exposure to pressurisation cycles for Pipe-in-Pipe applications. Subsea 7
4. Development of Supercritical CO₂ System to process waste hydraulic hoses for raw materials recovery. Test Centre Aberdeen Ltd
5. NDT of composites pipes and plates using Dolphitech imaging kit. Engineered Composites Services (ECS) Ltd

List of Abbreviations

AHP Analytical hierarchy process

AI Artificial Intelligence

AISI American Iron and Steel Institute

APB Annular Pressure Build-up

APDL ANSYS Parametric Design Language

API American Petroleum Institute

CAD Computer Aided Design

CCWD circumferential casing wear depth

CES Cambridge Engineering Selector

CEM cement elastic modulus

CI confidence interval

CT casing and Tubing

CRA Corrosion resistance alloys

CR consistency ratio

Creq chromium equivalent

DEA drilling engineering associations

DOE Design of experiment

ELECTRE ELimination Et Choix Traduisant la REalité (ELimination Et Choice Translating REality).

FAD failure assessment diagram

FDEMATEL fuzzy decision- making trial and evaluation laboratory

FEA finite element analysis

FEM finite element modelling

FP Fracturing pressure

ID inner diameter

ISO International organisation for standardisation

HPHT High pressure high temperature

HSE health safety and environment

KNN ‘K’ Nearest Neighbour

MAE Mean absolute error

mD Millidarcy
 MCDM multicriteria decision making
 MAUA Multi-Attribute Utility Analysis
 MOGA multi-objective genetic algorithm
 NDT non-destructive testing
 ODYSSEE Optimal Decision Support System for Engineering and Expertise
 OCTG Oil Country Tubular Goods
 OD outer diameter
 PCA principal component analysis
 PR Poisson's ratio
 PROMETHEE Preference Ranking Organization Method for Enrichment of Evaluations
 PREN pitting resistant equivalent number
 ROM Reduced Order Method
 RP recommended practice
 RT reservoir temperature
 RMSE root means square error
 ROC receiver operating characteristic
 SD slip displacement
 SP slip plane
 ST surface temperatures
 TOPSIS Technique for Order Preference by Similarity to Ideal Solution
 TR technical report
 ULS ultimate limit strength
 VIKOR VIseKriterijumska Optimizacija I Kompromisno Resenje, that means: Multicriteria Optimization and Compromise Solution
 WSM Weighted Sum Model
 WPM Weighted product model

List of Tables

Table 2.1 Provide a brief overview of the tubular hardware grades as contained in API spec. 5CT.....	13
Table 2.2 Summary of widely used casing buckling and related buckling mode.	22
Table 3.1 Presents cross -section of a hollow cylinder (pipe) with corresponding moments.....	71
Table 3.2 The material data properties for the P110 and BS 145	72
Table 3.3 Material mechanical and physical properties for the TOPSIS selection process.	88
Table 3.4 Calculated weighted normalised matrix	90
Table 3.5 Materials ranked according to performances using Euclidean distance measure.....	91
Table 3.6 Saaty's fundamental scale.....	93
Table 3.7 A pair-wise matrix obtained using the importance on an absolute scale from Table 3.6.....	93
Table 3.8 Weights of each criteria (A2 Matrix).....	95
Table 3.9 Random index according to Rao (2007).....	96
Table 3.10 Analytical hierarchy process performance and ranking	97
Table 3.11 Non-weighted method performance and ranking	101
Table 4.1 Material properties for the finite element model.....	113
Table 4.2 Top ten (10) materials selected for shale wells with induced stresses.	115
Table 4.3 Pearson's Correlation between methods.	118
Table 5.1 Materials description and properties used in the modelling	136
Table 6.1 Casing, cement and rock material properties.....	160
Table 6.2 Range of input parameters for the optimisation	161
Table 6.3 RMSE, Rsquared and MAE for various values of k.	171
Table 6.4 Variable importance to prediction accuracy on casing buckling phenomena based on KNN algorithm for von Mises stress.....	172
Table 6.5 presents this comparison between Lunar and "KNN" sensitivities on casing stress.	181

List of Figures

Figure 1.1 Example of casing lateral buckling. Adapted from Yan et al. 2017.....	3
Figure 1.2 The schematic diagram illustrating the knowledge gap.....	5
Figure 1.3 Schematic of research methodology overview	8
Figure. 2.1 (A) Presents a concise summary of casing utilisation by well type (B) Casing failure mix by grades based on the articles reviewed.	20
Figure 2.2 (A & B) Shows the effects of centraliser on casing deformations, while (C & D) presents buckling due to fracture and lead mould impression justifying casing deformation respectively.	27
Figure 2.3 Statistics on casing deformation points of 12 horizontal wells (After Xi et al., 2018). And specific example of Wei-204H7-3 with 5 deformation points as shown (After Yan et al., 2017).	31
Figure 2.4 (A) Casing imaging logging of an injection well (B) Illustration of shear formation slip inducing casing failure (After Yin et al., 2018).....	33
Figure 2.5 Simplified material selection chart (Millet et al. 2020).....	45
Figure 2.6 Data-structure of the CES EduPack for Material Science and Engineering database (Ashby, et al. 2018).....	46
Figure 2.7 schematic diagram of machine learning task showing the distinct phases between training and testing phase (inference phase).....	59
Figure 2.8: (a) classification (b) regression	60
Figure 2.9 An Overview of Lunar Workflow (Source: CADLM 2019) showing system data bank, input variable (X, Y), and new variable XN.....	63
Figure 3.1: An overview of casing material selection process for shale gas wells using CES Edupack and MCDM	69
Figure 3.2: 3-Point bending load displacement curve for P110 and BS 145 (a) Physical model (b) deform numerical model (c) Load versus displacement for P110 and BS145.	73
Figure 3.3 material candidates using CES Edupack.	76
Figure 3.4 Shortlisted candidates for shale gas well casing.....	77
Figure 3.5 Top ten (10) materials after further optimisation.	77
Figure 3.6 Selection for second scenario (induced stress and corrosion).	79
Figure 3.7 Initial screening for the second scenario.....	80
Figure 3.8 Shortlisted materials for high sour oil and gas wells.	81
Figure 3.9 Initial selection for service temperature and toughness.....	83
Figure 3.10 Shortlisted materials for shale gas wells with high impact energy and temperature.....	84
Figure 3.11 Optimum selection using tangent line for pareto solution.....	85
Figure 3.12 Shortlisted materials for shale gas wells with high impact potentials and service temperature.	85
Figure 3.13 Family envelope of the shortlisted material for high impact shales (brittle)	86
Figure 3.14 An overview of analytical hierarchical process showing goal, criteria and alternative materials	92
Figure 3.15 Non-weighted method of material selection.....	98
Figure 3.16 Summary of the methods.....	103
Figure 4.1(a) Buckling load for structural steel, P110 and BS 145 (b) Mesh density study for the numerical model.....	107

Figure 4.2 (a) P110 linear buckling mode 1 (b) P110 linear buckling repeat mode.....	109
Figure 4.3 Nonlinear buckling load for P110 casing.	110
Figure 4.4 Load deflection curve showing buckling response of structural steel, BS145 stainless steel and P110 steel grade.	111
Figure 4.5 Finite element Model showing casing, cement, rock and slip plane...	114
Figure 4.7 Plot of ranks against alternative materials for TOSPSIS, AHP and non-weighted methods.....	118
Figure 4.8 AHP ranking correlation matrix.	119
Figure 4.9 TOPSIS correlation matrix.....	120
Figure 4.10 Correlation matrix non-weighted method.	121
Figure 4.11 Strength distribution for non-weighted selection method.	122
Figure 4.12 Strength distribution for the AHP selection method.....	123
Figure 4.13 Strength distribution for TOPSIS method	124
Figure 4.14 Shows safety factor for the 10 shortlisted materials as evaluated from FEM for each material.	125
Figure 5.1 Linear traction-separation law for different modes (Wang 2015).....	132
Figure 5.2(A) 2D View of casing, cement and shale rock. (B) Finite element model (FEM) with 18414 elements	135
Figure 5.3 Finite element model (After Yin et al. 2018).....	137
Figure 5.4 The schematics of simulation scenarios ('a' and 'b')	139
Figure 5.5 The sample result comparison for validation	140
Figure 5.6 Tangential stress distribution along wells.....	141
Figure 5.7 Contour plots of casing displacements and von Mises stresses	145
Figure 5.8 (a) Hoop stress under different differential loads (b) Radial stress along path circumference (c) von Mises stress with corresponding differential loads along path.	145
Figure 5.9 (a) Presents radial displacement (b) Shear stresses	146
Figure 5.10 Plots of (a) Shear stress distributions along defined path at different time periods (b) Transverse displacements at various time interval and (c) 'Sort' von Mises stress distribution.	148
Figure 5.11 The angular deflection of casing under various slip periods.	149
Figure 5.12 Effect of temperature on casing stress and displacement.....	150
Figure 5.13 (a) Effect of temperature on casing strength as a function of time. (b) Effect of temperature on critical time to casing failure.....	151
Figure 6.1: XY-1 Well: Casing buckling in shale gas horizontal well located in Sichuan Basin, China (Yu et al., 2019).	154
Figure 6.2 Actual casing shear deformation based on microseismic data (Yan et al. 2019).	155
Figure 6.3 (a) Moment magnitude against slip distance (b) Moment magnitude against fault radius (Yan et al. 2019).	156
Figure 6.4 Flowchart on the overview of the study method showing top to down sequence of activities.	158
Figure 6.5 3D CAD and Mesh Models showing casing, cement and shale rock ...	159
Figure 6.9 Transverse displacement and von Mises stress after 30 hours of combined loading.....	163
Figure 6.10 Transverse displacement and von Mises stress after at critical.....	164

time of cobined loading	164
Figure 6.11 Correlation matrix showing the correlation between the 12 input and 3 output parameters	166
Figure 6.12 Local sensitivities of input parameters on casing total deformation, von Mises stress and safety factor.	167
Figure 6.13 Total deformation and von Mises stress for the optimised design ...	168
Figure 6.14 Optimised critical displacement and von Mises after 9 hours of combined loading.....	169
Figure 6.15 Scatter plots showing predicted von Mises stress for different_casings geometries (Inner diameter).....	170
Figure 6.16 Scatter plot for von Mises stress prediction:(a) before finetuning hyper parameter (b) after fine-tuning hyper parameter.	173
Figure 6.17: (a) Effect of changing slip plane 100 times (b) effect changing_casing Inner diameter 100 times showing the window in grey over time.	175
Figure 6.18 The inputs parameters influence on casing von Mises stress.	176
Figure 6.19 Principal component analysis of the casing performance based_on sensitive parameters.	177
Figure 6.20 The variance of the contributing sensitive parameters.....	177
Figure 6.21 Lunar software output for the optimised casing design shown_in blue line.....	178
Figure 6.22 The heatmap for the 10th hour von Mises stress for the_optimised casing.....	179

Contents

Declaration	iv
Dedication	v
Acknowledgement.....	vi
Abstract:	vii
Achievements.....	ix
List of Abbreviations	xii
List of Tables	xiv
Chapter 1: Introduction	1
1.1 Background.....	1
1.2 Gap in knowledge, motivation and significance of the research	4
1.3 Aim and Objectives	6
1.4 Methodology overview	7
Chapter 2: Literature Review	11
2.1 Introduction.....	11
2.2 API Casing Pipe Materials Grades and Standardisation	11
2.3 Casing–Cement-Formation Failure.....	14
2.4 Predictive Mechanical Models	17
2.5 Factors causing casing buckling during shale gas hydraulic fracturing	23
2.6 Casing Failure Mechanism in Shale Gas Horizontal Wells During Hydraulic Fracturing.....	25
2.6.1 Buckling Failure or Deformation of Casing Pipe	31
2.6.2. Casing Shear Failure in Shale Gas Wells.....	33
2.6.3. Collapse/burst failure.....	34
2.6.4. Fatigue Failure	35
2.6.5 Wear/erosion/corrosion failure	36
2.7 Conventional Casing pipe material selection.....	37
2.7.1 Materials selection Challenge for Unconventional Wells Application....	40
2.7.2 Material Selection and Verification of Selected Material Response	47
2.8 Horizontal Wells Drilling and Hydraulic Fracturing Associated Loads	51

2.9 Casing Buckling and Mitigation Strategies	53
2.10 Machine Learning.....	58
2.10.1 Data Mining Using “R”	61
2.10.2 Data Mining and Machine learning for critical deformations.....	63
2.11 Conclusion	63
Chapter 3: Casing pipe material selection for Shale gas wells application Using ANSYS Granta CES and multicriteria decision making (MCDM).....	67
3.1 Introduction.....	67
3.2 Methodology.....	68
3.2.1 Ashby Chart Method.....	70
3.2.2 Performance indices.....	71
3.3 Results and Discussion.....	74
3.3.1 Material Selection for shale gas well	74
3.3.2 Selection based on induced stress and corrosion.....	78
3.3.3 Selection based on induced stress, service temperature and External load (Impact)	82
3.4 TOPSIS: Technique for order performance by similarity to ideal solution	86
3.5 Analytical Hierarchy Process (AHP) Method.....	91
3.6 A non-weighted MCDM.....	98
3.7 Conclusions.....	103
Chapter 4: Casing Structural Evaluations, Correlations and Strength Analysis For TOPSIS, AHP and Non-Weighted	105
4.1 Introduction.....	105
4.2 Methodology	105
4.2.1 Linear and Nonlinear Pipe Buckling	105
4.2.2 Finite Element Modelling of 10 Material Candidates.....	111
4.2.3 Parameter Correlations for TOPSIS, AHP and Non-weighted Method.....	115
4.2.4 Matrix Concatenation for Strength Distribution	117
4.3 Results and Discussion Parameter correlation.....	117
4.4 Correlations and comparison: AHP, TOPSIS and Non-Weighted Methods.....	119
4.5 Results and Discussion for Strength Distribution	121

4.6 Conclusion.....	125
Chapter 5: Prediction of casing critical buckling during shale gas hydraulic fracturing	126
5.1 Introduction	126
5.2 Theoretical background	127
5.3 Methodology	134
5.3.1 Finite element model (FEM).....	134
5.3.2 Simulation Scenarios	137
5.3.2 Simulation Scenario 'a'	137
5.3.3 Simulation Scenario 'b'	138
5.4 Results and Discussions	139
5.4.1 Scenario 'a' Result Analysis	143
5.4.2 Scenario 'b' Result Analysis	146
5.5 Effect of temperature on casing performance	149
5.6 Conclusion.....	152
Chapter 6: An application of Finite Element Analysis and Machine Learning for the Prediction and Optimisation of Casing Buckling and Deformation Responses in Shale Gas Wells in an In-situ Operation.....	153
6.1 Introduction.....	153
6.2 The Casing Lateral Buckling/Deformation Phenomena	154
6.3 Methodology	156
6.3.1 Finite Element Modelling (FEM).....	158
6.3.2 Machine Learning Prediction and Optimisation.....	162
6.4. Results and Discussion	163
6.4.1 FE simulation results.....	163
6.4.2 Stress prediction using KNN model for casing design accuracy	170
6.4.3 Effect of slip plane and casing inner diameter on casing stress.....	173
6.4.4 Effect of design parameters on casing stress performance.....	175
6.5 Selection and optimisation for the casing design.	177
6.6 Conclusion.....	181
7.1 Conclusion.....	182
7.2 Recommendations for future work.....	186

References.....	189
Appendices	213
Appendix A: Proposed Experimental Rig.....	213
A1. Introduction	213
A2 Experimental setup.....	215
A3 Test materials	217
A4 Instrumentation	218
A5 Experimental procedure.....	218
Appendix B: R CODES.....	219
Appendix C: Tables Data and Mesh Sensitivities plots	225

Chapter 1: Introduction

1.1 Background

Shale gas resources is contributing to the global energy supply in recent times through horizontal wells and hydraulic fracturing technologies. This category of unconventional (shale gas horizontal wells) pose unique sets of challenges during drilling, completion, production and abandonment. Classic example of this challenge is casing lateral buckling or deformation (Xi et al. 2017; Yin et al. 2018; Yan et al. 2017). The interaction of hydraulic fractures and formation geomechanics is buckling and even shearing steel casing leading to lack of access into the well and costly delays in drilling out bridge plugs during shale gas well stimulation process. In severe cases, this can lead to complete loss of access to the lateral section of the wells. The casing failure under this circumstance is considered to be an intra-well phenomenon that can take several forms and has no universal driver (Jacobs 2020; Liang et al. 2017), and as such; not well understood. However, this phenomenon of casing deformation has several negative impacts on the production capacity of the well, both short- and long-term integrity of the production casing, other barriers of the well and ultimately environment during shale gas stimulation.

Recent statistics from around the world, on both conventional and unconventional wells, from countries that includes Canada, China, Netherlands, Norway, United Kingdom, and United States show that approximately 26, 600 wells out of 380,000 wells have one form of integrity failure or the other (Davies et al. 2014). Xi et al. (2017) reported a casing failure rate of 30% out of 101 wells drilled in Weiyuan shale play. However, in a related study Yang et al. (2018) examined the high failure

cases of casing in Changning Weiyuan shale and reported that 34% of the 101 wells that underwent hydraulic fracturing had casing deformation. Additionally, King and King (2013) said that there were 45% tubular failures out of 14,297 wells in the US Gulf of Mexico during 1980(s). Forty-eight casing collapses were reported due to reservoir compaction (Salehi et al. 2009), while Han et al. (2018) reported that 15-30% casing failure in thermal recovery well in An oil-field. Recent study by Noshi et al. (2018) reported that 20 production casing failed out of 80 examined in the Western Anadarko Basin of the North Texas and Oklahoma Panhandles that comprises Cleveland Sandstone, Granite Wash and Marmaton formations. Also, 85% of these occurred during or after hydraulic fracturing. The study further revealed that 75% of the failed casings inspected suffered from high hoop stress. Therefore, it is worthy of mentioning that both in-situ and induced stresses in conventional and unconventional wells affect casing structural health over the well lifespan.

A number of casing failures have been reported in shale gas horizontal wells. A classic example of this failure mode is casing deformation or buckling which is critical and could lead to catastrophe in an oilfield. Xi et al. (2017) pointed out that casing deformation has the potential to reduce production output of wells by around 30%. This could jeopardise well production efficiency; especially as shale gas reservoirs have low permeability (Yin et al. 2015). Additionally, casing buckling/deformation in shale gas horizontal wells could be devastating, leading to inaccessible wells. According to Yin et al. (2018), casing deformation can cause well integrity issues and endanger the natural setting of the environment.

Furthermore, Liang et al. (2017) pointed out that the problem of casing deformation can prevent efficient well completion, well stimulation and subsequent well re-completion. Moreover, casing buckling can present stiff resistance to bridge plugs and milling shoes during subsequent fracturing of the unfractured section in the well. Similarly, Furui et al. (2010) indicated that the casing deformation/failure problem could result in increased well construction cost and has the potential to prevent workovers and re-completions. An example case study is presented on Figure 1.1. As it can be seen; there are five different locations with casing buckling as shown. The 108mm gauge cutter was successfully run to 5205m measured depth (toe of the well), however, after the first stage fracturing the 108-gauge cutter was blocked at 3913.4m(first point), 106mm gauge blocked at 4202m (second point), 102mm gauge blocked at 4378m (third point), 100mm gauge blocked at 4388m (fourth point) and 96mm gauge blocked at 4394m (fifth point) as shown.

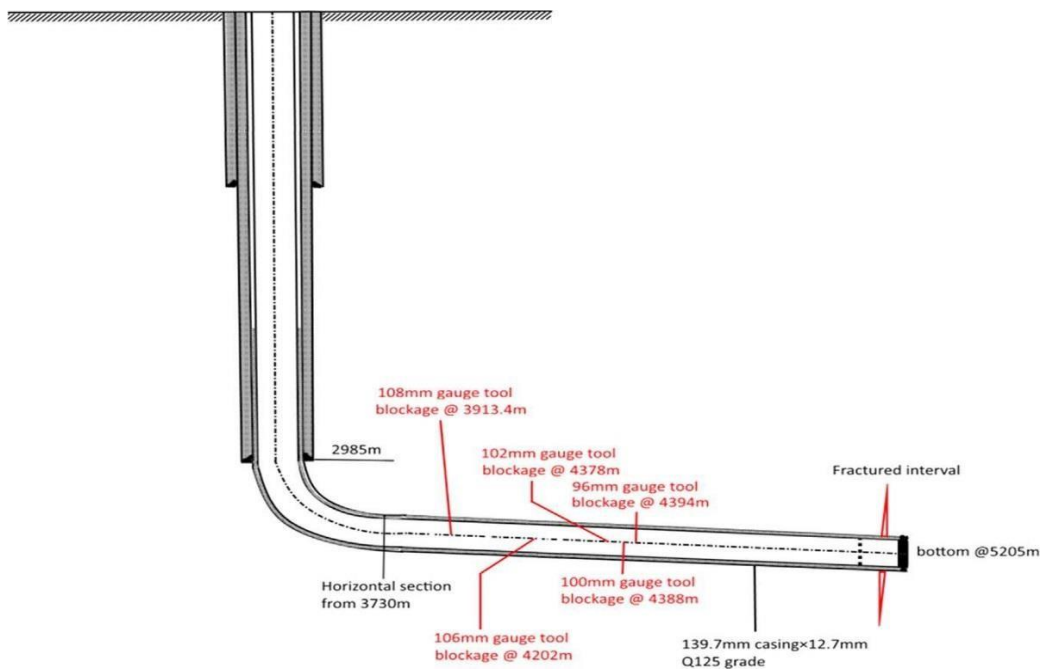


Figure 1.1 Example of casing lateral buckling. Adapted from Yan et al. 2017

Therefore, it is essential to identify and examine the magnitude of variables attributing to casing lateral buckling as a composites system (casing, cement and rock) through finite element analysis (FEA), data mining and machine learning algorithm. This will provide new knowledge and quicker way of establishing the interaction between the fracturing operations and the composites system and enable the prediction of casing structural integrity and /or responses and furnish the unconventional resources operators with the impending failure mode under a typical well scenario at the design stage.

1.2 Gap in knowledge, motivation and significance of the research

At present, casing is usually selected and design (from API and Propriety grades) based on anticipated downhole stresses using stress-check, wellcat and casing seat in both conventional and unconventional wells. However, this approach is limited and cannot sufficiently meet the design requirement for shale gas wells where casing –cement and formation system are bonded together with induced stresses during fracturing. Fortunately, finite element analysis, numerical simulation and machine learning can circumvent this limitation to predict the casing critical buckling parameters. Two possible solutions to this challenge are either to totally not developed the shale gas wells through hydraulic fracturing which will make shale gas wells unproductive/uneconomical or to find a suitable way to prevent casing buckling during hydraulic fracturing using existing resources.

Therefore, the purpose of this study is to develop detail understanding of the casing structural responses using both FEA and machine learning model in detecting impending casing lateral buckling in horizontal wells during stimulation and to

increase the success rate and prevent casing failure. It involves the identification of material (casing grade) for horizontal wells and conducting both static and dynamic stress analysis to determine critical buckling load. This was followed by parametric sensitivity analysis (design of experiment) to determine inter-relationships amongst key factors (Material, Geometry, Pressure, Temperature and Time) for casing lateral buckling. Figure 1.2 presents various phases of oil and gas wells construction and the boundary between known and unknown knowledge.

The known knowledge (Evaluation and Production) which involved quantifying the fractured volumes for each interval (microseimics), determining the casing integrity using caliper logs and/or gauge and by extension the fluids volumes that will be produce through the casing (production potential) is dependent on the unknown knowledge and the factors influencing the 'intact casing' and 'buckled casing' casing respectively.

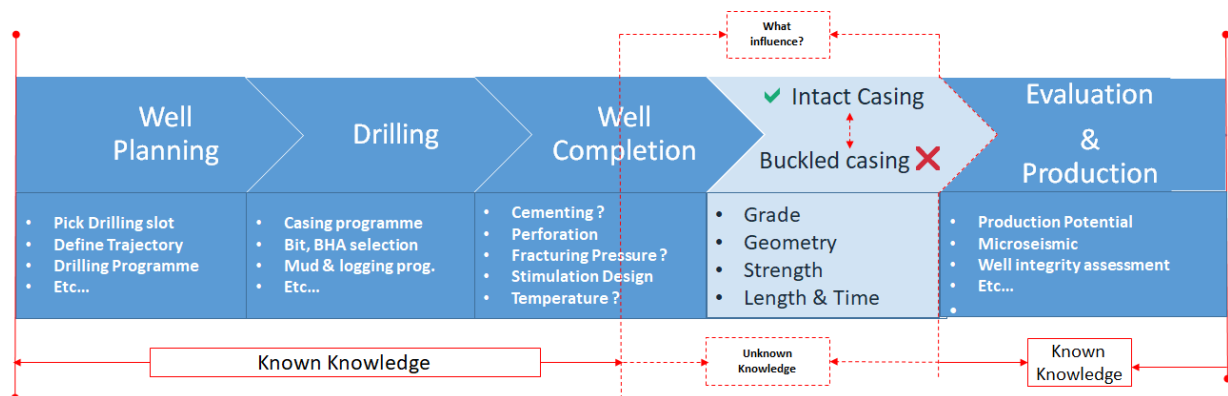


Figure 1.2 The schematic diagram illustrating the knowledge gap

The unknown knowledge manifest during the transition from well completion to final evaluation of the fracturing job resulting in buckled/deformations points along the

lateral section without the knowledge of what is influencing this buckling during the transition quantitatively.

1.3 Aim and Objectives

This thesis aims to investigate casing lateral buckling in shale gas horizontal wells using finite element analysis and machine learning to establish and quantify the relationship between variables causing the casing lateral buckling.

To achieve this aim, the thesis objectives are:

1. To conduct a critical literature review on casing failure to capture the current state of the art and to identify factors causing casing lateral buckling and determine casing grades applicable to shale gas wells development.
2. To utilise ANSYS Granta Selector (CES) material database and multicriteria decision making (MCDM) to assess the performance of API and non-API casings as well as search for an alternative casing material(s).
3. To perform linear finite element modelling (FEM) and simulations to determine the structural response of the selected materials and verification using hand calculation.
4. To conduct casing stress analysis to determine the casing health status under coupled loading conditions using lateral and radial configurations.
5. To evaluate casing lateral buckling in a given shale gas well operation condition with validation of the numerical model using relevant literature data.

6. To utilise machine learning models and artificial intelligence (AI) - ODYSSEE package for casing stress prediction and optimisation.

1.4 Methodology overview

This research began with a critical and strategic review on casing failures in a range of well types under different operating scenarios. This provided an understanding of casing grade utilisation, casing failure mix by grade, failure modes and failure mechanism. Although impeccable design and careful steps are taken, in running and operating the casing in horizontal wells; yet casing failures are still being recorded owing to the limitation of conventional methodology.

Stress analysis was conducted covering both static and dynamic condition of casing using finite element analysis (FEA) to distinguish the magnitude of stresses and displacements, underlying principles and cases, under combined loading conditions. This analysis was carried out using ANSYS APDL v.18.1. The parametric study on P110 & Q125 encompasses geometry, temperature, time and pressure to investigate how each correlates with stresses, displacements, and critical buckling loads. The predictive model employs machine learning techniques and use simulation results (data) to make quicker predictions and scenario realisations. Additionally, verification and validation were with real well data from the literature. Figure 1.3 presents a schematic overview of the research methodology.

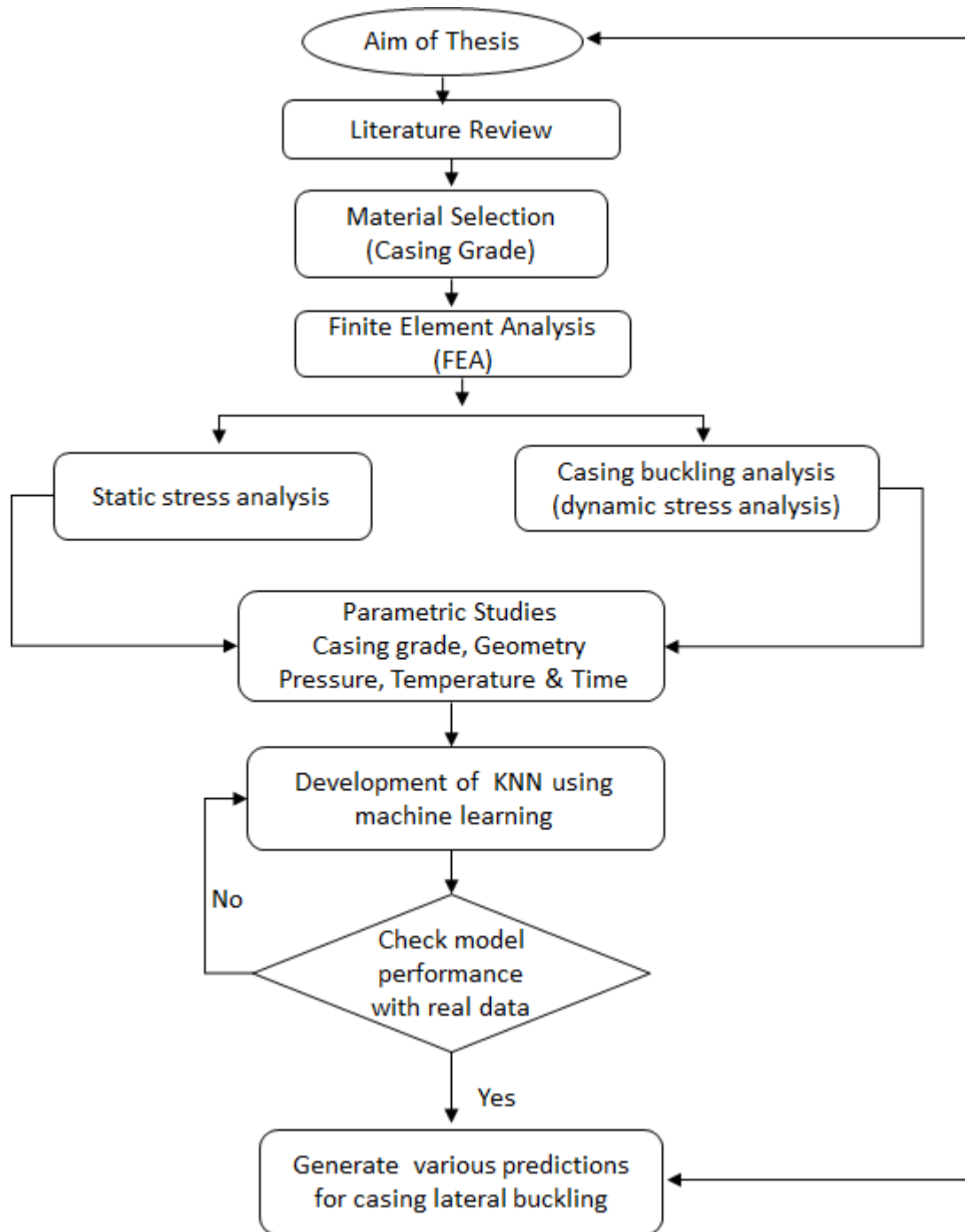


Figure 1.3 Schematic of research methodology overview

1.5 Thesis structure

This report is divided into seven chapters presenting the various simulations studies and systematic research achieved. Chapter 1 presents briefly about the research

background, aim and objectives, knowledge gap, motivation and methodology for the study. It gives information on research gap and the thesis structure/layout.

Chapter 2 provides information on API casing grades, critical and strategic review on casing failures oil and gas wells with particular emphasis on shale gas horizontal well. In particular, factors attributing to casing failure, failure modes, mechanism, underlying principles as well as cases in shale gas horizontal wells. Also, studies that investigated predictive mechanical model that are commonly applied to study casing buckling phenomena in shale gas wells are reviewed. It also briefly highlights material selection and multicriteria decision making (MCDM) for shale gas well casing and the literary solutions to the buckling phenomenon and conclusion drawn.

Chapter 3 study the casing material selection using CES EDUPACK and multicriteria decision making (MCDM) for three different scenarios of buckling tendencies. The 'expert' selection based on material performance indices is numerically evaluated using finite element modelling in chapter 4. This chapter applied exploratory data analysis to further explore and establish relationship between rank, safety factor and von Mises stress is covered in the chapter.

Chapter 5 utilise ANSYS parametric design language for the prediction of casing critical buckling during shale gas hydraulic fracturing. The chapter studied effect of temperature on casing performance and present the effect of time on stress and displacement during shale gas stimulation. The Chapter 6 cover detail studies on FEA and machine learning. It presents design exploration, parameter correlation, sensitivities and optimisation. This chapter further analysed the several simulation results and the application of machine learning and AI for prediction and scenario investigation on von Mises stress is accomplished.

While chapter 7 gives a summary of the key findings based on the outcome of the research carried in each chapter and presents concluding remarks on these observations. At the end of this chapter, recommendations for future work is proposed highlighting the potential opportunities to further studies are briefly discussed.

Chapter 2: Literature Review

2.1 Introduction

In this chapter, an overview of API casing grades is provided based on API specification 5CT. Definition and classification and the associated nomenclature used in describing the casing materials is provided. Horizontal well drilling and hydraulic fracturing technologies and resulting loads on the casing are studied. This is followed by reviewing articles that study failure mechanism of casing, cement and rock as an integrated system. Also, studies that investigated predictive mechanical model which are commonly applied to study casing buckling phenomena in shale gas wells are reviewed. The review cover casing failure mechanism and the typical failure modes that are commonly found in shale gas well development. Factors causing casing buckling, deformation and other failure modes in shale gas wells are examined and example cases from literature presented. Material selection and multicriteria decision making (MCDM) for shale gas well casing is studied and the literary solutions to the buckling phenomenon are investigated and conclusion drawn.

2.2 API Casing Pipe Materials Grades and Standardisation

Tubes are steel pipes or alloys of different sizes and grades which are couple together and run into oil and gas wells in form of strings and or liners to perform variety of functions. Byrom (2007) defined casing as 'steel tubes that become permanent part of oil and gas wells. On the other hand, tubes that are removable are called tubing. However, casing and tubing are two constituents of the group of tubular products known as Oil Country Tubular Goods (OCTG). The American

Petroleum Institute - API defines tubing as a pipe having an outside diameter OD from 1 1/2 in to 4 1/2 inches. Tubulars with OD of 4 1/2 inches or greater are classified as casing. 4-1/2 inch tubulars are often found quoted as both tubing and casing. In general, in terms of usage of the term 'tubing' is perhaps more accurate when applied to that pipe, or pipes, which comprise the completion of a well and 'casing' is that pipe which is permanently installed (cemented) in the well.

Tubular hardware (pipe) is manufactured in various connections, diameters, wall thickness, range length and strength to serve the function of maintaining structural support and integrity of the wellbore. It also prevents influx of formation fluids into the bore hole and to keep well fluids out of the wellbore. There are two manufacturing methods according to (Byrom 2007) in which oil and gas tubular are manufactured. These are the seamless and welded. The seamless is manufactured from solid cylindrical bar of steel. The steel bar is sized such that the join of a pipe manufactured from it is equal in length. The seamless tubes are the most commonly used in the industry today. However, the welded also have their place; because they are not expensive compared to the seamless tubes. In contrast, the welded are manufactured from heated steel slab that is rectangular as against the cylindrical shape in seamless.

Tubular hardware used in oil and gas wells are standardised by the American Petroleum Institute (API) and International Organisation for Standardisation (ISO). Typical example of this standardisation is API specification 5CT – which pertain to casing and tubing. However, there are non- API tubing and casing (propriety grades) which are also in used in the oil and gas industry. Oxford (1967) pointed out that the API standardisation is for safety, uniformity and guidance to both the

tubular manufactures and operators that uses this hardware. These standards are usually in form bulletin, recommended practice (RP), technical report (TR) material specification, design calculations ETC.

The casing, tubing, line pipes, couplings and their associated tests guidelines for used in oil and gas industry today; follow the American Petroleum Institute Specification- API specification - 5CT.

Table 2.1 Provide a brief overview of the tubular hardware grades as contained in API spec. 5CT.

S/no.	API Grade	Yield Stress (psi)		Minimum Ultimate Tensile (psi)	Maximum Elongation (%)
		Minimum	Maximum		
1	H-40	40000	80000	60000	29.5
2	J-55	55000	80000	75000	24.0
3	K-55	55000	80000	95000	19.5
4	N-80	80000	110000	100000	18.5
5	L-80	80000	95000	95000	19.5
6	C-90	90000	105000	100000	18.5
7	C-95	95000	110000	105000	18.5
8	T- 95	95000	110000	105000	18.0
9	P-110	110000	140000	125000	15.0
10	Q-125	125000	150000	135000	18.0

For example, in the P110 casing grade, the number represents the minimum yield strength in pounds per square inch, while the letter denotes steel grade.

However, because of the different characteristics exhibited by oil and gas wells; several alloys are developed to cope with varying environmental requirements. Example, some wells can contain acids gases that could not allow the use of carbon steel because this may lead to severe corrosion. As such, different propriety grades (also called non-API grade) with high corrosion resistance are manufactured by different manufacturers. A steel alloy is developed when other metals are added to

the basic combination of iron and carbon to improving its properties. The main objective; is for higher strength, corrosion resistance or better response to heat treatment. When the percentage of alloy material is below the level indicated by specialised terms such as "chrome" or "stainless," the product is simply called "alloy steel."

2.3 Casing–Cement-Formation Failure

Looking at casing, cement and formation as an integrated system, various well integrity issues, could manifest. However, mechanical failures of the steel casing and the cement sheath are two primary failures in such a system. Liu et al. (2017) pointed out that; casing-cement failure is caused by induced stresses and downhole stress changes due to hydraulic fracturing, steam injection and well test during well operations. In addition, casing and cement failure could be accelerated if chemical reaction degrades casing and cement barriers as a result of corrosive substances present in the well. Besides, failure of cement could endanger the health state of casing and its connection. Similarly, failure of casing undermines cement integrity- i.e., the integrity of casing cement system is mutually inclusive.

Ferla et al. (2009) simulated the effect of injecting surface fluids (sea water, CO₂ steam) in oil and gas reservoirs to ascertain the stresses in the composite system near the wellbore region. The result show that the casing is in compression due to the thermal stresses during injection, but the rock formation has an excessive impact on the stresses in the casing. Furthermore, analysis of the radial stresses on (hard-soft-hard rock sequence – under steady state) has shown that tensile radial stresses developed at the interface between the casing and the cement in the

neighbourhood of the boundaries between the rock layers (Jinan et al., 2012). These radial stresses are found in the simulations runs with and without casing pre-tensioning. Moreover, analysis of the shear stress produced at the interfaces of casing/cement and cement/rock indicates that increased shear stresses are produced near the central layer (Shen et al., 2016). However, this study concluded that; a complex stress environment form along the well that may include high axial stresses, shear stresses along the boundaries casing/cement and cement/rock, or even tensile radial stresses between the casing and the cement. These stress conditions may result in the material failure which can jeopardise the well integrity during steam injection.

Jinan et al. (2012) study the cement-formation interface adhesion in a horizontal well using elastic mechanics and composite structure model. This study found that at the interface (cement-formation) cement strength increases with a second interface adhesion. However, when the bottom hole temperature become severe casing-cement debonding may be the result (Li, 2008). In a separate research, Peng et al. (2007) examined a case study of casing failure in unconsolidated formation in Shengli oilfield of China. The study simulated the interactions between the casing and surrounding formation rock, and effects of sanding-induced cavities on the casing is determined. The simulation results show that the cavities in the rock due to sanding cause the formation rock more probable to fail and the casing to suffer much higher deformations. Further analysis on the results show that casing failures primarily occurred in unconsolidated sandstones, were caused by sanding-induced cavities. The results also revealed that most failures were caused by the

casing buckling and fracturing due to the cavities and varying stress distribution in the unconsolidated formation.

In addition, Lavrov et al. (2015) investigated tensile thermal stresses in casing-cement formation system with rock heterogeneities. The influence of thermal conductivity and material properties on tensile stresses and tensile damage development during heating and cooling of a downscaled casing-cement-rock assembly was examined. Tensile failure was predicted during thermal cycling of the casing/cement/rock assembly at both heating and cooling stages. The failure occurred mostly in damaged cement and damaged rock. The simulation results suggested that cement immediately adjacent to the casing pipe is most prone to tensile cracking during both heating and cooling. Heating the casing to a higher temperature activates tensile cracks located in cement increasingly farther away from the hole.

Modelling of casing-cement and formation system in steam injection wells show that casing expansion and stresses lead to cement failure behind the casing by cracking under high hoop stress. Additionally, due to thermal expansion of the casing, cement and formation system caused casing to fail in form of excessive deformation, buckling and collapse. In particular, when injection parameters are greater than 700psi and 500 °F (4.8 MPa and 260 °C) production casing often fail (Wu et al., 2006). Although, when casing is cemented in the well, it is assumed that it is totally restricted in axial direction, but it expand/contract radially and tangentially owing to temperature change. However, in steam injection projects, both casing, cement and formation are heated, and all expand/contract based on their coefficients of thermal expansion. This results in different radial stresses

developed at the casing-cement interface and cement-formation boundary respectively (Fang et al., 2015; Wu et al., 2006). This interface stress contrast promotes one form of failure or the other depending on the circumstance.

Figure 2.1 present a summary of casing grades utilisation in different well types base on articles reviewed in this research. It also shows casing failure mix by grades for oil and gas wells. Shale gas and deep-water wells utilised higher strength casing grades. Additionally, P110 and N-80 grades are more applied in injection wells than other grades owing to their stiffness and perhaps cost. Figure 2.1 (B) gives a summary of casing failure mixed by grades. It can be seen that; P110 casing grade have higher failure rate of buckling than other grades - probably due to its higher utilisation in shale gas, deep-water and injection wells (troublesome wells).

2.4 Predictive Mechanical Models

The research work of Li and Samuel (2016) developed an analytical model that can be used to predict a threshold pressure for a degraded casing with a crescent wear. The API specification 5CT established 12.5% wall thickness tolerance for design purposes; however, Li and Samuel (2016) argue that the API model is overly conservative. When compared to the crescent wear model, the crescent wear model gives higher burst capacity prediction than the API uniform wear model. Like the API model, the crescent wear model can be applied to estimate residual strength of the worn casing, tubing and riser pipes. Furthermore, Shen and Beck (2012) developed an analytical model that calculates stress profiles in a worn casing with consideration of downhole temperature effect and confining formation effects.

Results from the analytical study shows that the wear affects hoop stress more than the radial stress around the worn casing.

Furthermore, the worn part of the casing is likely to fail in compression when thermal load increased. In a similar study on casing wear, Yu et al. (2016) developed analytical model for the prediction of casing wear in a deviated well. This study utilised both experiment and simulation to establish the model. This model can calculate both von Mises stress and displacement at the wear point in the casing. In addition, Tan et al. (2018) developed a circumferential casing wear depth (CCWD) model. The basis for the development is based on energy principle and geometry. This new model assumes buckled drillstring to cause the wear, and on this basis the model provides practical method of accurately predicting casing wear in extended reach wells and horizontal wells.

Additionally, Yin and Gao (2015) developed an analytical model for the estimation of sustain casing pressure in shale gas horizontal well. The model is based on temperature change during fracturing that cause the pressure differential in the casing causing failure. The model incorporates temperature change and annular volume change to reliably predict casing behaviour under hydraulic fracturing. Sustain casing pressure displays a polynomial increase with well temperature. Using this model sustain casing pressure can be computed and used in design of production casing for shale gas horizontal well undergoing fracturing.

In addition, Brechan et al. (2018) build a model to developed ultimate limit strength (ULS) for the prediction of tubular collapse failure following a joint API/ISO work group (WG2b) guidelines and recommendation. Results obtained from this model (ULS) is in good agreement with actual collapse test conducted on 113 samples by

drilling engineering associations (DEA). Besides, Rodriguez-Prada (1990) developed a predictive simulator that calculates casing strains and stresses due to steam injection and/or hot fluid production. The simulator enabled the determination of radial and hoop stresses and displacements resulting from thermal induce stresses and pressure changes in the system. Results obtained from this study can take care of casing with slenderness ratio of less than 20 as the API model is only valid for slenderness ratio greater than 20. This model is built upon the energy distortion theory was used in the analysis of the combined stresses. All of these calculations can be carried out at any point along the casing and with any boundary conditions.

The slenderness ratio is simply the ratio of Diameter to pipe thickness that is;

$$SR = \frac{OD}{t} \quad 2.1$$

Where, SR = slenderness ration OD = casing outer diameter (inches) t = casing pipe thickness (inches).

The slenderness ratio of 20 is not an issue for casing buckling phenomena in shale gas wells, however slenderness ratio clearly delineates between various collapse regime of the casing which includes (elastic, plastic, yield and transitional collapse). Based on this ratio, different empirical coefficients are provided corresponding to each of the collapse regime mention above. At the design stage these constants are looked up in table for design calculations to ascertain the collapse pressure rating of the selected pipe.

Figure 2.1 (a) presents a summary of casing utilisation by well type (b) casing failure mix by grades. The buckling failure appears to be second highest for all the

grades investigated owing to loading conditions and structural forms of these pipes as well as the orientation of the wells (vertical, horizontal and inclined wellbores).

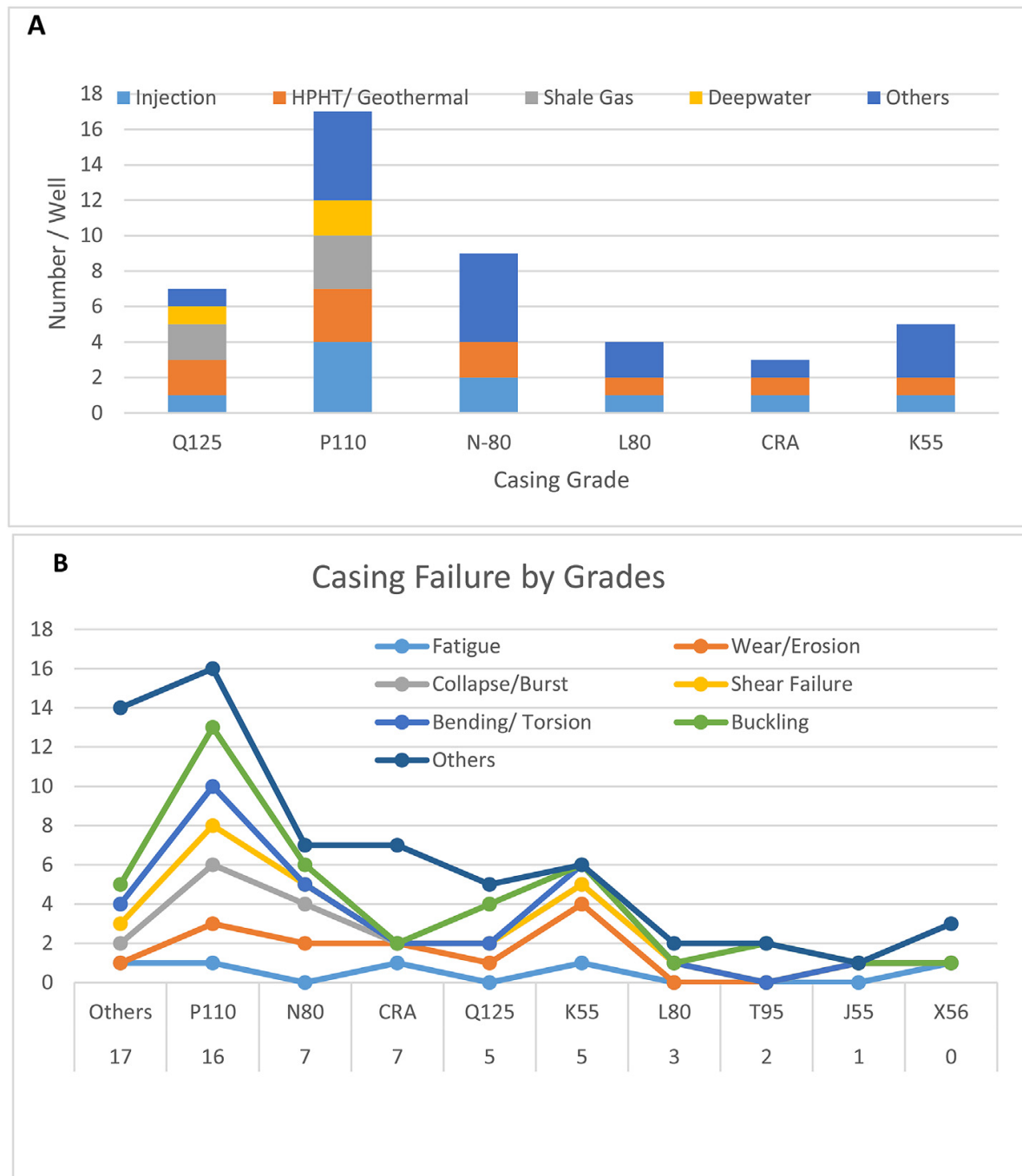


Figure. 2.1 (A) Presents a concise summary of casing utilisation by well type (B) Casing failure mix by grades based on the articles reviewed.

Buckling is a type of failure resulting from a compressive force applied leading to structural instability and/or sideways deflection of a tubular in oil and gas wells. Casing and tubing buckling could occur during installation in the well, completion, stimulation and production operations. However, recent literature indicated rising cases of casing lateral buckling/deformation particularly during shale gas development process (Lian et al., 2015, Mohammed et al. 2019; Yin et al. 2018). Historically, the underlying theory for buckling was first introduced by Euler in 1757. This model is specifically meant to determine critical buckling limit of a weightless rod in vertical column members (Hearn, 1997). However, Lubunski (1950) was the first to developed pipe buckling in oil and gas wells accounting for weight of the pipe. Lubunski model was developed to predict both sinusoidal and helical buckling. Other models developed are that of Mitchell for helical buckling and Dawson (1984) model for sinusoidal buckling of pipes in inclined wells (Kyllingstad, 1995). Menand et al. (2011) developed analytical model and compares the model results with a full-scale buckling test. The new buckling model considers the actual tortuosity of the wellbore. Menand et al. (2011) argued that field observation reveal that the existing models do not predict buckling phenomena like lockup and assume the wellbore to be idealistically perfect devoid of any deviations. Mitchell and Miska (2006) developed a three-dimensional buckling of pipes with connectors with an applied torque. The formulation of the model builds upon Lubunski buckling theory; the wellbore is vertical and straight. The beam-column equations considered in the plane buckling analysis are used, but now there are deflections out of the plane in this model. A solution for helical buckling is developed that produces pipe sag,

maximum dogleg angle, contact force, and bending stress magnification as a function of pipe effective axial force and torque.

Moreover Mitchell et al. (2011) developed a semi-empirical model for the prediction of drillstring buckling in horizontal and extended reach wells. The semi-empirical model predicts contact forces in the string and result from this model matches very well with drill-drag software. Furthermore, Mitchell et al. (2019) developed a predictive dynamic model that could estimate tubular stresses in horizontal wells. In particular, this model provides an ideal means of prediction critical cyclic stresses that result due to excessive stimulation stages in shale gas horizontal well development. In addition, recent study by Sathuvalli et al. (2019) presented an analytical model for the determination of mechanical response of concentric cemented casing from a far field geomechanical stress. Results obtained from this model show that it can effectively quantify the effect of the loads on the concentric casings and the intervening cement sheaths, and to assess the effect of the formation.

Table 2.2 Summary of widely used casing buckling and related buckling mode.

Buckling Model	Assumptions	Operations	Reference
Euler	Beyond critical load casing deflect/ buckled in vertical wells	Injection of water leads to slippage of weak structural interfaces which cause buckling of the casing	Yin et al. (2018); Lin et al. (2017); Xi et al. (2018);
Lubunski	Buckling occurs when effective axial force is applied	Volume fracturing lead to casing axial deflection	Lian et al (2015); Liang et al. (2013); Li and Samuel (2016)

Dawson	Beyond critical load casing deflect/ buckled in deviated wells	Volume fracturing activates faults and fractures which cause several deformation sections in horizontal wells	Guo et al. (2019). Yin et al. (2018); Chen et al. (2018); Xi et al. (2018)
Mitchell	Sinusoidal buckling occurs when critical force is less than effective axial force and effective axial force less than $2.8F_{\sigma}$ Helical buckling occur before reaching $2.8F_{\sigma}$	Horizontal well stimulation lead to complex stresses resulting in sinusoidal buckling of the casing	Zhao et al. (2018); Yin et al. (2018); Zhang et al. (2016)

These buckling theories are based on linear elastic and the prediction are not conservative. In practice real buckling load are less than what it is typically calculated using linear elastic prediction. These theories consider single mode buckling with the only exception of Mitchell's model that examines mixed mode.

Heathman and Beck (2006) used DIANA software to modelled casing, cement and formation system to re-evaluate the design basis of casing due to significant failure experience in East Texas HPHT wells. Their analysis shows that when all critical aspect of the well is included in the design; previous failures encountered in this field will be avoided and ensure cost effective well being drilled and stimulated effectively in future development. However, casing buckling recently encountered in horizontal well during shale gas development take various forms and modes. Hence, casing buckling can be closely related to some of these models mentioned above. Table 2.2 presents a comparison of selected cases of casing/deformation to the models.

2.5 Factors causing casing buckling during shale gas hydraulic fracturing

Tight oil and gas reservoirs and shales are difficult to exploit. However, the development hydraulic fracturing and horizontal well drilling are enabling the

extraction of these difficult reservoirs/ resources. During the process of multistage hydraulic fracturing for oil/gas extraction, a number of challenges limits the efficient stimulation of these shale/tight oil reservoirs. One example is casing lateral buckling / deformation – which occurs in the process of hydraulic fracturing, due to high internal pressure and unequal external support (Yan et al., 2017; Mohammed et al., 2019). Furthermore, shale gas horizontal wells are associated with long lateral sections, this feature of shale gas horizontal well present difficulties to effective installation of the casing in the drill hole. This is often related to gravity pulling the casing to lie on the low side of the well and tight spots preventing the casing concentrically in the hole (Mainguy and Innes, 2018; Mohammed et al., 2019).

In addition, several stimulation stages and high pump pressures in the process of hydraulic fracturing affect casing's mechanical behaviour resulting in shear failure and deformation of the casing in the horizontal segment of the well as established by (Lian et al., 2015; Yin et al., 2018). As a result, many stages are not stimulated due to lack of access into well (Brantley et al., 2014; Tang et al., 2013; Yu et al., 2016). The study of Xing et al. (2017) established that complex downhole stresses in shale gas wells lead to the failure of the production casing. Also, the study of Lian et al. (2015) revealed that stress deficit, slip displacement and perforation completions made the casing axial buckling into an 'S' shape in shale gas horizontal well during fracturing. However, the works of Xi et al. (2017) and Wang et al. (2018) both pointed that the activation of a weak rock layers and overburden stress shale reservoirs result in the casing buckling failure.

On the other hand, reason given by the study of Haghshenas et al. (2017) and Liu et al. (2017) on casing buckling is the additional load exerted by fracture slip

penetrating through the well. Furthermore, in-situ stresses and weak rock layers are identified to be sources of variable stresses leading to casing buckling during stimulation (Liu et al. 2017). The in-situ stresses are orthogonally acting at a point, and depending on the magnitude of these stresses, rock mechanical properties and operational practice executed in stimulation process; the well and casing instabilities (buckling and deformation) are strongly connected to these variables (Mohammed et al. 2021).

The study of Yin et al. (2018) based the casing failure phenomena on slip of shear fractures which occurred during fracturing operation. Yin et al. (2018) further show that fracture slip result in large transverse displacements and stress concentration points on the casing. Meanwhile, Yu et al. (2019) and Chen et al. (2017) argue that hydraulic fractures and subsurface distortions during fracturing operations are the main factors leading casing buckling in shale gas horizontal wells.

2.6 Casing Failure Mechanism in Shale Gas Horizontal Wells During Hydraulic Fracturing

Shale gas and tight oil reservoirs exhibit very low permeability justifying the need for excessive stimulation stages to aid commercial oil and gas production through hydraulic fracturing. Another key feature of shale gas horizontal well is the very long horizontal lateral section. In the process of hydraulic fracturing, with high-flowrate, fluid retention in cement voids contract due to sudden temperature decrease inside the casing. Consequently, pressure drops inside the cement sheath voids causing uneven load distribution on the casing paving way for potential casing deformation (Yan et al., 2017).

The study by Chen et al. (2017) identified fracture and bedding as the main internal factors responsible for casing deformation during hydraulic fracturing. In addition, when casing is placed in a poor lateral support with high pumping pressure requirement to fracture the formation, this creates high internal pressure inside the casing which is the basis of casing failure. Yan et al. (2017) pointed to the fact that under the combined effect of high internal pressure in a high tortuous wellbore, external stress becomes critical and casing deformation risk is higher in such a situation. However, owing to long lateral sections, casing standoff is a challenge especially in the horizontal section due to gravity. Lack of good standoff (70% and above) could lead to potential points for lateral buckling in a horizontal well. Casing standoff is a measure of the ratio of how the casing is centrally placed relative to the well diameter (concentricity). Furthermore, Gorokhova et al. (2014) compared soft string and stiff string models for casing centralisation and established that both approaches yield similar standoff ratio during planning phase. However, the study concluded that the stiff string model gives more accurate prediction in the presences of well tortuosity and open hole enlargements. Operational efficiency, models predictions and optimum number of centralisers and type (spring-bow or rigid) play crucial role in establishing good standoff and potentials buckle points along the lateral section of the well.

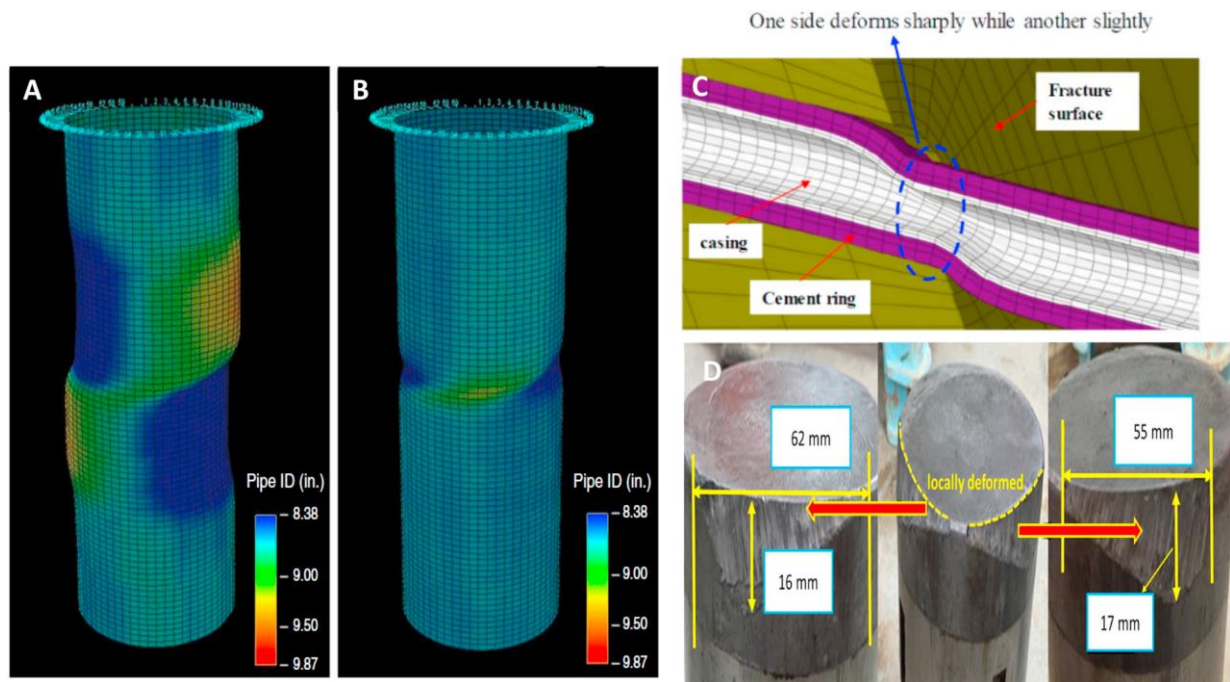


Figure 2.2 (A & B) Shows the effects of centraliser on casing deformations, while (C & D) presents buckling due to fracture and lead mould impression justifying casing deformation respectively.

The key factors attributed to casing failure are unequal external and internal loads acting on the casing during fracturing operation. For example, Yin et al. (2018), showed that shear deformation of casing was due to slip of shear fractures in shale gas reservoirs, based on curvature screening criteria. The study further revealed that slip displacement led to large transverse displacement and stress concentration points on casing. Furui et al. (2012) established that simultaneous fracking and acidising can lead to compaction, wellbore integrity issues and casing failure. In a different study, Yu et al. (2016) examined the effect of hydraulic fracturing on reservoir deformation and concluded that fractures caused casing and subsurface deformations.

In summary, hydraulic fracturing cause structural stresses that lead to wellbore integrity decline (Yin et al., 2017, Furui et al., 2012; Yuan et al., 2016; Li et al., 2017; Abou-Sayed et al., 2005). Similarly, both Xi et al. (2017) and Wang et al. (2018) indicated that when weak plane is activated in shale reservoirs, such activation and bedding caused casing shear deformation. Another reason for casing deformation was proposed by Hagshenas et al. (2017) and Liu et al. (2017) who noted that additional load is exerted on casing by fracture slip through the wellbore. Again, Yin et al. (2018) pointed that fracture slip during hydraulic fracturing can cause casing shear failure. During this process, fracture slips through the wellbore, which induce a shear load on the casing resulting in - casing damage under the action of rock shear slip.

The study of Xi et al. (2018) identified key factors such as fracturing pressure, formation anisotropy, lithologic interface, temperature and cement to increase casing stress. Consequently, casing deform under combined stresses. Figure 2.3 provides statistical analysis showing deformation points of 12 wells out of 25 horizontal wells during hydraulic fracturing. It could be seen three different categories of casing deformations were encountered i.e., during fracturing, tripping bridge plug and those related to drilling out the bridge plug. However, based on the formation characteristics and the cementing process in Sichuan Basin and Annular Pressure Build-up (APB) noticed in conventional wells, physical and finite element models were established to study this phenomenon. Many factors, like void, bedding plane angles, temperature change, magnitude of the internal pressure and in-situ stress were examined. Results obtained show that cement void contract due to high fracturing flow rate and sudden temperature reduction inside the casing. As a result,

pressure inside the cement sheath voids dropped significantly within a short time; thereby imposing varying load on the casing. Hence, the buckling failure results under such a situation.

In almost all fracturing projects, high pumping pressure is needed to overcome rock compressive stress particularly in a high geo-stress shale block. This high pumping pressure is necessary to fracture the formation, which in turn induce a higher internal pressure inside the casing (Yan et al., 2017). Under this opposing load events occurring downhole on the casing, deformation and buckling failure become imminent. This study adjudged factors responsible for casing deformation to be high internal pressure and non-uniform external loading on the casing during fracturing. Furthermore, cement sheath defects and shale characteristics are amongst the features responsible to casing deformation.

Also, Yan et al. (2017) claimed that for deformations around 'heel' region (end of build section in horizontal well) shearing force is exerted on casing, as a result causing such deformations. However, the curved section of the casing experienced significant shear force during fracturing. Some field specialists recognised that casing deformation in shale gas might be also caused by formation/fault slip induced by hydraulic energy. It could be an acceptable explanation for deformation around build section. Evidence of casing buckling beyond the build section is presented by lead mould printing (refer to Figure 2.2 D). It is however a non-trivial task to explain these deformations that occurred far away from the build section in horizontal part especially deformation near the toe (tail end of horizontal section). Taking the Wei-204H7-3 well as an example, this well is expected to be fractured in 21 stages.

Before the first stage fracturing, milling shoe (108 mm) was driven through the casing to the bottom at 5205m without any resistance.

However, after the first stage stimulation, the gauge cutter (108mm diameter) was blocked at 3913.4 m, and even the 96mm diameter gauge cutter could not pass through the casing (block at 4394 m). After several attempts, five casing deformation points were determined, and these deformation points distributed along the entire horizontal well as shown on Figure 2.3 (Yan et al., 2017). Li et al. (2017) examined casing failure mechanism using finite element model (FEM) during volume fracturing technique in low permeability gas reservoirs. The study established casing deformation based on field data including completions, reservoir rock and micro seismic surveillance data. Tight horizontal gas well was investigated for casing deformation and result obtained showed that the natural fracture slip is accompanied by extreme local casing shrinkage with slight deformation one side and severe at other, as shown on Figure 2.2 (C).

Lian et al. (2015) indicated that stress deficit and clustering perforations make horizontal well deformed radially and s-shaped deformation axially. Excessive stimulated segments and big pumping delivery rate during volume fracturing process, complicate casing's mechanical behaviour which results in shear failure, leap and slip, around the horizontal section and change in in-situ stress field (Chipperfield et al., 2007; Hossain et al., 2010). All these factors mentioned frequently lead to in-accessible well caused by casing deformational failure. Consequently, usual completion and stimulation cannot be performed as planned during fracturing operations (Tang et al., 2013; Yu et al., 2016; Brantley et al., 2014). To address this challenge, Furui et al. (2010) suggest an advanced

comprehensive model that can analyse wellbore stability and casing linear deformation during hydraulic fracturing and acidising. But this model is limited to highly compacting chalk formation and cannot be employed to analysed shale gas well casing stability.

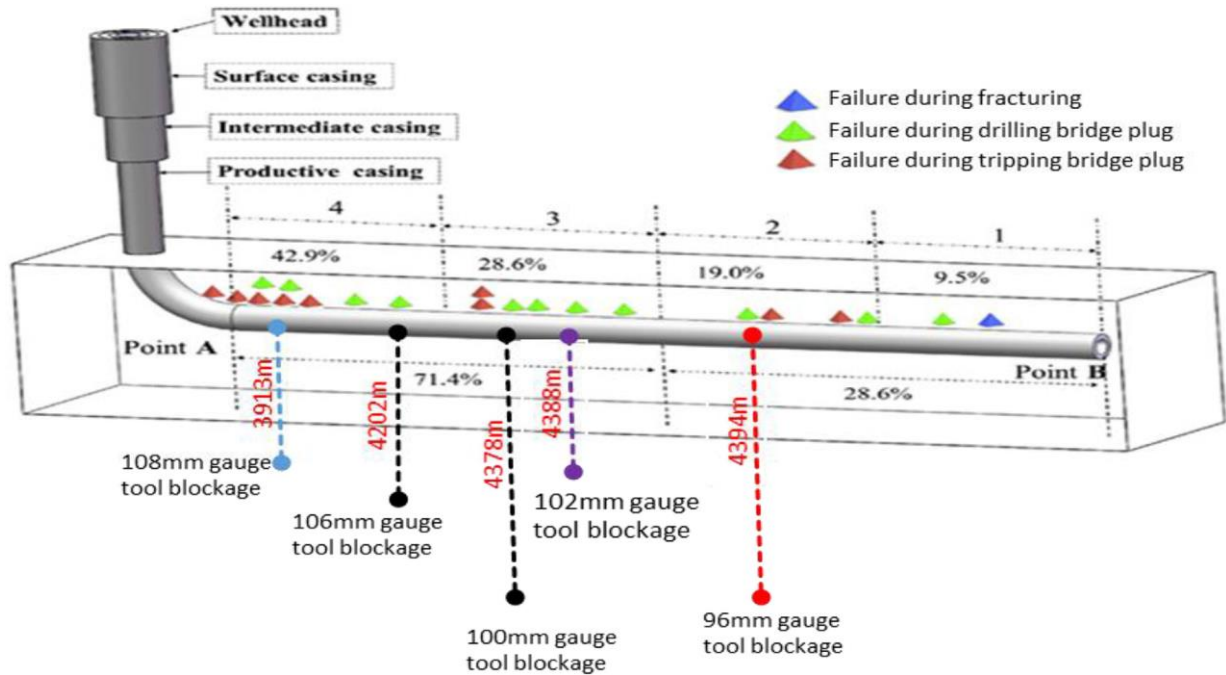


Figure 2.3 Statistics on casing deformation points of 12 horizontal wells (After Xi et al., 2018). And specific example of Wei-204H7-3 with 5 deformation points as shown (After Yan et al., 2017).

2.6.1 Buckling Failure or Deformation of Casing Pipe

This section is specific to factors causing casing lateral buckling and the failure mechanism. Buckling is a pipe structural instability that cause sudden change in shape owing to applied compressional load which lead to bowing or deformation when subjected to shear load. Wang et al. (2014) described local buckling as a failure mode along the wall of a casing that does not extend to its centre. While, in column buckling (deformation) the casing is completely deformed with the centre

of the casing bending leading to lack of access through the casing. In addition, Chen et al. (1989) classified two types of buckling for casing in horizontal well, which are sinusoidal and helical. Axial compression load gives rise to sinusoidal buckling configuration but depend on casing stiffness, weight, and hole size. In contrast, with increased axial compression sinusoidal buckling changes to helical buckling.

In addition, Yin et al. (2018) and He et al. (2014), established through finite element analysis (FEA) that fracture slip during fracturing causes casing lateral buckling in shale gas wells. Additionally, with increase in pumping rates, a critical value is reached which cause natural fracture to shear rock mass, leading to casing lateral deformation. Moreover, Zhaowei et al. (2017) indicated that at some critical pressure, natural fracture is activated which move and induce casing failure.

According to Guo et al. (2019); sudden temperature change between reservoir and fracturing fluids increases casing failure probability. Similarly, Yu et al. (2016) shows casing failure to be caused by formation alternation, in situ stress variation, irregular fracturing zones.

Under this situation in situ stress increases and become very severe downhole to deform the casing radially. Moreover, Zeng et al. (2018) attributed casing deformation to change in in-situ stress because of large scale fracturing which led to sliding of strata of rocks. However, the study added that well trajectory, cement quality and temperature may influence casing deformation under this situation. In situ vertical stress (overburden) is a function of depth, and rock densities and always vary due to different rock mineralogy, porosity and volume of open fractures within the rock. On the other hand, in situ horizontal stresses vary because of topography of the formation, tectonic activity and proximity to faults. When oil and

gas wells are drilled, the rock removal create an imbalance between the overburden and horizontal stress. Consequently, wellbore stability issues manifest leading to buckled casing.

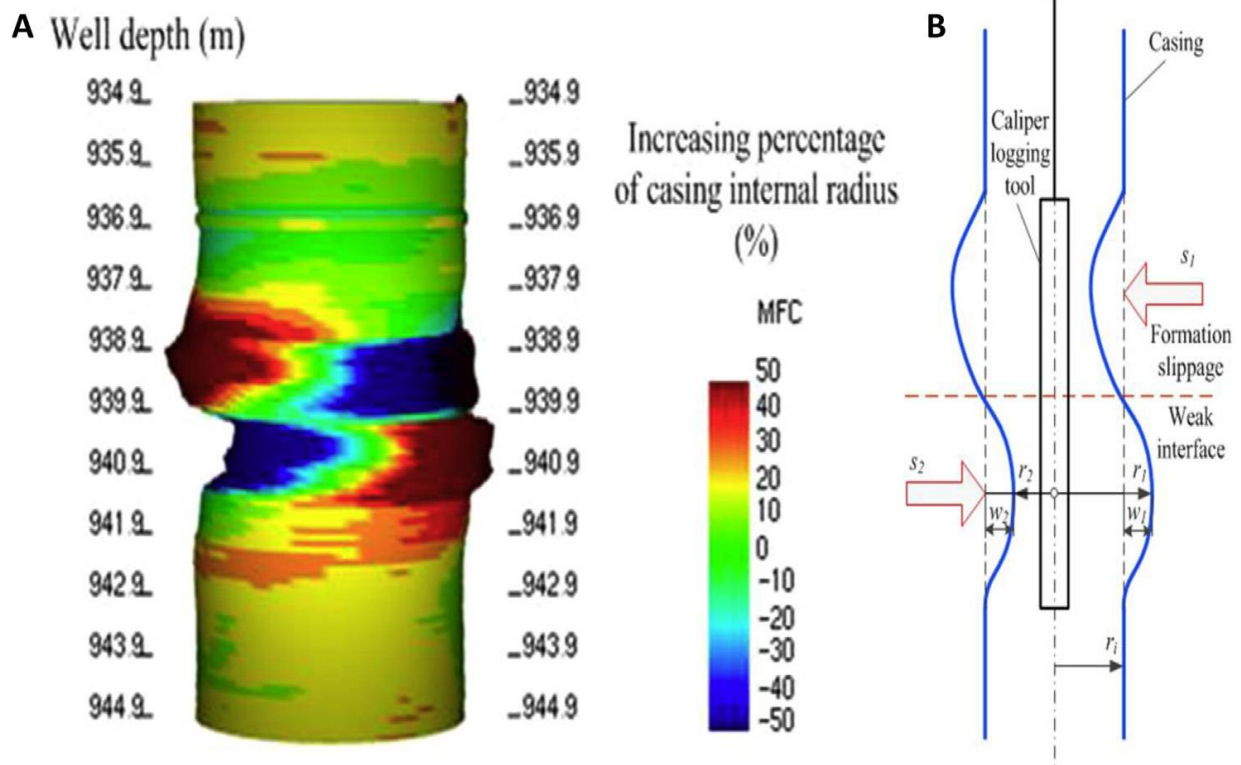


Figure 2.4 (A) Casing imaging logging of an injection well (B) Illustration of shear formation slip inducing casing failure (After Yin et al., 2018).

2.6.2. Casing Shear Failure in Shale Gas Wells

Dusseault et al. (2004) described casing shear because of formation shear that happen due to changes in stress and pressure caused by the type of exploiting condition-depletion, injection and heating. Wang et al. (2011) described shear failure mechanism due to displacement of the rock strata along bedding plane or steeply inclined fault planes. Yin et al. (2018) reported that fracture slip during

hydraulic fracturing can cause casing shear failure as shown on Figure 2.4. Fracture slips through the wellbore during hydraulic fracturing induce shear load on the casing resulting in casing damage under the action of formation shear slip. It can be seen on Figure 2.4 (A) that one side of casing dips inward and the opposite side bulges outward reflecting shear deformation and hence support the notion of formation slippage during water flooding i.e., the slippage of weak structural interfaces Figure 2.4(B).

Hu et al. (2016) calculated the critical displacement that can induce casing shear within a weak structural interface using numerical simulation. However, this study suggested that lower casing grade could be utilised around the weak structural interface if it meets all downhole requirements. The study concluded that if casing elongation could be improved by 60%, then critical casing failure slip displacement can be increased by 21.4%. For example, Daqing Oilfield in China has been known for casing shear failure and/or deformation.

2.6.3. Collapse/burst failure

Vudovich et al. (1988) reported that casing failure modes are interrelated with casing failing in one or more of the failure modes – collapse or burst, which is attributed to radial stress. Tensile failure due to axial tension and connection jump out as the result of compression or tension. However, one factor may reduce the occurrence of a failure mode but promote another kind of failure. According to Wang et al. (2014) collapse failure is a result of different mechanical loading from sand, cement and casing itself. Kiran et al. (2017) also suggested that presence of voids and cement channels at casing-cement interface could induce up to 60% reduction on casing collapse resistance. Meanwhile, when compared to eccentricity, the

presence of voids and channels is by far more troublesome than eccentricity. Conversely, eccentricity has its own attendant effect on the casing structural integrity. Additionally, during production, stress consistently change due to variable flow rates and dynamic loading; this stress variation has also been established to cause casing collapse failure.

The mechanism is mainly attributed to unequal external load exceeding casing yield strength which change the circular orientation to oval (Huang and Gao, 2015; 2016). Collapse of the casing are mainly classified into yield, transitional, elastic and plastic. The industry standard approach to differentiating these collapses is based on slenderness ratio which is a ratio of casing diameter to its thickness. However, Abdideh and Khah (2018) presents casing collapse phenomena as abnormal displacements of rock formations on the casing leading to collapse (Kuanhai et al., 2017). Bastola et al. (2014) examined the factors influencing pipe's collapse resistance and concluded that effects are small for 3D models with length to diameter (d/t) ratios above 10, and that an increase in initial ovality would lead to a decrease in the pipe's resistance to collapse (Bastola et al. 2014).

2.6.4. Fatigue Failure

Fatigue is the progressive and localised structural damage that occurs when a material is subjected to cyclic loading (Bai and Bai 2005). Fatigue is also described as simply a mechanism associated with cyclic loading and is an irreversible and cumulative damage that occurs when a material is subjected to cyclic stress (Gao and Hsu, 1998). The cyclic loading or stresses could either be fully reversed, repeated or fluctuating loads. Moreover, these loadings are either low cycle or high

cycles (Liu et al., 2015; Cirimello et al., 2018; Chen et al., 2018). Casing fatigue failure could occur when the well exhibit alternating temperatures during production. Also, during stimulation fatigue loading is induced due to temperature difference between stimulation fluids and the reservoir fluids. Casing gains high temperatures during steam injection, while in soak periods its temperature reduces significantly.

2.6.5 Wear/erosion/corrosion failure

Mao et al. (2018) described casing wear failure; as failure resulting from frictional contact of the drillstring with casing thereby shelving or removing part of the surface of the casing. Consequently, the friction point wear (thickness reduces) which depends on the contact force magnitude, contact area, angle, fluids and material strength. On the other hand, corrosion is one example of metal loss in casing that can leads to potential leaks, (Wilson, 2018). According to Zhang et al. (2016) wear is a kind of material loss by removal of solid surface under mechanical action (friction). Wear can also be described as a fundamental type of material loss that is characterised as the removal of material from solid surfaces by mechanical action (Fischer and Bobzin, 2009). It can be classified into adhesive wear, abrasive wear, surface fatigue wear and corrosive wear in terms of the fundamental mechanisms and characteristics of wear surface (Andersson, 2011).

Casing wear caused by drill string rotation may be classed as typical adhesive wear and abrasive wear. Adhesive wear is the transfer of material between solid surfaces during relative friction motion and adhesive interactions between rubbing surfaces

(Best, 1986). Abrasive wear is the material loss caused by hard tool joint protuberances (two body abrasion) or by hard particles (three-body abrasion). It is characterised as a series of grooves on softer surface caused by hard surface or hard particles. Adhesive and abrasive wear may coexist in downhole casing wear. The adhesive wear takes a leading mechanism under high contact pressure between tool joint and casing. The abrasive wear is dominant when drilling mud contains high content of hard weighting agent or cutting.

Other failures that could manifest are either that of casing connections and/or auxiliary equipment such as wellhead etc during the producing life of the well. Each of these has specific effect on the well integrity as a whole. Sathuvalli and Suryanarayana (2016) and Aasen et al. (2003) both examined the relationship between structural casing and formation effects on wellhead motion due to temperature loads and resulting casing deformation. The studies established that casing deformation cause noticeable movement of the wellhead. As such, they developed a semi-analytical model that can be applicable to study various wellhead loading situations that can potentially cause motion in the upward direction. In contrast, Awe et al. (2015) and Jellison and Brock (1998) identified connection failure, local buckling and shear failure as the main types of failures on casing strings.

2.7 Conventional Casing pipe material selection

The development of shale gas, oil and gas reservoirs has been pushing the limits of casing materials in recent times resulting in casing deformations. Hausler et al. (2017) pointed out that the performance of tubular hardware (tubing and casing) depends on tubes properties, existing and applied stresses and the environment in

which the tube is operating. Selecting safe and economical materials for unconventional wells is challenging. Materials (pipes) that could withstand the harsh downhole condition are generally of higher strength capacity and thicker geometries, but expensive compared to inexpensive lower strength capacity materials. Besides, Kaldal et al. (2015) indicated that substantial temperature changes pose many design challenges in a diverse range of structures – including casing in oil and gas wells. For example, Yang et al. (2018) pointed out that the yielding strength of N80 and P110 casing grades decreases with the increase in temperature. Specifically, below 350 °C, both N80 and P110 meet the API requirement on yielding strength. However, when the temperature is above 450 °C, neither N80 nor P110 casing strengths' meets the API specification.

Although the API standards guidelines such as API Spec 5CT, API Spec 5C2 and 5C3 have proved to be good reference materials for casing material properties, tests protocols and minimum design calculations for conventional oil and gas wells. The challenge however pose by unconventional wells are numerous and entirely different from conventional wells (Mohammed et al. 2020). The study of Gouveia et al. (2020) on the current search for oil and gas show that the casing is being increasingly exposed to higher depths, extreme pressure and temperatures in (HPHT), deep-water, shale gas and tight oil and gas reservoirs (Unconventional reservoirs). In addition, these wells have long been identified to posed different kinds of challenges raging from material selection, design, drilling and completion to abandonment (Lihong et al. 2013; Wang et al. 2014; Mohammed et al. 2019). Depending on the well type and the circumstance, striking a balance between cost and safety is an essential consideration for casing grades selection, design,

installation and subsequent operations in oil and gas wells. The selection and design of casing for shale gas application is an essential aspect of the well construction process in order to ensure well integrity and safeguard the environment during such process.

The standard procedure is to select and design these casings using either API or propriety grades(non-API) and apply safety margin based on anticipated downhole condition. This procedure is adequate for conventional wells that do not threatening the integrity of the casing pipes. On the other hand, unconventional wells such as shale gas – this procedure may not be adequate.

For example, Marbun et al. (2020) established that production casing of well HCE29 failed in Dieng Field, Indonesia, after the well was drilled and completed. The well which is an unconventional is characterised by a water-dominated geothermal system with temperature of up to 330°C and pressure of up to 19.4 MPa. In a separate study on pitting corrosion, Yan et al. (2019) found out that two pits in circumferential direction on the casing are more likely to cause failure than the double pits located along the axial direction on the casing. Also, the study of Correa et al. (2020) suggests the use of the failure assessment diagram (FAD) tool to prove the structural integrity of riser pipes is essential for the evaluation of crack and determining the critical crack size and its likely failure method for application in deep-water. These are very few examples indicating the need for a more methodical approach to unconventional wells. However, one key aspect that is essential and is still a gab in the literature; is the use of CES Granta selector to select alternative casing materials using performance indices for oil and gas wells. Materials selected

using this method for casing application are further evaluated and rank using TOPSIS, AHP and the Non-weighted methods.

2.7.1 Materials selection Challenge for Unconventional Wells Application

Exploration and production for oil and gas resources is now venturing into difficult terrain which lead to drilling higher depths, extreme pressure and temperatures in (HPHT), deep-water, shale gas and tight oil and gas reservoirs. These difficult terrains are often associated with high stresses resulting from pressure, temperature and induced hydraulic energy during shale gas development that negatively impact casing (Gouveia et al. 2020; Çasliskan et al.2013). Furthermore, wells that possessed these kinds of characteristics are identified to present challenges ranging from material selection, drilling completion/stimulation to abandonment (Lihong et al. 2013; Wang et al. 2014; Mohammed et al. 2019). However, depending on the well type and the downhole condition, establishing a balance between cost and safety is a critical consideration for casing grades selection, design, installation and consequent operations in oil and gas wells. Moreover, the selection and design of casing for shale gas application is an essential aspect of the well construction process in order to ensure well integrity and safeguard the environment during such process.

Statistics and analysis of articles reviewed in this research revealed that the development of shale gas, oil and gas reservoirs often utilised P110 and Q125 API casing grades. Refer to Figure 2.1 for additional evidence on this. The application and the resulting performance of these materials is based on the pipes mechanical properties and the loading conditions present in that scenario (Hausler et al. 2017). In unconventional like shale gas horizontal wells, the selection of inexpensive

materials for casing that will ensure safe wellbore is challenging. This is because the pipes that could endure extreme downhole stresses are usually of higher strength and thickness but expensive than the inexpensive ones.

The study of Kaldal et al. (2015) showed that significant temperature changes can present difficulty in designs – including casing pipe in oil and gas wells. Although, extreme temperatures (greater than 300°C) are rarity in oil and gas wells, but recent study by Yang et al. (2018) established that the yield strength of N80 and P110 casing grade both meet the strength requirement at temperatures below 350°C. However, beyond this temperature, both N80 and P110 do not meet the API strengths specification. In addition, this extreme temperature is not commonly encountered in oil and gas wells, however geothermal wells exhibit elevated bottom hole temperature ranging from (232–399 °C) or 450 to 750 °F (Smithson 2016).

While API Specification 5CT, API Spec 5C2 and 5C3 have proved to be good reference materials for casing material geometrical and mechanical properties as well as establishing test guidelines and design calculations for conventional wells (Hay and Belczewski 2003). However, on the other hand unconventional such as shale gas well has been established to exhibit different characteristic during development (Mohammed et al. 2020). An example of this characteristic is slip displacement resulting after a stage stimulation. Therefore, this new challenge requires a new guideline and a pragmatic solution.

The standard procedure for casing design usually begins with casing grade selection (API and non-API) based on available materials and anticipated stresses in the downhole conditions. The materials selected are further screen to select the best by applying safety margin. The material whose strength meet this safety margin is

selected and applied in the well being constructed. This procedure is acceptable for conventional wells that do not threaten the integrity of the casing pipes. On the other hand, unconventional wells such as shale gas – this procedure may not be adequate due to induce stress during multi- stage hydraulic fracturing in shale gas well for example.

The new case of geothermal well casing failure in Indonesia is another example where the well was drilled and completed, but the production casing failed in a water dominated geothermal system with a temperature of 330°C and pressure of 19.4 MPa (Marbun et al. 2020). Although the specific cause of the casing failure has not been clearly explained in the study, but poor material choice and harsh downhole conditions of Dieng geothermal field may be behind the casing failure. Corrosion studies by Yan et al. (2019) showed that two pits of pitting corrosion in the circumferential direction in the casing have higher potential to cause casing failure than double pits in the axial direction the casing assuming the same distance between the pits. In addition, the study of Correa et al. (2020) demonstrated the use of the failure assessment diagram (FAD) tool to prove the structural integrity of riser pipes is essential for the assessment of crack and determining the critical crack size and its likely failure method for application in deep-water. While this procedure for establishing the critical crack size is crucial, one will argue that material selection for riser pipe is an integral part of the riser design as it concerns weight, water depth, flexibility etc.

These examples describe the challenges associated with material selection in different situations and in specific scenarios. However, a meticulous and methodical approach to unconventional wells is paramount in view of these examples and the

limitations of the present procedure. As the industry grapple with unconventional well development, it is essential to examine the potentials of huge collection and robust ANSYS Garnta selector CES database for an alternative casing material for oil and gas application. This can be accomplished using performance indices based on scenario for oil and gas wells. Materials selected using this method for casing application are further evaluated using finite element modelling to predict its structural response in a shale gas well scenario. Similar strategy of predicting defects and materials response to applied loads and/or stress are covered by (Ferro and Bonollo 2019; Fazekas, and Goda, 2020, Liu et al. 2016; Feng et al. 2019).

The driving force for material selection generally are performance's improvement and cost minimisation. However, criteria such as critical loads and weight reduction are also strong motivations for proper material selection. For example, in the aerospace industries weight reduction is one of the foremost targets for design enhancements. Conversely, in oil and gas wells strength and stiffness may be the main objectives in selecting casing and tubing pipes in order to ensure well integrity. Kumar et al. (2014) pointed out that inappropriate material selection may lead to requirement of customers and manufacturers not being satisfied. Poor selection of materials can cause premature failure of an assembly and reduction in product performance, thus efficiency and profitability affected adversely and organisation reputation damaged (Kabir et al. 2014; MATSUMOTO, K. et al., 2018). In order to solve the problem of material selection, different technique have been applied in the literature and one of the popular methods that have been applied is the MCDM method. Some of the popular MCDM tools that have been applied in the literature for material analysis are AHP, VIKOR, ELECTRE, and TOPSIS.

As established above, there are many multi-criteria decision-making process for material selection. However, this study examined Ashby bubble chart method to select alternative material for casing based on key pertinent parameters for the first time in the literature. The shortlisted materials from Ashby method are further rank and compared based on material properties and anticipated loading on casing during shale gas well stimulation using TOPSIS, AHP and non-weighted method.

Multi-criterion Decision-Making (MCDM) methods are applied in selecting an optimum decision in circumstance that has to do with multiple alternatives having multi-conflicting and non-commensurable decision criteria. The MCDM is a recognised tool for solving complex engineering problems due to their inherent ability to judge diverse alternatives with reference to various decision criteria in order to choose to best alternative (Emovon and Oghenenyerovwho 2020). Technique for Order Preference by Similarity to Ideal Solution (TOPSIS), VIKOR, Analytic Hierarchy Process (AHP), PROMETHE, Weighted Sum Model (WSM), Weighted product model (WPM), ELECTRE, and Multi-Attribute Utility Analysis (MAUA) are amongst the popular MCDM techniques that are commonly utilised for solving decision problem.

The tradition in the industry is to select these casings from available grades or place an order to manufacturers with certain specifications in order to meet the anticipated downhole conditions. This traditional approach is very much dependent on experience as well as constructing oil and gas wells at minimum budget. However, due to increase complexity experienced in development of unconventional wells like HPHT wells that are associated with significant amount of acid gases; Sumitomo alloys selection chart was developed to cope with the selection challenge.

This chart is based on calculating the partial pressures and the chloride content on a limited casing grade. Additionally, Millet et al. (2020) developed a simplified selection chart for Super Martensitic Stainless-Steel Solution for High CO₂/H₂S Environment based on partial pressures and temperature.

As it can be seen on Figure 2.5 the selection is limited to few steel alloys and partial pressures of hydrogen sulphide and carbon dioxide and cannot be applied in wide range of scenarios like shale gas wells and deep-water wells. Also, in situations where there is inter-relationship and dependencies between the attributes to a particular objective, both Sumitomo and the simplified material selection chart cannot give the desired result/outcome.

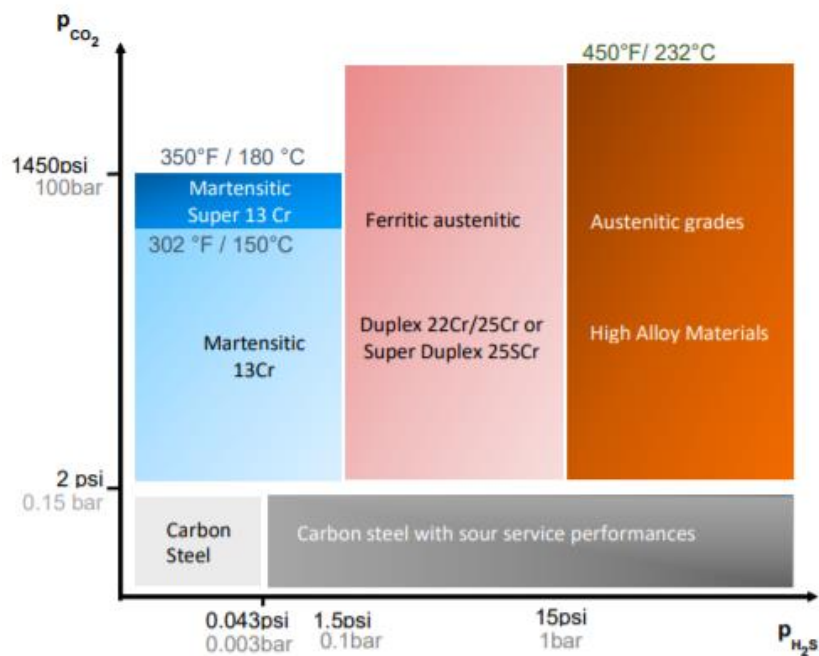


Figure 2.5 Simplified material selection chart (Millet et al. 2020).

Therefore, using advanced level 3 aerospace CES EduPack database with rich physical, chemical and mechanical properties as well as the capability of manipulating materials' performance indices numerical evaluations can resolve the challenge of material selection for unconventional wells.

The materials and processes data-tables lie at the heart of the database. The first contains records for the properties of structural, functional, and biological materials (Figure 2.6). The second gives access to records for shaping, joining and finishing processes, with schematics and images of processes.

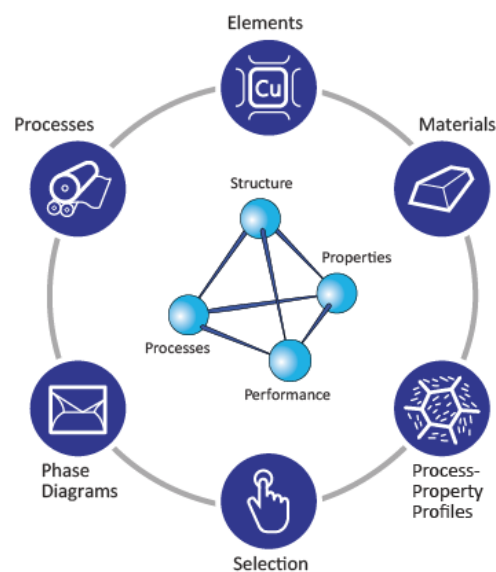


Figure 2.6 Data-structure of the CES EduPack for Material Science and Engineering database (Ashby, et al. 2018).

The elements data-table contains records for the basic properties of the elements of the Periodic Table; they are linked, where appropriate, to records in the other tables giving one-click access to relevant fundamental atomic properties. The Phase Diagrams data-table contains the most-used phase diagrams and an interactive tool

to illustrate how to interpret them. The Process-Property Profiles data-table allows the effect of processing on properties to be explored and the associated Structure and Mechanism. Notes give insight into structural changes that are used to manipulate properties. This makes the CES a preferred choice for material science and engineering across many fields of study since it establishes relationship between processing, structure, properties and performance as shown on Figure 3.3 (Ashby et al. 2018). Depending on the scenario material selection can significantly affect buckling phenomena.

2.7.2 Material Selection and Verification of Selected Material Response

In certain circumstances and situations, the material selection for engineering designs involves evaluating the materials' functional requirements, relevant materials' properties and materials performance under such situations. The study of Liao et al. (2015) pointed out that the material selection is a key aspect in engineering design which often involves the designer (Engineer) applying his knowledge and experience in deciding which material to select. However, the evaluation of the materials performance based on its physical, chemical, mechanical and functional requirement lead to the challenge of multi-objective, or multi-attribute optimisation (Fazekas and Goda 2020). This challenge is further increase when there are conflicting criteria, such as low cost and high performance with additional constraints.

Material selection is a difficult task due to complex inter- relationship amongst various conflicting decision criteria for selecting alternatives (Kumar et al. 2014). The main objective or goal in many material selections are based on performance's enhancement and reducing cost but criteria such as failure and weight reduction

are also strong variables for proper material selection depending on the situation (Li et al. 2020, Chen et al. 2013). For example, in the aerospace industries weight reduction is one of the leading targets for design enhancements and optimisations. On the other hand, in oil and gas wells casing, the main driver may be strength for ensuring well safety and integrity over the entire life cycle of the well. The study of Rubio-Aliaga et al. (2020) on optimal groundwater pumping solutions based on a variety of energy resources and water storage options are assessed and classified using AHP and TOPSIS. In a different study, Li et al. (2020) applied fuzzy decision-making trial and evaluation laboratory (FDEMATEL), entropy weighting to assign weights to the objectives and VIKOR to rank the optional alternatives for machine tool selection.

In resolving material selection problems, different methods are established in the literature each with its strength and weakness. One popular method that is often applied in material selection is the MCDM. This method provides a means of ranking multicriteria decision making method for material selection using different approaches. However, advances in material selection over the last three decades has led to developments new MCDM methods such as Weighted Sum Model (WSM), Weighted product model (WPM), Technique for Order Preference by Similarity to Ideal Solution (TOPSIS), PROMETHEE, VIKOR, ELECTRE, and Multi-Attribute Utility Analysis (MAUA) as noted by (Emovon and Oghenenyerovwho 2020). Using any of the mention approaches, simultaneous evaluation of the multiple criteria is accomplished to subjectively obtained the most appropriate decision/or selection from the range of alternatives (Csiszar et al. 2020; Kabir and Sadiq 2014).

In determining the best materials for specific application different techniques are established from previous studies in the literature each with its merit and demerits. The multicriteria decision making (MCDM) is common and popular method that is often applied in material selection. The MCDM methods provide a way of ranking available options for material selection using different approaches. However, advancements in material selection over the last three decades has led to developments of new MCDM methods such as Weighted Sum Model (WSM), Weighted product model (WPM), Technique for Order Preference by Similarity to Ideal Solution (TOPSIS), VIKOR, PROMETHEE, ELECTRE, and Multi-Attribute Utility Analysis (MAUA) as noted by (Emovon and Oghenenyero who 2020). Using any of the mention approaches, simultaneous evaluation of the multiple criteria is accomplished to subjectively obtained the most appropriate decision/or selection from the range of alternatives (Kabir and Sadiq 2014).

After an initial selection of materials for application in a particular engineering project/design, it is a common practice to further scrutinise these materials to establish performance, relationship among key variables. However, in the process of applying limits and constrains which involves rigorous examination of the material functional requirements, physical and mechanical properties to select the best material. This procedure provides the overall best material using any of the multicriteria decision making process (MCDM) based-on performance ranking. The material selection is a major aspect of engineering design, but selection using most of the MCDM methods is often subjective. The subjectivity arises in assigning weight based on knowledge and experience of the Engineer to favour a particular material (Liao 2015).

The study of Kumar et al. (2014) pointed out that material selection is a challenging task owing to intricate inter- relationship amongst designs variables. Although, different engineering design have different objectives/goals to material selection. However, many engineering designs for materials selection is usually based on performance improvement and/or reducing cost. For example, criteria such as failure and weight reduction can be strong variables in many engineering designs and/or considerations (Emovon and Oghenenyero 2020). For instance, in the design of aeroplanes, a key parameter for performance enhancements is reducing the weight, while casing pipe for oil well application, the leading factor/criteria may be the strength that will ensure safety and integrity over the entire lifecycle of the well. Using AHP and TOPSIS, the study of Rubio-Aliga et al. (2020) assessed optimal choice of water/energy requirement for an irrigation project in Spain. Meanwhile, Li et al. (2020) applied fuzzy decision- making trial and evaluation laboratory (FDEMATEL), entropy weighting to assign weights to the objectives and VIKOR to rank the optional alternatives materials for machine tool selection.

Therefore, in order to meet designs considerations and/ or customer specifications a robust material selection must incorporates all material properties that are pertinent to the design objective (Chen et al. 2013). On the other hand, unsuitable material selection can lead to dissatisfaction of the customer specification or premature failure of an assembly and reduction in product performance, resulting in reduced efficiency and profitability. Additionally, depending on the design and the impact of material failure in design; the effect can adversely damage organisation reputation (Kumar et al. 2014). However, having carried the selection and suitable alternative to the P110 casing grade identified. The evaluation of the

alternatives using numerical simulation to determine structural responses is vital in order to ascertain these materials with P110 and Q125 to prove their effectiveness using data mining and in particular exploratory data analysis for stress distribution and correlations between variables (Mohammed et al. 2021).

Inappropriate material selection and design may lead to not meeting certain conditions of customers and manufacturers (Karande et al. 2012). The improper selection and design can also lead to premature failure of an assembly and reduction in product performance, resulting in reduced efficiency and profitability. Additionally, depending on the severity, the effect can adversely damage organisation reputation as indicated by (Kumar et al. 2014). However, having carried the selection and suitable alternative identified. It is essential to evaluate the structural responses of these alternatives from the reference P110 casing material. Doing this will further establish the potentials of these alternative materials; eliminate doubts and justify the selection from the structural point of view. Based on this argument therefore, the numerical evaluation of the P110 and the alternatives are individually carried out in ANSYS.

2.8 Horizontal Wells Drilling and Hydraulic Fracturing Associated Loads

Horizontal wells and hydraulic fracturing are key technologies that are commonly employed to develop shale gas and low permeability oil and gas reservoirs in recent years. However, numerous challenges prevent efficient drilling, completing and stimulating these wells as planned. For example, drill-cuttings accumulation increases with increase in wellbore inclination as established by (Busahmin et al., 2017). Shale gas and tight oil reservoirs exhibit very low permeability justifying the

need for multi-stage stimulation to increase recoveries of oil and gas through hydraulic fracturing. Another feature of shale gas horizontal well is the very long lateral section. This characteristic of the well prevent efficient deployment of casing in the lateral due to gravity, ledges and tight hole particularly in shale reservoirs. In the process of hydraulic fracturing, the production casing is subjected to high internal pressure as noted by (Yan et al., 2017). Excessive stimulated segments and big pumping delivery rate during the volume fracturing process, complicate casing's mechanical behaviour which results in shear failure, leap and slip, around the horizontal section and change in in-situ stress field due to both drilling and stimulation (Chipperfield, 2007; Yin et al., 2018a; Lian et al., 2015). Consequently, the planned multi-stage stimulation cannot be completed as expected (Tang et al., 2013; Yu et al., 2016; Brantley et al., 2014). Xing et al. (2017) established that shale gas horizontal wells suffered casing deformation because of complex stresses downhole during fracturing operations.

Moreover, Lian et al. (2015) indicated that stress deficit and clustering perforations made horizontal well deformed radially and 'S'-shaped deformation axially. Similarly, both Xi et al. (2017) and Wang et al. (2018) indicated that when a weak plane is activated in shale reservoirs, such activation and bedding caused casing shear deformation. Another reason for casing deformation was proposed by Haghshenas et al. (2017) and Liu et al. (2017) who noted that additional load is exerted on the casing by fracture slip through the wellbore. Liu et al. (2018) pointed out that local stresses and shear of weak formation are the main causes of casing deformation during fracturing. These local stresses are typically tangential, axial and radial resulting from in situ stresses. Depending on the degree of rock

consolidation and the formation characteristics wellbore stability problems issues can develop during fracturing operations.

For example, Yin et al. (2018a), revealed that shear deformation of casing was due to slip of shear fractures in shale gas reservoirs, based on curvature screening criteria. This study further revealed that slip displacement led to large transverse displacement and stress concentration points on the casing. In a different study, Yu et al. (2016) examined the effect of hydraulic fracturing on reservoir deformation and concluded that fractures caused casing and subsurface deformations. The study by Chen et al. (2017) identified fracture and bedding as the main internal factors responsible for casing deformation during hydraulic fracturing. Besides, when the casing is not properly centralised potential buckle points could manifest in the lateral section of the horizontal well (Mainguy and Innes, 2018). In summary, many factors are attributing to casing failure during hydraulic fracturing, resulting in different casing failure modes are being studied and documented in the literature (Yin et al., 2018b, Zhaowei et al., 2017; Li et al., 2012; Abou-Sayed and Zaki, 2005). Nonetheless, another aspect that is presently receiving attention is multiple casing deformation points on lateral section of the well during fracturing as established by Xi et al. (2018) and Yan et al. (2017).

2.9 Casing Buckling and Mitigation Strategies

Recent technological advancement of hydraulic fracturing and horizontal wells drilling is enabling the exploitation of shales, tight oil and gas resources. Nonetheless, in the process of shale oil and gas extraction (stimulation), both natural and hydraulic fractures exert a shearing load on steel casing leading to its

buckling failure (Jacobs 2020; Guo et al. 2018). Depending on the severity of the shearing load exerted on the casing, there are situations in which access into the well becomes difficult owing to deformations leading to delays in drilling out bridge plugs (Xing et al. 2017; Lian et al. 2017). In addition, in extreme situations, substantial section of the lateral may be lost – resulting in non-stimulation of the other stages of the well as planned. However, it is established that circumstances around casing buckling is tricky even in the same field it can be an intra-well phenomenon that do not have a single leading factor (Jacobs 2020).

The main factors responsible for casing buckling and deformation phenomena are being argued and debated in the literature from shale gas fields around the world. The study of Xi et al. (2019) argued that fault slip displacement during shale gas well stimulation is responsible for casing shear failure. Furthermore, Wang et al. (2018) and Xi et al. (2018) both pointed out that hydraulic fractures activate natural fractures which lead to shear buckling of the casing during fracturing operations. In contrast, Carpenter (2019) based the casing buckling on substandard cementing in Granite Wash Play – Western Anadarko Basin.

Also, the study of Lin et al. (2016) established that shale rocks strength in Longmaxi Formations reduced most at an angle of 45° and further reduces with increase in fracturing stages along the lateral section of the well. This results in lack of access into the well and significantly affect both the well and casing integrity. Casing mechanical behaviour is affected by combined effect of thermal stress and fracturing pressure as noted by Xi et al. (2018). While Haghshenas et al. (2017) and Liu et al. (2017) adjudged fracture slip displacement and activation of weak

bedding plane during hydraulic fracturing to be the factors causing casing deformation.

However, Yin et al. (2018) and Mohammed et al. (2020) studies on casing deformation revealed creep load to increase casing displacement and stress during shale gas well stimulation. According to the study of Yu et al. (2019) axial deformation of the casing is caused by overlap in adjacent stages which increase the shear load on the casing leading to its 'S' shape failure. Also, Lian et al (2015) and Wang et al. (2016) indicated that the variations in in-situ stresses during fracturing process are responsible for casing buckling. However, a review study on casing buckling pointed out that induce stress in stimulation process, in-situ stress variation, slip and shear stress lead to different kinds of casing failures (Mohammed et al. 2019).

Conversely, different solutions are being proposed by engineers and researchers in the field in order to mitigate this challenge of casing buckling phenomena. The study of Guo et al. (2018) proposed avoiding fractures and faults during stimulation can prevent casing buckling. In addition, this study further pointed out that utilising a casing with high flexural strength and employing cement whose elastic modulus is less 10GPa can substantially reduce casing buckling tendencies in shale gas wells (Guo et al. 2018). However, Yin et al. (2018) argued that increasing the casings' flexural strength do not eliminate casing buckling. However, low slip angle and cement whose elastic modulus is low, is sufficient to reduce casing deformational failure (Guo et al. 2018; Xi et al., 2017; Yan et al., 2019). In addition, Yan et al. (2019) shows that reducing the pump pressure in the process of hydraulic fracturing can ensure casing integrity in shale gas wells. Furthermore, according to Lian et al.

(2015) and Lin et al. (2017) propositions, casing buckling can be resolved by ensuring significant spacing between stages during shale well stimulation.

Advances in horizontal well drilling and hydraulic fracturing is now enabling the extraction of shale gas and oil in commercial quantities. However, during shale gas fracturing process (stimulation), the interaction of hydraulic fractures and rock formation is buckling and even shearing the steel casing leading to lack of access into the well and expensive rig time in drilling out bridge plugs in the process (Jacobs 2020; Guo et al. 2018; Xing et al. 2017; Lian et al. 2017). In more severe cases, this can lead to complete loss of access to the lateral section of the wells. The casing failure under this circumstance is an intra-well phenomenon that can take several forms and has no universal driver.

The literature has documented some of the major reasons attributed to the casing buckling and deformation phenomena based on field experience from notable shale gas provinces. For example, in China - Xi et al. (2019) pointed out that fault slippage in multistage fracturing caused casing shear failure. Also, according to Xi et al. (2018) and Wang et al. (2018) fracturing activates pre-existing fractures that lead to casing shear buckling. Analysis of casing failures in the Granite Wash play in the western Anadarko Basin also identified poor cementing to be responsible for casing buckling (Carpenter 2019).

However, Lin et al. (2017) established that rock mechanical strength reduces most in Longmaxi Formations at a slip angle of 45° and continue to be de-stabilise with increase in number of stimulated stages along the lateral section of the wells. As a result, the casing structural integrity is compromise which translate to lack of access into the wells to drill-out bridge plugs and recompletions. The casing stresses are

further amplified due to thermal and pressure in volume fracturing of shale gas wells (Xi et al. 2018). In addition, Haghshenas et al. (2017) and Liu et al. (2017) pointed out that casing deformation is due to imposed additional load by fracture slip and weak bedding plane through the wellbore in the process of hydraulic fracturing. The studies of Mohammed et al. (2020) and Yin et al. (2018) show that creep load (slippage) lead to an increase of transverse displacement and stresses on the casing.

According to Yu et al. (2019) overlapping, asymmetric stimulated zones in adjacent stages effectively increase the resultant shear force on the casing that may lead to its failure ("S" shaped deformations). Besides, Lian et al. (2015) and Wang (2016) attributed casing buckling to fluctuations in in- situ stresses as a result of fracturing pressure. Furthermore, Mohammed et al. (2019) review on casing failure pointed that the casings are subjected to material degradation due to perforations, varying local loads - in situ stresses, induced stresses due to stimulation, natural fracture activation and propagation, slip and shear during their installation and operation leading to different kinds of casing failure modes.

In contrast, different countermeasures are being proposed in the literature corresponding to specific scenarios to avoid casing failures. For example, simulation results on shale gas horizontal wells suggest avoiding natural fractures and nearby faults during shale gas stimulation can reduce casing failure (Guo et al. 2018). Furthermore, using cement with an elastic modulus smaller than 10GPa and higher casing grade can significantly reduce casing buckling phenomena in such wells (Guo et al. 2018).

In addition, Yin et al. (2018) investigated casing shear deformation induced by fracture slip during multistage hydraulic fracturing in a particular well in China. The study established that increasing casings' flexural strength does not prevent deformation. However, low slip angle and using cement with low elastic modulus is minimising the potentials of casing failure phenomenon (Guo et al. 2018; Yin et al., 2018; Xi et al., Yan et al., 2019). Meanwhile, Yan et al. (2019) suggested that reducing the fracturing pressure is sufficient to maintained casing integrity during stimulation process. The study of Lian et al. (2015) and Lin et al. (2017) indicated that the key to solving casing deformation and/or buckling is reasonable spacing in the design of multi- stage hydraulic fracturing.

2.10 Machine Learning

Historically, Arthur Samuel coined the term Machine Learning in the year 1959. He was a pioneer in Artificial Intelligence (AI) and computer gaming, and defined Machine Learning as "Field of study that gives computers the capability to learn without being explicitly programmed".

Machine learning is the use of a machine/computer to learn in analogy to how the brain learns and predicts. It combines statistics and computer science techniques and depends on a new class of learning algorithms that improve with time, as well as the availability of large datasets to train the systems.

In some cases, the methods are directly inspired by the way the brain works, as is the case with neural networks (Theodoridis, 2015). According to Mitchell (2006) machine learning is defined as a well modelled learning problem - where a computer programme learns from experience (E) with respect to some tasks (T) and some performance measure (P) if its performance on (T) as measured by (P) increase

with experience (E). Figure 7 presents schematic diagram of how the machine learning task is accomplished. As it can be seen on Figure 6, machine learning involves two distinct phases, namely the training and the inference or testing phase on a very basic level.

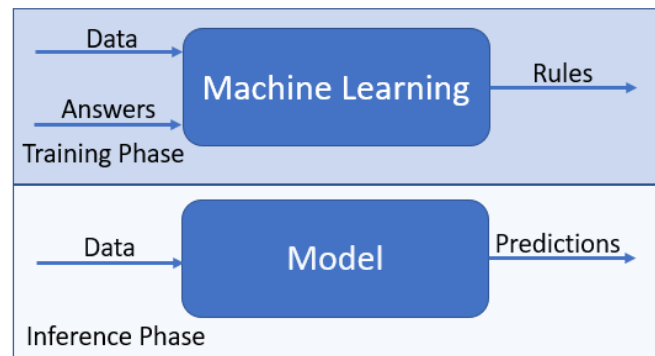


Figure 2.7 schematic diagram of machine learning task showing the distinct phases between training and testing phase (inference phase)

The first step in manipulating any machine learning task is the depiction of each pattern in the computer (Duda et al. 2012; Talebi et al. 2015; Bartlett and Cussens 2017). This is achieved during the pre-processing stage; where one has to “encode” related information that resides in the raw data in an efficient and information-rich way. This is usually done in a process called data transformation. The raw data in a new space with each pattern represented by a vector, $x \in R^l$. This is known as the feature vector, and its “l” elements are known as the features. In this way, each pattern becomes a single point in l-dimensional space, known as the feature space or the input space. This is referred to as feature generation stage.

Based on the training data, one then designs a function, f , which predicts the output label given an input. Once the model has been designed, the system is ready for predictions. Given an unknown pattern, we form the corresponding feature vector,

x , from the raw data, and we plug this value into the classifier; depending on the value of $f(x)$ (usually on the respective sign, $\hat{y} = \text{sgn } f(x)$) the pattern is classified in one of the two classes as shown on Figure 8(a).

Two problems at the heart of machine learning task are the classification and regression. The classifier has been designed in order to separate the training data into the two classes (Figure 8a), having on its positive side the points coming from one class and on its negative side those of the other. The 'red' point, whose class is unknown, is classified to the same class as the 'star' points, since it lies on the positive side of the classifier as shown. The goal in classification is to assign an unknown pattern to one out of a number of classes that are considered to be known. For example, in casing deformation, using known scenarios of casing deformations we can classify a new scenario as either deform or undeform (intact).

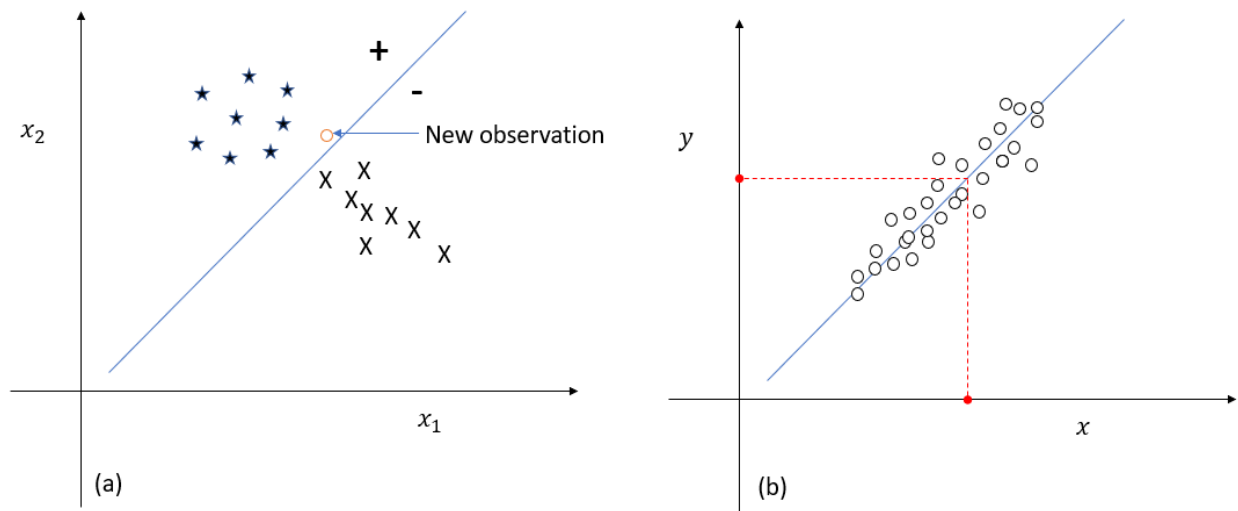


Figure 2.8: (a) classification (b) regression

Similarly, regression shares to a large extent the feature of classification at preprocessing stage, however, the output variable, y , is not discrete but it takes values in an interval in the real axis or in a region in the complex numbers plane. The regression task is basically a curve fitting problem (Duda et al. 2012). This is usually done by transforming the raw data in a new space with each pattern represented by a vector, $x \in R^l$. This is known as the feature vector, and its l elements are known as the features. In this way, each pattern becomes a single point in an l -dimensional space, known as the feature space or the input space. This is referred to as the feature generation stage. For a given a set of training points, $(y_n, x_n) \ y_n \in R, x_n \in R^l, n = 1, 2, \dots, N$, and the task is to estimate a function, f , whose graph fits the data. Once we have found such a function, when an unknown point arrives, we can predict its output value. This is shown in Figure 8b.

2.10.1 Data Mining Using “R”

Like any other machine learning tasks, the relevant libraries deployed in this study include caret, pRoc, mlbench and ggplots2. The classification and Regression Training (“caret”) package contains functions to streamline the model training process for complex regression and classification problems. The pROC package contains tools for visualising, smoothing and comparing receiver operating characteristic (ROC curves). The basic unit of the pROC package is the ‘ROC’ function. It will build a ROC curve, smooth it, if requested (if smooth=TRUE), compute the area under the curve AUC (if auc=TRUE), the confidence interval (CI) if requested (if ci=TRUE) and plot the curve if requested (if plot=TRUE). The mlbench library converts X (which is basically a list) to a data frame. Lastly, the

ggplot2 library initializes a ggplot object. It can be used to declare the input data frame for a graphic and to specify the set of plot aesthetics intended to be common throughout all subsequent layers unless specifically overridden.

The “K” Nearest Neighbour Method (KNN) is utilised in this study in that k-nearest neighbour classification for test set from training set looks at each row of the test set, using distances such as Euclidean or Manhattan. The training set vectors are found, and the classification is decided by majority vote, with ties broken at random. If there are ties for the kth nearest vector, all candidates are included in the vote.

On the other hand, the k nearest neighbour regression (knnreg) is utilised which returns the average values of the neighbours. The default value of k is 5, however this parameter has been modified to improve the regression analysis in order to arrive at the most accurate predictive model.

One of the most significant advantages of kNN is that it is relatively easy to implement and interpret (Duda et al. 2012., Theodoridis 2015). Also, with its approach to approximate complex global functions locally, it can be a powerful predictive model. The weaknesses are that kNN is very sensitive to the curse of dimensionality. This refers to scenarios with a fixed size of training examples but an increasing number of dimensions and range of feature values in each dimension in a high-dimensional feature space (Donoho et al. 2000). It can be expensive to compute with a $O(n)$ prediction step however, smart implementations and use of data structures such as “K” dimensional-trees and Ball-trees can make kNN substantially more efficient (Donoho et al. 2000; Duda et al., 2012). In general, compared to other machine learning algorithms, the kNN algorithm has relatively

few hyperparameters, namely k and the distance metric; however, the choice of an appropriate distance metric is not always obvious. This is because the performance of the KNN algorithm is dependent on the distance/similarity measure used (Prasatha et al., 2017).

2.10.2 Data Mining and Machine learning for critical deformations

The Lunar is an Artificial Intelligent (AI) software platform that utilised different solvers to perform real time parametric simulation interactively to make prediction and optimisation. Lunar uses past experiences (results – supervised learning) in order to predict new responses with ROM methods (Reduced Order Model method). In contrast, Quasar is a web-based machine learning software that is used for prediction and forecasting (Kayvantash 2019). This analysis in Lunar is carried out using the simplified workflow shown in Figure 9.

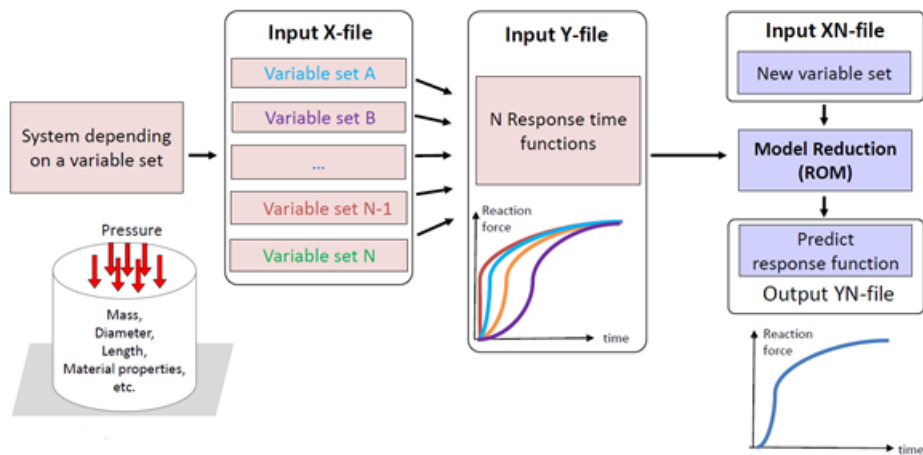


Figure 2.9 An Overview of Lunar Workflow (Source: CADLM 2019) showing system data bank, input variable (X, Y), and new variable XN.

2.11 Conclusion

The Data available from the literature have shown that there is an increasing cases of casing failure during shale gas development process. However, well integrity as

whole is comparatively new in relation to drilling, completion, production and health safety and environment (HSE). It is anticipated that well integrity will therefore see both quantitative and qualitative step changes in technology and procedure in short and long term (Brechan et al., 2018).

The casing integrity is reviewed for a range of well types and operating conditions. Factors that undermine casing robustness and their effect on well integrity failure are presented. It is noted that these factors can cause casing failure and lead to accident, negative financial implications, loss of asset and damage to environment. In particular, the severity and magnitude of casing failure depend hugely on wellbore environment (material, pressure, temperature, fluid content, time) and the type of well. The induced stresses due to stimulation tend to promote casing failure more than in-situ geo-mechanical stresses.

This study found that Q125 and P110 casing grades are mainly employed in high pressure high temperature wells (HPTHT wells), shale gas wells, injection wells and deep-water oil and gas wells. This is due to the characteristic of these wells requiring higher strength materials. Additionally, the review has examined both sources and causes of casings failures currently faced in the industry from drilling, completion production to abandonment. Recent advances in materials, material selection, and casing buckling mitigation strategy are studied and presented. Future opportunities that exist around twinning – a digital twin is a virtual representation that serves as the real-time digital counterpart of a physical object or process. Additionally, numerical modelling and machine learning algorithms can assist to predict quantitative effect of geometry and material selection for casing structural integrity at the design phase. Also, development of accurate predictive models that will

predict casing failure based on historical data and/or experiment will further provide potential next step in tackling casing failure in oil and gas wells.

In the literature, different causes of casing failure have been identified (Chen et al. 2018, Lian et al. 2015, Liu et al. 2017, Xi et al. 2018, Lin et al. 2016, Liu et al. 2016, Yin et al. 2018, Zhang et al. 2017). However, casing lateral buckling as a function of time, geometry, pressure and temperature as well as the critical buckling load has not been studied. Additionally, no effort was made at detecting such critical loads and potential buckle failures on the casing in the horizontal wells.

The gap in knowledge is, however, few of the published articles used 'FEA' to study casing deformation in shale gas horizontal wells, have either oversimplified the physical model, or do not consider important factors such as temperature and pressure combined effect on casing deformation. In addition, many do not consider effect of combined slip displacement, geometry, pressure and temperature over time on the casing buckling resistance under the combined influence of cement and formation coupling. Furthermore, most of the articles reviewed looked at the factors responsible for casing failure independently and drawing a conclusion. Therefore, one could argue that; most of these failures take place under the combined influence of more than one factor at a time. Hence, on this basis, the results presented, and conclusions are unsatisfactory justifying further research.

In view of the foregoing; robust simulation approach will no doubt; if coupled with realistic assumptions and verification establish the failure mechanism and be able to determine and relate the effect of each factor on casing structural integrity. Therefore, this study examined the role of each factor individually and in

combination to distinguish the magnitude of each factor, underlying principles as well as cases under combined loading conditions.

Chapter 3: Casing pipe material selection for Shale gas wells application Using ANSYS Granta CES and multicriteria decision making (MCDM)

3.1 Introduction

The conventional method of casing selection is based on availability and/or order placement to manufacturers based on certain design specifications to meet the anticipated downhole conditions. This traditional approach is very much dependent on experience as well as constructing oil and gas wells at minimum budget. However, this material selection approach is very limited in meeting the requirement of shale gas wells. As a result, this chapter derived, utilises the material performance indices and ANSYS Granta database to examine three different casing pipe buckling scenarios including the buckling with corrosion potentials and buckling with impact and long-term service temperature conditions.

In addition, having obtained the expert shortlist of potential casing materials, further analysis and ranking is carried out using, TOPSIS, AHP, and Non-Weighted methods to examines multiple conflicting criteria for casing selection and application in oil and gas wells for the first time. In particular, shale gas wells with buckling tendencies, corrosion and impact potentials resulting from rock shear as well as long term service temperature constrains are investigated. The factors examined are Young's modulus, yield strength, density, cost, elongation, buckling load, corrosion, service temperature and suitability to application in sour oil and gas wells. This chapter study and compare the performance of both API and propriety grades with the alternative materials in CES database to establish a balance between cost and safety levels to be reached in a typical well scenario. Doing this will assist the

designer (Engineer) to justify the selection of casing safely and technically for unconventional wells. The significance of this new method is added advantage in terms of integrating materials' physicochemical, thermal and mechanical properties and the casing functional performance to establish ideal selection within the design space or requirements.

3.2 Methodology

Using advanced level 3 aerospace database in CES Granta selector, Ashby plot (bubble diagram) are employed for casing material selection with emphasis given to shale gas wells casing performance indices. Figure 3.1 present high-level overview of the selection process as implemented in this study. As it can be seen on Figure 3.1, the preparatory stage involves defining the main objective(s) followed by distinguishing the key factors or requirement to meet a particular design. As soon as the driving parameters are identified, the performance indices are derived using relevant equations. The selection process is basically plotting the performance indices on a XY plot using the advanced plotting techniques in CES. This is followed by applying constraints and limits to further refine the initial selection. Depending on the situation, an alternative material or best material choice may be obtained at the end of this stage. If, there is need for further screening or evaluation then, further screening can be carried out using TOPSIS, AHP, Finite element analysis FEA to make the final decision/selection as shown on Figure 3.1.

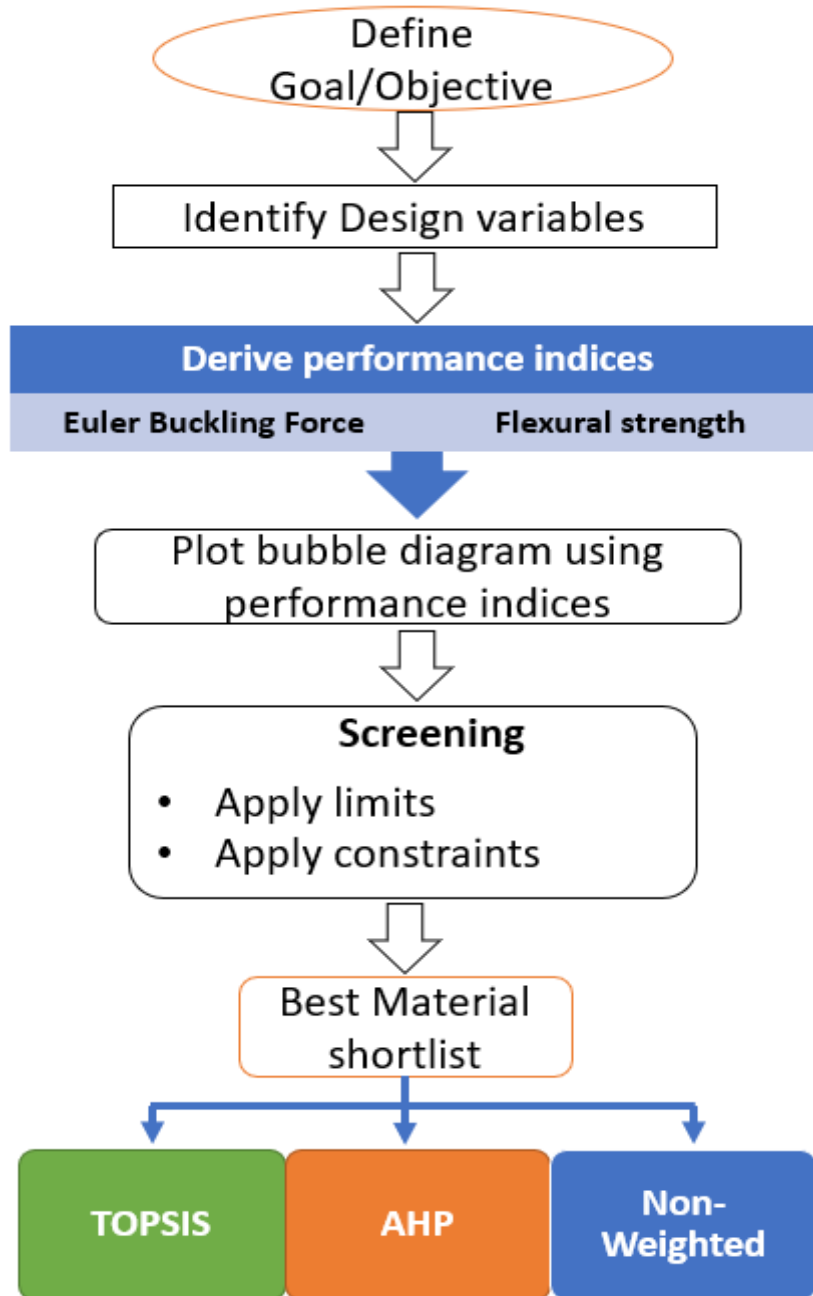


Figure 3.1: An overview of casing material selection process for shale gas wells using CES Edupack and MCDM

Where, TOPSIS stands for Technique for order performance by similarity to ideal solution while AHP stands for Analytical Hierarchy process.

3.2.1 Ashby Chart Method

Ashby M. F. in 1992, invented the technique based on ratio to develop a means of assessing the performance of alternative materials between material properties (Chen et al. 2013; Emovon and Oghenenyerovwho 2020; Ferro and Bonollo 2019). This ratio translates to bubble diagram for initial screening between the available materials based on their properties. The best candidate (material) is the one with the highest performance index. This approach is very effective for the initial screening process of materials based on the performance index developed to suits a particular requirement. It also enjoys the advantage of robust database from which the screening is made, as well as the relative comparison with another potential candidates.

The main requirement for the casing is to ensure well integrity throughout the well producing life. However, in unconventional wells such as shale gas wells where hydraulic fractures induce casing buckling and deformations during stimulation, stiffness and strength becomes a major requirement in the selection and design of the casing. In addition, high buckling load, low cost, and low-density material will be identified amongst key design variables to meet this requirement.

Based on these variables, the performance indices are derive using flexural strength and Euler buckling equations. The constant terms are separated from the indices in each case. Using the CES Edupack level 3 database, the entire material family is plotted and subsequent screening – that involves applying limits and constraints is accomplished to obtain the best performing candidates. The three scenarios investigated using this database are the shale gas with buckling tendencies. The first scenario investigates casing buckling owing to external load during shale gas

well stimulation. The second scenario considered casing buckling with emphasis on corrosion resistant materials. The third scenario is based on service temperature and impact to the casing. As such material with higher service temperature and fracture toughness are selected.

3.2.2 Performance indices

Using the Ashby method, this section developed the performance indices that will enable the selection of relevant material from the CES – EDUPACK database. For the casing that experience bending stress (external load) as a result of induce stress during shale gas well stimulation. Equation (3.1) is utilised to derive the performance index assuming the flexural load on the casing to act as in simply supported beam.

$$\sigma_f = \frac{my}{I} \quad 3.1$$

Where:

σ_f = flexural strength

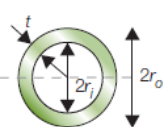
y = displacement measure from the neutral axis of the beam

I = Moment of area of the hollow pipe

m = internal bending moment of the pipe neutral axis

The second moment of area I , measures the resistance of the section to bending about a horizontal axis.

Table 3.1 Presents cross -section of a hollow cylinder (pipe) with corresponding moments.

Section Shape	Area A m^2	Moment I m^4	Moment K m^4	Moment Z m^3	Moment Z_p m^3
	$\pi(r_o^2 - r_i^2)$ $\approx 2\pi r t$	$\frac{\pi}{4}(r_o^4 - r_i^4)$ $\approx \pi r^3 t$	$\frac{\pi}{2}(r_o^4 - r_i^4)$ $\approx 2\pi r^3 t$	$\frac{\pi}{4r_o}(r_o^4 - r_i^4)$ $\approx \pi r^2 t$	$\frac{\pi}{3}(r_o^3 - r_i^3)$ $\approx \pi r^2 t$

The moment, K , measures the resistance of the section to twisting, and Z is the section modulus – which determines how strong a beam of a given cross section is. Z_p measures the resistance of the beam to fully plastic bending. The moment of inertia for a hollow pipe is $I = \frac{\pi}{4}(r_o^4 - r_i^4)$ as shown in Table 3.1. However, $r_o^4 - r_i^4 = t^4$ represent the thickness of the casing pipe. Implies $t = \left(\frac{4I}{\pi}\right)^{1/4}$. Again, the cross-sectional area of a hollow pipe $A = \pi(r_o^2 - r_i^2)$ as shown in Table 3.1.

For a minimum mass that will give the optimum flexural strength of certain cross-sectional area – the mass can be express in terms of area, length and density. Mass, $m = A.l.\rho$ substituting for A , I and t and simplifying leads to expression for optimum mass is obtained with the index term as shown in equation 3.2.

$$M = (4\pi m y l^2)^{1/2} \left(\frac{\rho}{\sigma_f^{1/2}} \right) \quad 3.2$$

On taking the reciprocal of the index term, we get

$$\left(\frac{\sigma_f^{1/2}}{\rho} \right) = \mathbf{M1} \quad 3.3$$

The flexural strength strictly only applies to brittle materials. For ductile materials, the flexural strength is the "effective" yield strength measured from the load at which a beam loaded in bending first becomes fully plastic, as in Figure 3.2(b). As such, in this study, we assumed the flexural strength of all the materials to be equal to material yield strength (elastic limit) for the derivation of the performance index and hence equation (3.3) applies.

Table 3.2 The material data properties for the P110 and BS 145

Material	Young's Modulus (MPa)	Poisson's ratio	Inner Diameter (inches)	Outer Diameter (inches)
P110	210000	0.300	4.5	5.5
BS 145	206000	0.295	4.5	5.5

The boundary condition is applied as in Figure 3.2(a) One end fixed while the other is a roller support and a 5 inches displacement is gradually applied shown on Figure 3.2(a).

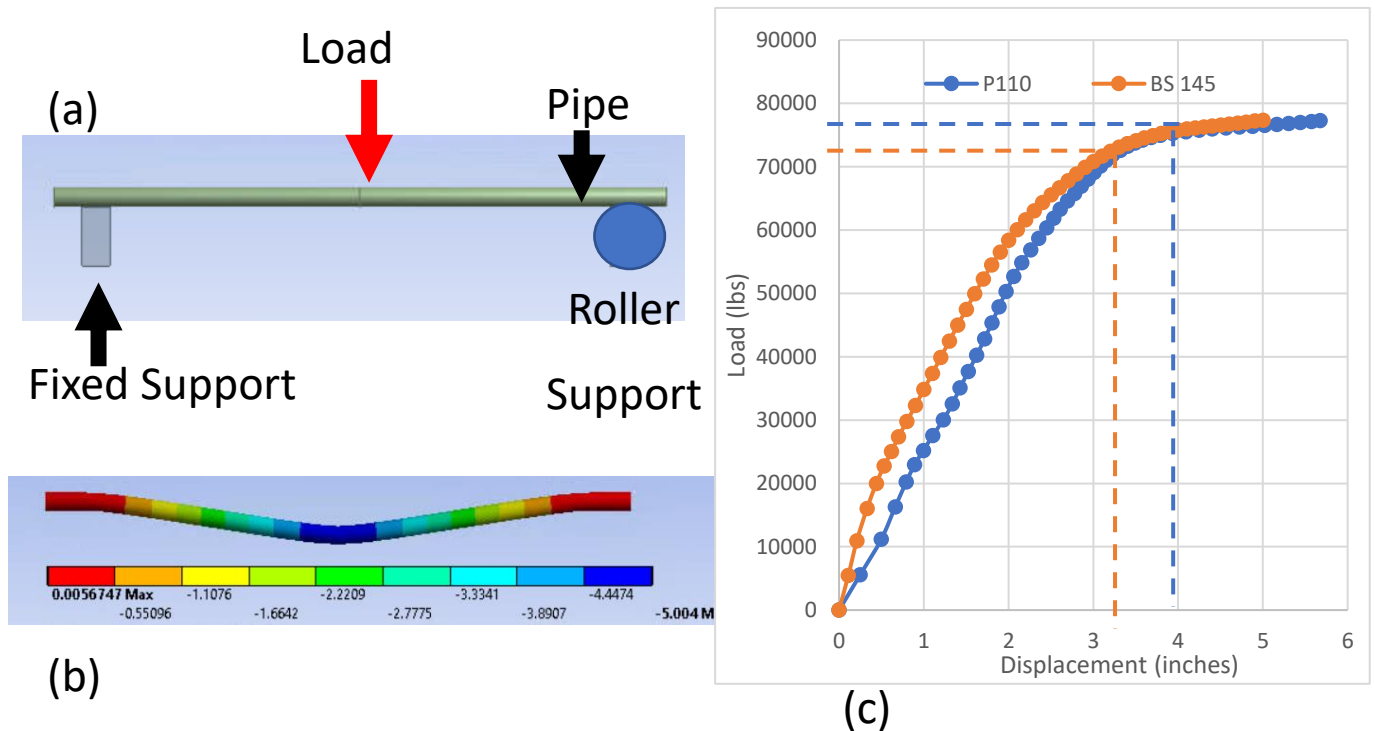


Figure 3.2: 3-Point bending load displacement curve for P110 and BS 145 (a) Physical model (b) deform numerical model (c) Load versus displacement for P110 and BS145.

Flexural strength is calculated from the load F at which beam fractures (brittle materials) or becomes fully plastic for ductile materials as shown on Figure 3.2(c).

This plot reveals the flexural load of P110 and BS 145 to be 75750lbs and 73098lbs respectively.

Another assumption is based on Euler buckling equation. Using this equation (3.4); the performance index is derived to determine ratio from CES database which will avoid critical buckling of the casing under load at minimum thickness.

$$F = \frac{\pi^2 EI}{(KL)^2} \quad 3.4$$

The moment of inertia for a hollow pipe is $I = \frac{\pi}{4}(r_o^4 - r_i^4)$ as shown in Table 3.1. While K is the buckling load constant – which depend on the end conditions. K= 1 for one fixed end and translation and rotation free at the other end. However, $r_o^4 - r_i^4 = t^4$ represent the thickness of the casing pipe. Implies $t = \left(\frac{4I}{\pi}\right)^{1/4}$ Again, the cross-sectional area of a hollow pipe $A = \pi(r_o^2 - r_i^2)$ as shown in Table 3.1. Now substituting for A, I and t and simplifying, to obtain the material with minimum thickness and mass that will avoid the buckling of the casing at minimum mass m is we get:

$$m = 2r(\pi F)^{1/4} \cdot L^{3/2} \left(\frac{\rho}{E^{1/4}}\right) \quad 3.5$$

The index term is $\left(\frac{\rho}{E^{1/4}}\right)$

$$\text{And the reciprocal gives: } \left(\frac{E^{1/4}}{\rho}\right) = \mathbf{M2} \quad 3.6$$

3.3 Results and Discussion

3.3.1 Material Selection for shale gas well

The initial selection begins with the advanced plotting features for all the materials in the CES database. As it can be seen on Figure 3.3 the various material family are highlighted based on these performance indices on X and Y axes. Also, the powers (indices) and mathematical operators assign accordingly as shown on Figure 3.3. Materials on lower-left hand side are cheap and of low performance, while material

on the top-right corner are of high performance but more expensive. Additionally, different material families cover a significant range so there is room for further screening of the potential candidates.

The material family (Ferrous) and based material (Iron) limiting constraints of are applied to the initial selection in order to search for materials that will meet the casing material requirements. Material family ferrous with iron as based material are selected because of their high strength, low cost and ductility. Furthermore, a 195GPa is applied as the minimum threshold for materials Young's Modulus to get most stiff materials from this family. A Young's Modulus of 195GPa is similar to the reference P110 casing's Young's Modulus at 100°C which is also stiff.

However, using API 5CT, and other mechanical properties from the casing manufacturers, user define materials records are created in the selection at this stage for comparison with other materials in the CES Edupack. It should be noted that both API and non-API steel grades are considered. However, for the non-API steel grades only V150 and SM125 are included owing to their applicability in harsh gas wells high pressure, high temperature, and high H₂S as pointed by (Wang et al. 2019).

Also, based on study conducted by (Jacobs 2020; Mohammed et al. 2020) established the casing to buckle at very low shear loads. Typically, 10-15MPa for P110 casing) as established by (Mohammed et al. 2020). As, such, a minimum shear load of 13MPa was applied to modify the selection. As a result, Figure 3.4 was developed from CES database which shows the bubble diagram of the materials that meet selection criteria and show their corresponding performance.

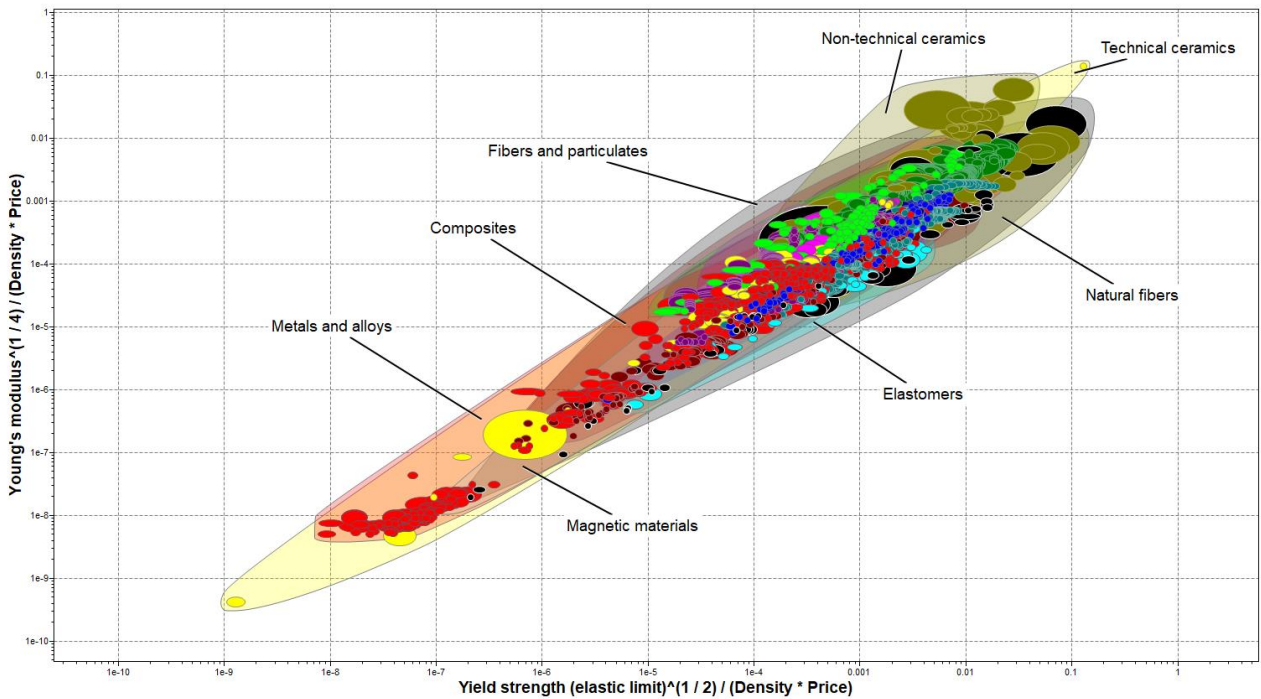


Figure 3.3 material candidates using CES Edupack.

Based on Figure 3.4 the design engineer can select and justify the selection for a particular well application. Furthermore, material on the lower left are of low performance and cheaper and lighter. In contrast, materials on top right are of higher performance but more expensive and heavier. Under this circumstance the trade-off has to be made.

As it can be seen on Figure 3.4 the API casing perform very well with P110 casing grades being the highest while SM 125 being the best for the non-API material grades. Furthermore, high strength low alloy (YS460 hot rolled) from the metal and alloys family appears to be the best performing material from the EDPACK Database for this application.

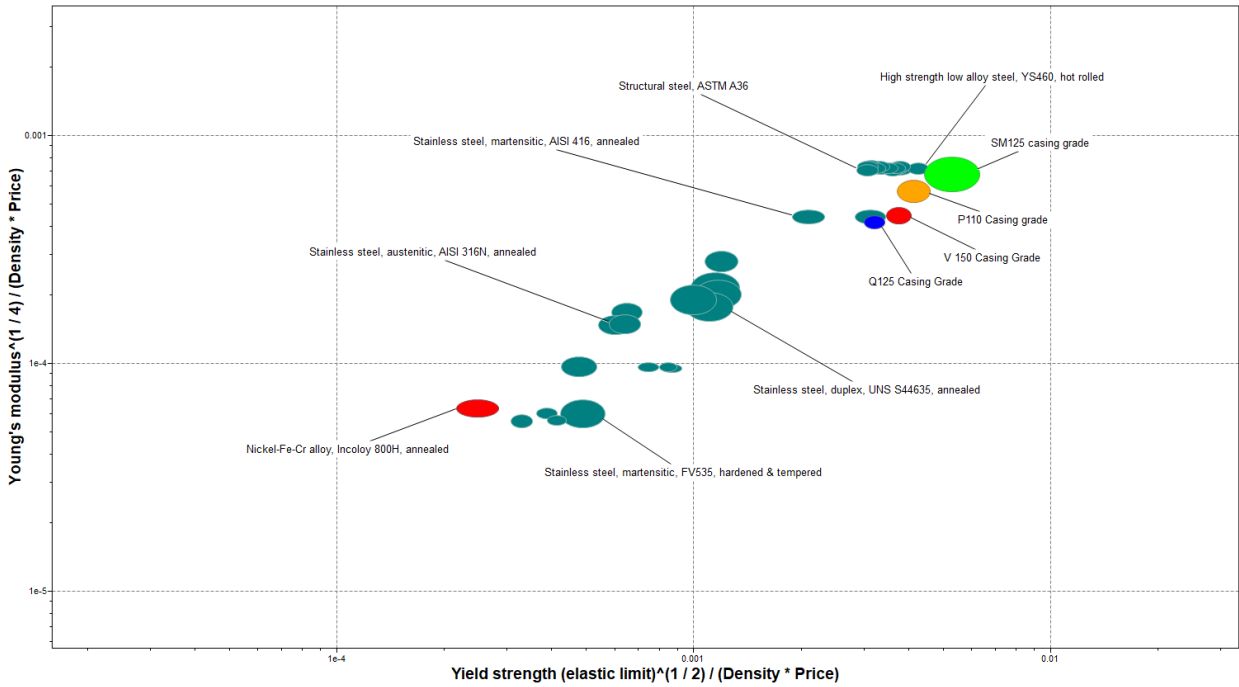


Figure 3.4 Shortlisted candidates for shale gas well casing

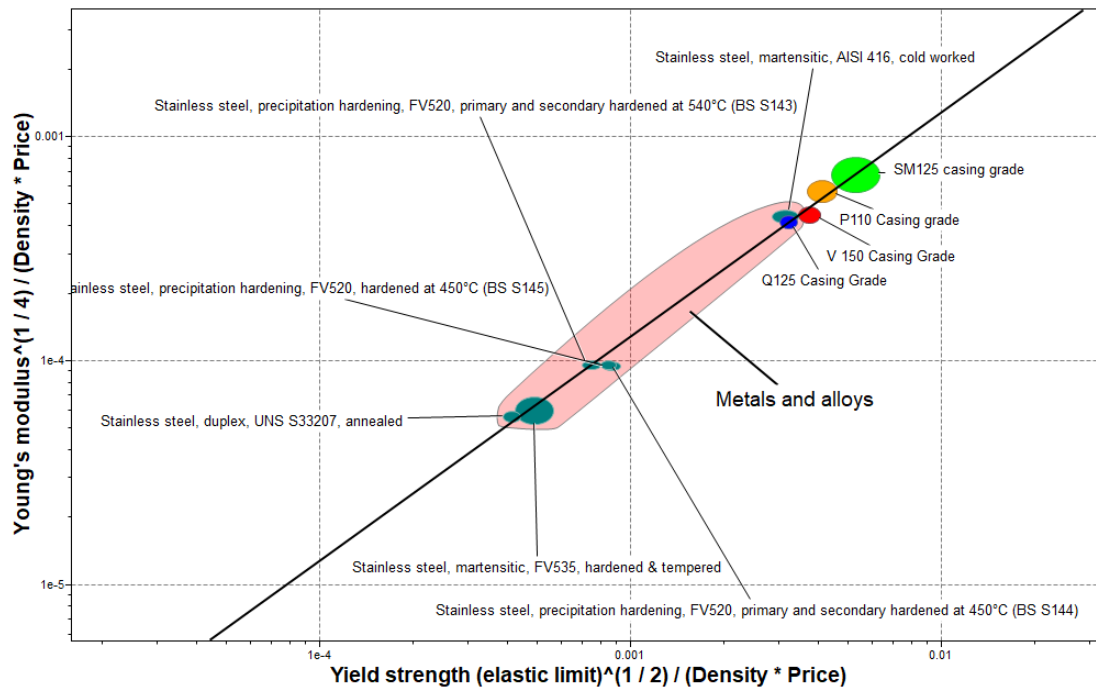


Figure 3.5 Top ten (10) materials after further optimisation.

Using equation of a straight line with slope equals 1($x=y$). Further refinement is achieved as shown on Figure 3.5. This reduced the number of materials to 10. The “active constraints” method can be applied to further optimised the selection – a process which allows the selection of a specific material that optimally meet two or more constraints. As it can be seen based on the performance indices SM125, P110 and V150 appear to be the best in terms of performance but more expensive and heavier than stainless steels (BS143, BS144, BS145) and FV535 stainless steel.

3.3.2 Selection based on induced stress and corrosion

Again, using the same material indices as in the previous section and different selection criteria another shortlist of materials is obtained from the database. In similar manner, the entire database was used in order not to discriminate any material, as a result similar material family was obtained as in the previous scenario as shown on Figure 3.6.

The study of Marbun et al. (2020) pointed out the material selection for the production casing and production liner in the Dieng Field, Indonesia was estimated according to corrosion equations established by Ekasari and Marbun (2015). Using this equation, the chromium equivalent (Creq value) is calculated. Based on the temperature, pH data of the fluid in the field and the corrosion rate target (0.1 mm/year) the Creq diagram for production casing and production liner plotted. However, this methodology is limited to geothermal wells in the Dieng Field and cannot be in shale gas wells casing wells selection.

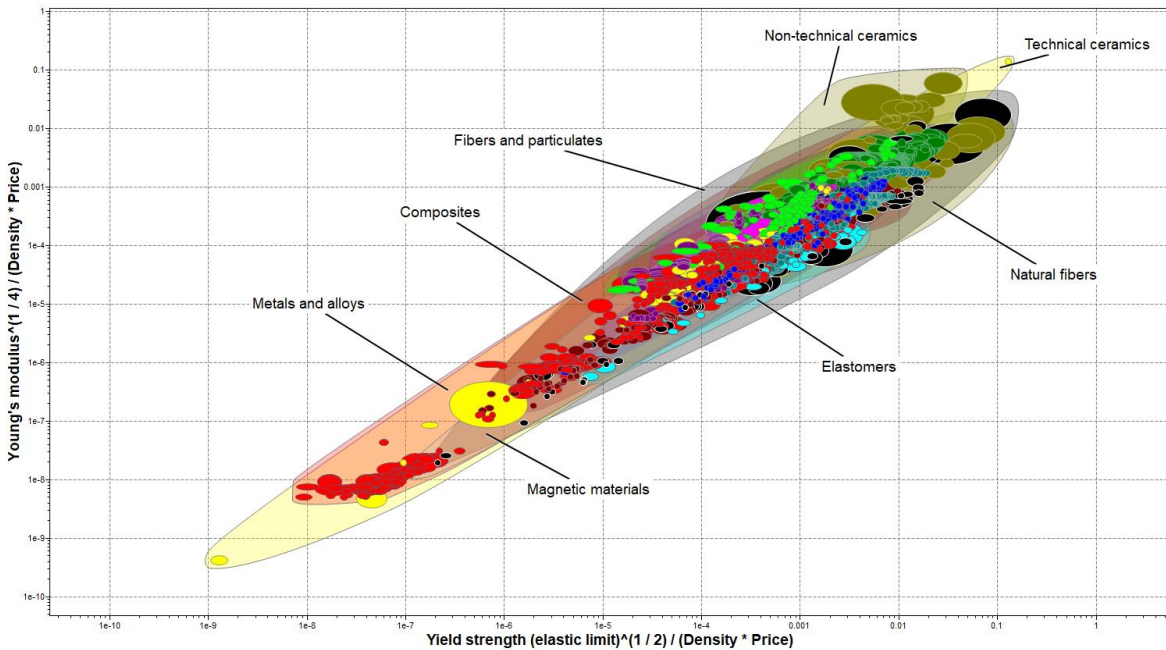


Figure 3.6 Selection for second scenario (induced stress and corrosion).

The second scenario for the selection of potential materials of the casing looks into different limiting criteria. The young's modulus was selected as a range from 160-200GPa for a typical casing grade (SM125). Another, constraint impose was the strain ($\geq 14\%$) to get the stiffest materials from the database based on this equality constraint. Under this stage, out of 4169 potential materials, 569 materials meet the criteria. Those materials that do not meet these criteria are shown in grey and subsequently removed (Figure 3.7).

The resulting selection is further limited with yield strength of 758MPa (P110 casing grade). This yield strength is applied as limiting constraints considering the deformation of P110 casing grade reported in the literature (Mohammed et al. 2019, Yin et al 2018; Wang et al. 2019). In addition, assuming a high pressure, high temperature, high H_2S gas well, the corrosion potential for this class of wells is severe.

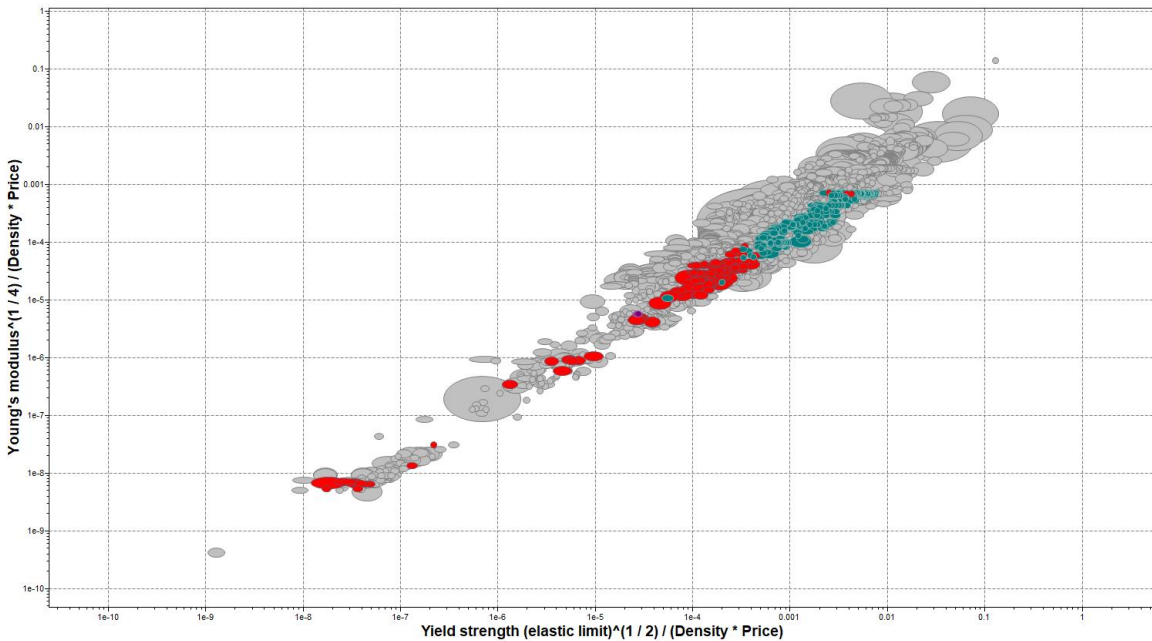


Figure 3.7 Initial screening for the second scenario.

The pitting resistant equivalent number (PREN) for metals and alloys ranges from 0-56.4 and proprietary austenitic stainless steels for directional drilling (PREN between ~ 20 to ~ 45 (Marya 2020). Based on this, 15 to 30 PREN was applied as the minimum and maximum respectively. Moreover, the resistance of the materials to sour oil and gas, i.e., that which contains high levels of hydrogen sulphide. This qualitative attribute is categorised as either; Excellent, Good, Moderate, restricted and poor. Therefore, excellent, good and moderate materials are chosen to further optimise the selection. This selection is as shown on Figure 3.8 with the material family envelop – metals and alloys.

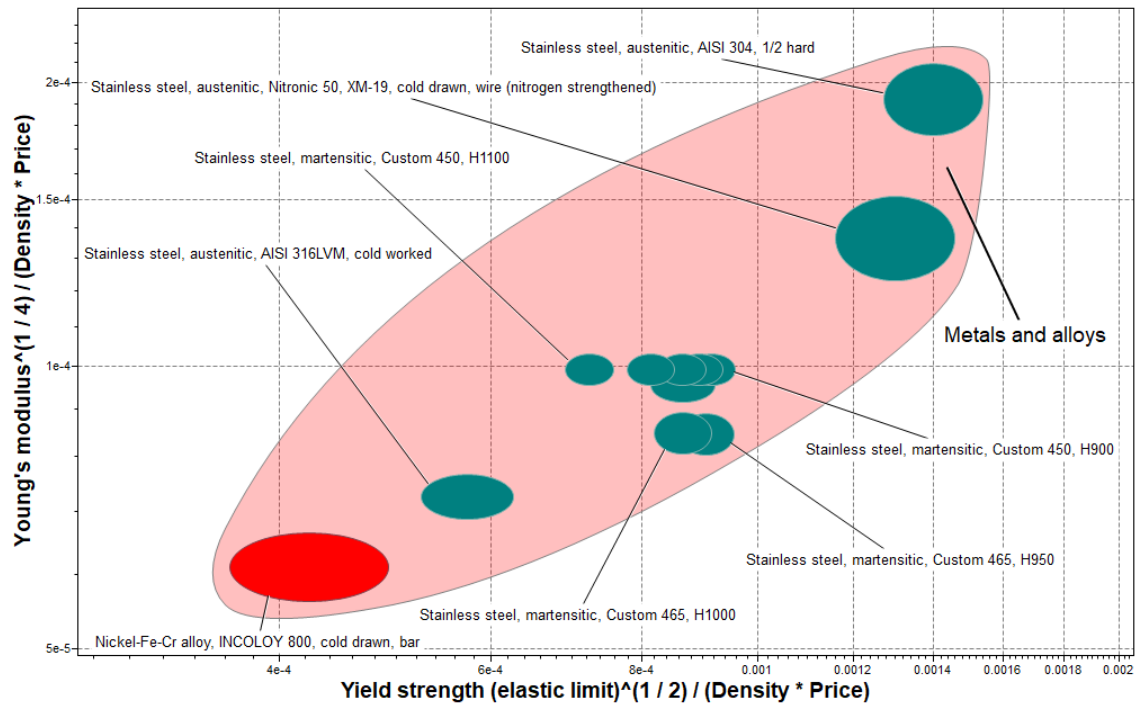


Figure 3.8 Shortlisted materials for high sour oil and gas wells.

Figure 3.8 presents stainless steel and Nickel alloys material families. Both Nickel and stainless steel have good corrosion resistance as established in the studies of (Craig and Smith 2011; Liu et al. 2020; Qi et al. 2020). Similarly, materials on the top right-hand corner demonstrates good performance but are relatively expensive and heavy compared to those on the bottom left-hand corner. These materials such as Nickel alloys are lighter, cheaper but of low performance. This is expected considering the limiting criteria. However, none of the API steel grades meets these criteria as such not shown on bubble diagram (Figure 3.8).

3.3.3 Selection based on induced stress, service temperature and External load (Impact)

There are circumstances in which the casing is installed in an environment where thermal loads are present apart from the localised stress due to fracturing pressure. Moreover, shale development is often associated with impact resulting from shearing of the rock during fracturing process (Yang et al. 2018). Significant fracture toughness in materials is essential factor for performance under this situation. The study by Correa et al. (2020) computed the fracture toughness of API 5CT P110 steel using crack tip opening displacement (CTOD) through FEA in order to determine the acceptability of the cracks in rigid risers. Risers can be rigid, flexible or hybrid. However, rigid risers (Pipes) are susceptible to external threats such as accidental impacts, and environmental factors such as the high corrosion potential during operations (Correa et al. 2020).

As such, it is therefore essential to select material using these indices but can withstand significant amount of impact energy. A recent study by Zhu et al. (2020) on experimental studies on dynamic behaviour of pipes under repeated impact loadings shows that the pipe mainly experienced local dent close to the upper side, while the global bending was very small. This phenomenon is similar to casing deformation commonly encountered during shale gas wells stimulation. However, materials with high impact energy absorption (KJ/m^2) absorbs high impact energy before deformation while materials with low toughness absorbs little impact energy, and as result permanent deformation of the casing may be the result.

The P110 casing grade did not meet selection criteria as its ranges between 15-30ft-lbs (0.020-0.04KJ/m²) which is well below the minimum threshold of 30KJ/m² for fracture toughness. As such, not appear in the selection for this scenario. While the selection and design of casing for oil and gas wells is largely based on downhole conditions (pressure, temperature and fluids properties). For example, the study of Kaldal et al., (2015) and Marbun et al. (2020) pointed the danger of the combine influence of high temperature and pressure on casing strength degradation and casing thickness reduction and eventual failure of the casing. Therefore, meticulous selection using CES database and performance indices for casing materials would be more robust and effective method in preventing corrosion and prolonging the lifetime of the well than the conventional approach.

Figure 3.9 presents the various material families based on the performance indices from advanced level 3 aerospace database was obtained for the initial casing selection for this scenario.

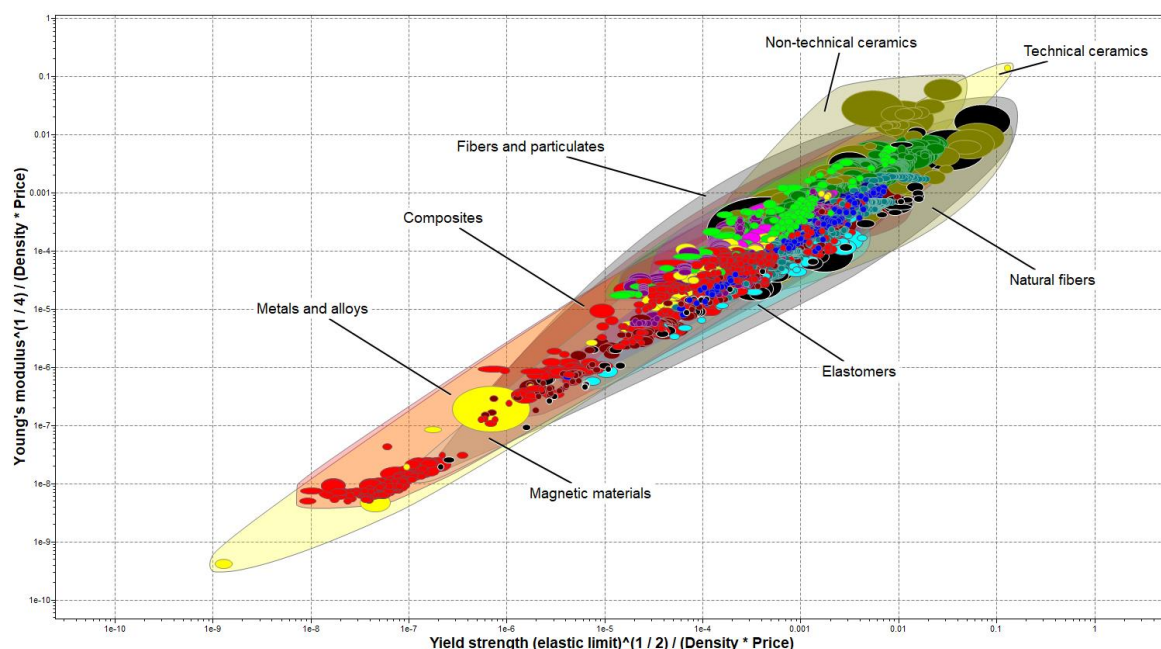


Figure 3.9 Initial selection for service temperature and toughness

Similarly, all those materials that do not meet the selection are eliminated/screened out which reduce the materials to 568 from initial 4164 of the advanced level 3 aerospace databases. Figure 3.10 presents the resulting materials bubble plots based on these constraints.

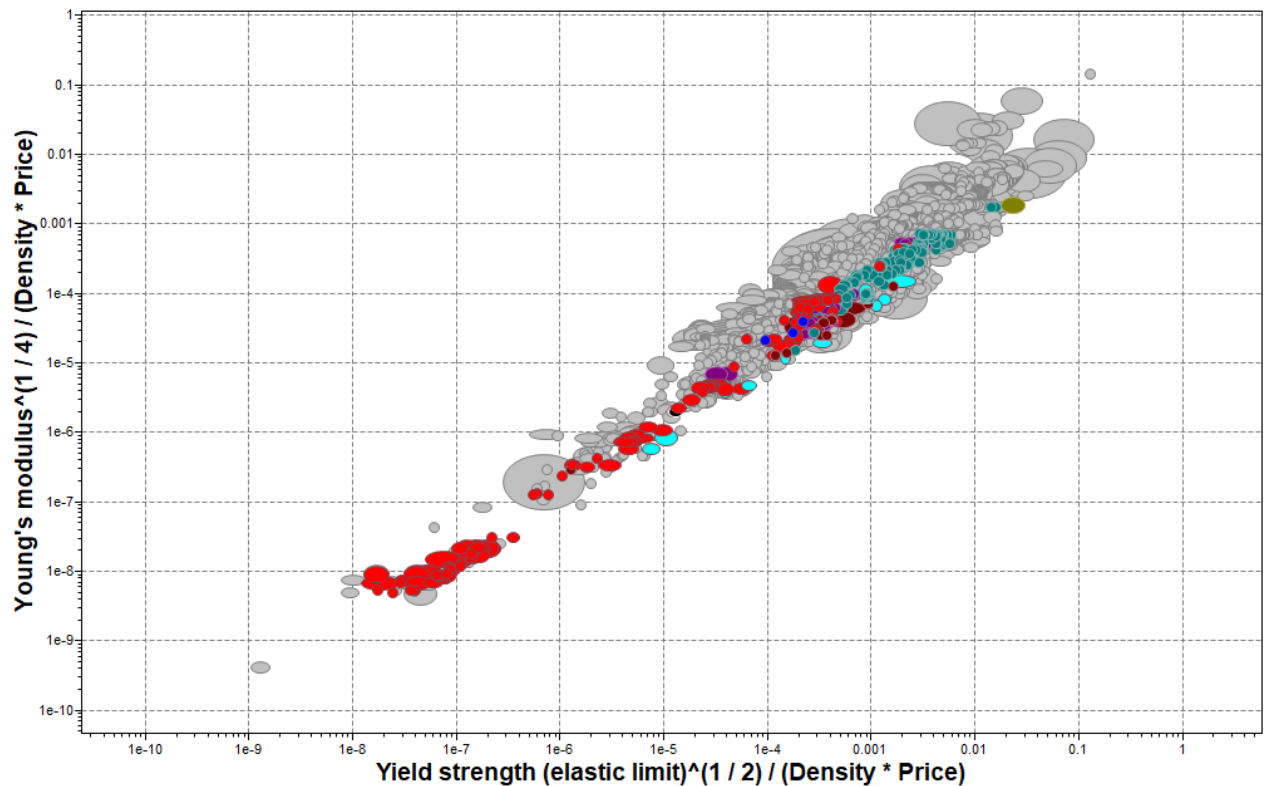


Figure 3.10 Shortlisted materials for shale gas wells with high impact energy and temperature.

The resulting selection is shown on Figure 3.11 with a tangent line delineating optimum selection. This selection is further expanded to aid in visualisation with a tangent line drawn connecting the optimum candidates for this selection so as to further reduce the list to the most qualified materials (pareto optimal solution).

Having applied the additional limiting criterion such as ferrous and nonferrous metals, base materials and service temperature ≥ 120 -degree Celsius, and pareto optimal selection; the selection reduces to 10 materials from the previous 568

shortlisted. As it can be seen the final list is mostly stainless-steel family (80%) and Titanium and Nickel alloys accounting for 20% as shown on Figure 3.15.

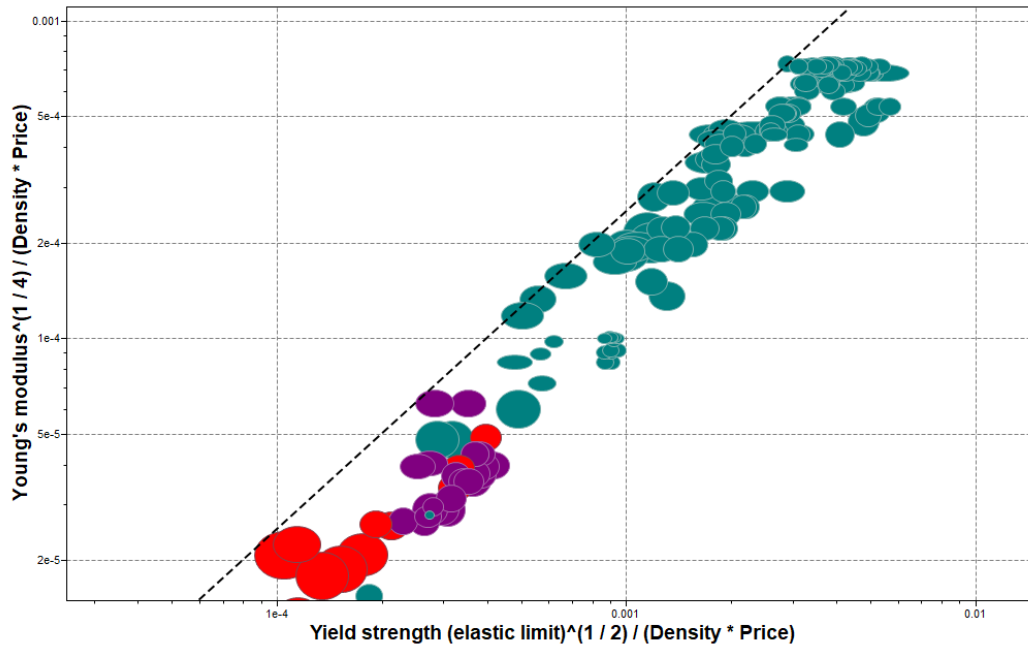


Figure 3.11 Optimum selection using tangent line for pareto solution

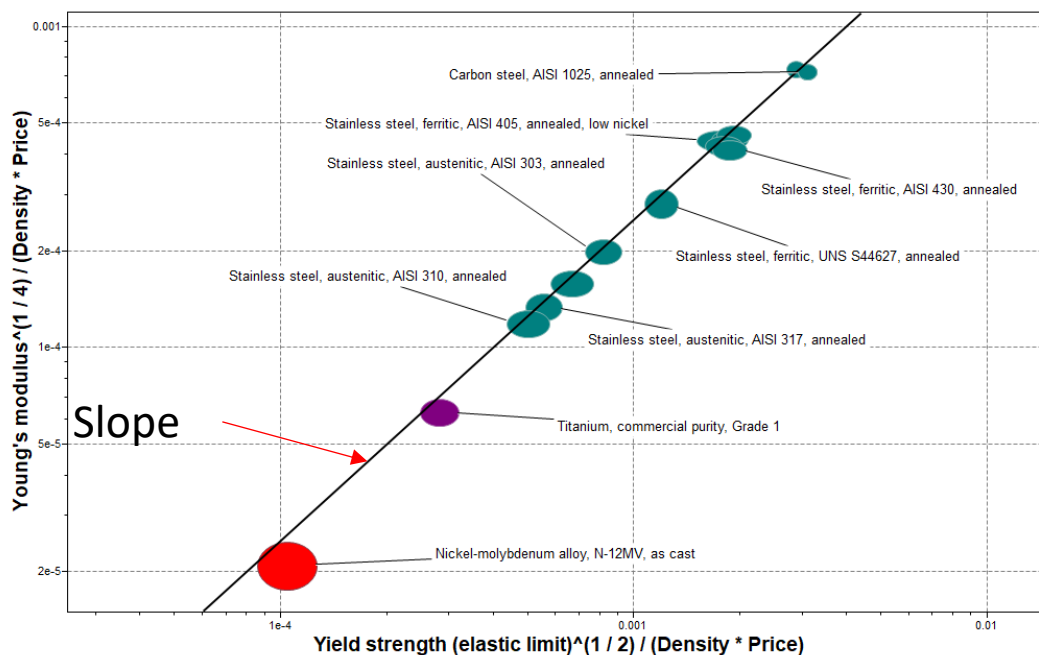


Figure 3.12 Shortlisted materials for shale gas wells with high impact potentials and service temperature.

The final shortlist that comprises Nickel and Titanium as well as the carbon steel are presented on Figure 3.13. This optimised selection revealed that carbon steel (AISI 1025 annealed) is the overall best material for impact loads and service temperature based on this scenario. Moreover, these materials all belong to the metals and alloys group as shown on Figure 3.13.

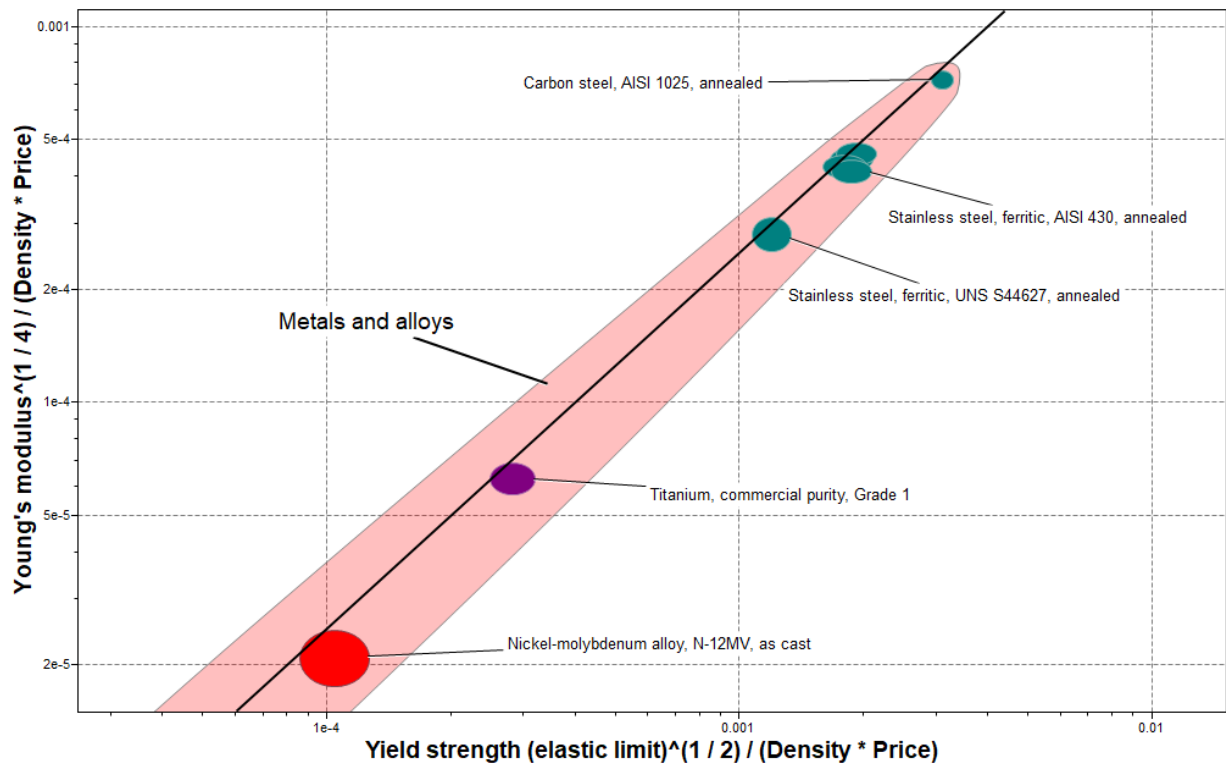


Figure 3.13 Family envelope of the shortlisted material for high impact shales (brittle)

3.4 TOPSIS: Technique for order performance by similarity to ideal solution

In 1981, Hwang and Yoon developed the TOPSIS process which is quite simple, and the solution procedure does not change irrespective of number of decision criteria and alternatives. The method estimates the optimum material candidate by applying distances to positive and negative solution. However, the main setback of this approach is that correlation between criteria is not considered in the evaluation

of Euclidean distance. In addition, weights are assigned to the various criteria to favour are particular material by the designer.

The main objective is to select material for the casing that will not buckled during hydraulic fracturing as a result of induced stress and resulting displacements in the process. Therefore, we need a high strength and high stiffness and low cost and elongation as well as light material (low density). Using the shortlisted materials in Table 3.3 form CES GRANTA SELECTOR – TOPSIS method is applied for the material selection.

From Table 3.3 it could be seen that Young's Modulus, Yield strength, Density, elongation, price per kilogram, service temperature are the criteria used to shortlist these materials from CES EDUPACK based on performance indices derived for the casing selection in section 3.3.2 of this chapter. While, buckling load are computed for each material using Euler buckling equation. Also, for the API casing grades, the cost is an average based on similar grade obtained online.

Table 3.3 Material mechanical and physical properties for the TOPSIS selection process.

Material Description	YM (GPa)	YS (MPa)	Density (Kg/m³)	% Elong.	Price (£/Kg)	Service Temperature (°C)	Buckling Load (lbf)
Stainless Steel Duplex UNS S33207	205	816	7740	16.5	9.05	365	73330
Stainless Steel (BS S145)	206	1280	7830	15	5.24	427	73688
Stainless steel martensitic FV535	216	1030	7830	22	9.28	550	77265
Stainless steel Precipitation FV520	216	955	7830	22	5.24	427	77265
Stainless steel Precipitation FV520	216	1200	7830	18	5.24	427	77265
Stainless Steel AISI 416	210	820	7880	18	1.17	750	75119
Q125 Casing grade	216	862	7800	18	*1.25	250	77265
P110 Casing Grade	210	758	7800	15	*0.929	250	75119
V150 Casing Grade	220	1034	8150	18	*1.16	250	78696
SM 125	202	862	7790	18	*0.85	250	72257

*Denotes average cost online.

From the shortlisted materials in CES EDUPACK database, the ranking of these materials is implemented using TOPSIS method. The first step for the TOPSIS method is the calculation of normalise matrix. This is accomplished using Equation (3.5).

$$\overline{X}_{ij} = \frac{X_{ij}}{\sqrt{\sum_{i=1}^n X_{ij}^2}} \quad 3.5$$

Where:

X_{ij} = Elements magnitude in the selection based on different criteria

\overline{X}_{ij} = Normalise values

Using equation (3.5), the values in Table 3.3 are normalised to have level playing field for all the selection criteria, subsequently all the elements in Table 3.3 are converted between 0 and 1 exclusive leading to Table 3.4.

All the criteria are assumed to be 15% weights with the exception of cost which is assigned a value of 10%. This is to ensure equal distribution among the criteria.

Based on these weights, Table 3.4 is obtained using Equation (3.6) which is basically the product of Equation (3.5) and Equation (3.6)

$$V_{ij} = \overline{X}_{ij} * W_j \quad 3.6$$

Table 3.4 Calculated weighted normalised matrix

Weights	0.15	0.15	0.15	0.15	0.1	0.15	0.15
Material	YM (GPa)	ρ (kg/m ³)	YS (MPa)	% Elong	Average Cost (£/kg)	Service Temperature (Deg. C)	Buckling Load
Stainless Steel Duplex UNS S33207	0.0482	0.0492	0.0411	0.0449	0.0685	0.0425	0.0482
Stainless Steel (BS S145)	0.0485	0.0498	0.0645	0.0408	0.0397	0.0497	0.0485
Stainless steel martensitic FV535	0.0508	0.0498	0.0519	0.0599	0.0703	0.0640	0.0508
Stainless steel Precipitation FV520	0.0508	0.0498	0.0481	0.0599	0.0397	0.0497	0.0508
Stainless steel Precipitation FV520	0.0508	0.0498	0.0605	0.0490	0.0397	0.0497	0.0508
Stainless Steel AISI 416	0.0494	0.0501	0.0413	0.0490	0.0089	0.0873	0.0494
Q125 Casing grade	0.0508	0.0496	0.0435	0.0490	0.0095	0.0291	0.0508
P110 Casing Grade	0.0494	0.0496	0.0382	0.0408	0.0070	0.0291	0.0494
V150 Casing Grade	0.0518	0.0518	0.0521	0.0490	0.0088	0.0291	0.0518
SM 125	0.0475	0.0496	0.0435	0.0490	0.0064	0.0291	0.0475

The calculated ideal best and ideal worst values are values that are positively and negatively close to the ideal solution. This basically is the selection of maximum values for Yong's modulus and strength as the ideal best and minimum values for density, price and elongation as the ideal best. On the other hand, the ideal worst for the Young's modulus are the minimums while for density, elongation and price; the ideal worst are the maximums calculated. Using the ideal best calculated, the Euclidean distance for the ideal best is computed using Equation (3a)

$$S_i^+ = \left[\sum_{j=1}^m (V_{ij} - V_j^+)^2 \right]^{0.5} \quad 3.7a$$

Also, in similar approach calculate Euclidean distance from the ideal worst is achieved using (3b)

$$S_i^- = \left[\sum_{j=1}^m (V_{ij} - V_j^-)^2 \right]^{0.5} \quad 3.7b$$

The performance score of the different material is computed using Equation 4

$$P_i = \frac{S_i^-}{S_i^+ + S_i^-} \quad 3.8$$

Table 3.5 Materials ranked according to performances using Euclidean distance measure

Material	Si+	Si-	Pi	Rank
Stainless Steel Duplex UNS S33207	0.0803	0.0206	0.2037	10
Stainless Steel (BS S145)	0.0504	0.0492	0.4940	6
Stainless steel martensitic FV535	0.0717	0.0378	0.3455	9
Stainless steel Precipitation FV520	0.0561	0.0385	0.4070	8
Stainless steel Precipitation FV520	0.0510	0.0447	0.4672	7
Stainless Steel AISI 416	0.0249	0.0854	0.7740	1
Q125 Casing grade	0.0625	0.0622	0.4989	5
P110 Casing Grade	0.0639	0.0661	0.5085	4
V150 Casing Grade	0.0601	0.0643	0.5166	2
SM 125	0.0627	0.0650	0.5091	3

As it can be seen using the TOPSIS approach Stainless steel AISI 416 appears to be the best candidate based on these criteria and the assumption stated above. This is followed by V150 casing grade as the second-best choice and SM 125 making the third on the list.

3.5 Analytical Hierarchy Process (AHP) Method

AHP developed in the year 1980 by Saaty has been popular in application in areas of planning, selecting best alternative materials, resource allocation and resolving conflict. Like TOPSIS method, the AHP is accomplished through 4 systematic steps as follows:

1. Develop a model for the business case (goal)
2. Derive priorities (weights) for the criteria governing the selection
3. Check for weights consistency

4. Derive the overall priorities and final decision.

The procedure is usually structured in hierarchical order with the main goal or objective at the top. This is followed by the criteria and the alternatives from which the choice is going to be made. Optimum solution is obtained based on the degree of importance of criteria and alternatives. Using the Thomas Saaty's (1970) fundamental scale, the different criteria are assigned weights depending on their contribution to overall objective or goal. However, the technique becomes more complicated as criteria and alternatives increases.

Step 1: Defining main goal

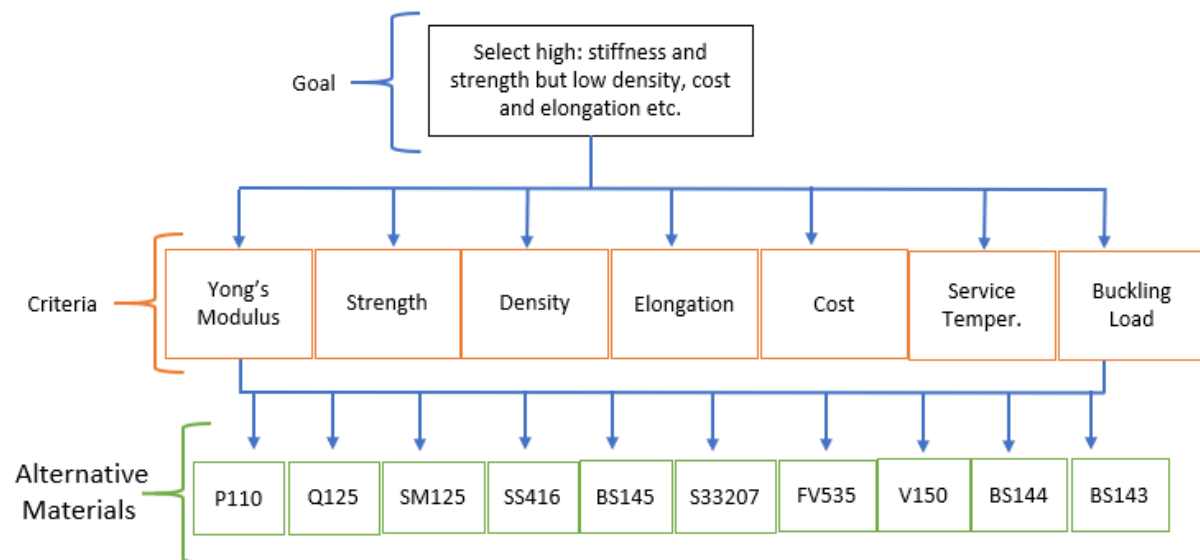


Figure 3.14 An overview of analytical hierarchical process showing goal, criteria and alternative materials

As it can be seen on the flowchart (Figure 3.1), the first thing is to define the goal or objective. This is followed by applying the weights using Saaty's fundamental scale to all the criteria depending on the goal or objective to be achieved from the available materials.

Step 2: Derive weights for the selection criteria based on Saaty's fundamental scale

As it can be seen in Table 3.6 the value of on the scale represent equal importance between two criteria. The value of 3 and 5 is assign to moderate and essential importance. Furthermore, 7 and 9 represent strong and extreme importance, while 2,4,6 and 8 are intermediate values between two adjacent judgements – when a compromise is needed.

Table 3.6 Saaty’s fundamental scale

Intensity of importance on an absolute scale	Definition	Explanation
1	Equal importance	Two activities contribute equally to the objective
3	Moderate of one over another	Experience and judgement strongly favour one activity over another
5	Essential or strong importance	Experience and judgement strongly favour one activity over another
7	Very strong importance	An activity is strongly favoured, and its dominance demonstrated in practice
9	Extreme importance	The evidence of favouring one activity over another is of the highest possible of affirmation
2,4,6,8	Intermediate values between two adjacent judgements	When compromise is needed

$$\text{A pair-wise comparison matrix } A_1 = \begin{bmatrix} C_{11} & C_{12} & C_{13} & C_{14} & C_{15} & C_{16} & C_{17} \\ C_{21} & C_{22} & C_{23} & C_{24} & C_{25} & C_{26} & C_{27} \\ C_{31} & C_{32} & C_{33} & C_{34} & C_{35} & C_{36} & C_{37} \\ C_{41} & C_{42} & C_{43} & C_{44} & C_{45} & C_{46} & C_{47} \\ C_{51} & C_{52} & C_{53} & C_{54} & C_{55} & C_{56} & C_{57} \\ C_{61} & C_{62} & C_{63} & C_{64} & C_{65} & C_{66} & C_{67} \\ C_{71} & C_{72} & C_{73} & C_{74} & C_{75} & C_{76} & C_{77} \end{bmatrix} \quad 3.9$$

Table 3.7 A pair-wise matrix obtained using the importance on an absolute scale from Table 3.6.

A pair-wise matrix A1

Using the fundamental scale suggested by Saaty 1980 to develop the pair matrix A1							
criteria	YM (GPa)	ρ (Kg/m3)	YS (MPa)	% Elong	Average Cost (£/kg)	Service Temp. (Deg. C)	Buckling Load
YM (GPa)	1.00	2.00	0.33	2.00	4.00	3.00	0.25
ρ (Kg/m3)	0.50	1.00	0.50	2.00	2.00	2.00	0.50
YS (MPa)	3.00	2.00	1.00	2.00	4.00	4.00	0.50
% Elong	0.50	0.50	0.50	1.00	2.00	3.00	2.00
Average Cost (£/kg)	0.25	0.50	0.25	0.50	1.00	2.00	0.33
Service Temperature (Deg. C)	0.33	0.50	0.25	0.33	0.50	1.00	0.25
Buckling Load	4.00	2.00	2.00	0.50	3.00	4.00	1.00

As it can be seen in Table 3.7 the diagonal elements indicate equal importance or same criteria correlation. Additionally, the importance of buckling load on Young's Modulus is taken as 4. While the importance of Young's Modulus on buckling load is the inverse which correspond to 0.25 tabulated on the top right-hand corner on Table 3.6.

The next step is the summation of each of the column in the pair-wise matrix.

$$C_{ij} = \sum_{i=1}^n C_{ij} \quad 3.10$$

Next is to divide each of the elements of criteria by the total summation to get the weight of each criterion. As it can be seen in Table 3.8 buckling load and yield strength have the highest weights of 24% each (column 2) followed by elongation and Young's Modulus with 15 and 13% respectively. On the other hand, service temperature and cost have the least weight as shown in Table 3.8- column 2.

Table 3.8 summarised A2, A3 and A4 matrices. A2 matrix gives the weight of each criterion as a ratio of the total sum. A3 matrix is the product of A1 and A2 matrices while A4 matrix is a ration between A3 and A2 matrix.

Table 3.8 Weights of each criterion (A2 Matrix)

Criteria	A2 Matrix	A3 Matrix	A4 Matrix
YM (GPa)	0.15	1.22	8.0
ρ (Kg/m ³)	0.12	0.93	7.5
YS (MPa)	0.24	1.79	7.5
% Elong	0.13	1.15	8.7
Average Cost (£/kg)	0.07	0.47	7.2
Service Temperature (Deg. C)	0.05	0.36	7.1
Buckling Load	0.24	2.03	8.5

Step 3

The consistency vector is calculated by multiplying the pair-wise matrix by the weights vector.

$$\begin{bmatrix} C_{11} & C_{12} & C_{13} & C_{14} & C_{15} & C_{16} & C_{17} \\ C_{21} & C_{22} & C_{23} & C_{24} & C_{25} & C_{26} & C_{27} \\ C_{31} & C_{32} & C_{33} & C_{34} & C_{35} & C_{36} & C_{37} \\ C_{41} & C_{42} & C_{43} & C_{44} & C_{45} & C_{46} & C_{47} \\ C_{51} & C_{52} & C_{53} & C_{54} & C_{55} & C_{56} & C_{57} \\ C_{61} & C_{62} & C_{63} & C_{64} & C_{65} & C_{66} & C_{67} \\ C_{71} & C_{72} & C_{73} & C_{74} & C_{75} & C_{76} & C_{77} \end{bmatrix} * \begin{bmatrix} W_{11} \\ W_{12} \\ W_{13} \\ W_{14} \\ W_{15} \\ W_{16} \\ W_{17} \end{bmatrix} = \begin{bmatrix} C_{v11} \\ C_{v12} \\ C_{v13} \\ C_{v14} \\ C_{v15} \\ C_{v16} \\ C_{v17} \end{bmatrix} \quad \text{A3 Matrix} \quad 3.11$$

where,

$C_{v_{ij}}$ is the consistency vector

Also, the A4 matrix is computed by dividing A3 Matrix by A2 matrix. The average value of A4 matrix is represented by λ . Lambda (λ) together with number of criteria n the value of consistency index is calculated.

The consistency index is calculated using Equation (3.12)

$$CI = \frac{\lambda - n}{n - 1} \quad 3.13$$

Where n , is the number of criteria in the selection and CI is the consistency index.

In order to be consistent with weights assignment in the pair-wise matrix, Saaty recommends the consistency ratio to be less than 0.1

λ is calculated by averaging the value of the consistency vector (matrix A4)

$$\lambda = \sum_{i=1}^n C v_{ij} \quad 3.14$$

Average = **7.799237** of A4 Matrix

The consistency index CI is calculated using Equation 5

Consistency index = **0.1332**

Next is consistency ratio **cr**

$$C_r = \frac{CI}{RI} \quad 3.15$$

The random index is obtained from Table 3.9 for the number of criteria. In this selection, the number of criteria is 7, based on Table 3.8 (column 1) therefore, **1.35** (yellow highlight) is taken to compute the consistency ratio.

Table 3.9 Random index according to Rao (2007)

Attributes	3	4	5	6	7	8	9	10
Random index	0.52	0.89	1.11	1.25	1.35	1.4	1.45	1.49

Consequently, the consistency ratio is found to be:

$C_r = \mathbf{0.0951}$ which agrees with has been established in the literature.

Step 4 Derive performance and rank

Table 3.10 Analytical hierarchy process performance and ranking

AHP method									
Weights	0.152	0.125	0.238	0.132	0.065	0.051	0.238		
Material	YM (GPa)	ρ (Kg/m ³)	YS (MPa)	% Elong	Average Cost (\$/kg)	Service Temperature (Deg. C)	Buckling Load	Performance	Rank
Stainless Steel AISI 416	0.9545	0.9669	0.6406	0.8182	0.1261	1.0000	0.9545	0.8117	7
Q125 Casing grade	0.9818	0.9571	0.6734	0.8182	0.1347	0.3333	0.9818	0.7958	8
P110 Casing Grade	0.9545	0.9571	0.5922	0.6818	0.1001	0.3333	0.9545	0.7456	10
V150 Casing Grade	1.0000	1.0000	0.8078	0.8182	0.1250	0.3333	1.0000	0.8396	5
SM 125	0.9182	0.9558	0.6734	0.8182	0.0916	0.3333	0.9182	0.7680	9
Stainless Steel Duplex UNS S33207	0.9318	0.9497	0.6375	0.7500	0.9752	0.4867	0.9318	0.8203	6
Stainless Steel (BS S145)	0.9364	0.9607	1.0000	0.6818	0.5647	0.5693	0.9364	0.8782	3
Stainless steel martensitic FV535	0.9818	0.9607	0.8047	1.0000	1.0000	0.7333	0.9818	0.9280	1
Stainless steel Precipitation (BS143)	0.9818	0.9607	0.7461	1.0000	0.5647	0.5693	0.9818	0.8775	4
Stainless steel Precipitation (BS144)	0.9818	0.9607	0.9375	0.8182	0.5647	0.5693	0.9818	0.8990	2

Using the AHP method, stainless steel FV535 appear to be overall best material for shale gas well application.

3.6 A non-weighted MCDM

Considering the irregularities and subjectivities involve in both TOPSIS and AHP approaches the non-weighted method is proposed to tackle this limitation of the two approaches. The non-weighted method is executed using the simplified flowchart shown on Figure 3.15.

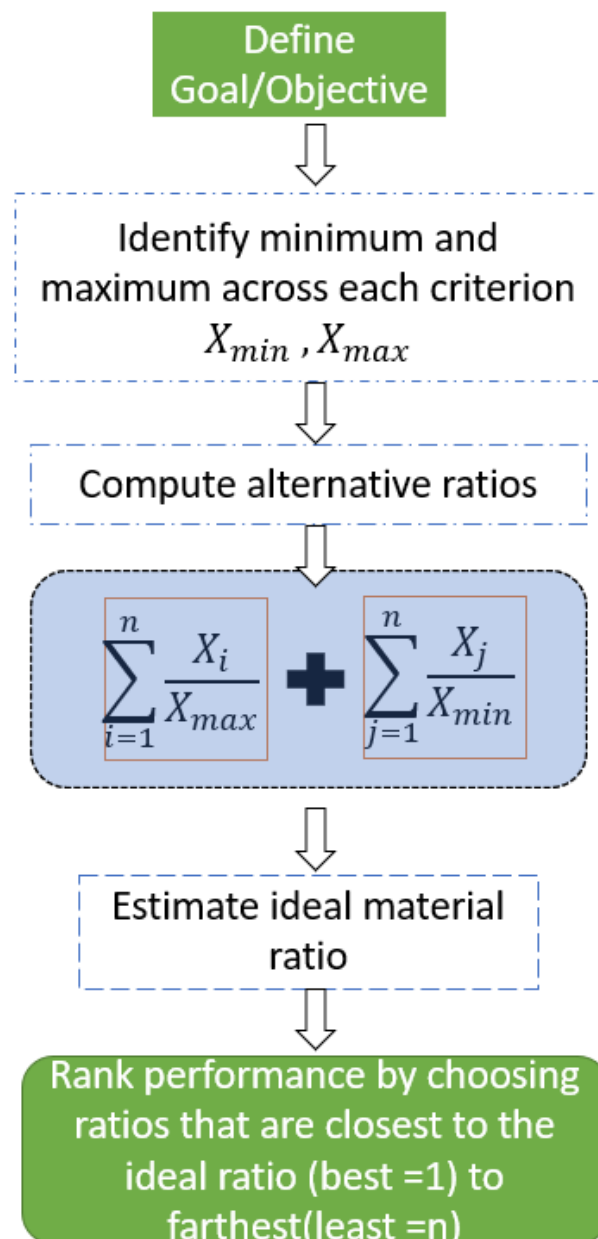


Figure 3.15 Non-weighted method of material selection.

As it can be seen on Figure 3.15 starting with defining the goal or objective, the maximum and the minimum corresponding to each criterion are identified. For whose ratio add favourably to the objective, the maximum value is utilised while for the criteria whose ratio reduced the objective, the minimum value is used. This stage similar to TOPSIS ideal best and ideal worst for multicriterial decision making process with the exception that weights are not assigned in this method. In doing so, the aggregation of the various ratios for each alternative material is computed using summation notation shown on the flowchart.

The ideal material is the material that 100% satisfy the goal or objective of the multicriteria decision making (MCDM). Obviously, this ideal material (dummy) does exist in theory – but not in practice. However, the non-weighted method tries to estimate the best material that will be as close to this ideal material.

The estimation of the 'ideal material ratio' is a dummy material whose ratio is unity (1) across all the criteria under consideration. For example, material selection that 5 selection criteria the 'ideal material ratio' is 5, for 6 criteria the ratio is 6 and for 3 criteria the ratio is 3. Therefore, the non-weight method under this particular study has 7 selection criterion and as such the ideal material ration gives 7 as shown in Table 3.11. This is computed under each criterion but search across all the alternatives to determine the best that will match the maximum such that ratio is 1. Summation of the resulting ideal ratios will guide the ranking.

The alternative ratio for each material is simply the summation of the ratios that positively add and negatively add to goal and/or objective since there is no such thing as ideal material. The ratios that positively add to the goal/objective are denoted by $\frac{X_i}{X_{max}}$ while all those ratios that negate the goal/objective are designated

by $\frac{X_j}{X_{min}}$.

The ranking comparison is simply based on choosing ratio that is closest to ideal ratio (best =1) and the farthest (least= n). The n represents the number of alternatives being considered for selection. In this way the best and the least material are rank in relation to ideal material. This is as shown in Table 3.11.

The non-weighted method avoids the subjectivity which inherent in the other two method as demonstrated in Table 3.11.

Table 3.11 Non-weighted method performance and ranking

Material	YM (GPa) <i>Hi</i>	ρ (kg/m3) <i>Lo</i>	YS (MPa) <i>Hi</i>	% Elong <i>Lo</i>	Average Cost (\$/kg) <i>Lo</i>	Service Temperature (Deg. C) <i>Hi</i>	Buckling Load (MPa) <i>Hi</i>	Ratio	Performance	Rank
Stainless Steel Duplex UNS S33207	205	7740	816	16.5	9.05	365	32158	15.8179	14.2	9
Stainless Steel (BS S145)	206	7830	1280	15	5.24	427	32315	11.70183	9.4	6
Stainless steel martensitic FV535	216	7830	1030	22	9.28	550	33884	16.98509	15.5	10
Stainless steel Precipitation FV520	216	7830	955	22	5.24	427	33884	12.00955	9.8	8
Stainless steel Precipitation FV520	216	7830	1200	18	5.24	427	33884	11.93429	9.7	7
Stainless Steel AISI 416	210	7880	820	18	1.17	750	32942	7.144274	1.4	1
Q125 Casing grade	216	7800	862	18	1.25	250	33884	6.736236	1.9	3
P110 Casing Grade	210	7800	758	15	0.929	250	32942	5.935305	3.7	5
V150 Casing Grade	220	8150	1034	18	1.16	250	34511	6.847932	1.5	2
SM 125	202	7790	862	18	0.85	250	31687	6.131413	3.4	4
Ideal Material	1	1	1	1	1	1	1	7.00		
Max	220	8150	1280	22	9.28	750	34511	16.98509		
Min	202	7740	758	15	0.85	250	31687	5.935305		

For example, the ratio of P110 casing grade is calculated: $\left(\frac{210}{220}\right) + \left(\frac{7800}{7740}\right) + \left(\frac{758}{1280}\right) + \left(\frac{15}{18}\right) \left(\frac{0.929}{0.85}\right) + \left(\frac{250}{750}\right) + \left(\frac{32942}{34511}\right) = 5.935305$

As it can be seen in Table 3.11, the overall best material is stainless steel AISI 416 using non-weighted approach with only 1.4 units from the ideal material. On the other hand, the farthest material from the ideal is stainless steel martensitic FV535 with a corresponding distance of 15.4 units.

The top ten (10) candidates are further ranked using TOPSIS, AHP and the new non-weighted method as demonstrated in this chapter. The resulting ranking is plotted to establish the relation between the methods on the alternative material selected for each technique.

Figure 3.16 shows a comparison between the TOPSIS, AHP and the new- method. As it can be seen, the TOPSIS and the new method correlate very well. Both TOPSIS and the new method select AISI 416 as the overall best material, while the AHP indicate stainless steel FV535 as the best. Overall, there is a negative relation between, the AHP and both TOPSIS and the new method. The comparison for the 10 potential candidates shows similar trend for most of the candidates based TOPSIS and the New method. However, a different prediction was observed using AHP method owing to subjectivity and Saaty's scale for assigning weights to the criteria.

The non-weighted method is a simple procedure as demonstrated on the flowchart (Figure 3.15). Its key strengths lie in the user not assigning any weights to the criteria, and the ranking is based on the closest distance as shown in Table 3.11.

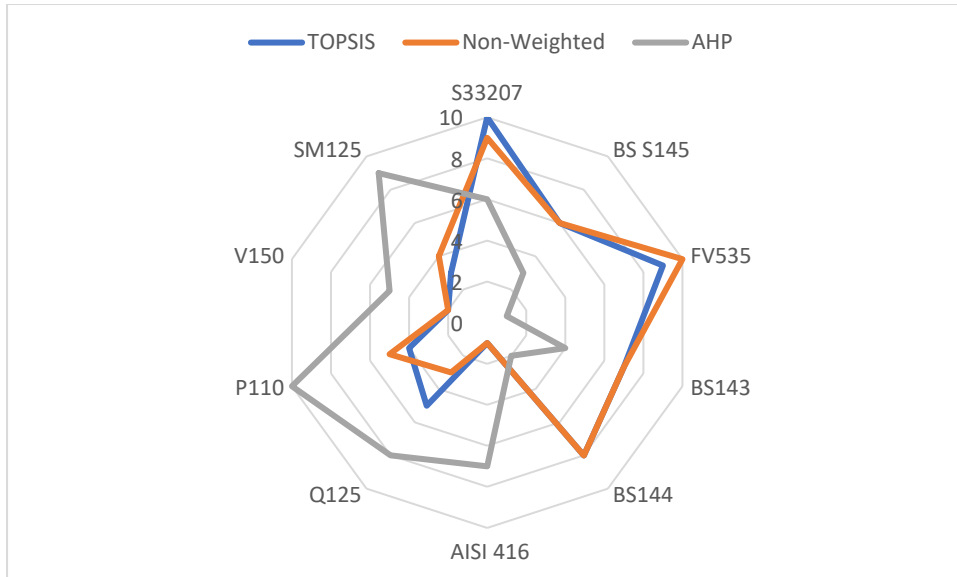


Figure 3.16 Summary of the methods

3.7 Conclusions

The material selection of steel casing was carried out for shale gas wells considering scenarios such as buckling tendencies, long term corrosion, impact and service temperature of such wells using CES Edupack and multi-criteria decision making (MCDM). Casing material selection for shale gas wells requires an additional step than the conventional selection approach to address the unusual multiple yet conflicting challenges. This additional step would to a large extent depend on the specific scenario for a particular shale gas well. It can be concluded that different scenarios will give different sets of materials as demonstrated in this chapter. The shortlisted materials using this new procedure are much more reliable both in terms of performance and MCDM- which involves TOPSIS, AHP and the new non-weighted method than the conventional method.

This approach offers enhanced assurance with regards to establishing appropriate operational boundaries based on materials properties as per performance requirements. This is especially important as there have been cases of failures of casing materials in gas wells despite the meticulous steps taken using the conventional selection methods. While the conventional approach overlooks many selection considerations and the inter-relationship between design variables – this limitation of the conventional method may have been a key factor contributing to the failures of the casing. The proposed procedure for casing material selection and analysis for downhole tubulars (pipes) performance evaluation for gas well applications is justified as presented in this chapter. Although the P110 (API casing grade) meet the first scenario, there are alternative materials that outperform it based on TOPSIS, AHP and the non-weighted method.

The overall best material based on TOPSIS is AISI 416 while the least is Stainless Steel Duplex UNS S33207. Also, the AHP selection revealed Stainless steel martensitic FV535 as the best while P110 Casing Grade is the 10th material based on this ranking. The new non- weighted method on the other hand, indicate Stainless Steel AISI 416 and Stainless steel martensitic FV535 as the 10th material. The proposed methodology can be applied in material selection to eliminate the need on assigning weights in the process of both TOPSIS and AHP.

Chapter 4: Casing Structural Evaluations, Correlations and Strength Analysis For TOPSIS, AHP and Non-Weighted

4.1 Introduction

This chapter study both linear and nonlinear buckling of P110 and BS145 to reveal the buckling load in each case. This gives a baseline idea of the structural response of the pipes without cement and formation rock. This is followed by simulation of the ten (10) top materials using ANSYS static structural to determine the structural response of these materials as an integrated system involving cement, and rock formation (shale).

The chapter benchmark the AHP, TOPSIS and non-weighted methods using finite element analysis data to further determine the ranking trend and establish correlations for these methods. Also, the chapter applied exploratory data analyses in assessing the correlation between von Mises stress, ranking, safety factor and transverse displacement. Moreover, additional analyses using matrix concatenation established the performance of AHP, TOPSIS and the non-weighted method on strength distribution and the results are presented and discussed. The significance of these analyses is to take the material selection to the next level through numerical simulation and establishing correlation between key variables and evaluation of the AHP, TOPSIS and the non-Weighted methods for strength distribution.

4.2 Methodology

4.2.1 Linear and Nonlinear Pipe Buckling

Buckling of pipe is a structural instability as established in the literature owing to applied load (Chen et al. 1990; López-Almansa et al. 2012). Buckling has also

been described as a failure mode which deforms the wall of the casing that do not extend to its centre (Wang et al.2014). When a beam is loaded in compression; sinusoidal or helical buckling may be the result, but depend largely on the beam stiffness, geometry and the applied load (Chen et al. 1989).

Two of the materials selected using ANSYS Granta selector for shale gas applications and structural steel are studied through analytical and numerical simulation to determine their buckling loads in each case. The pipe buckling structural stability is carried out for these materials under compressive load applied at one end and the other end is fixed in all degree of freedom. The justification for this boundary condition (fixed and free end) is based on Euler buckling theory and the numerical modelling of buckling in ANSYS which require columns and beams to be pre-stressed before calculating the eigen buckling load. The analytical calculation applied Euler buckling model to compute the buckling load of Structural steel, P110 and the BS145 stainless steel. The Euler Buckling equation $F = \frac{\pi^2 EI}{(KL)^2}$ and ANSYS static structural couple with eigen buckling tool in ANSYS are used to determine the linear buckling load. On the other hand, the nonlinear buckling load was computed using deformed model (geometric nonlinearity) of the linear buckling and application of sideways displacement to account for perturbation in nonlinear buckling analyses. The P110 and the BS145 are representative of the 10 selected candidates. The hand calculation and the ANSYS linear (eigenvalue buckling) are determine for these three materials and presented on Figure 4.1(a) The nonlinear buckling analysis which takes into consideration large deflection and a little perturbation (displacement) was computed using ANSYS as presented on Figure 4.1(a). Mesh density studies

conducted to verify the numerical model solution accuracy as shown on Figure 4.1(b). Based on the mesh sensitivity studies carried out it was found that 11988 elements are enough to give accurate results for this model as shown on Figure 4.1(b). The geometry of the pipe (P110 and BS145) is 114.3mm (4.5inches) inner diameter by 139.7mm (5.5inches) outer diameter respectively with a length of 4000mm.

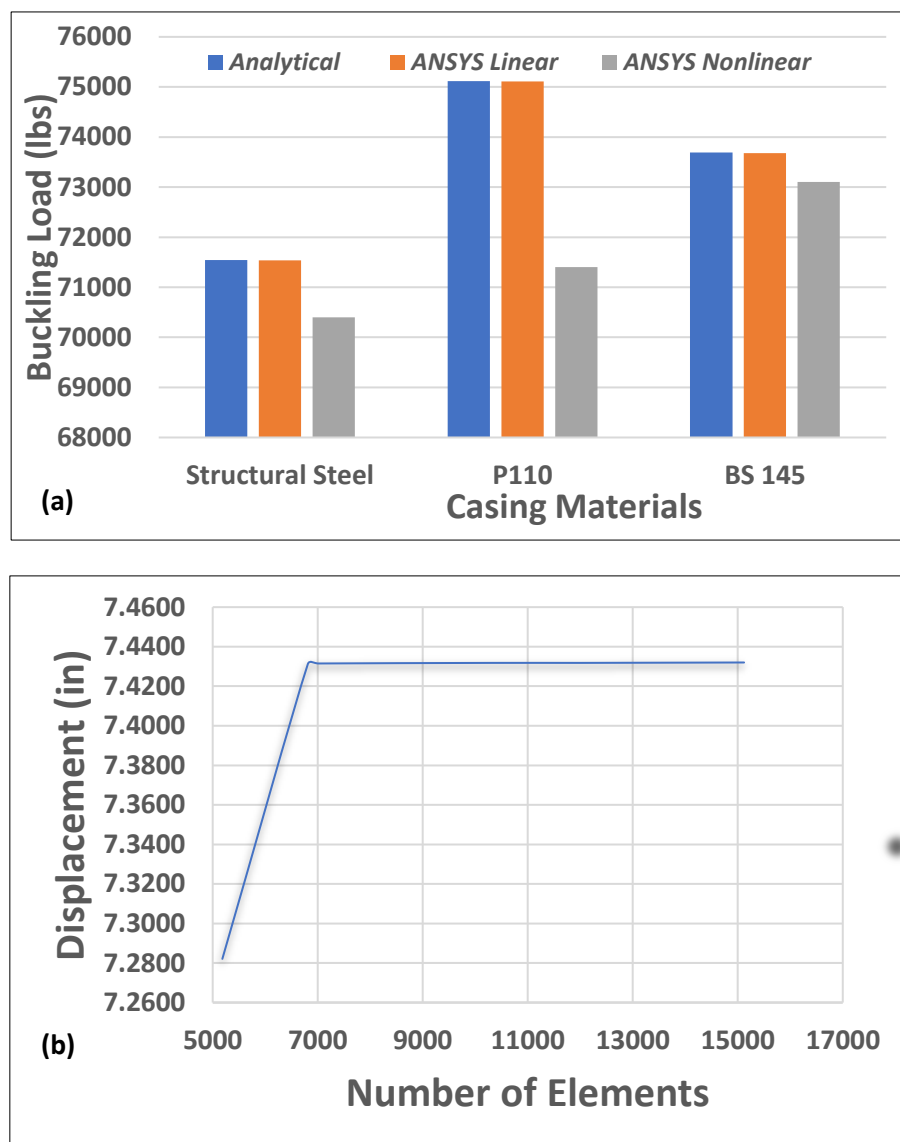
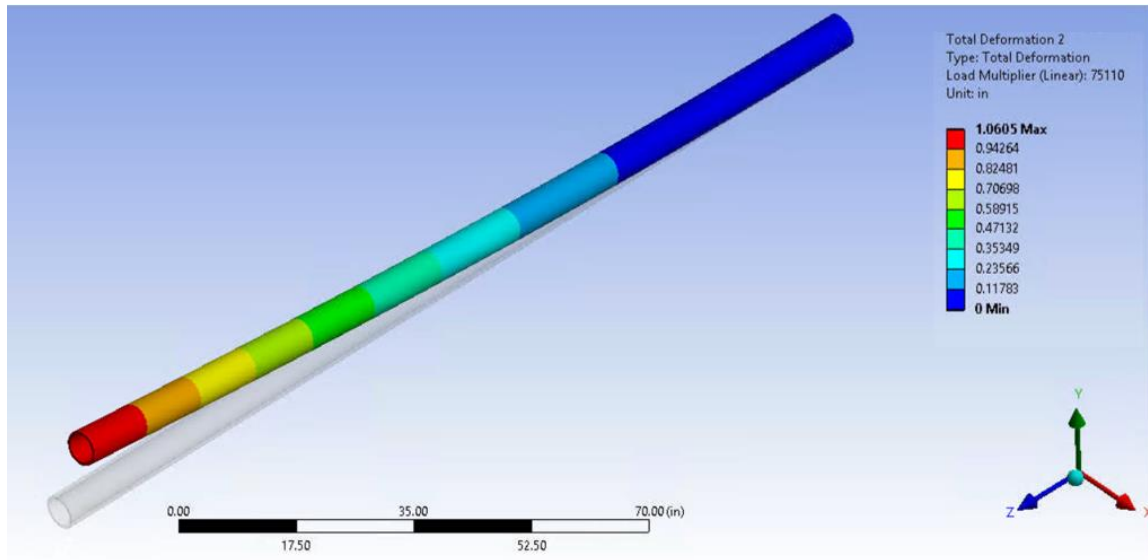


Figure 4.1(a) Buckling load for structural steel, P110 and BS 145 (b) Mesh density study for the numerical model

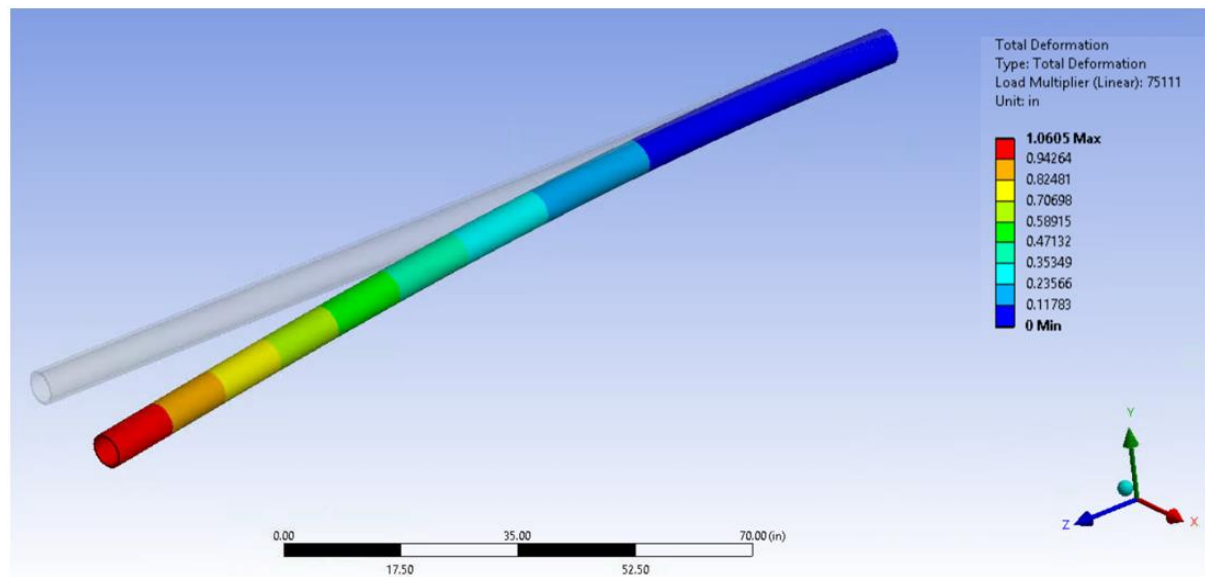
It can be seen on Figure 4.1(a) that both the analytical and ANSYS linear eigenvalue buckling are nearly the same for all the three materials. However, the results obtained for the nonlinear buckling analysis lower than the linear buckling load for structural steel, P110 and BS 145. This is due to the perturbation and/or imperfection and geometric nonlinearity that is introduced in conducting nonlinear buckling.

The linear buckling in ANSYS is performed using Static Structural and Eigenvalue buckling analysis toolkits. A unit load (1 pound) is applied in the static structural in order to obtain a trivial static solution and then eigen buckling analysis is drop onto the solution of the static structural. This makes the two analyses (Static structural and Eigenvalue buckling) to share the same mechanical outline and activate the pre- stress on in the eigenvalue buckling.

Depending on the requirement of buckling modes, one, two or three mode shapes can be scoup in an analysis and the corresponding load multiplier is displayed. For example, two modes shapes are scouped for the P110 casing materials – mode 1 and repeat mode as shown. Figure 4.2 presents eigen mode 1 and repeat mode for the P110 casing grade.



(a)



(b)

Figure 4.2 (a) P110 linear buckling mode 1 (b) P110 linear buckling repeat mode.

As it can be seen on Figure 4.2 (a) the maximum buckling load for mode 1 is 75110lbs while for repeat mode the maximum buckling load is 75111lbs. However, the computed linear buckling load in ANSYS is 75119lbs. This value (75119) is

very similar to both mode 1 and repeat mode as shown. In addition, a nonlinear buckling that consider geometric nonlinearity and large deflection reveal the P110 buckling load to be lower than the eigenvalue buckling load. The nonlinear buckling load of 71400lbs was computed which approximately represent 5% reduction from the linear buckling load.

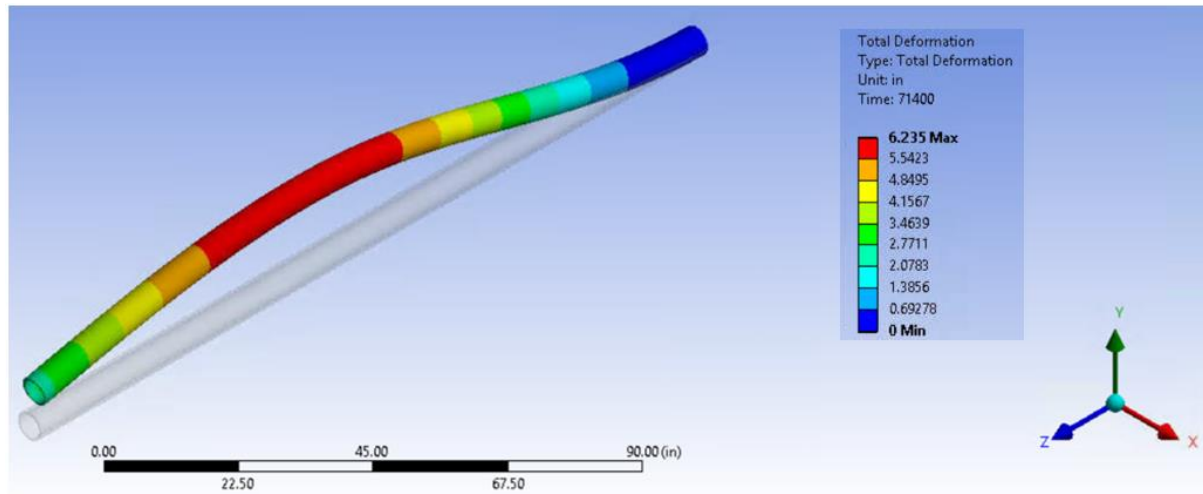


Figure 4.3 Nonlinear buckling load for P110 casing.

Based on Figure 4.3 the total transverse displacement of 6.235inches denotes the critical buckling displacement at 71400lbs buckling load. This critical displacement signifies that beyond this point plastic or permanent buckling of the pipe is the result on a 4000mm pipe.

The nonlinear buckling is computed by setting up the nonlinear analysis with time step and large deflection on and the load multiplier converted to load time step to capture the buckling point. The significance of determining the linear buckling load will give an idea on the boundary condition to be used during nonlinear buckling analysis. In similar, manner both structural steel and BS 145 stainless are simulated to determine at which point will these materials buckled. Using load

deflection chart, a simple comparison is presented between these materials showing the structural response of these materials.

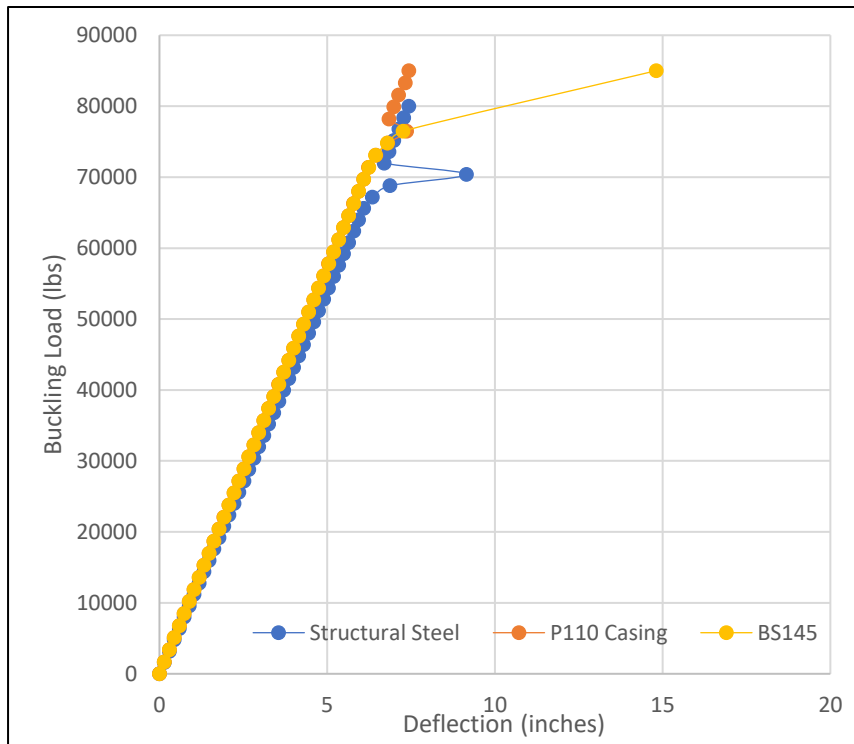


Figure 4.4 Load deflection curve showing buckling response of structural steel, BS145 stainless steel and P110 steel grade.

The eigenvalues also called bifurcation points (deviated data points on plots) denotes onset of buckling for these materials which are clearly presented on Figure 4.4. This shows BS145 to have a higher buckling load than P110 and structural steel.

4.2.2 Finite Element Modelling of 10 Material Candidates

The shortlisted materials from CES Granta Selector are further analysed through finite element analysis to determine the structural response of the casing in shale

gas well. The FEM revealed the von Mises stress, transverse displacement, and safety factor for each potential or alternative material. Using these responses, alternative materials are compared with most popular casing grade (P110) commonly applied in shale gas well development. The finite element model consists of casing, cement and the shale rock as shown on Figure 4.5. This will enable the prediction of casing structural response under a particular scenario in shale gas well.

As it can be seen in Figure 4.5 the scenario examined the casing structural response based on applied slip displacement assuming bonded relationship between, the casing, cement and shale rock (composites). Using this approach, the shortlisted materials' performance is evaluated through numerical simulation. Consequently, the materials are compared with P110 casing grade based on safety factor, stress, and displacement. The material properties for casing cement and shale rock are listed in Table 4.1. The shale rock is a square cross-section with dimension measuring 47.24 X 47.24 inches to avoid boundary effect on stress.

In order to ensure result accuracy a mesh sensitivity studies revealed 54816 computational elements and 286352 nodes are sufficient for this model. The element type chosen for this analysis is 'SOLID186'. SOLID186 is a higher order 3-Dimensional 20-node solid element that exhibits quadratic displacement behaviour. The element is defined by 20 nodes having three degrees of freedom per node: translations in the nodal x, y, and z directions. The element supports plasticity, hyperelasticity, creep, stress stiffening, large deflection, and large strain capabilities. It also has mixed formulation capability for simulating deformations

of nearly incompressible elastoplastic materials, and fully incompressible hyperelastic materials. It is used for 3-D modelling of solid structures.

Table 4.1 Material properties for the finite element model

Material	Young's Modulus (MPa)	Poisson's ratio (μ)	Yield Strength (MPa)	OD (inches)
Casing P110	210000	0.3	758	5.5
Cement	7000	0.23	-	6.625
Shale Rock	20900	0.18	-	-

In Finite Element Analysis (FEA) two or more components coming into contact or touching one another are modelled as contacts. Contact types can be bonded, no separation contact, Frictional, Frictionless and rough contact. It is necessary to specify various settings in order to achieve reliable results from contact analyses, these can be either set by the user, or program controlled – that is, determined by the FEA software. A bonded contact is assumed between casing pipe and the cement with no separation. This contact type gives a linear solution (no equilibrium iteration) is good enough to obtain an accurate solution for materials that are bonded together. It has the advantages of reaction forces are always balanced comparing with the existing one iteration Normal Lagrange solution.

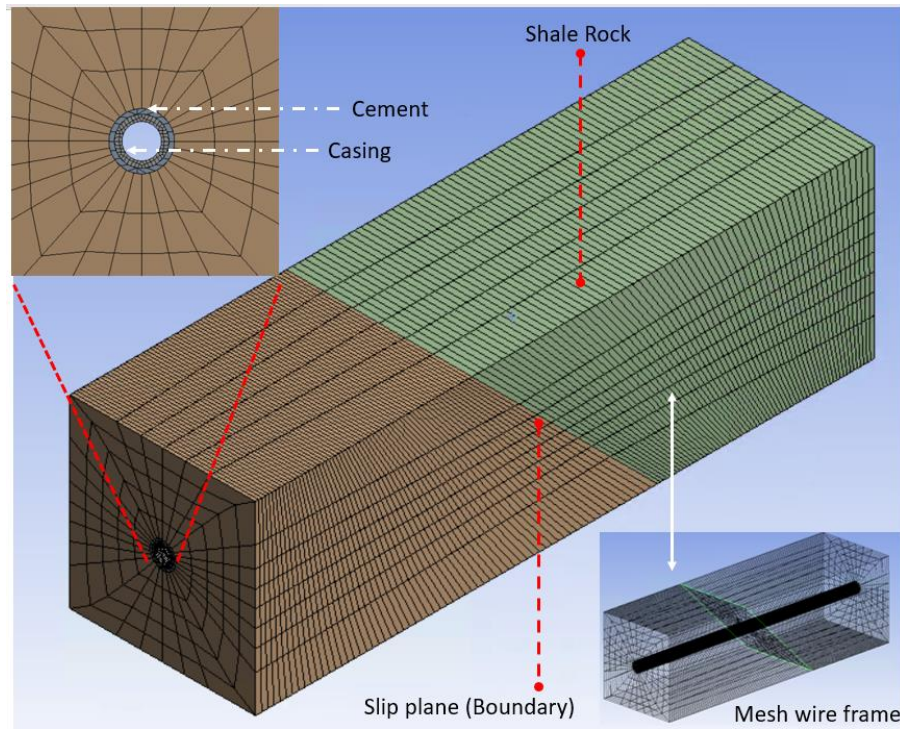


Figure 4.5 Finite element Model showing casing, cement, rock and slip plane

This analysis will enable the prediction of casing response to fracture slip displacement during hydraulic fracturing. The boundary condition is applied in such a way to replicate fracture slip traversing the well at an angle of 45° as established in the study of Lin et al. (2017). A value of 3mm for slip displacement is applied based on the recommendation of Yan et al. (2019) for moment magnitude due to microseismic in shale gas horizontal wells which is in the range of -2 to 5 on the green surface of the shale rock while the brown surface is fixed in all degree of freedom.

Table 4.2 listed the top ten material that meet the selection criteria for shale gas well application from Granta selector. It indicates pertinent material properties for the numerical simulation. The Young's Modulus varies from 202 to 220GPa, while Poisson's ration ranges from 0.3 to 0.32. The minimum value of Yield strength

from the shortlist is 758MPa and the Maximum is 1280MPa and the Tensile strength varies from 862 to 1470MPa. These properties are defined for each material in ANSYS static structural, and the 3D CAD model is meshed, boundary condition applied, and solution performed to determine the stress, displacement and safety factor in each case.

Although, the best materials are identified from Granta Selector, performance evaluation through finite element modelling will further ensure the certainty and safety of utilising these materials in a typical scenario. The shortlisted materials from CES Edupack are exported to ANSYS for structural analysis. The material properties are taken from the database while for the API and the non-API casings materials, the properties are determined from API specification 5CT and manufacturers catalogues respectively.

Table 4.2 Top ten (10) materials selected for shale wells with induced stresses.

Material	Young's Modulus (MPa)	Poisson's Ratio	Yield Strength (MPa)	Tensile Strength (MPa)
BS143	216000	0.31	955	1130
BS144	216000	0.31	1230	1330
BS145	206000	0.31	1280	1470
FV535	216000	0.31	1030	1140
AISI 416	210000	0.3	820	965
S33207	205000	0.32	816	893
Q125	216000	0.3	862	896
P110	210000	0.3	758	862
V150	220000	0.3	1034	1103
SM125	202000	0.3	862	896

4.2.3 Parameter Correlations for TOPSIS, AHP and Non-weighted Method

Correlation is a statistical technique which enable the understanding of how variables or parameters are related. This technique gives an idea on how strong a relationship is, how weak the relation, or no relationship between parameters. The correlation helps to distinguish an anomaly from an established trend or suggest an outlier. For example, the total displacement is inversely related to von Mises stress.

Initial data analysis in excel is carried out to plot the rank against alternatives materials for the TOPSIS, AHP and the non-weighted method – in order to visualise the ranking trend. Additional analysis reveals the relation between these ranking methods based on Pearson's correlation. The Pearson correlation is a type of correlation that represents the relationship between two variables that are measured on the same interval or ratio scale (Benesty et al 2009). On the other hand Pearson coefficient measure the strength of the association between two continuous variables. The Pearson coefficient is a mathematical correlation coefficient representing the relationship between two variables, denoted as X and Y. Pearson coefficients range from +1 to -1, with +1 representing a positive correlation, -1 representing a negative correlation, and 0 representing no relationship (Benesty et al 2009).

The simulation data for the von Mises, displacement, and safety factor for these materials are saved as csv files and read in 'R' using the read command. Further, 'corrplot' library is utilised in order to visualise the various correlation matrices for the TOPSIS, AHP and the non-weighted method respectively. In addition, default

settings are left unchanged, as such the method of Pearson correlation to determine the correlation between variables.

4.2.4 Matrix Concatenation for Strength Distribution

Further analysis in 'R' using the simulation data enabled the determination of strengths distribution to be computed for each method for further insight into selection methods and subsequent comparison. Matrix concatenation is the process of joining one or more matrices to make a new matrix. Therefore, for the strength distribution, this is achieved through the product of safety factor and von Mises stress matrices. This is crucial in modelling the strength distribution of these methods base on their respective rankings for strength. The libraries relevant for this plotting is the 'rgl' library. RGL is a 3D real-time rendering system for 'R'.

4.3 Results and Discussion Parameter correlation

The ranking obtained from these methods are plotted to determine the trend on all the alternative materials. The ranking obtained using TOPSIS is relatively similar to the non-weighted method. This can be seen Figure 4.7.

The 10 shortlisted materials are ranked from 1 to 10. Using exploratory data analysis 'XY' scatter plots the rank is plotted against the number of alternatives for each of the multicriteria models (TOPSIS, AHP and Non-Weighted method). The rank represents dependent variable 'Y' while the number of alternative materials represent the independent variable 'X'. For example, both TOPSIS and Non-weighted method have top rank of 10 and 9 to represent material number 1 as shown.

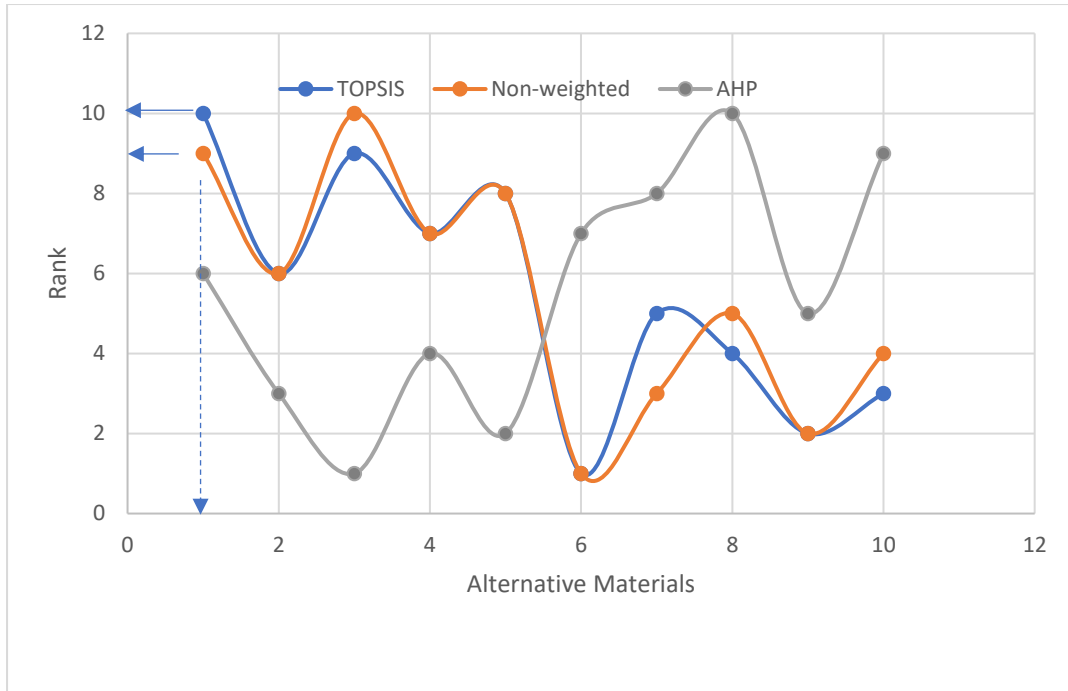


Figure 4.7 Plot of ranks against alternative materials for TOPSIS, AHP and non-weighted methods.

On the other hand, the ranking obtained for AHP method indicate an inverse relation to both the TOPSIS and the non-weighted method. Furthermore, using Pearson correlation function in excel Table 4. 3 reveal this trend. As it can be seen in Table 4.3, the correlation between TOPSIS and non-weighted is 0.95 this indicates very strong positive correlation between the two methods.

Table 4.3 Pearson's Correlation between methods.

<i>Methods</i>	<i>TOPSIS</i>	<i>Non-weighted</i>	<i>AHP</i>
TOPSIS	1	0.95	-0.58
Non-weighted	0.95	1	-0.60
AHP	-0.58	-0.60	1

However, a relatively strong but inverse correlation is obtained for the AHP in relation to both the TOPSIS and non-weighted method. This is found to be -0.58 for AHP/TOPSIS while -0.6 for the AHP/non-weighted as shown in Table 4.3.

4.4 Correlations and comparison: AHP, TOPSIS and Non-Weighted Methods

As it can be seen on Figure 4.8, safety factor is inversely (negatively) correlated to rank. While von Mises stress and transvers displacement are moderate correlation but negatively and positively correlated respectively.

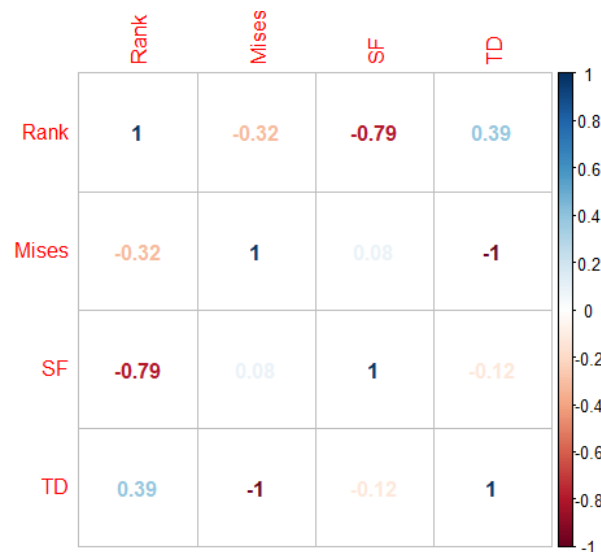


Figure 4.8 AHP ranking correlation matrix.

In similar approach, using correlation the relation between rank, von Mises stress, safety factor, and transverse displacements for the TOPSIS is performed. Using the TOPSIS ranking data, the correlation is generally weak across all the variables with the exception of von Mises to transverse displacement as shown on Figure 4.9.

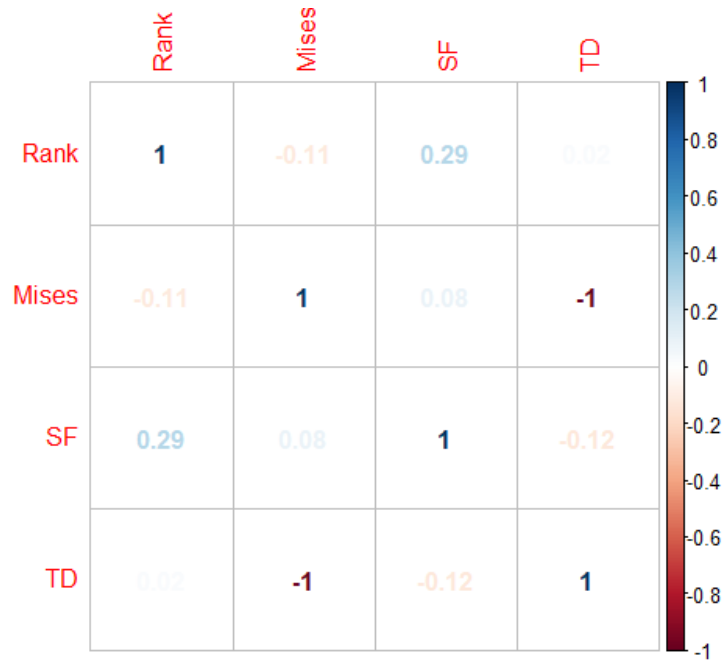


Figure 4.9 TOPSIS correlation matrix

It is interesting to point that both AHP, TOPSIS and non-weighted methods established similar correlation between von Mises stress and transverse displacement – which is negative (-1). However, unlike AHP, the TOPSIS correlation is generally weak as shown on Figure 4.9.

Furthermore, similar analysis is performed on the new non-weighted method to study the correlation between the variables. Like TOPSIS, the new non-weighted method shows weak correlation between the variables. The only exception is correlation between rank and safety factor. It is observed that the new non-weighted correlation shows similar trend with TOPSIS's correlation. For example, the correlation between rank and safety factor is 0.29 for the TOPSIS's correlation, while for the non-weighted method is 0.33. Also, it is observed that the correlation

between safety factor and transverse displacement for all the method is the same (0.12).

Based on this simple analysis, it can be said the new non-weighted do not deviate from the norm in selection and ranking materials. In addition, the new non-weighted method predicted the same correlation for von Mises and transverse displacement exactly with AHP and TOPSIS.

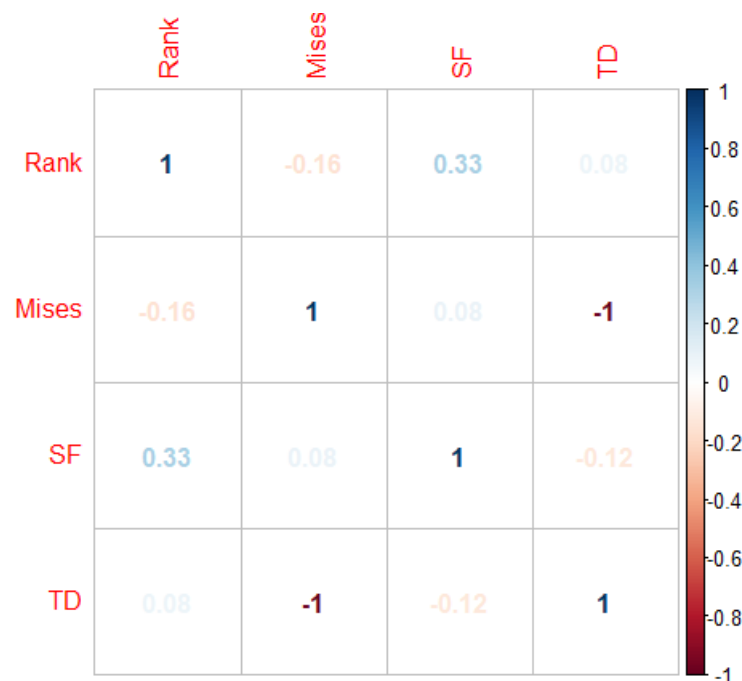


Figure 4.10 Correlation matrix non-weighted method.

The new non-weighted enjoy the advantage of no weight is applied to any criteria in the process of establishing the best alternative material.

4.5 Results and Discussion for Strength Distribution

However further analysis and matrix concatenation, data normalisation and scaling in 'R' to visualise the strength of the material based on these ranking is performed. The normalisation and scaling transform the data between 0 and 1 as

shown on the contour plots. The matrix concatenation involves the von Mises stress and safety factors – strength scale for these rankings (AHP, TOPSIS and non-weighted methods). Figure 4.11 presents a contour plot for the non-weighted method in which the strength distribution varies from 940 to 1160MPa.

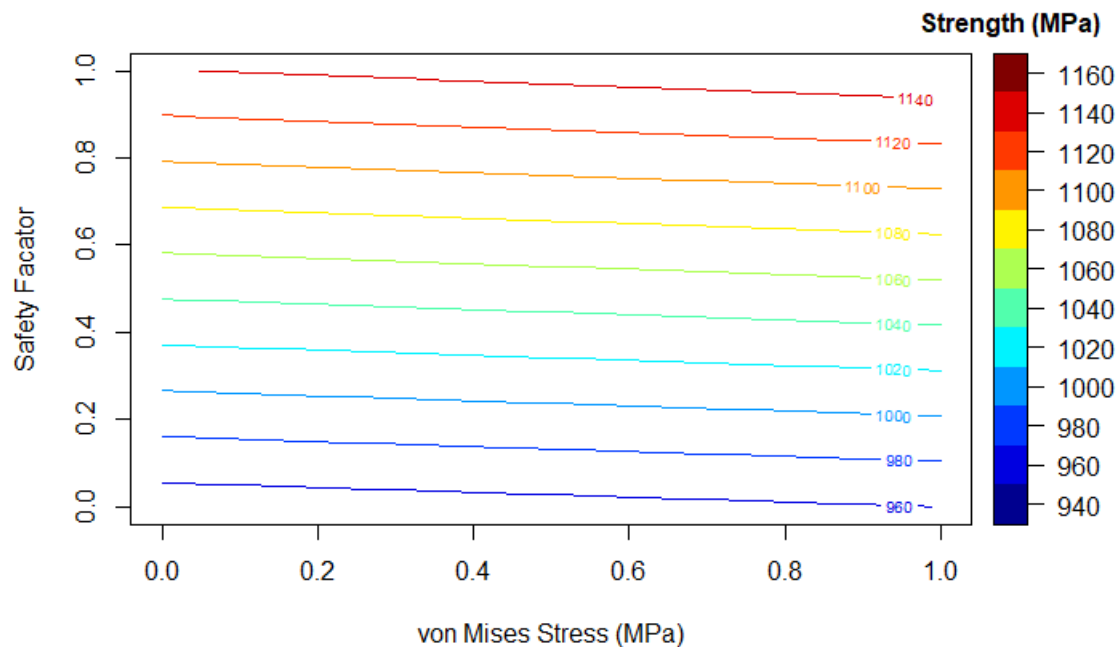


Figure 4.11 Strength distribution for non-weighted selection method.

The selection based on non-weighted is analysed to develop the contours using the safety factors and von Mises stress. The difference between the first material AISI 416 and the 10th material stainless steel FV535 for von Mises and safety factor is exploited to generate the distribution for strength. This gives a 220MPa within this interval as shown on Figure 4.11. This represents the differential stress based on the scaling and data normalisation and as shown on the scale. However, it is worthy to mention that this does not represent strength of the 10 top materials selected from the CES Edupack Granta Selector.

In similar procedure, the selection from the analytical hierarchy process (AHP) is carried out to investigate the strength distribution. Again, the difference between stainless steel FV535 and P100 casing for both safety factor and von Mises stress are explored and plotted on Figure 4.12.

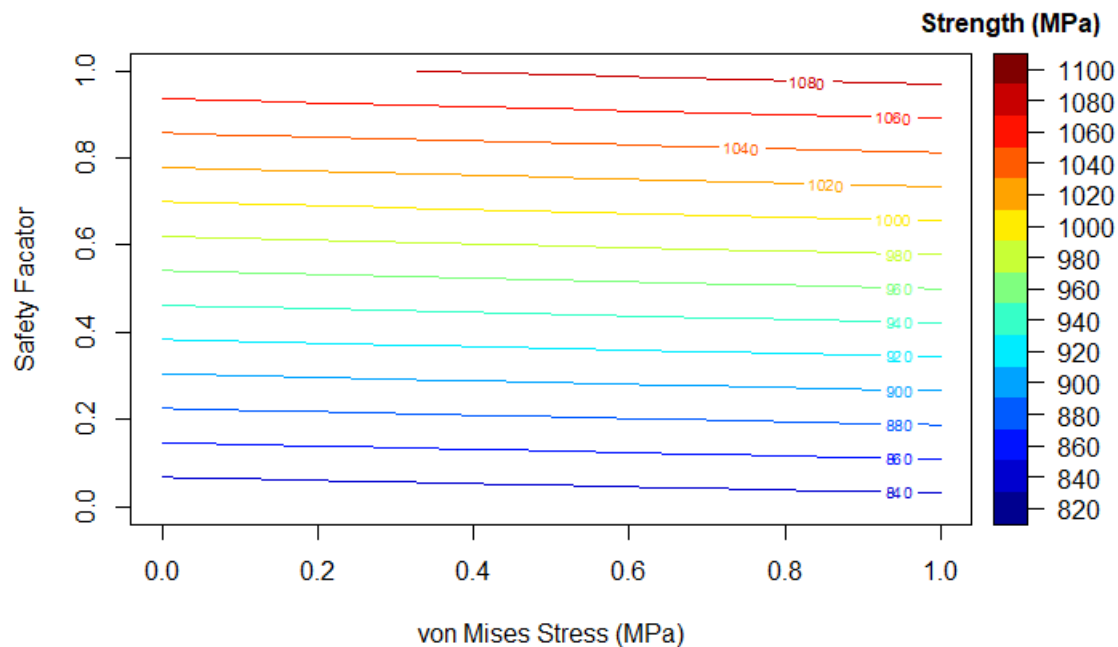


Figure 4.12 Strength distribution for the AHP selection method

As it can be seen on Figure 4.12 the strength varies from 820 to 1100MPa. This shows a slightly lower strength distribution than the non-weighted method. However, the strength distribution for the AHP is slightly higher than the non-weighted method. Unlike the non-weighted method which gives a 220MPa, the AHP gives 280MPa strength differential as shown.

Furthermore, the TOPSIS selection was analysed in similar manner to estimate the strength distribution. Figure 4.13 presents the strength contrast between the intervals. It is observed that the strength distribution for TOPSIS appears to be

unique – in that the strength differential is only 70MPa within interval for AISI 416 to S33207.

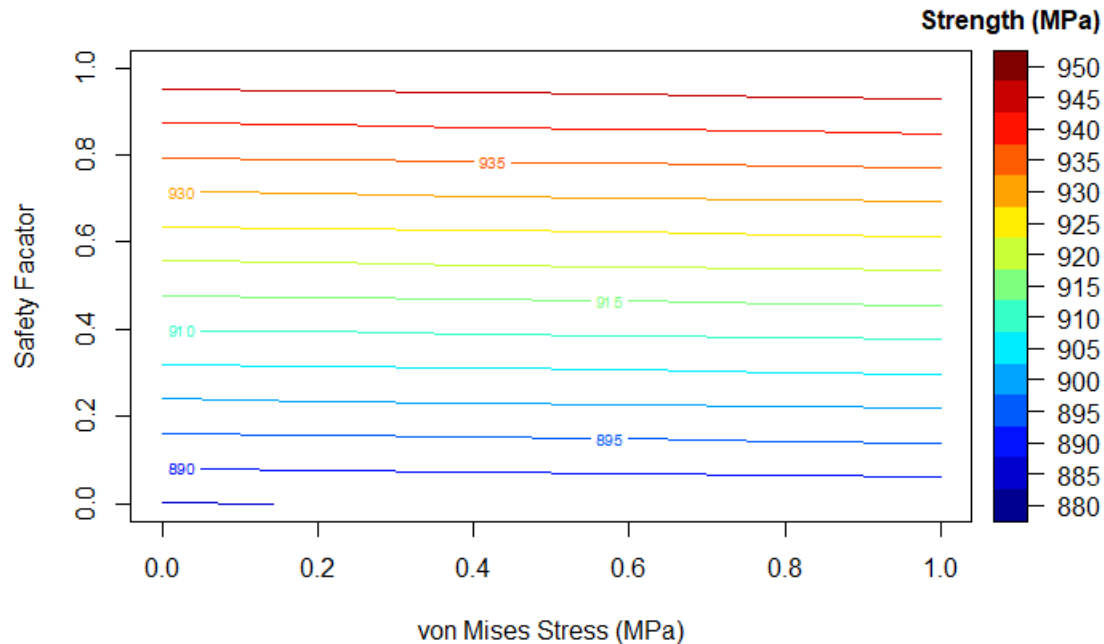


Figure 4.13 Strength distribution for TOPSIS method

Despite the low stress contrast observed in the TOPSIS method lower spectrum is higher than the AHP which 820MPa. The data analysis carried out in this section gives the respective strength distribution for these methods. Further comparison on the safety factor shows that there are alternative materials that can be used to replace the P110 or Q125 casing for shale gas well development using CES Edupack database.

As it can be seen on Figure 4.14 (green bar) which represent the stainless steel (BS145) with 2.4 safety factor while the reference material P110 (red bar) is only 1.4. Meanwhile, other alternative materials have their respective values as shown.

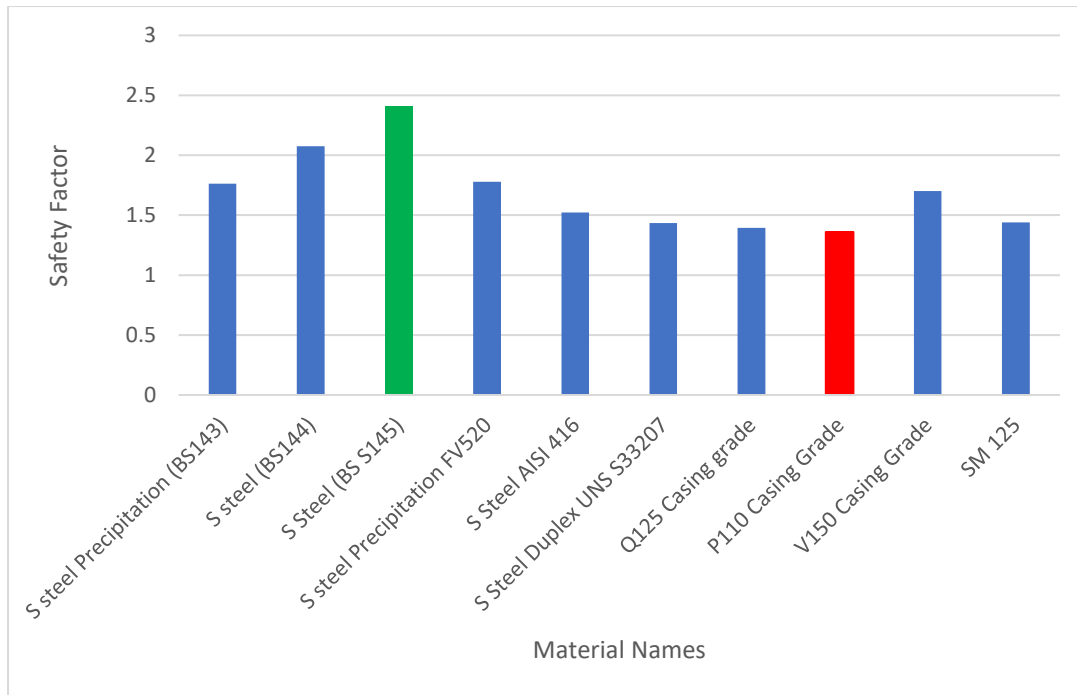


Figure 4.14 Shows safety factor for the 10 shortlisted materials as evaluated from FEM for each material.

4.6 Conclusion

The stress analysis is carried out to determine the resulting stress, displacement and safety factors for both P110 and the alternative materials for shale gas wells application under fracture slip scenario. Although, these ten (10) materials differ from each other, the simulation results obtained are relatively similar. This suggests the “expert” selection of the top 10 materials using CES GRANTA SELECTOR indicate the efficacy of each in terms of structural performances. In addition, although, there is popular usage of P110 casing grade, simulation and ranking results in this chapter shows alternative better materials in terms of safety and strength.

Chapter 5: Prediction of casing critical buckling during shale gas hydraulic fracturing

5.1 Introduction

Chapter 5 study the casing critical buckling using ANSYS parametric design language (APDL). Therefore, this chapter examined the time dependent viscoelastic property of the rock (creep) and thermal stress complexities during stimulation to quantify critical parameters on the production casing. The objective is to predict critical displacement, shear and von Mises stresses in the casing as a function of time. Using these parameters (results) and casing properties, the casing structural integrity is categorised as either elastically or plastically buckled over time. Knowledge in the stresses that will develop in the casing during fracturing under a particular circumstance is beneficial. In particular, one of the significances of this study is the results obtained from these analyses show that even without considering induce thermal loads, P110 and Q125 casing grades cannot withstand shale slip displacement of 20 mm over a 30-h period. Hence, predicting critical parameters (under creep and temperature) as a function of time during multi-stage stimulation for shale gas wells is important. This will influence the selection, design and installation of casing to optimise the process and increase success rate in shale gas horizontal wells stimulation.

The standard practice in the industry is to select, design, install, and operate the casing string based on anticipated downhole stresses using stress-check, wellcat and casing seat (Aasen and Pollard, 2003; Wu and Knauss, 2006; Liu et al., 2015) in both conventional and unconventional wells. However, this approach is limited

and cannot sufficiently address the design requirement for unconventional wells where casing –cement and formation system are bonded together with induced stresses during fracturing. Finite element analysis and numerical simulation can circumvent this limitation to predict the casing critical buckling parameters. Hence, using 2D and 3-dimensional finite element model, casing critical buckling and factors influencing it are investigated based on the simulations and analyses. In this study we examined both time dependent viscoelastic property of the rock (creep) and temperature during shale gas wells development (stimulation). Predicting the stresses and displacement that will be generated under a particular fracturing scenario in P110 casing grade is essential during this process. Ideally, a stage stimulation and tripping could simply take few hours under normal circumstance during shale gas fracturing. However, viscoelastic property of the rocks (particularly shales) can lead to a major wellbore instability such as collapse and fracture closure under creep load. This can lead to an expensive rig time of days if not weeks. Therefore, knowledge in critical parameters (under creep and temperature) as a function of time during multi-stage stimulation for shale gas wells is urgently required to further support design and installations to increase in stimulation success rate.

5.2 Theoretical background

Both in-situ and induce stresses during shale gas development contributed to casing deformation. A wellbore drilled during drilling removes rock within the subsurface formation, which distorts the initial equilibrium of in-situ stress field. The distortion in the in-situ stress is responsible for the resulting wellbore

instability problems such as tight hole, casing collapse/buckling and perforation/fracture closure (Daneshy et al., 1998).

Depending on the rock characteristics, well configuration, geometry, drilling fluids type; several wellbore stability issues could manifest. Besides, in almost all fracturing projects, high pumping pressure is required to overcome rock compressive stress particularly in a high geo-stress shale region (Xi et al., 2018). This pumping pressure and the hydrostatic pressure of the fracturing fluids intensify the distortion of the in-situ stresses-leading to a complex stress field around the wellbore (Lian et al., 2015).

As explain above, a well drilled through a rock formation introduces a new stress field at the wellbore vicinity that can be large enough to cause borehole collapse. In addition, when a wellbore is loaded with hydrostatic pressure or other pressures at underbalance/overbalance with pore fluid pressure; wellbore collapse/ 'wellbore breakdown' may be the result (Economides et al., 1998; Turon et al., 2006). Feng and Gray (2017) study established that fracture evolution could significantly change the in-situ stress near the wellbore. The direction of minimum principal stress near the hydraulic fracture path becomes parallel to the fracture, while in the area immediately ahead of the fracture tip the minimum principal stress tends to be perpendicular to the fracture. This led to a situation where the minimum horizontal stress grows without limit and cause casing lateral buckling during fracturing (Beugelsdijk et al., 2000).

A larger perforation angle may cause a longer curving fracture section and a higher breakdown pressure. This phenomenon additionally causes major structural failure of both casing, cement and surrounding formation. Wang et al. (2016) and Zhang

et al. (2010) pointed out that with arrays of hydraulic fractures along horizontal wells-stress field changes induced by hydraulic fractures can lead to fracture interference and coalescence. The resulting complex fracture geometry may compromise or improve the effectiveness of the stimulation job, depending on the nature of the context. However, Mohr's Coulomb and Drucker Prager are among applied models to study rock failure criteria in geomechanics. The Mohr's Coulomb rock failure criteria is linear estimation of the maximum uniaxial stress a rock can withstand assuming its confining pressure is zero. While the Drucker-Prager failure criterion, is a pressure dependent model in which the rock material strength is dependent on the confining pressure. This criterion was originally introduced to deal with the plastic deformation of soils (Drucker and Prager 1952).

To understand a failure mechanism, one must apply a specific and compatible failure criterion. Geo-materials, such as sandstones and consolidated shales fails in shear, while for soft material such as clays, plastic compaction dominates the failure mechanism. For example, shear failure give rise to casing and cement failure while plastic deformation and compaction may cause casing buckling and collapse. Similarly, rock tensile failure can potentially cause casing connection failure such as part and creep loading may induce permanent deformation of the casing downhole.

Assuming a homogeneous, isotropic, linearly elastic rock mass being stressed below its yield limit, a stress field expressed in polar coordinates as vertical, tangential, and radial is given by the Kirsch solution (Jaeger et al., 2009)

$$\sigma'_v = g \int_0^H \rho_b dH - \alpha p_r \quad 5.1$$

where:

ρ_b is the bulk density of the overburden layers and H is the depth.

g = Acceleration due to gravity

σ'_v = Overburden stress α = Poroelastic constant usually between 0 and 1.

p_r = Pore pressure

The radial stress is expressed as:

$$\sigma'_{rad} = \frac{1}{2}(\sigma'_{Hmax} + \sigma'_{Hmin}) \left\{ 1 - \frac{r_w^2}{r^2} \right\} + \frac{1}{2}(\sigma'_{Hmax} - \sigma'_{Hmin}) \left\{ 1 - \frac{4r_w^2}{r^2} + \frac{3r_w^2}{r^4} \right\} \cos 2\theta + \frac{r_w^2}{r^2} (p_w - p_r) \quad 5.2$$

$$\sigma'_{tan} = \frac{1}{2}(\sigma'_{Hmax} + \sigma'_{Hmin}) \left\{ 1 - \frac{r_w^2}{r^2} \right\} - \frac{1}{2}(\sigma'_{Hmax} - \sigma'_{Hmin}) \left\{ 1 + \frac{3r_w^2}{r^4} \right\} \cos 2\theta - \frac{r_w^2}{r^2} (p_w - p_r) \quad 5.3$$

where;

p_w = is the bottomhole pressure

p_r = is the reservoir pressure

θ = is the angle measured from the direction of stress at wellbore radius $r = r_w$

However, creep experimental tests on rocks under constant stress as a function of time resulted in two different displacements. That is:

$$\varepsilon_t = \varepsilon_e + \varepsilon(t) \quad 5.4$$

In addition, Munson (2004) developed a dual mechanism creep model that consider rock creep behaviour under both temperature and differential stress as:

$$\dot{\varepsilon}_r = \dot{\varepsilon}_0 \left(\frac{\sigma_{eff}}{\sigma_0} \right)^n e^{\wedge \left(\frac{Q}{RT_0} - \frac{Q}{RT} \right)} \quad 5.5$$

Where: ε_t = is the total strain due to applied load

ε_e = is the elastic strain

$\varepsilon(t)$ is the creep as a function of time which depend on the rheological properties of the rock

$\dot{\varepsilon}_0$ is the strain rate caused by steady state creep at a reference condition, σ_{eff} is the effective creep stress; σ_0 is effective stress at reference conditions. n is the exponent determine from laboratory test and Q is activation energy; R is universal gas constant, T & T_0 are the reference temperature and rock temperature respectively.

However, if one considers the loading conditions that lead to rock failure during fracturing three failure modes may result. These are rock failure in tension, shear failure under sliding and shear failure from tear. For rock failure in tension (plane strain fracture), the critical energy equals the area under the traction – separation curve as noted by Wang (2015) on Figure 5.1. This, however, can be related to rock fracture toughness according to (Melvin et al. 1985, Daneshy et al., 1998).

$$G_i^c = \frac{K_{Ic}^2}{E} (1 - \nu^2) \quad 5.6$$

Where E is Young's Modulus of the rock and ν is the rock Poisson's ratio. K_{Ic} is a material parameter known as fracture toughness to describe the resistance of the material against fracture, G is the elastic energy release rate during fracture.

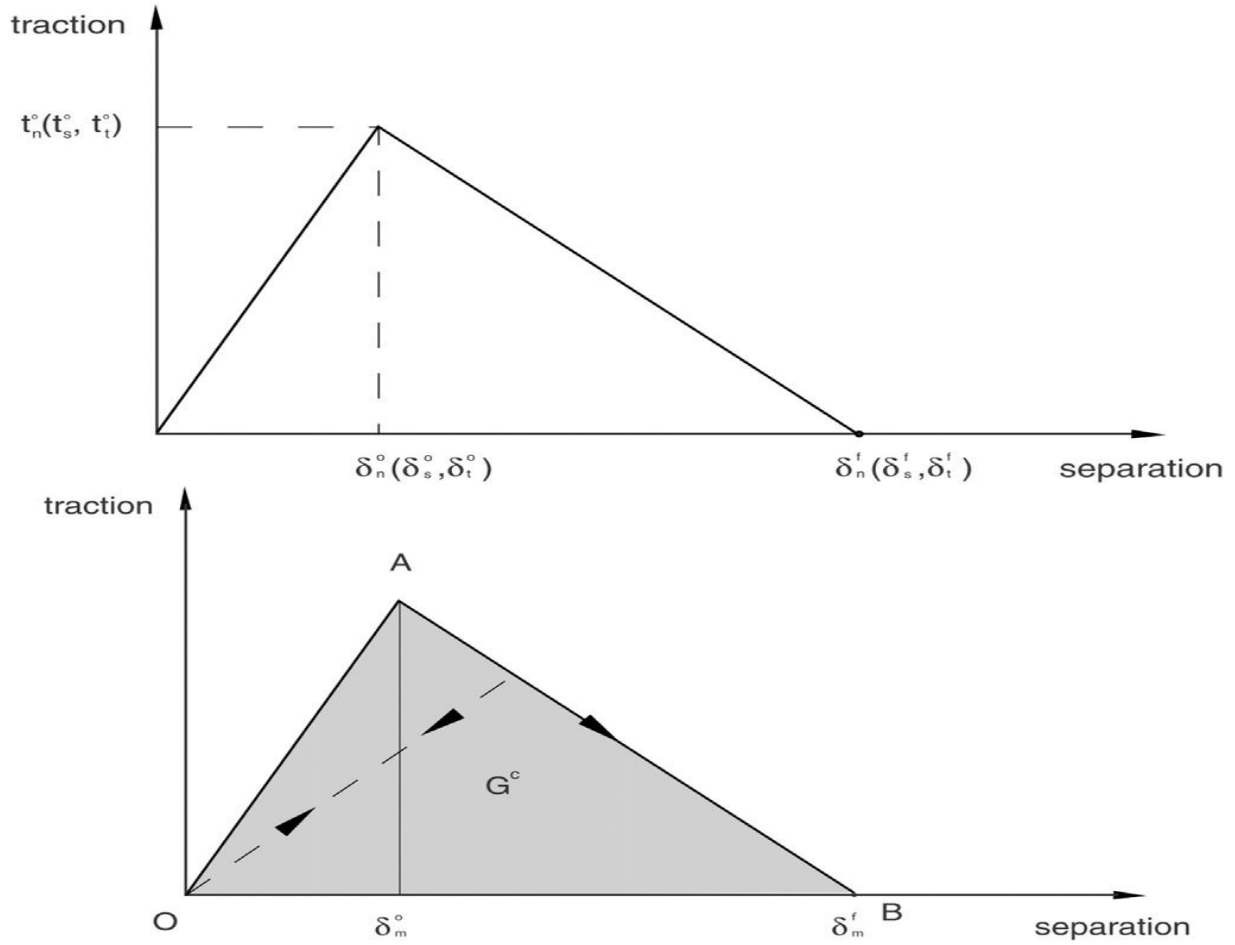


Figure 5.1 Linear traction-separation law for different modes (Wang 2015)

If any of the mentioned failure modes occur at any one instance during fracturing and the stress components reaches the maximum value in each case, the rock strength in that direction is expressed as:

$$\left\{ \frac{t_n}{t_n^0} \right\}^2 + \left\{ \frac{t_s}{t_s^0} \right\}^2 + \left\{ \frac{t_t}{t_t^0} \right\}^2 = 1 \quad 5.7$$

Where:

t_n, t_s, t_t are the normal, first and second shear stress components respectively.

In addition, t_n^0, t_s^0, t_t^0 represent the tensile strength of the rock when deformation is purely perpendicular to interface and the shear stress in the first and second

directions denoted by $\delta_n^0, \delta_s^0, \delta_t^0$ which correspond to the initial displacement and $\delta_n^f, \delta_s^f, \delta_t^f$ represent the complete failure of the rock in these three directions as shown on Figure 5.1. While the Macaulay bracket symbolised pure compressive stress that does not initiate damage to the rock.

For the steel casing, the tendency of plastic deformation depends on the radial, axial and tangential stresses. This phenomenon is essentially governed by the von Mises yield criterion; in which the casing strength is estimated by:

$$\sigma_{VME} = \sqrt{\frac{(\sigma_A - \sigma_t)^2 + (\sigma_t - \sigma_r)^2 + (\sigma_r - \sigma_A)^2}{2}} \quad 5.8$$

Plastic deformation can be estimated from yield index (YI) which is defined by:

$$YI = \frac{\sigma_m}{\sigma_y} \quad 5.9$$

Where:

σ_m Von Mises stress, σ_A , σ_t , σ_r represent the three principal stresses respectively. σ_y is the casing yield strength.

In particular, axial stress is expressed as:

$$\sigma_A = \frac{F_A}{A_{pb}} \quad 5.10$$

For radial stress two components are internal radial stress and external radial stress are:

$$\sigma_{re} = -p_e \quad 5.10a$$

Similarly for internal radial stress

$$\sigma_{ri} = -p_i \quad 5.10b$$

For external tangential stress, we have;

$$\sigma_{te} = \frac{2p_i r_i^2 - p_e (r_e^2 + r_i^2)}{r_e^2 - r_i^2} \quad 5.10c$$

Also, for internal tangential stress;

$$\sigma_{ti} = \frac{p_i (r_e^2 + r_i^2) - 2p_e r_e^2}{r_e^2 - r_i^2} \quad 5.10d$$

It should be noted that radial and tangential (hoop stress) are derived from Lamé's equation for stresses in a cylinder (Klementich and Jellison 1986). Moreover, Carslaw and Jaeger (1959) established the governing equation for heat transfer after an energy balance in solids materials.

5.3 Methodology

5.3.1 Finite element model (FEM)

The initial stress analysis is linear static in ANSYS parametric design language (APDL) v.18.1 which examines shale rock, cement and P110 as one entity. A 2D geometry was developed and consist of casing, cement and formation rock modelled using solid element (8 nodes 183) which is ideal for modelling 2D structural solids with plane strain behaviour. This element is defined by 8 nodes having two degrees of freedom at each node: translations in the nodal x and y directions.

Next, a 3D finite element model that comprises the casing, cement and shale rock was developed in ANSYS v18.1 (ANSYS parametric design language - APDL) to simulate the mechanical behaviour of casing undergoing time dependent slippage during fracturing. Mesh sensitivity was first carried out to ensure convergence and results accuracy during simulations study. A mesh sensitivity studies in FEA is a mesh size determination that ensure a numerical model solution is converged. Its significance is to ensure result accuracy and reliability. Also, mesh sensitivity assists in the decision-making process in FEA design and analysis for product development. On the other hand, mesh convergence justifies the number of elements required in a model to ensure that changing the number or mesh size does not affect the result. The FE model has total of 18414 elements as shown on

Figure 5.2. The modelling of scenario 'b' utilised 3D geometry with a 4000mm casing length. The outer diameters of casing, cement and formation rock are 127mm, 168mm and 468mm respectively. The shale rock is assumed to undergo a 20mm displacement over a 30-hour time dependent slippage during fracturing. The element type chose for this analysis is 'SOLID185'. It is used for 3-D modelling of solid structures. The front view (2D) of casing, cement and shale rock is shown on Figure 5.2 (A) below. While the finite element model (FEM) is as shown on Figure 5.2 (B).

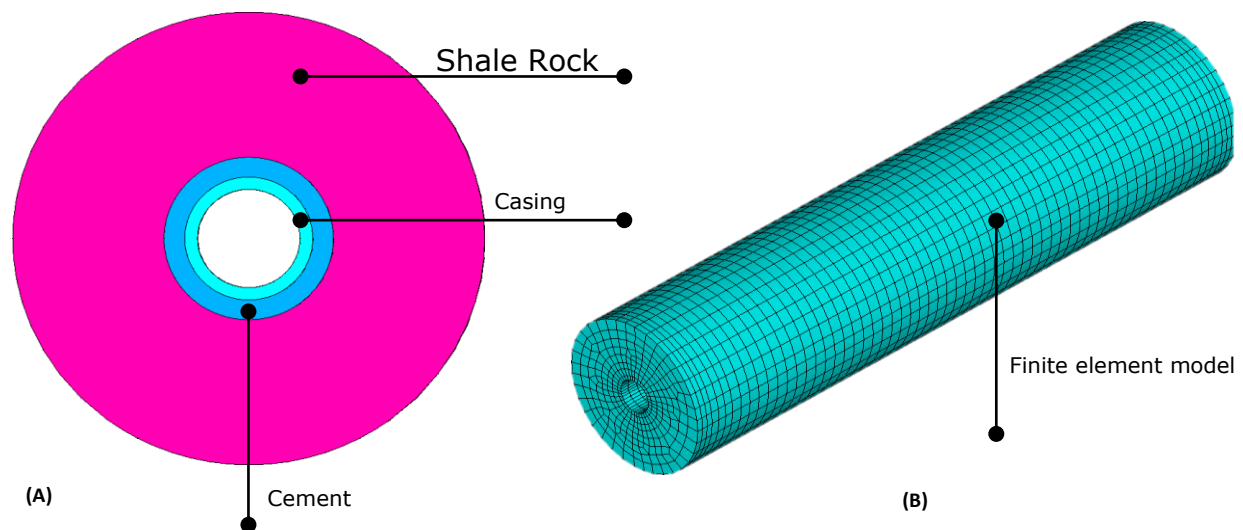


Figure 5.2(A) 2D View of casing, cement and shale rock. (B) Finite element model (FEM) with 18414 elements

It is defined by eight nodes having three degrees of freedom at each node: translations in the nodal X, Y, and Z directions. The element has plasticity, hyperelasticity, stress stiffening, creep, large deflection, and large strain capabilities. It also has mixed formulation capability for simulating deformations

of nearly incompressible elastoplastic materials, and fully incompressible hyperelastic materials.

The feature of large deflection was used in this analysis to ANSYS accounts for changes in stiffness due to changes in the shape of the parts under simulation. This gives the ability to capture the large deflection of the casing in ANSYS parametric design language (APDL) while other features of this element (solid 185) settings are left unchanged – programme controlled.

Table 5.1 Materials description and properties used in the modelling

Material	Young's Modulus (MPa)	Poisson's Ratio	Coefficient of thermal expansion (/°F)	Internal diameter (mm)
Casing P110	210000	0.3	6.9×10^{-6}	101.6
Cement	7000	0.23	9.2×10^{-6}	127
Shale rock	20900	0.18	1×10^{-5}	468

In order to build confidence on the finite element model, a 3D nonlinear finite element model was utilised based on the study performed by Yin et al. 2018 (Figure 5.3). The cuboid rock block has the dimensions of 4000mm X 1200mm X 1200 mm. A natural fracture with the dip angle α and width of Δd is created in the rock block (Figure 5.3). The rock block is divided into a static part and a mobile part (or two mobile parts). The normal displacements on the settled part surface are zero. The slip displacement of the mobile part is represented as s .

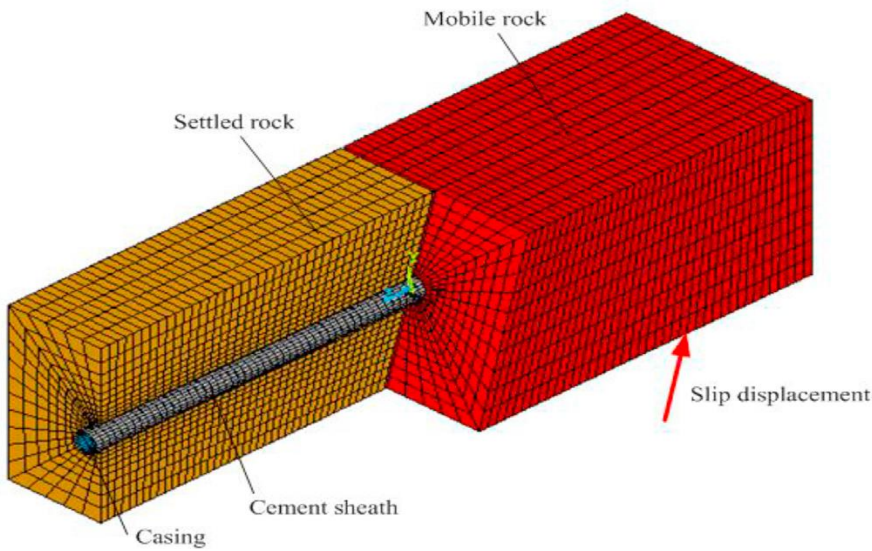


Figure 5.3 Finite element model (After Yin et al. 2018)

5.3.2 Simulation Scenarios

Two scenarios are investigated to compute the production casing's critical parameters during fracturing operations.

5.3.2 Simulation Scenario 'a'

This scenario assumed differential overburden stress owing to rock removal acts on the casing externally resulting from hydraulic fracture after a stage stimulation. The scenario examined the mechanics of a combined system (casing, cement and shale rock) to reveal how differential stress (overburden) lead to casing deformation. We also assumed the stress analysis to follow thin wall cylinder theory and the external pressure act perpendicular to the cross-sectional surface of the outer shale rock as shown on Figure 5.4 (a). Therefore, this scenario analyses P110 casing grade under different loading conditions based on casing specifications provided in Table 5. 1. 45MPa, 60Mpa, 75MPa and 90MPa are applied and the corresponding simulation performed to investigate the casing structural integrity.

5.3.3 Simulation Scenario 'b'

Scenario 'b' refers to the simulation of a time dependent formation slippage (creep) during hydraulic fracturing. Similarly, this scenario examined the mechanics of a combined system (casing, cement and formation rock) as one single entity. The linear static stress analysis on P110 casing grade predicted the critical displacements, stresses and time for such critical values to be attained. In addition, the scenario also examined the effect of static temperature on the critical parameters. The physical model of this scenario is shown on Figure 5.4 (b).

The casing was constrained in all degree of freedom to avoid rotation. Systematic investigation of the casing deformation was carried out based on casing data and slip displacements for a time dependent slippage of 30 hours. A 20mm displacement was applied on the shale rock to simulate its effect on the casing. Again, linear elastic is assumed to predict the critical displacements and stresses in the casing. Further, simulation scenario 'b', results relating to time dependent slip displacement after a stage stimulation are analysed. A representative sample of contour plots of both von Mises stress and transverse displacement along the axial length of the casing within critical time (hours) at which the casing will likely buckled was studied. A path was defined along the axial length of the casing (4000mm) and extracted data points of shear stress, transverse displacement and von Mises stresses corresponding to different times of concern.

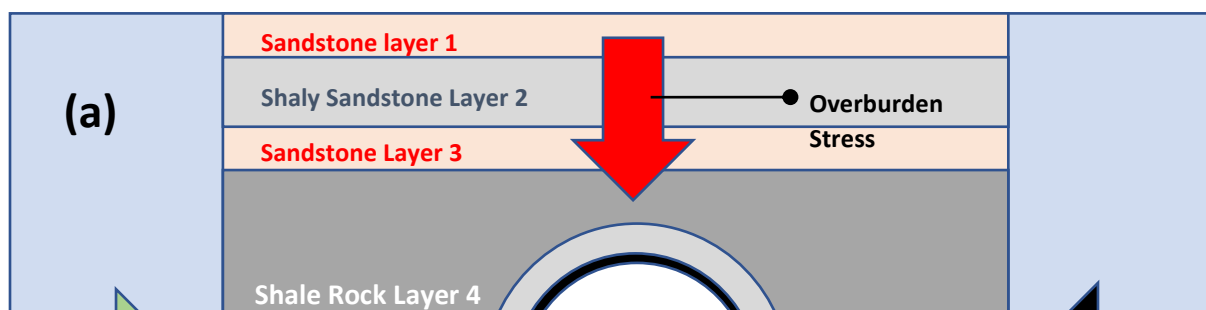


Figure 5.4 The schematics of simulation scenarios ('a' and 'b')

5.4 Results and Discussions

Although Yin et al. (2018) assumed frictional contact between shale, cement and formation rock, this study assumed bonded relationship between casing, cement and formation rock. Simulation results for lateral displacements are in good agreement as per the study of Yin et al. (2018) with less than 5% error accounting for geometric and material nonlinearity. The 5% difference between the present study and Yin et al. 2018 indicates very strong agreement and the validation of

the numerical model utilised in this chapter. These results are plotted and presented in Figure 5.5.

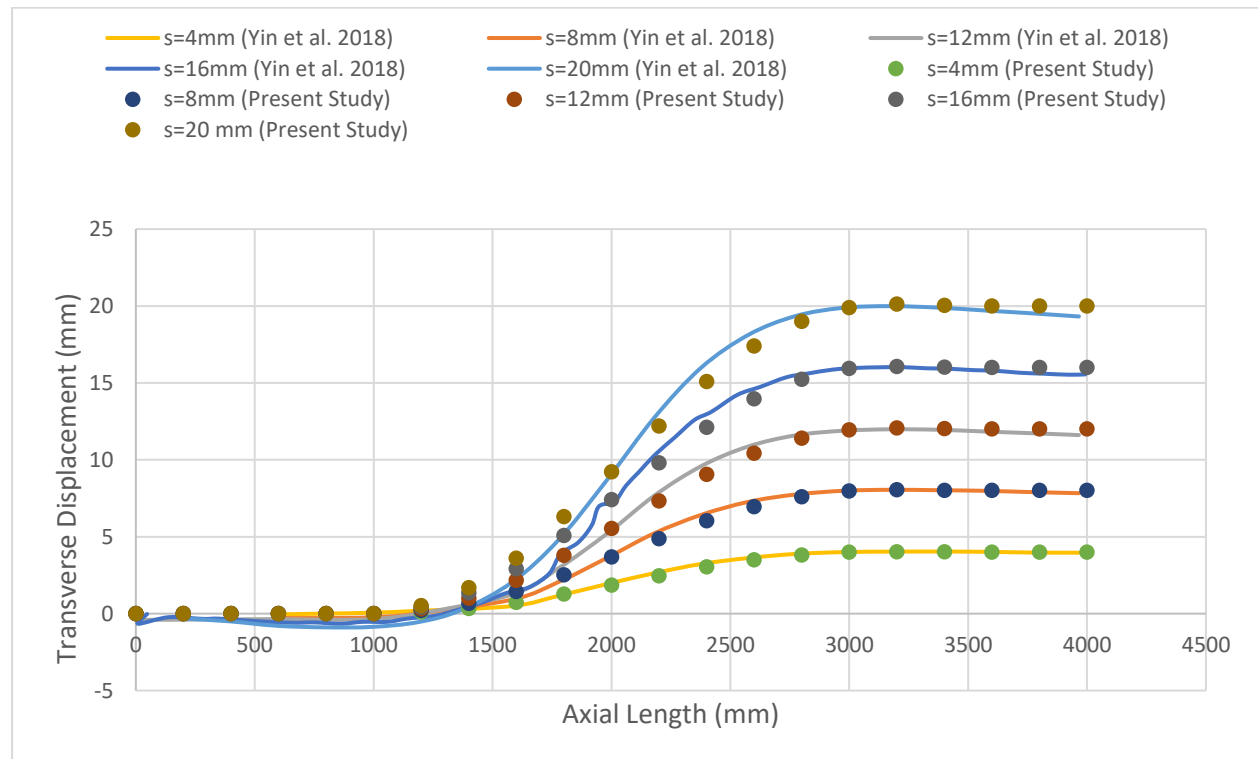


Figure 5.5 The sample result comparison for validation

The two simulation scenarios described above are examined independently. For simulation scenario 'a', radial displacements, von Mises stresses, shear stress, hoop stresses under different external loads on a defined 'circular path' of radius 115mm (appx. mid-point) through the casing thickness were investigated.

In-situ stress field could lead to a severe tangential stress (hoop stress) or even cause wellbore collapse attesting the view of (Daneshy et al., 1998; Turon et al., 2006). Also, using in-situ stress data and analyses Figure 5.6 presents the criticality of tangential stress in both vertical and horizontal wells before and after drilling. The initial tangential stress in vertical well was 48MPa before drilling and

69MPa after drilling. In contrast, the initial tangential stress in horizontal well before drilling was 48MPa. However, owing to rock removal, the tangential stress reaches a maximum of 110MPa. As seen on Figure 5.6, stress variation in horizontal well is much more severe than in vertical well due to overburden pressure. Under this situation wellbore stability becomes critical. Using equation (11), the tangential stress can be calculated as follows:

$$\sigma_{\theta} = \sigma_{Hmax} + \sigma_{hmin} - 2(\sigma_{Hmax} + \sigma_{hmin})\cos 2\theta - (P_w - \alpha P_r) \quad 5.11$$

Where, σ_{θ} = is tangential stress, σ_{Hmax} = Maximum horizontal stress, σ_{hmin} = Minimum horizontal stress, P_w = well pressure, P_r = reservoir pressure, α rock poro-elastic constant lies between 0 and 1 θ = is angle across the wellbore in tangential direction.

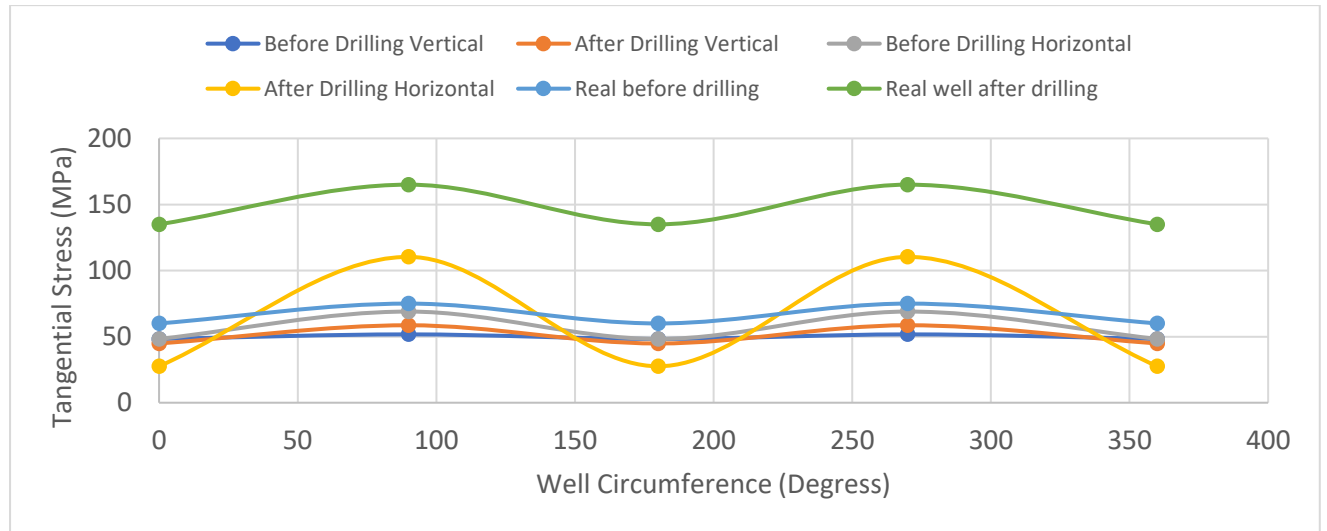


Figure 5.6 Tangential stress distribution along wells

Figure 5.7 (a and b) presents contour plots of the radial displacement and von Mises stress in the casing under 90MPa differential overburden stress. As it could be seen that the casing deforms slightly owing to external load applied. The

maximum radial displacement recorded under this loading was 0.163637mm on the high side of the casing. While the minimum occurred at the low side of the casing is 0.106×10^{-03} mm. However, this indicates that the differential stress resulting from overburden affects the casing only slightly. Moreover, the von Mises stress generated (201MPa) is below the casings' yield strength of 758 MPa. Therefore, provided the casing is centrally cemented there is low risk of its failure under the influence of differential overburden - external load. These contour plots are presented on Figure 5.7(a and b). Hence, and elastic stresses of the casing results under this circumstance.

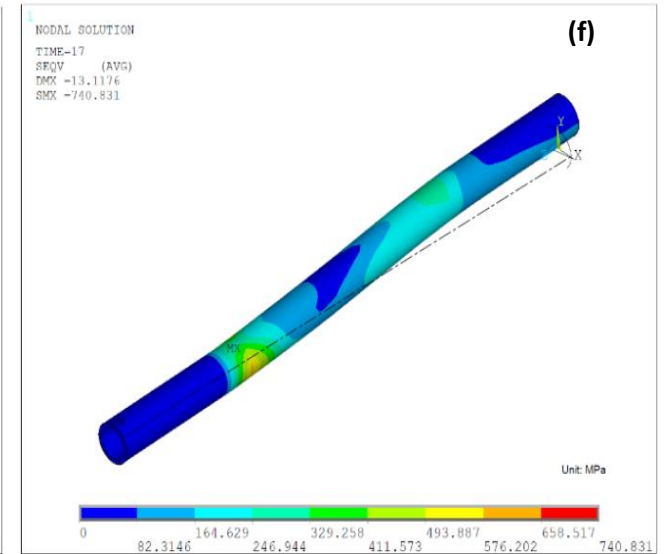
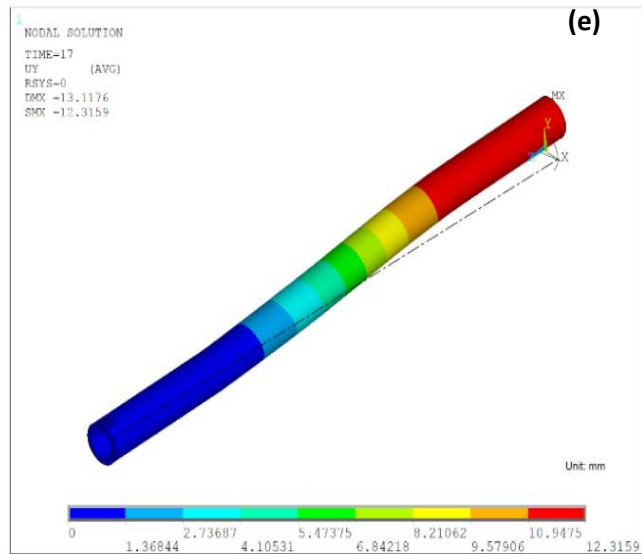
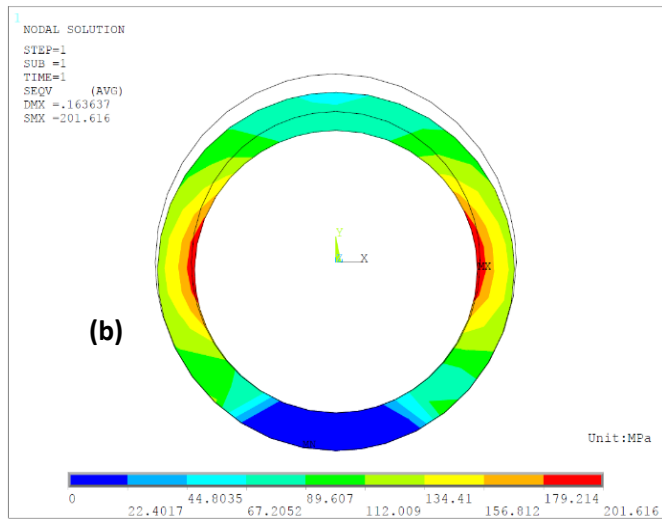
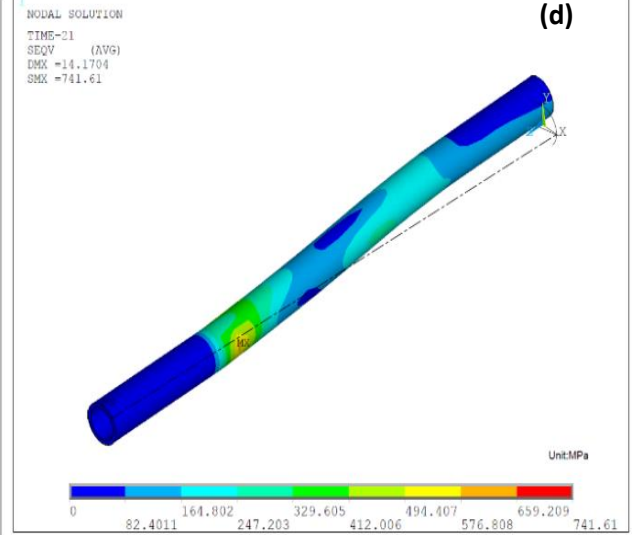
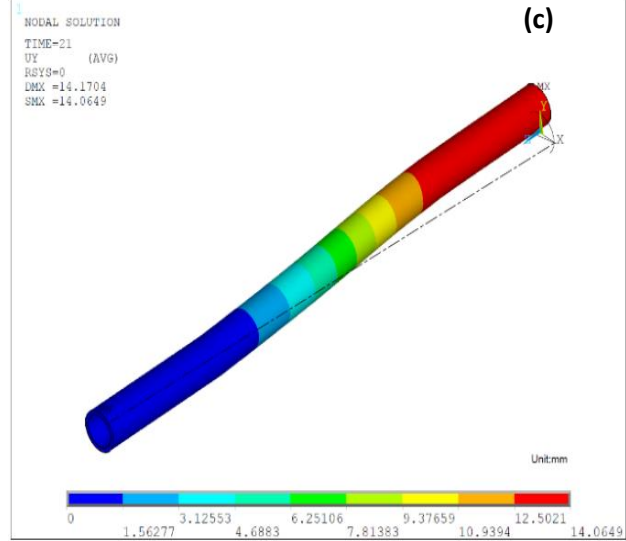
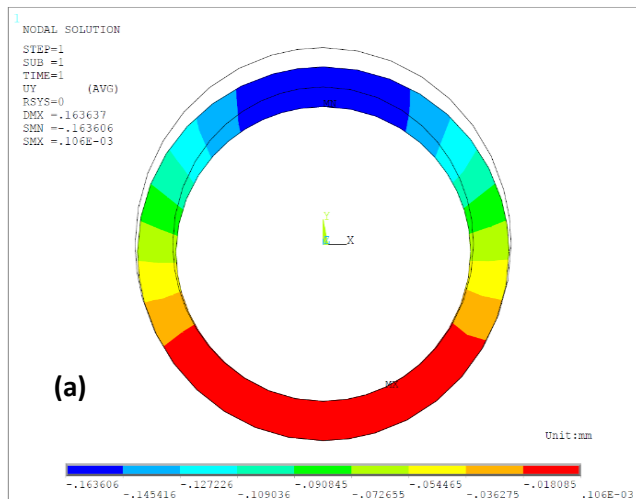
Figure 5.7 (c and d) presents a representative sample of contour plots of both critical displacement and von Mises stress. The rock failure during fracturing leads to the corresponding differentials in stress and displacements as established theoretically by (Wang et al. 2015). Hence, the rock failure leads to casing buckling depending on the stress and displacement of the rock and the orientation of the principal stresses downhole. As it can be seen, simulation result shows the critical displacement calculated is 14mm, while the corresponding critical von Mises stress is approximately 742MPa, which will be attained in the time-space of 21hours as shown. These results show the casing's critical time of buckling after a stage stimulation because 742MPa is 97.8% of the 758MPa limit for P110 casing grade.

Furthermore, under the same boundary condition, different reservoir temperatures are examined, and corresponding simulations performed. For example, at a temperature of 300°F (232°C), the displacement recorded was

13.117mm while corresponding von Mises stress is 714MPa. However, under this temperature, the time taken to reach critical displacements and stresses is reduced from 21 to 18.5hours. This represents a 11.9% reduction in time taken to reach critical load in comparison to initial simulation results. Also, when the temperature is further increased to 450°F, critical displacement and von Mises are 12.3mm and 741MPa respectively as shown on Figure 5.7 (e and f). When compared to initial simulations; temperature has caused a reduction of time taken to attain critical values from 21 to 17 hours, representing a 19% reduction. In the end, considering the complete 30 hours period, 24mm displacement and 1375MPa von Mises stress is generated under the combine loading conditions (creep and temperature). Based on this result the casing is plastically buckled and permanently failed (Figure 5.7 g & h).

5.4.1 Scenario 'a' Result Analysis

Due to the significance of hoop stress in pressure vessel design, different differential external load ranging from 45 to 90MPa are applied and simulation performed in each case. Figure 5.8(a) presents various hoop stresses along the circumference of the casing. As it can be seen fluctuating compressional stresses are generated along the casing circumference as shown. However, this fluctuating compressional stresses are inadequate to cause the casing permanent failure as shown on Figure 5.8(a-c). Although, the maximum radial stress recorded on contour plot is 201MPa, the corresponding radial stress recorded along the path was 186MPa in compression as shown on Figure 5.8(b) and similarly, the maximum von Mises on this path is 150MPa Figure 5.8(c).



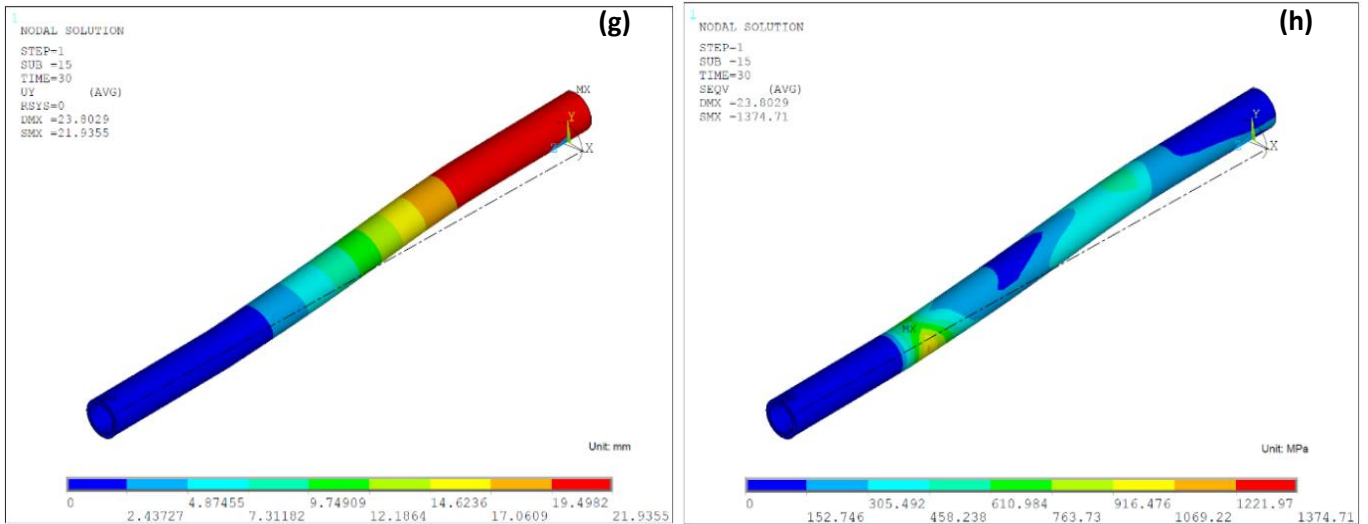


Figure 5.7 Contour plots of casing displacements and von Mises stresses

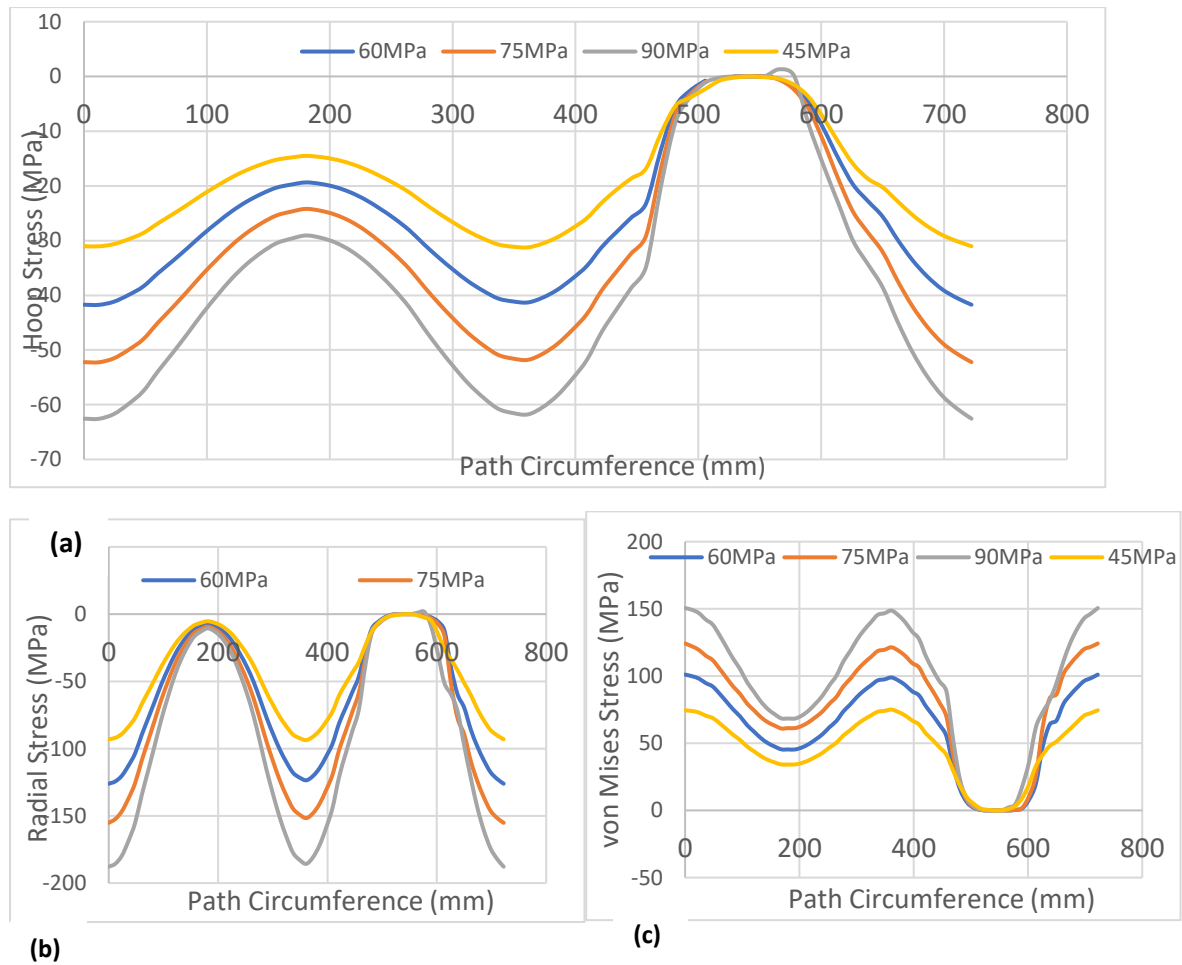


Figure 5.8 (a) Hoop stress under different differential loads (b) Radial stress along path circumference (c) von Mises stress with corresponding differential loads along path.

In addition, different radial displacement and shear stresses corresponding to these differential overburden loads are presented on Figure 5.9 (a and b) respectively. The maximum displacement occurring at high side as shown.

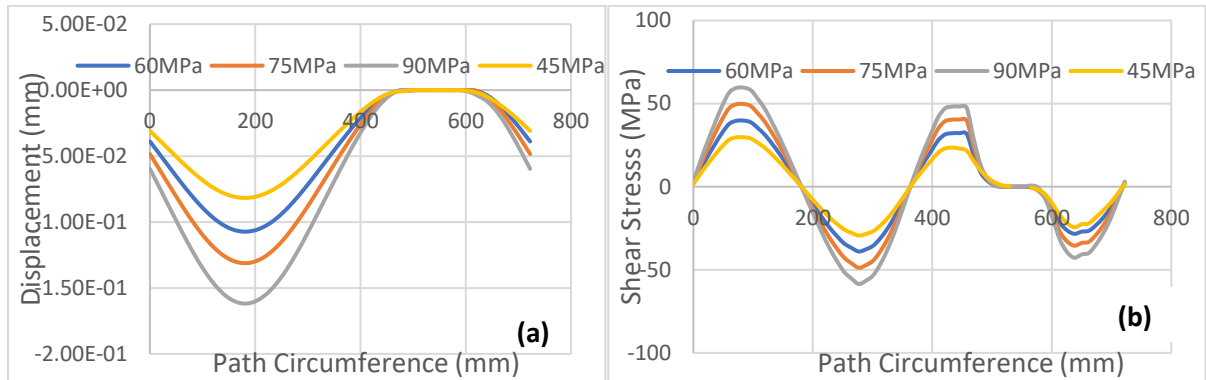


Figure 5.9 (a) Presents radial displacement (b) Shear stresses

5.4.2 Scenario 'b' Result Analysis

Even though the modelling considers formation rock, cement and the casing as one entity, however, formation rock, cement were suppressed to enable the visualisation of the innermost casing's result as it is the objective of the analysis. Furthermore, a path was created along the axial length of the casing to observe the distribution of shear stresses, displacements, von Mises within the range of 5-30 hours as shown.

Figure 5.10 (a) presents various shear stresses at five hours interval for the period simulated. This modelling scenario is transient simulation covering 30 hours in static structural. It indicates the tension and compression exists within the casing with a neutral section around the mid-point (1500-2500mm). In addition, this plot revealed that with an increase in the stimulation period, a corresponding increase in the shear stresses develops. However, the fundamental message on this plot is

that casing may plastically buckle at low shear stresses (10-15MPa) which is well below the casing yield strength of 758 MPa.

Figure 5.10 (b) presents the transverse displacement distribution along the defined path for various periods. At the axial distance of 1000mm, transverse displacement is constant because the casing is constrained in all degree of freedom. However, beyond this point, transverse displacement continues to increase with an increase in the time interval. This reaches a maximum of 20mm at the end of 30-hour period at an axial distance of 3100 to 4000mm. This should not be confused with contour plots result that predicted the critical displacement of 14mm corresponding to 21 hours slip period in Figure 5.7 (c and d). The casing will fail before the 30hour period based on the comparison with casing strength.

Figure 5.10 (c) presents mapped von Mises stresses plotted along the axial length of the casing. This plot represents 'sort' data points along the defined path. It also shows that von Mises stresses increase with an increase in displacement and period. Additionally, by using $2^{\circ}/100\text{ft}$, the corresponding deflection is calculated and plotted on Figure 5.11. As expected, the maximum deflection on the casing occurred after a 30hour displacement corresponds to 7.8° . Meanwhile, the minimum deflection computed is at 1.2° , which occurred after five hours of slippage

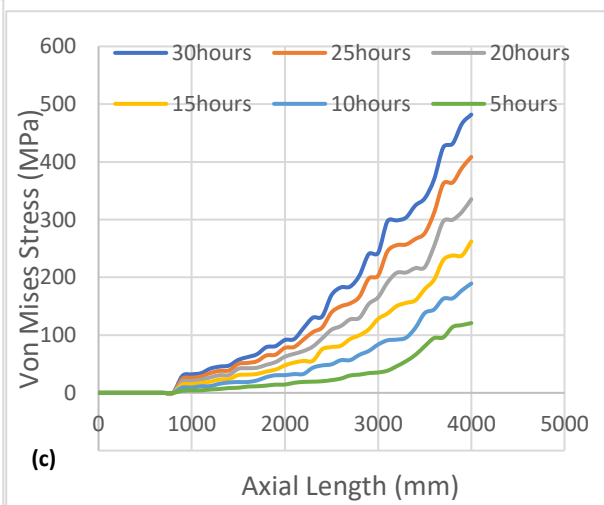
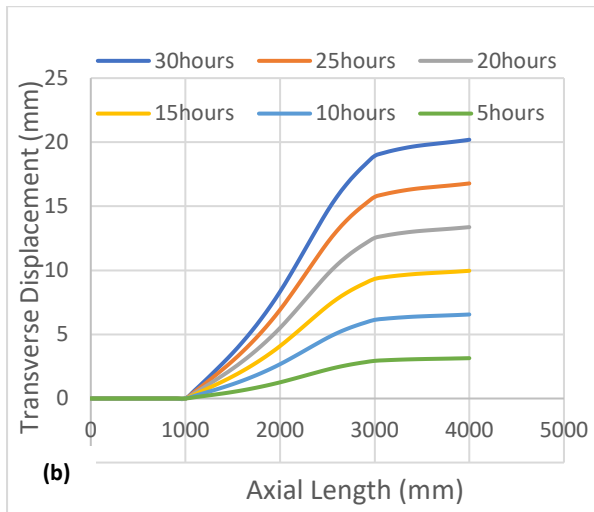
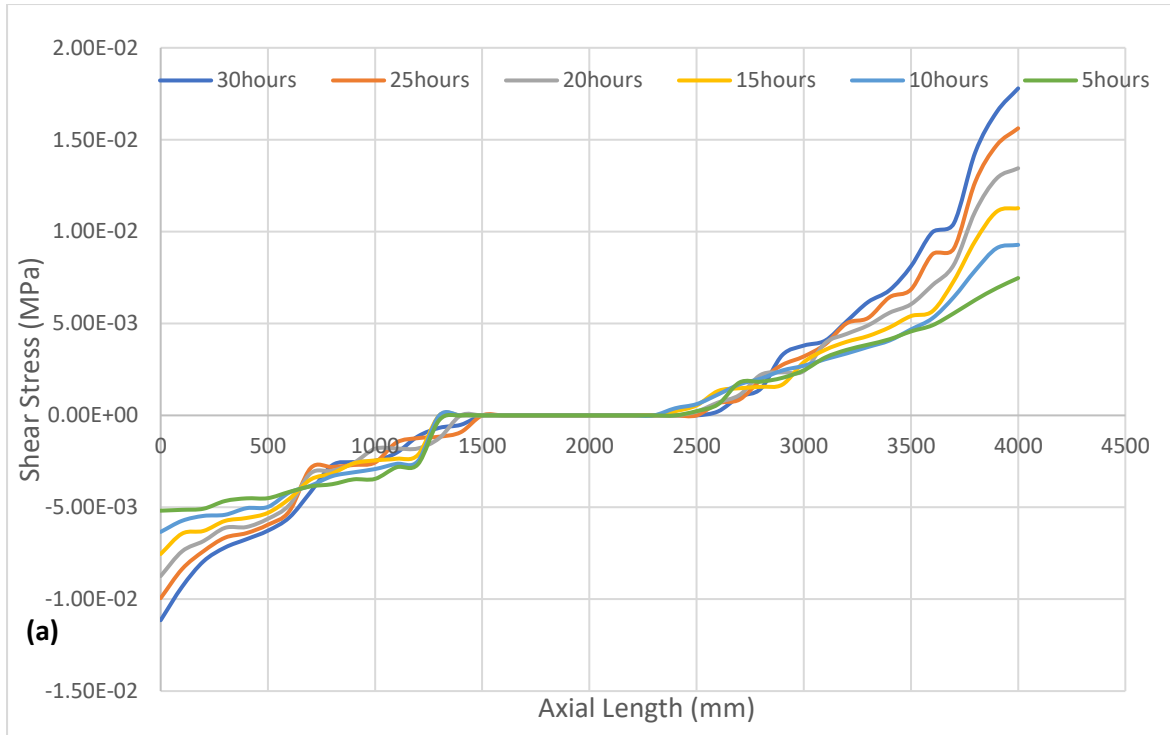


Figure 5.10 Plots of (a) Shear stress distributions along defined path at different time periods (b) Transverse displacements at various time interval and (c) 'Sort' von Mises stress distribution.

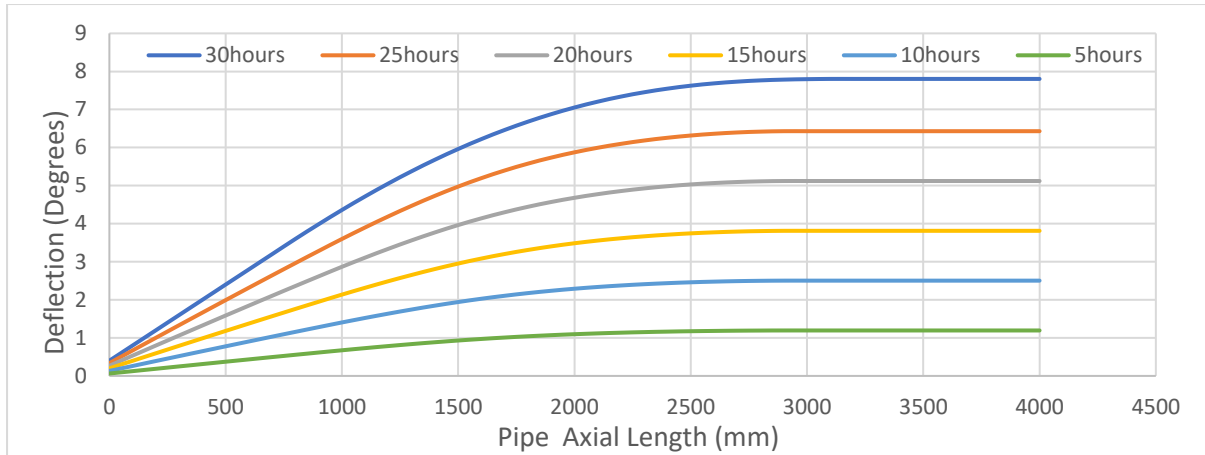


Figure 5.11 The angular deflection of casing under various slip periods.

5.5 Effect of temperature on casing performance

Using the same scenario 'a' influence of static temperature on casing under 45MPa external loading is investigated. Four different temperatures of 68, 150, 300 and 450°F are simulated to compute the incremental stress and von Mises stresses in the casing. As, expected, it was found that the increase in temperature leads to an increase in both stress and displacement as shown on Figure 5.12 respectively. The key finding here is that at a temperature of 150°F (65°C) displacement increased by 62.09%. Also, it is deduced based on this finding that higher thermal gradient would increase the magnitude of induce stress. Additionally, under these conditions of external load and thermal loads von Mises stress increased to 633 MPa from the initial 100.7 MPa. As such, under the combine influence of differential overburden stress and temperature, casing failure is highly likely. For example, at 45MPa differential load and temperature of 300°F (149°C) von Mises was 1125 MPa which is much higher than the casing yield strength of 758 MPa. It can

therefore be concluded under these combined loading conditions; both P110 and Q125 casing grade will fail plastically as shown on Figure 5.12.

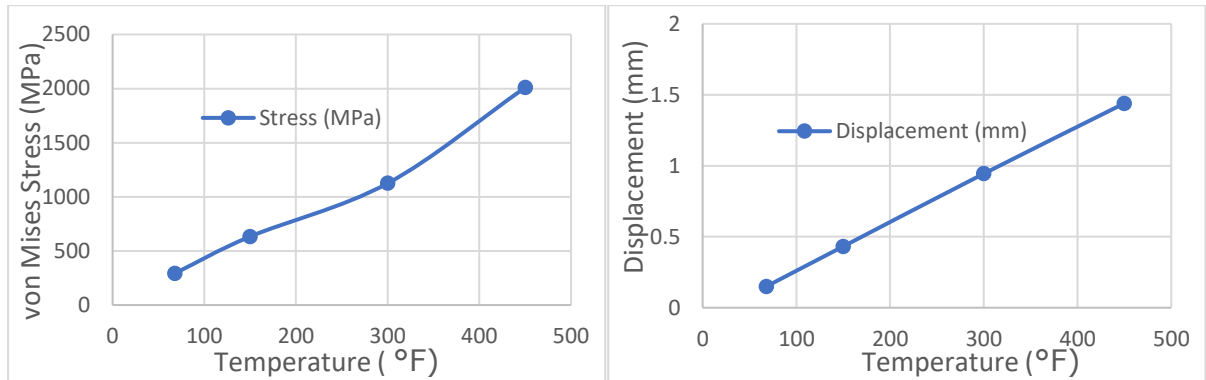


Figure 5.12 Effect of temperature on casing stress and displacement.

To understand the role of temperature on critical displacements, shear and von Mises stresses, as well as the time to attain these critical values; another simulation was conducted with P110 at temperatures of 68, 150, 300 and 450°F. Results obtained show that temperature induces additional stress and displacement thereby reducing the time taken to attain critical values. For example, at a temperature of 150°F, the critical displacement is 13.76mm with corresponding von Mises 713MPa. Furthermore, when the temperature is increased to 300°F, the displacement reduces only a little with approximate von Mises stresses of 714MPa.

Figure 5.13 (a) presents the effect of various temperature on casing strength. It indicates that the increase in temperature induces additional stress and displacement in the casing. For example, when the reservoir temperature is assumed to be 450°F, the P110 casing could not sufficiently meet the stress requirement. In addition, higher strength casing grade Q125 will only bear these

stresses below the 19-hour slip period. Beyond this time, it will fail as shown on Figure 5.13(a). As it is expected, higher temperatures lead to additional thermal loads on the casing; the critical time also reduces significantly owing to temperature increase as shown on Figure 5.13(b).

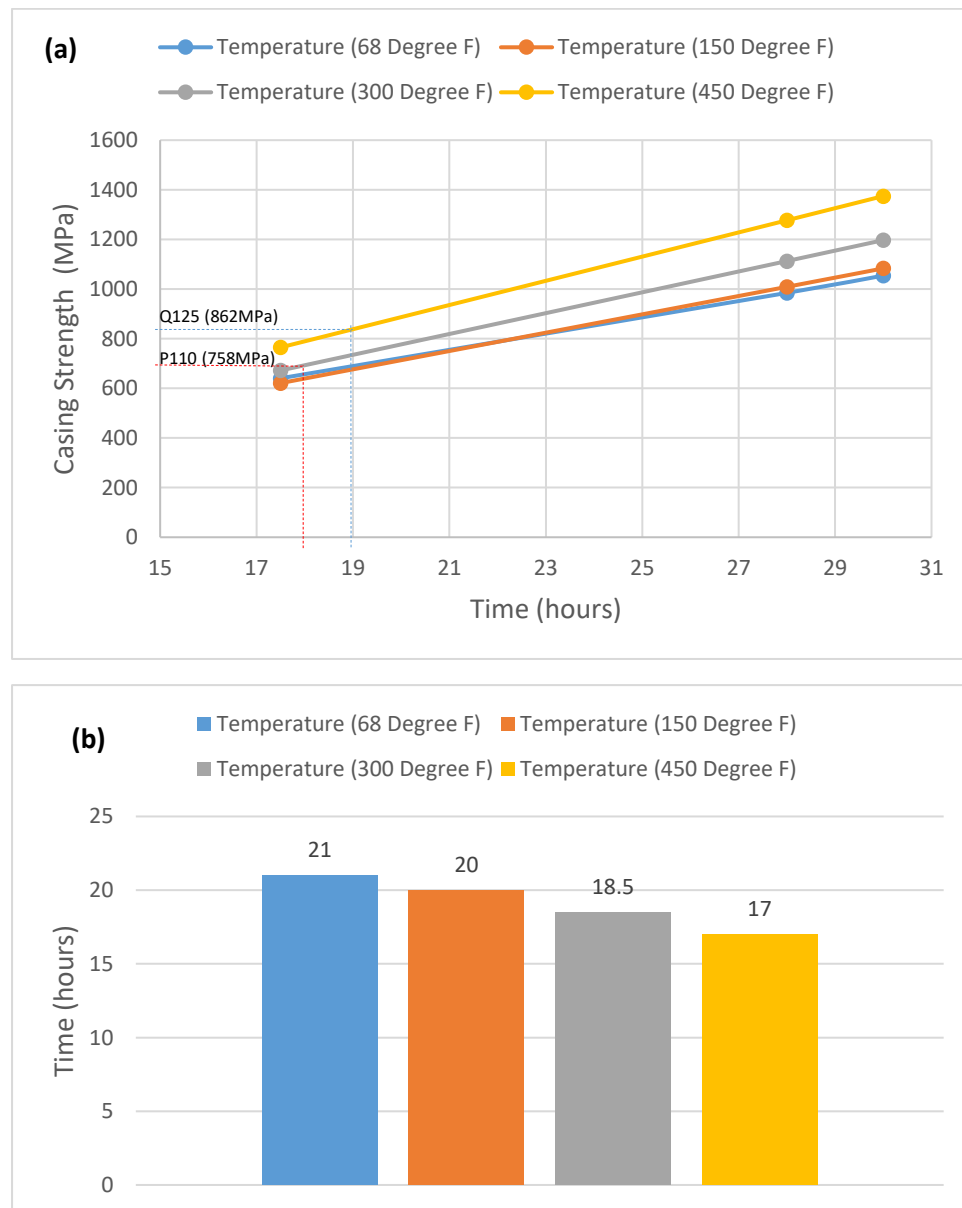


Figure 5.13 (a) Effect of temperature on casing strength as a function of time. (b) Effect of temperature on critical time to casing failure.

5.6 Conclusion

Casing failure as a function of time, temperature and constant slip displacement was simulated and critical parameters influencing casing buckling identified and quantified. Simulation results from these analyses show that even without considering induce thermal loads, P110 casing grade cannot withstand shale slip displacement of 20mm over a 30hours period. Moreover, at 14mm casing displacement, shear stresses of 10- 15 MPa developed along the defined path. This suggests that at very low shear rates casing buckling could occur.

Chapter 6: An application of Finite Element Analysis and Machine Learning for the Prediction and Optimisation of Casing Buckling and Deformation Responses in Shale Gas Wells in an In-situ Operation

6.1 Introduction

The established procedure in the design of casing for oil and gas wells involves casing grade selection and an estimation of the various loads expected to occur on the casing with some safety margin based on predicted downhole conditions of that particular well. However, this procedure is inadequate and cannot be generalised to adequately meet the design requirement for shale gas wells where casing –cement and formation rock are bonded together with induced stresses during fracturing.

The propositions in the literature are case specific and cannot be generalised to address casing buckling phenomena as noted above. Therefore, in this chapter, finite element modelling (FEM) is conducted together with design exploration using ANSYS design explorer and Lunar to determine the relationship between the main attributing parameters. In addition, using Lunar, Quasar and machine learning approaches ('R' coding), strength and weakness of the parameters that are sensitive to casing lateral buckling in the process of shale gas wells hydraulic fracturing are evaluated and optimisation performed to guide future casing selection and design strategy in shale gas well development.

As noted above, despite designing of the casing for shale gas wells, during shale gas stimulation, the interaction of hydraulic fracturing and formation geomechanics is buckling and shearing the casing leading to buckling and deformation. Hence, different finite element modelling has been conducted (see Figure 6.4 for an overview) to evaluate the structural responses of the casing in shale gas wells covering static and dynamic situations. The significance of these modelling is to

avoid the limitation of conventional design to predict the casing responses and aggregate the various scenarios of finite element modelling (FEM) for optimisation using machine learning.

6.2 The Casing Lateral Buckling/Deformation Phenomena

As pointed above, the casing lateral buckling phenomena is a combination of more than one attributing factor (Mohammed et al., 2019). The predominant factor is often depended on the casing specific failure mode. The complex interrelationship between these factors remains an engineering challenge to engineers and researchers in tackling this problem during shale gas horizontal wells development. For instance, Yu et al., (2019) presented a complicated casing buckling failure owing to in-situ stress and stress re-distribution during shale gas well development. This is presented in Figure 6.1. The stress keeps on increasing from stage 8-10 as shown. After the 10th stage, the P110 casing grade is permanently buckled reaching a maximum of 773.8MPa (Yu et al., 2019).

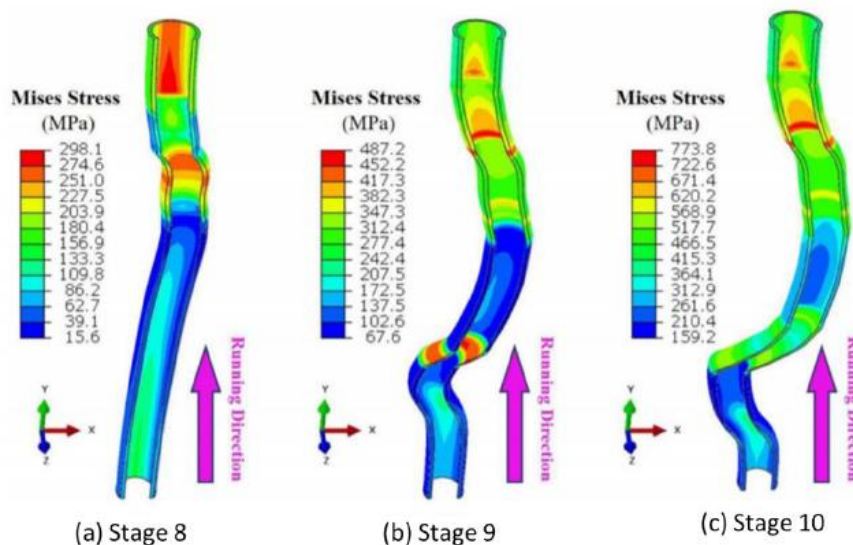


Figure 6.1: XY-1 Well: Casing buckling in shale gas horizontal well located in Sichuan Basin, China (Yu et al., 2019).

The magnitude of the microseismic moment is usually in the range of 2–4 as established by Bao and David, (2016). However, Yan et al., (2019) pointed out that exceptional microseism appeared on fault groups, indicating that the fault is activated during multistage fracturing. Further analysis into the well section that experience unique microseismic moment, corresponds to casing shear failure as shown on Figure 6.2. As it can be seen on Figure 6.2, the section of the casing associated with fault slip is buckled while the section that is not is “intact” as shown.

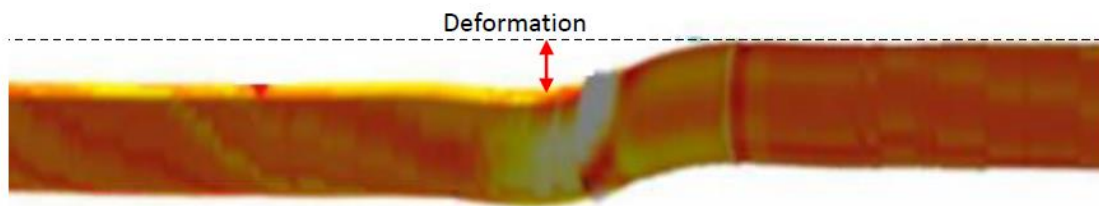


Figure 6.2 Actual casing shear deformation based on microseismic data (Yan et al. 2019).

Figure 6.3 (a and b) presents the relationships between microseismic moment magnitude, fault radius and slip distance calculated based on analysis by (Yan et al., 2019). It can be seen on Figure 6.3 (a and b) that the increase in the degree of microseismic moment magnitude, the radius and slip distance increases; with the increase of stress drop, the radius decreases, and the slip distance increases (Yan et al., 2019). Microseismic data from an actual shale gas well was used to verify the accuracy of this approach by Yan et al., (2019).

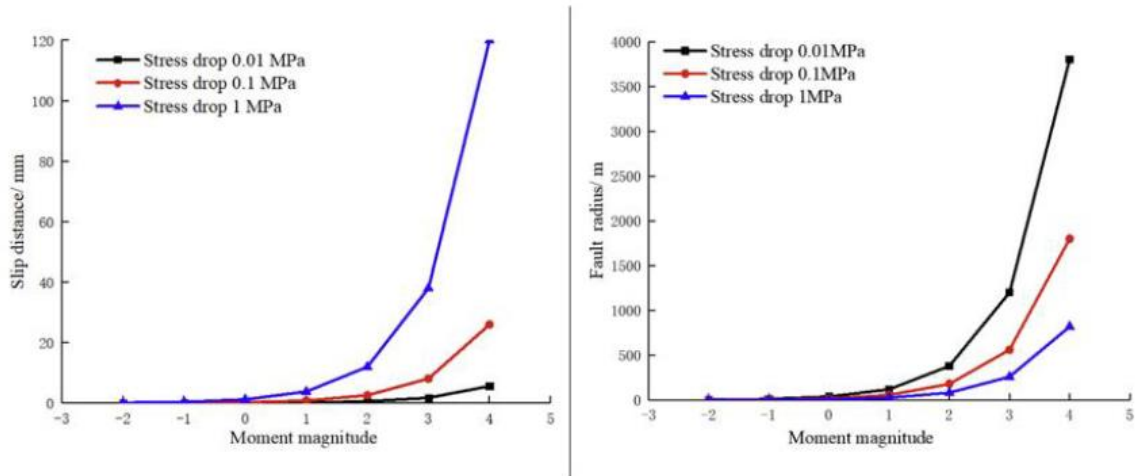


Figure 6.3 (a) Moment magnitude against slip distance (b) Moment magnitude against fault radius (Yan et al. 2019).

6.3 Methodology

The design explorer component of ANSYS Workbench could help to simplify complex designs efficiently and make more robust prediction, parameterisation and optimisation. Using “what if analysis” different designs were carried-out to study the P110 casing grade responses. The computed results are used as the basis for parameter correlation.

In addition, the local sensitivity of an input parameter relative to the output can be establish using “parameter correlation tool”. Parameter correlation tool uses Latin Hypercube sampling to ensure even distribution with no repetition of the design points. It can be used to determine what parameter matter and what do not in a design. The correlation can be positive, negative or neutral. Based on this analysis one can horn to a specific objective and/or target in the design and get rid of the attributes that do not matter without compromising the safety of the structure (casing). The initial simulation takes into consideration the influence of a combined loading of thermal and slip displacement to determine the effect of temperature

difference between surface and the downhole (reservoir). Moreover, 5mm slip displacement is assumed to occur during flowback period of 30 hours.

Figure 6.4 presents a flowchart on the research overview implemented in this chapter. As it can be seen, different independent modelling (FEM 1-3) which cover both static and dynamic conditions with multiple boundary conditions in each case was simulated. This is followed by design exploration, correlation and sensitivity analysis. This led to generation of 517 simulation scenarios as shown on Figure 6.4. Using ANSYS design explore tool, a direct optimisation is conducted, and sample result presented on page (Figures 6.13 and 6.14). On the other hand, machine learning prediction and optimisation is carried out using KNN algorithm and ODDYSSEE package.

Finite Element Modelling on Casing Buckling

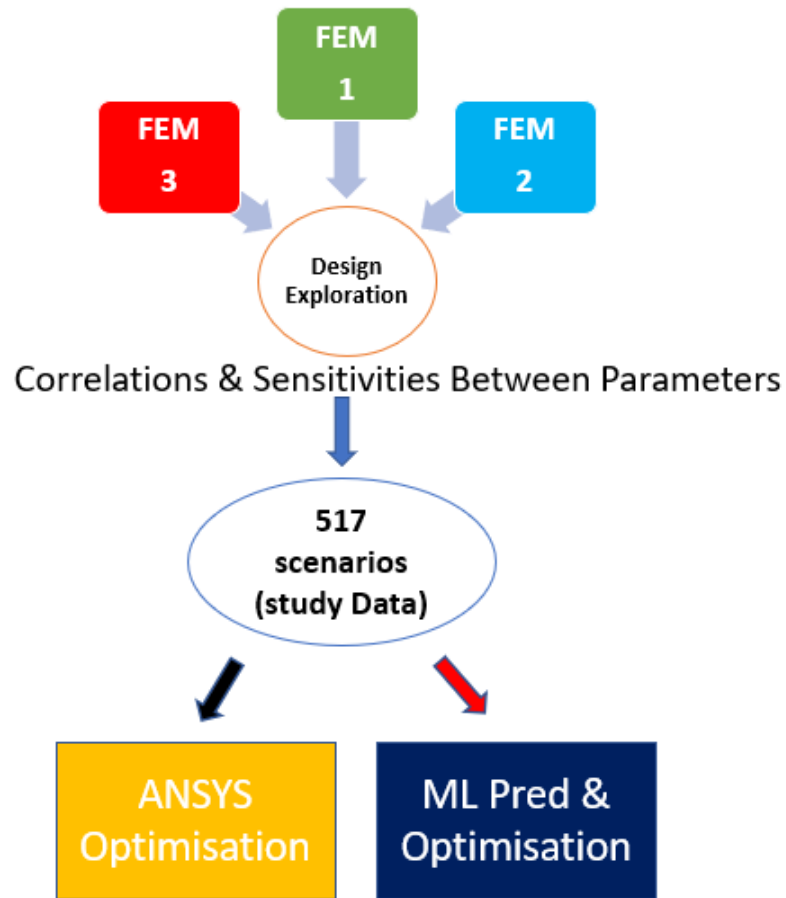


Figure 6.4 Flowchart on the overview of the study method showing top to down sequence of activities.

6.3.1 Finite Element Modelling (FEM)

The numerical modelling in this study is an advancement of the previous work by Mohammed et al. (2020). The objective is to predict critical displacement, von Mises stresses and the applicable safety factor in order to establish robust design for the casing as a function of hole diameter, cement mechanical properties (Elastic modulus and Poisson's ratio), surface and downhole temperatures, slip plane angle and casing geometry.

The 3D computed aided design (CAD) models comprises of the casing, cement and shale rock is shown on Figure 6.5. As it can be seen, the shale rock is distinctively separated by the slip plane. The shale rock has a square cross-section with a dimension of 599.95mm to avoid boundary effect on stress and displacement.

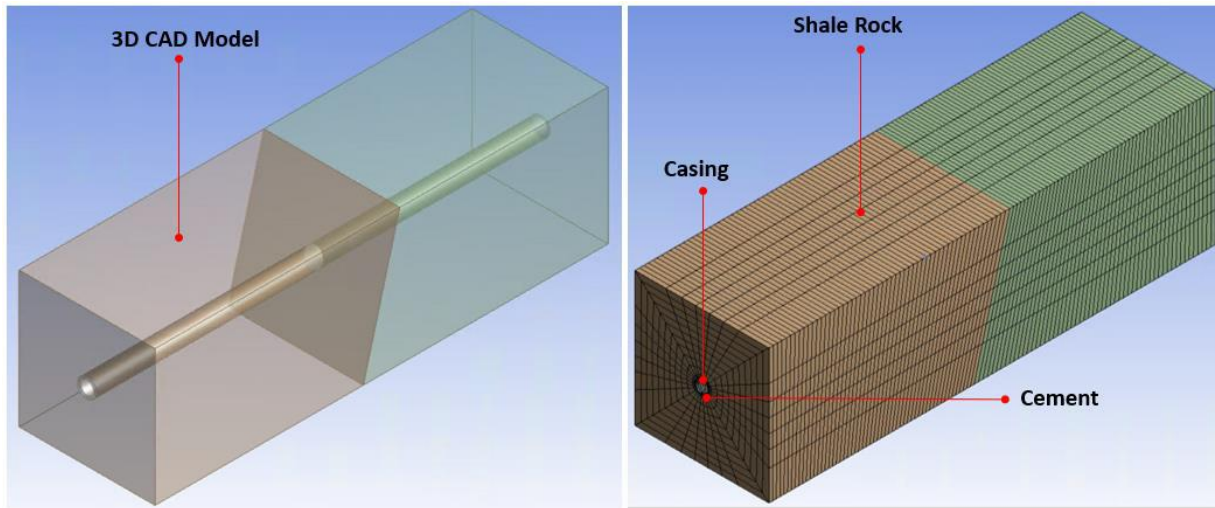


Figure 6.5 3D CAD and Mesh Models showing casing, cement and shale rock

The element type chosen for this analysis is 'SOLID186'. This is a higher order 3D, element which exhibit quadratic displacement behaviour. This element supports plasticity, large deflection and strains with mixed formulation capabilities for simulating deformations in layered and homogenous solid materials.

The material properties for the casing, cement and the shale rock for the initial simulation scenario are presented in Table 6.1.

Table 6.1 Casing, cement and rock material properties.

Materials	Elastic Modulus (MPa)	Poisson's Ratio (μ)	Coefficient of Thermal Expansion ($^{\circ}/C$)	Casing Outer Diameter (mm)
P110 Casing Grade	210000	0.3	6.9×10^{-6}	139.9
Cement	7000	0.23	9.2×10^{-6}	168.275
Shale Rock	20900	0.18	1×10^{-5}	-

A bonded relationship is established between the casing, cement and the rock formation to mimic -rock- cement-casing bonding and to simulate casing structural response under this situation. Buckling under thermal loading with zero displacement (static) is carried out to predict casing response owing to variation between surface and reservoir temperature. Additionally, the same scenario is simulated with a consideration of slip displacement (dynamic). Furthermore, hundreds of simulations are performed to cover wide range of possible scenarios to establish the prevailing factor to the buckling phenomena.

A 5mm displacement was applied on the shale rock to account for the flowback (fault slip activation) after stimulation and to predicts its effect on the casing. Based on this loading, the mechanics of a composites system (casing, cement and shale rock) and in particular the structural responses of the casing are investigated.

The ANSYS design explorer has demonstrated a robust design as established in this study with improve design factors under combined loading for the casing. Table 6.2 presents the range of input parameters utilised in the screening optimisation. The novelty of this approach is the concurrent investigation of the main factors attributing to casing buckling phenomena as opposed to previous studies of investigating individual attribute (parameter).

As stated above, the ANSYS design explorer can simplify and optimise structural designs which can be carried out using either screening optimisation, multiobjective genetic algorithm (MOGA) and goal driven optimization method. However, for simplification and making use of good computational resources; the screening optimisation method is selected. This is a simple approach based on sampling and sorting. It supports multiple objectives and constraints as well as all types of input parameters.

Table 6.2 Range of input parameters for the optimisation

Input Parameters	Lower Bound	Upper Bound
Coefficient of Thermal Expansion (C^{-1})	8.28E-06	1.012E-05
Cement Modulus (MPa)	6500	10000
Cement Poisson's Ratio	0.207	0.4
Reservoir Temperature (C)	60	250
Ambient Temperature (C)	10	45
Fracturing Pressure (MPa)	30	90
Slip Displacement (mm)	-5.5	-2.75
Slip Plane (degree)	30	75
Inner Diameter (in)	4.05	4.95
Outer Diameter (in)	4.95	5.5
Cement Diameter (in)	5.9625	7.2875
Hole Diameter (in)	5.9625	7.2875

As it can be seen in Table 6.2 twelve attributes (parameters) are investigated simultaneously to estimate the influence of each on casing buckling phenomena. Each attribute (parameter) covers wide range of conditions as shown in Table 6.2. For instance, casing diameter ranges from 4.05inches(102.89mm) to 4.95inches (125.73mm). Similarly, the outer diameter ranges from 4.95 (125.73mm) to 5.5inches (139.70mm), fracturing pressure from 30 to 90MPa. The cement elastic modulus is kept below 10000MPa based on studies (Guo et al. 2019; Yin et al., 2018; Xi et al., Yan et al., 2019) that established making use of cement with low elastic modulus reduces the potentials of casing buckling.

6.3.2 Machine Learning Prediction and Optimisation

In this section, using pragmatic approach, numerical modelling and machine learning techniques were applied to evaluate quantitatively the magnitude of these factors under a combined loading scenario. Using "K" nearest neighbour (KNN) machine learning algorithm the simulation data is further studied to establish a predictive model for the von Mises stress. The 517 simulation (instances) is divided into training and testing in the ratio of 70:30, respectively. Preliminary data manipulation involved removing noise and missing values. This is followed by data partitioning in the ratio state above and normalisation. Training and testing are next and finally finetuning the hyper-parameter "k" to establish the best model for the prediction of von Mises stress.

Specifically, in the Lunar and Quasar the parametric prediction and optimisation this study utilised 258 instances which represent 50% of the simulation data for the training set. On the other hand, the testing set comprises of 129 instances which represent 25% of the simulation data. Furthermore, the relevant data associated with casing (Design of experiment - DOE) and the corresponding responses are predicted, and optimisation performed to determine parameter sets for a desired target.

Additional data modelling in Quasar (machine learning package) is performed using principal component analysis (PCA) to determine the distribution of the sample's designs. The variance of attributing parameters is computed and plotted to estimate how these attributes are diminishing. Furthermore, matrix concatenation operation

is carried out on the DOE datasets and the corresponding responses for the generation of heatmap of von Mises stress on the casing.

6.4. Results and Discussion

6.4.1 FE simulation results

Simulation results for the combined loading of slip displacement and thermal loading when the fracture slip plane is 60° reveal casing transverse displacement and von Mises stress to be 13.029 mm and 932.46 MPa respectively after 30 hours of combined loading. This is as shown on Figure 6.9. Under this loading condition the casing is plastically failed since the yield strength of this casing is 758MPa.

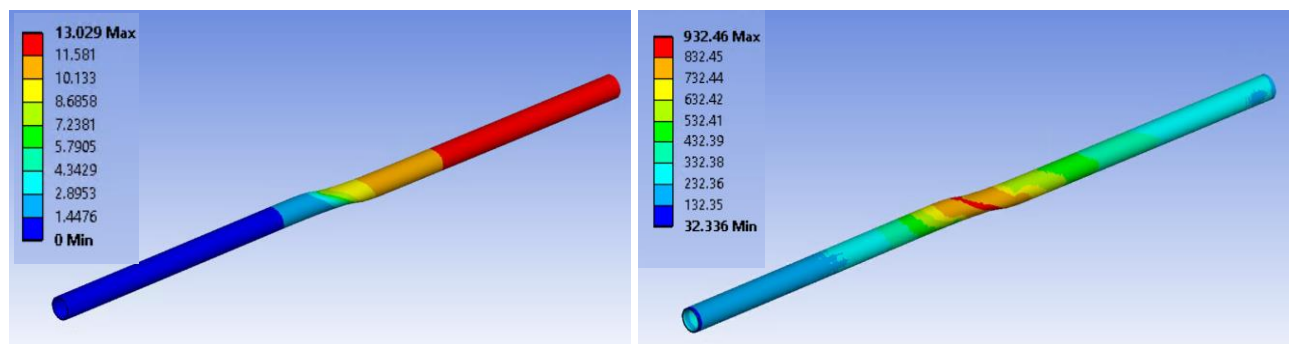


Figure 6.9 Transverse displacement and von Mises stress after 30 hours of combined loading.

In contrast, the predicted critical transverse displacement and von Mises stress is attained after 9 hours of combined loading. Figure 6.10 represent contour plots of critical displacement and von Mises stress on the casing under combine loading. Based on these results the casing failure looms after 9 hours of combined loading as shown. Therefore, using design explorer, we work out the optimum design based on the pertinent parameters earlier explained.

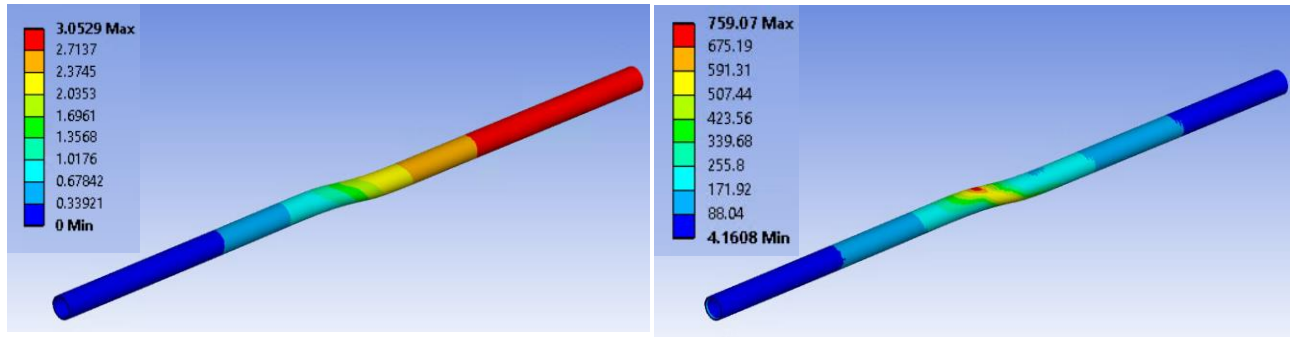


Figure 6.10 Transverse displacement and von Mises stress after at critical time of cobined loading

As shown on correlation matrix (Figure 6.11), slip displacement is negatively correlated to deformation and von Mises. While safety factor minimum is positively correlated with slip displacement as shown. Additionally, slip plane has a neutral relationship with von Mises stress and safety factor as shown. The red colour codes on the diagonal denotes strong correlation of the same parameter.

For example, coefficient of thermal expansion is 1 to 1 correlation (horizontal and vertical), and as such the colour code is red as shown the top left of the correlation matrix. The 12 input parameters are casing coefficient of thermal expansion, cement Young's Modulus and Poisson's ratio. The reservoir temperature (thermal condition magnitude), surface temperature, fracturing pressure (pressure magnitude), slip displacement, slip plane, inner and outer diameter of the casing. Other parameters are cement and well diameter (Hole Diameter). On the other hand, the output parameters are casing von Mises stress, transverse displacement and safety factor.

Furthermore, the local sensitivity of the pertinent parameters is evaluated and plotted on Figure 6.12. It indicates that hole diameter affects casing deformation

positively. Increase in inner diameter, fracturing pressure drives von Mises stress to increase. However, increase in outer diameter reduces the von Mises stress and total deformation respectively.

The casing geometry is a factor that affects the stress in the casing as can be seen on the local sensitivity chart (Figure 6.12). Increase in inner diameter reduce the pipe thickness which in turn increase the von Mises stress. Also, fracturing pressure increase the downhole stress which results in increase in von Mises stress. However, increase in outer diameter make the pipe thicker and reduces the von Mises stress accordingly. 32MPa fracturing is moderate which ensure moderate slip displacement on the casing and consequently the stress in the casing remains well below the yield strength 299MPa and 0.76mm transverse displacement.

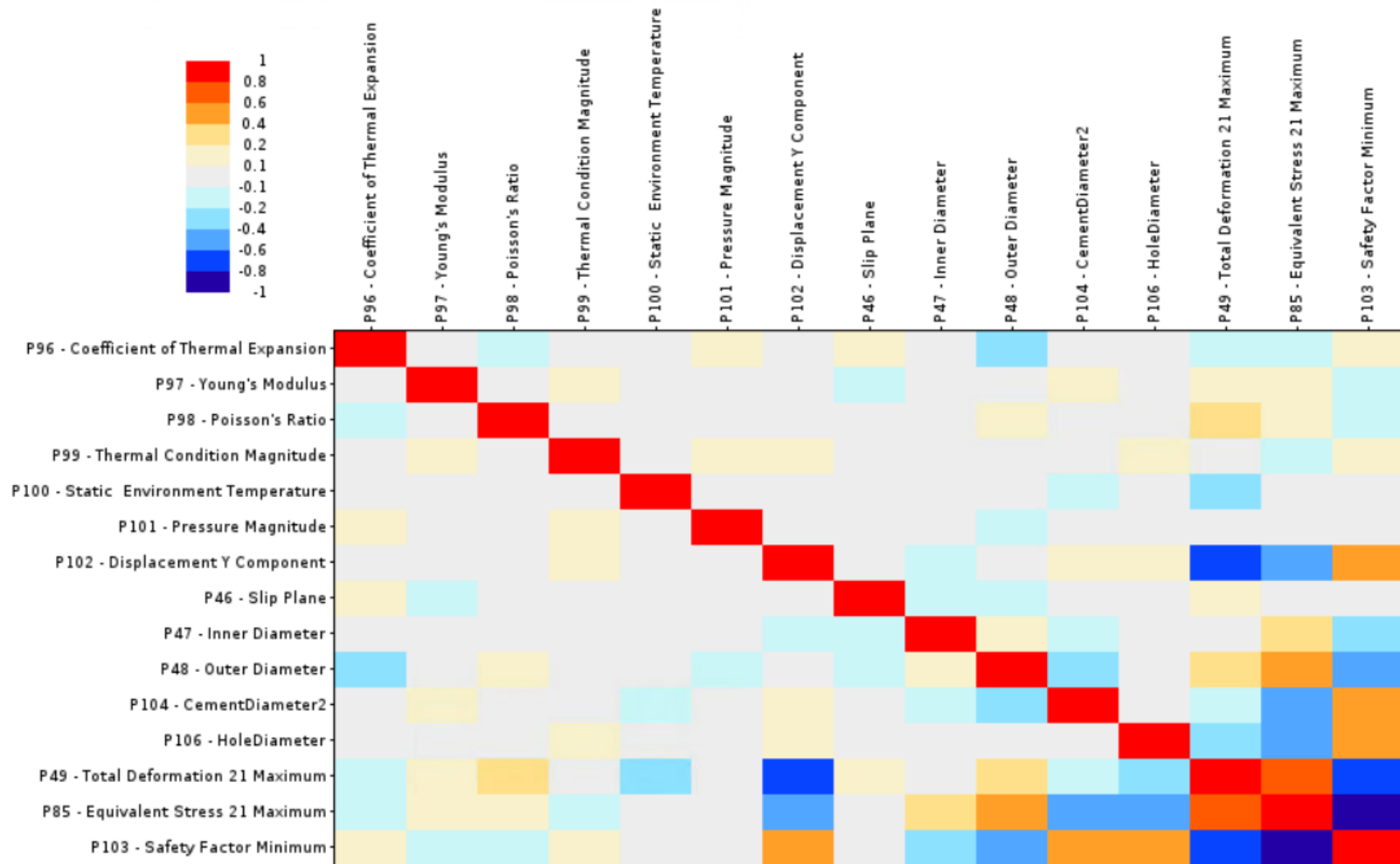


Figure 6.11 Correlation matrix showing the correlation between the 12 input and 3 output parameters

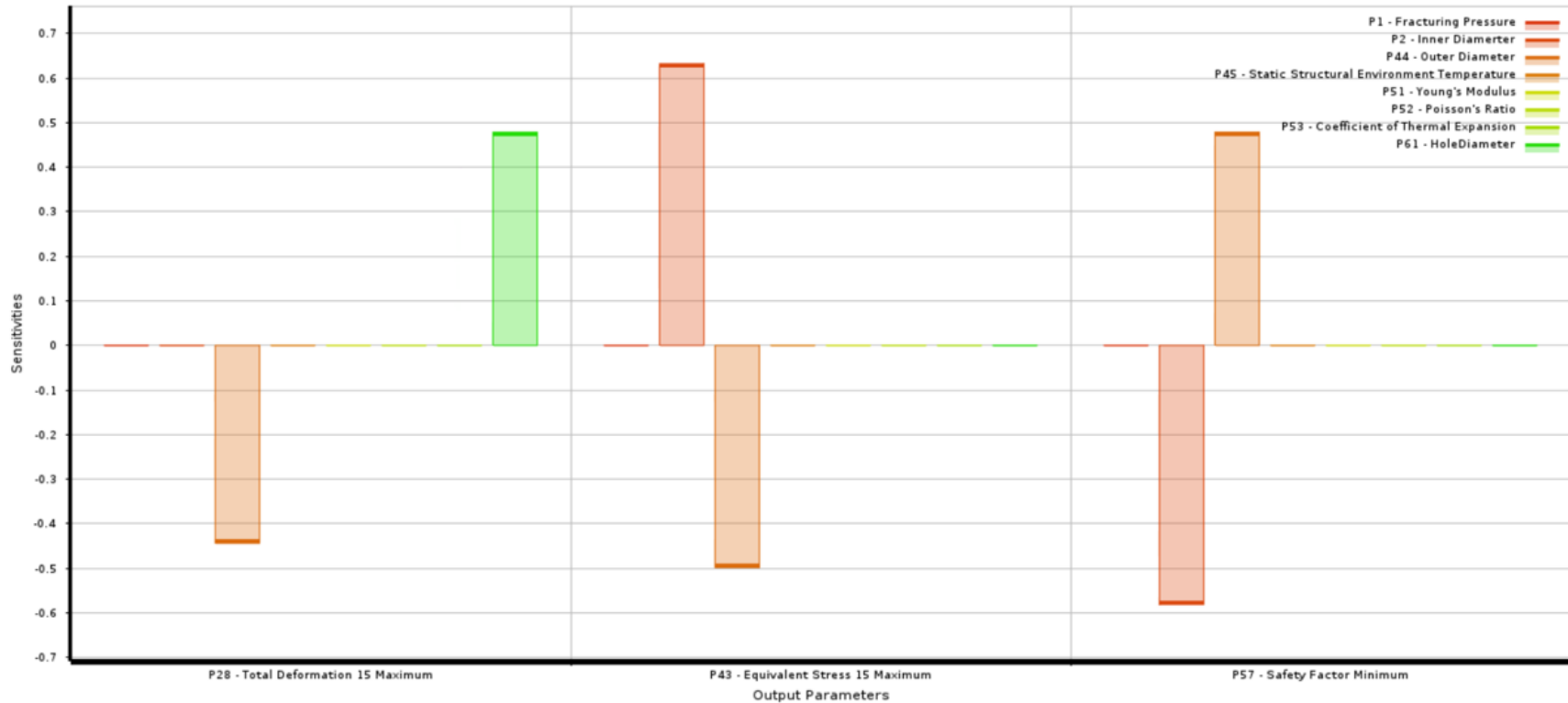


Figure 6.12 Local sensitivities of input parameters on casing total deformation, von Mises stress and safety factor.

The optimise results presents three candidates design that meet all the objectives and constraints. Figure 6.13 presents a sample contour plots of total deformation and von Mises stress for one of the optimised designs.

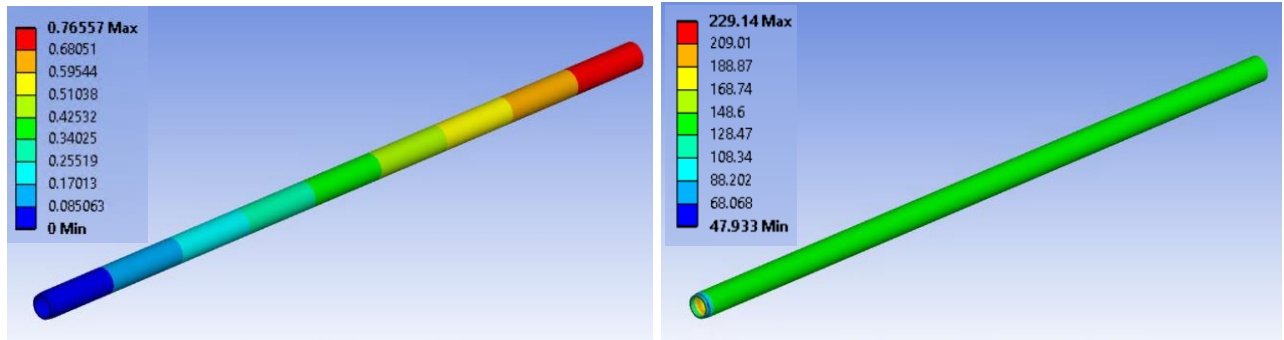


Figure 6.13 Total deformation and von Mises stress for the optimised design

The design variables that yielded the optimised von Mises and displacement of 299MPa and 0.76mm on Figure 6.13 are: 4.08inches (103.632mm) and 5.00 inches (127mm) inner and outer diameter respectively. Cement elastic modulus and well diameter is 6635MPa and 6.0-inch hole. The fracturing pressure and surface temperature is 32MPa and 25.52°C. On the other hand, fixed parameters or constraints corresponding to this scenario of combined loading of 5.29mm slip displacement during flow back with a thermal load of 143.3°C from the reservoir. This result agrees with what has been established in literature on limiting the cement elastic modulus to below 10000MPa and reducing the fracturing pressure as pointed by Guo et al. (2018) and Yan et al. (2019) in their respective studies. Besides, a new study by Huang et al. (2020) on rubberise cement established that; the rubberise cement absorb micro expansion and shrinkage, which reduces the brittleness of the concrete and improves its deformation performance.

As it can be seen the total deformation recorded after the optimisation is only 0.7655mm after the 30 hours of combined loading. Also, the computed von Mises stress corresponding to this deformation is 299MPa as shown on Figure 6.14. This value is below the casing yield strength of 758MPa. As such, based on this result it

can be said casing's structural integrity is guaranteed. This gives a safety factor of 3.3 against the previous predicted stress of 932.46 MPa with a safety factor of 0.8129.

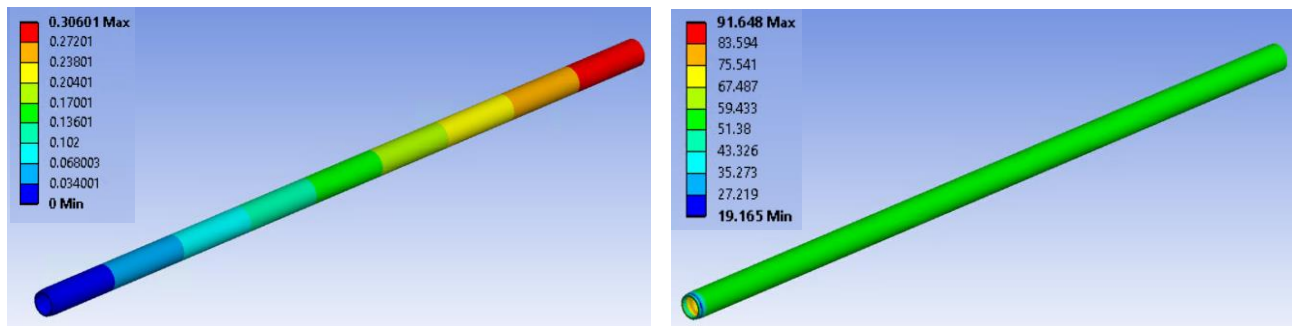


Figure 6.14 Optimised critical displacement and von Mises after 9 hours of combined loading.

However, if the circumstance change, then a much thicker casing geometry will be needed to cope with the change. Under this example design, 5.29mm slip displacement at an angle of 30 degree to the horizontal axis, 32MPa fracturing pressure and 143.3°C thermal stress will not deform the casing whose internal and outer diameter is 4.08 and 5.00 inches respectively.

On the other hand, the extracted result after 9 hours of combine loading for displacement and von Mises corresponding to earlier critical simulations results, are shown on Figure 6.14. This shows a remarkable reduction in the values of the total deformation and von Mises after optimisation. This represents 89% reduction in total deformation compared to initial simulation results.

6.4.2 Stress prediction using KNN model for casing design accuracy

The significance of this section is to demonstrate the use of KNN machine learning algorithm for the classification and prediction of casing health status, as well as quicker stress prediction than ANSYS. The data utilised comprises of both “buckled” and “intact” scenarios obtained from FEA. The analysis on the simulation data generated classify the casing status into “buckled” and “intact” as shown.

Figure 6.15 presents the scatter plots of the raw simulation data for von Mises plotted against casing inner diameter for the range of 4.5 - 6.625 inches diameters (114.3-168.275mm) as shown.

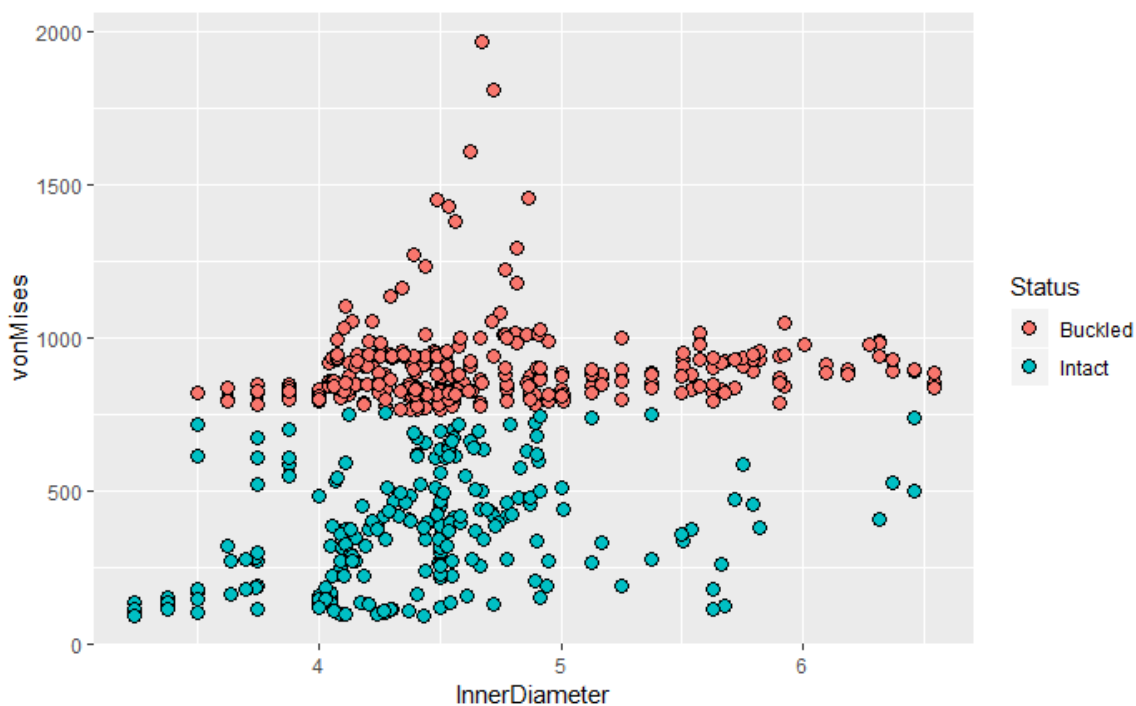


Figure 6.15 Scatter plots showing predicted von Mises stress for different casings geometries (Inner diameter).

Train-control which control the computational variation of the train function is applied for the regression, while the argument of “repeated cross-validation” is

selected for the resampling method in this study. The root means square error (RMSE), Rsquared and Mean absolute error (MAE) are used to select the optimal model that give the result as shown in Table 3. After several trials adjusting the hyperparameter, a model with K= 3 gives the best possible prediction based on “Rsquared” as shown in Table 3. This gives a metric accuracy of 42.72% as shown in Table 3 for k=3. Also, Table 3 presents “k” values and the corresponding values of RMSE, Rsquared and Mean absolute error (MAE) of the final model.

Table 6.3 RMSE, Rsquared and MAE for various values of k.

k	RMSE	Rsquared	MAE
1	147.8524	0.4030724	242.8430
2	153.1275	0.4250579	223.7322
3	154.0407	0.4272247	220.5380
4	159.0814	0.4104764	222.5914
5	164.3681	0.4059004	222.5398
6	165.8822	0.4068940	222.5053
7	166.1047	0.4132182	221.5441

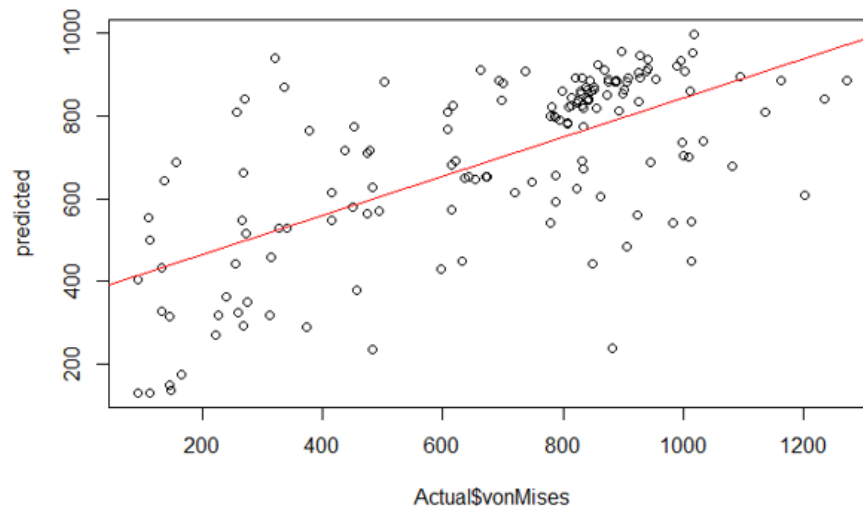
Figure 6.15 presents scatter plots for the prediction of von Mises stress based on the 12 attributes listed in Table 2. It can be seen Figure 6.16(a) show the scatter plots of actual von Mises stresses against the predicted before fine tuning the hyperparameter. However, after fine tuning of hyperparameter, a significant improvement in prediction accuracy is achieved. This yielded the most improve prediction model shown on Figure 6.16(b).

Table 6.4 Variable importance to prediction accuracy on casing buckling phenomena based on KNN algorithm for von Mises stress.

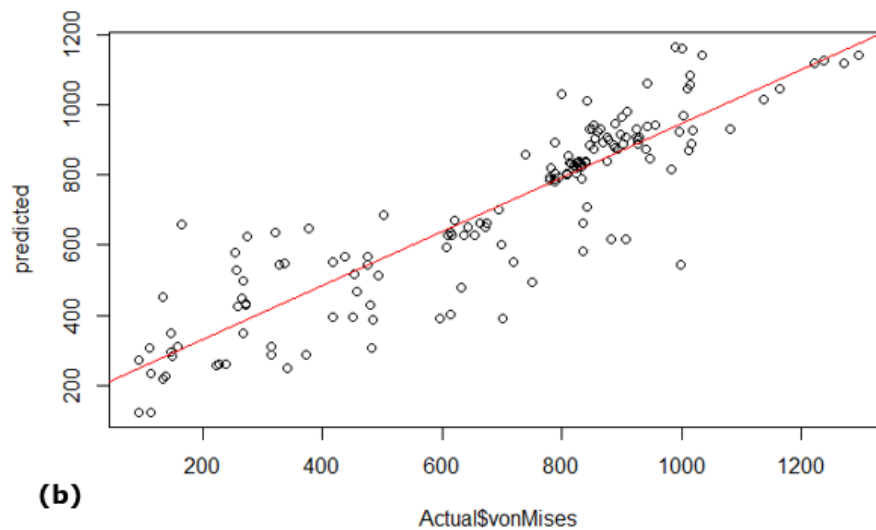
Slip Displacement	100.000000
Outer Diameter	79.673703
Slip Plane	70.206126
Inner Diameter	43.533671
Reservoir Temperature	24.969509
Cement Diameter	22.179621
Cement Modulus	20.701206
Fracturing Pressure	20.174114
Cement Ratio	11.486119
Hole Diameter	10.102478
Ambient Temperature	8.422043
Coefficient of Thermal Expansion	0.000000

Furthermore, the variable importance varies from 0 to 100 is shown in Table 6.4 based on regression analysis on the data using the KNN algorithm.

The parameters that substantially affects the von Mises stress are slip displacement, casing geometry (inner and outer diameters), hole diameter and cement mechanical properties. This is also true on the correlation matrix on Figure 6.11 and Lunar (Figure 6.17). However, coefficient of thermal expansion and ambient temperature do not significantly affect casing structural integrity provided the casing is properly cemented in place (Mohammed et al. 2020). Other factors with their respective influence on the casing von Mises stress are as presented in Table 6.4.



(a)



(b)

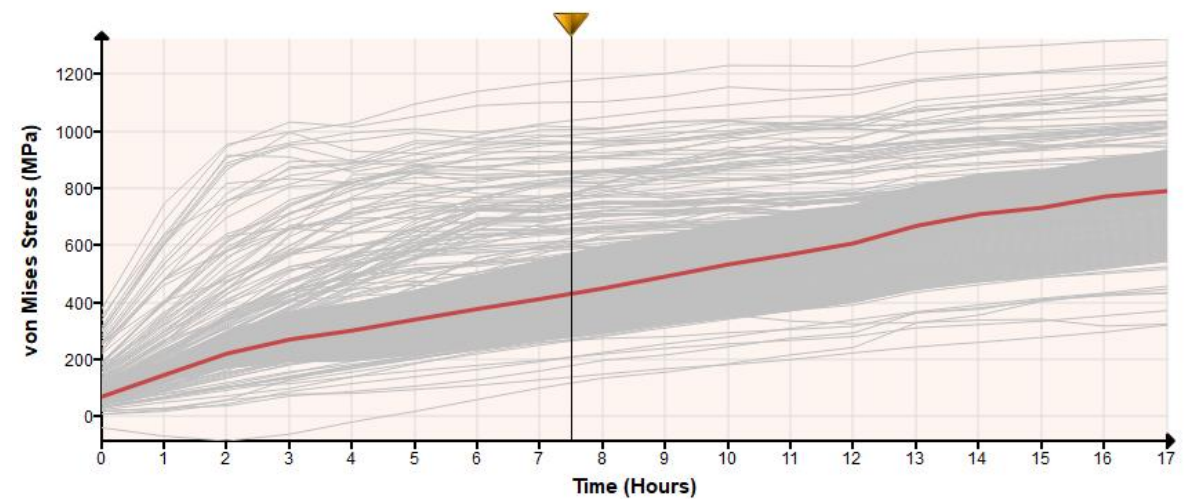
Figure 6.16 Scatter plot for von Mises stress prediction:(a) before finetuning hyper parameter (b) after fine-tuning hyper parameter.

6.4.3 Effect of slip plane and casing inner diameter on casing stress

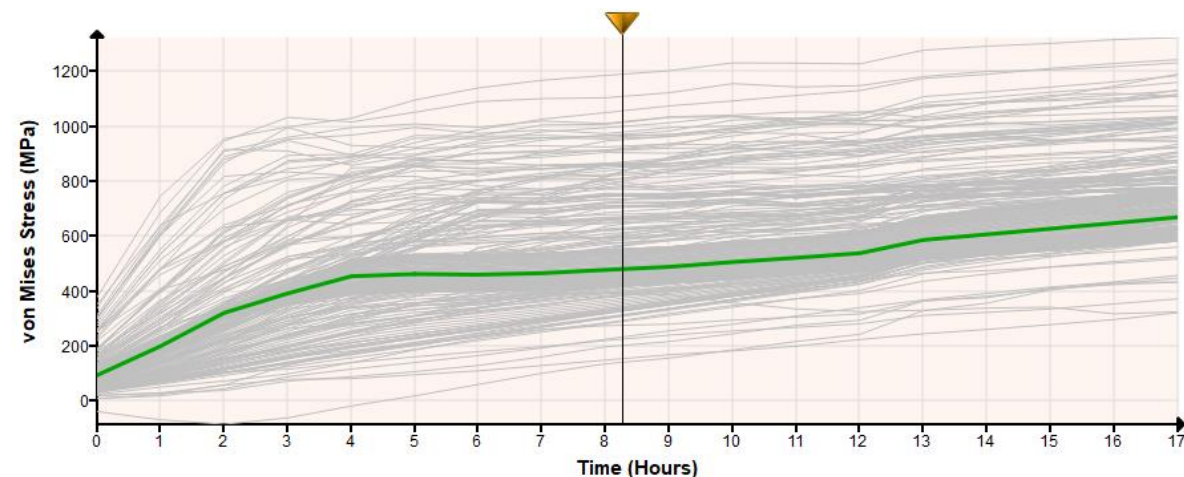
Lunar evaluated the effect of changing slip plane and inner diameter on casing von Mises stress over time is examined on the testing dataset (DOE). The (grey shadow)

is generated assuming the slip plane and inner diameter were to change 100 times for selection and design purposes.

The analysis in Lunar predicted the corresponding responses for the new design of experiment (DOE). The influence of each parameter is investigated and corridor of each evaluated. Figure 6.17 (a and b) present the corridor for slip plane and inner diameter respectively on von Mises stress over the period of investigation.



(a)



(b)

Figure 6.17: (a) Effect of changing slip plane 100 times (b) effect changing

casing Inner diameter 100 times showing the window in grey over time.

As expected, and as it can be seen, different parameters (see Table 4) have different influence on casing von Mises stress particularly for time dependent data as shown on the Figures 6.17. This is particularly crucial as it allows the engineer to examine range of scenarios for an inform decision within a very short time. As it can be seen on Figure 6.17(a) the corridor is wider than on Figure 6.17(b) for slip plane and inner diameter respectively.

6.4.4 Effect of design parameters on casing stress performance

The Lunar predicted the influence and the variance/standard deviations of the design parameters on casing structural performance using fraction of the simulation data earlier explain in section 3.2.2. The sensitivities of all parameters are presented on the bar chart plotted on Figure 6.18. As it can be seen the slip displacement (SD) has the highest impact on the casing stress. This is obvious and completely agree with variable importance based on KNN metric prediction accuracy shown in Table 6.4. Other parameters that strongly affect the target variable (von Mises) is slip plane (SP) and inner diameter (ID). Meanwhile, outer diameter (OD), Fracturing pressure (FP), and Poisson's ratio (PR) have very little / no influence on the von Mises stress. However, cement elastic modulus (CEM) and reservoir temperature (RT) affect the casing stress moderately as shown on Figure 19.

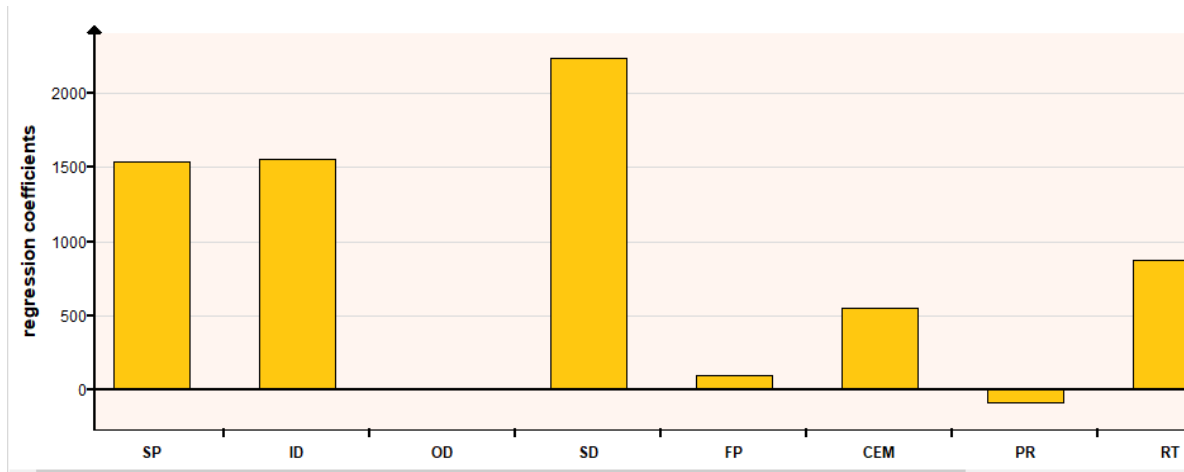


Figure 6.18 The inputs parameters influence on casing von Mises stress.

The PCA presents the standard deviation between the parameters. As it can be seen on plot the standard deviation ranges from -4 to +4 on both axes. Although, the data is highly variable (imbalance), the PCA show good distribution as shown on Figure 6.19. On Figure 6.19, Inner and outer diameter (ID & OD), surface and reservoir temperatures (ST & RT) are strongly correlated.

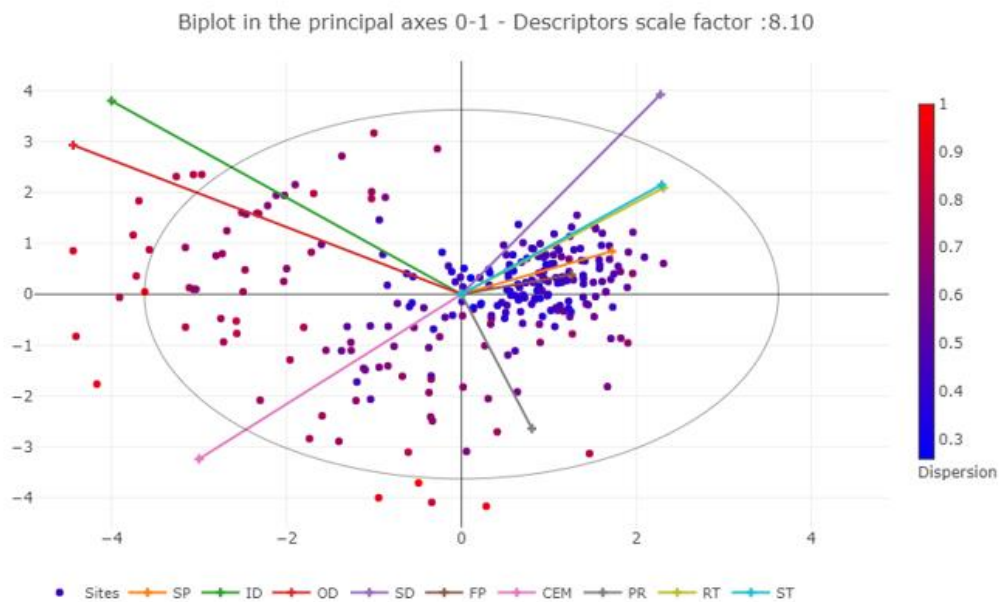


Figure 6.19 Principal component analysis of the casing performance based

on sensitive parameters.

Figure 6.20 presents the variance contribution of each of the 9 parameters under investigation. The gradual diminishing of the bars indicates a good principal component analysis.

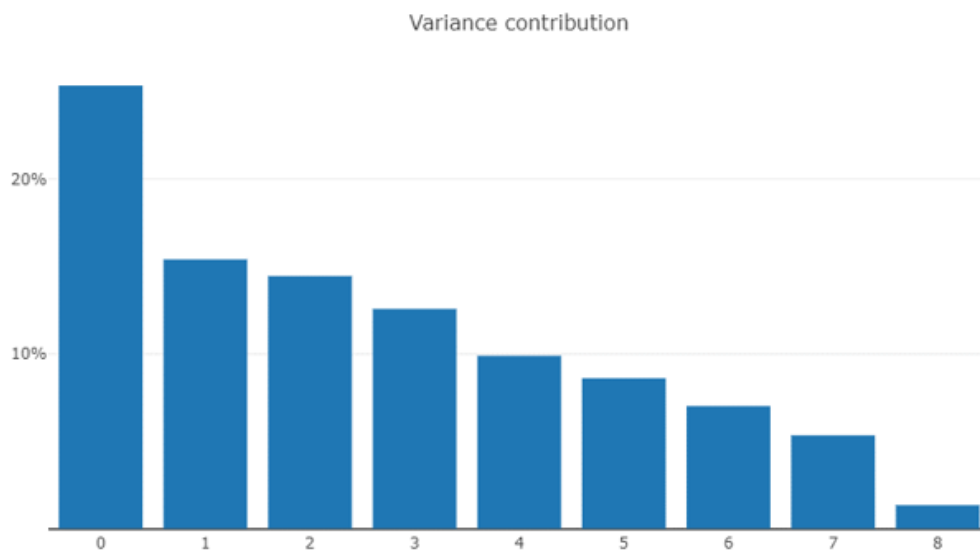


Figure 6.20 The variance of the contributing sensitive parameters.

6.5 Selection and optimisation for the casing design.

The optimisation functionality of Lunar iteratively goes through the design variables to select the right values (bounds) of those parameters that enable the determination of a predetermined casing stress threshold specified by the user.

Consequently, Lunar revealed the parameter sets that enable determination of right combination of values that can achieve predetermine target (optimum) without reaching the casings' strength limit. For this purpose, 650MPa was selected as the

maximum value for the P110 casing which has a minimum yield strength of 758 MPa. After the analysis, the optimised parameters are presented on Figure 6.21.

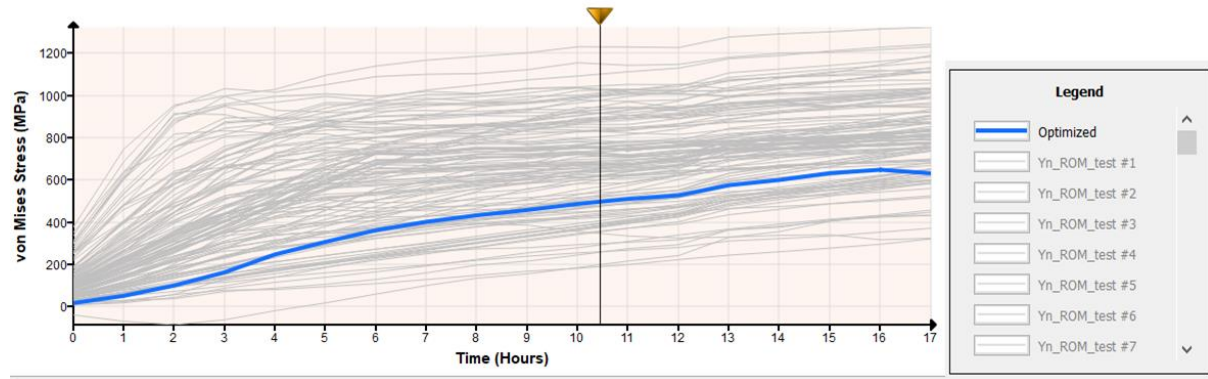


Figure 6.21 Lunar software output for the optimised casing design shown in blue line.

Under this specific example optimisation with Lunar, limiting the von Mises stress for P110 to 650MPa is shown on Figure 6.21. This is achieved with a casing geometry of 113.593 and 164.7mm for inner and outer diameter respectively. Also, the maximum fracturing pressure of 49.29MPa was computed to meet this objective.

Furthermore, cement with 19258.5MPa and 0.39 Poisson's ratio with fluids temperature of 25.24°C are the corresponding design variables for this situation. However, in keeping this stress level (650MPa) in the casing, the maximum permissible slip displacement is only 2mm on the casing. Also, other fixed variables such as slip plane, and reservoir temperature are 41 degrees and 133.1°C respectively. This agrees with the previous study of Yin et al. (2018) and Xi et al. (2018) that established low slip angle reduce buckling tendencies.

The heatmap presents the von Mises distribution for the 18th column which corresponds to the 10th hour casing responses under the combined loading. It is showing the distribution of the von Mises stress for this particular column to varies between 200- 1200MPa as shown on the scale.

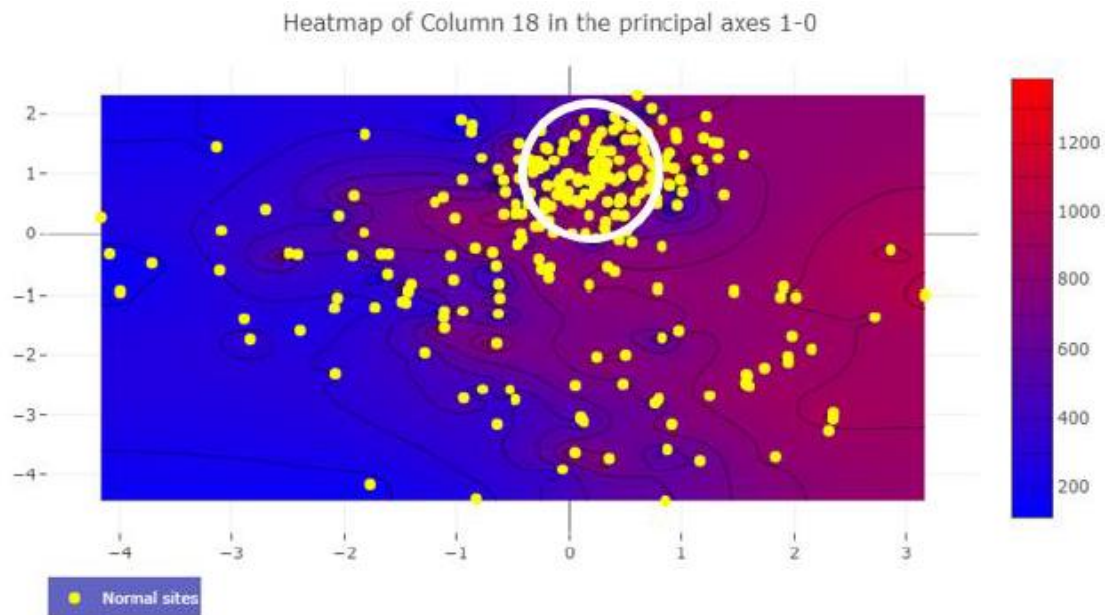


Figure 6.22 The heatmap for the 10th hour von Mises stress for the optimised casing.

It indicates low and high regions for this particular column as shown by the left and right extremes of the heatmap on Figure 6.22. It is important to point that the optimal region resides where there is high density cluster (circled region) in the middle. From the analysis accomplished in this study, both Lunar and Quasar results have proved to be an effective tool that can optimise the casing selection, design, and completion of shale gas horizontal wells.

In summary, investigation of casing structural responses under various slip displacements and a wide range of scenarios between reservoir and surface temperatures, fracturing pressures, casing geometries and downhole conditions and optimisation performed. However, this investigation is limited to induced stresses resulting from slip displacements - during flowback and fracturing pressures in hydraulic fracturing operations and thermal loads for a 30-hour period. In addition, this investigation covers many conditions but limited to the range of parameters and magnitude indicated in Table 2. In particular, cement elastic modulus magnitude is restricted from 6500 to 10000MPa as established by literature.

A quick comparison between the two approaches on the sensitivities of the casing structural responses - specifically the von Mises stress is summarised in Table 5. As it can be seen, there is good agreement between Lunar and KNN" on most of the parameters investigated. Slip displacement, Inner diameter and slip plane appears to have highest influence on the casing stress based on their magnitude. On the other hand, cement coefficient of thermal expansion, fracturing pressure and Poisson's ratio have low impact on the casing stress magnitude. Although, the two approaches do not use the same amount of data, yet good trend has been established in terms of the sensitivities with the exception of outer diameter which appears to be unique. This is partly due to the constant nature of the outer diameter within a particular casing geometry group.

Table 6.5 presents this comparison between Lunar and “KNN” sensitivities on casing stress.

Parameter	Lunar	KNN
Slip Displacement	2300	100
Outer Diameter	0	79.6737
Slip Plane	1580	70.20613
Inner Diameter	1600	43.53367
Reservoir Temperature	800	24.96951
Cement Modulus	600	20.70121
Fracturing Pressure	100	20.17411
Poisson's Ratio	-100	11.48612
Coefficient of Thermal Expansion	0	0

6.6 Conclusion

This paper proposes a novel way to investigate and optimise the casing structural integrity using two approaches of finite element analysis (FEA) and machine learning. The approach in this study is unique, as it is able to capture the pertinent parameters influencing the casing buckling and the evaluation of the magnitude of each. In this work, the effect combined loading using multiple parameters to establish the relationship and effect of each on stress, displacement and ultimately casing safety factor is revealed. Similar approaches of combining machine learning and FEA are established in the study of Kim, M., Yi, S. and Hong, S., (2021) which, acquire a training data for machine learning from 100 simulations to determine an optimal design.

Simulation results for the combined loading of slip displacement and thermal loading when the fracture slip plane is 60° reveal casing transverse displacement and von Mises stress to be 13.029 mm and 932.46 MPa respectively after 30 hours. Similarly, the critical stress and displacement computed after 9 hours of combined loading is found to be 759.07MPa and 3.0529mm respectively.

Chapter 7: Conclusion, Recommendation and Future Works

7.1 Conclusion

Shale gas and tight oil and gas resources are currently being developed in the quest to increase energy supply and reduce carbon footprint on the planet. Researchers and engineers are currently investigating ways of producing these resources as efficiently as possible since natural gas produces 35% less CO₂ than oil and 65% less than coal. This lower CO₂ emissions of shale gas makes its development attractive to unconventional operators even though, many countries do not subscribe to the process through which shale gas is developed and produced. Despite this reluctance, the potentials of shale gas resource development are still high in the future, but hugely depend on human ingenuity and technology advancement.

The two main technologies that are utilised in shale gas development is horizontal well drilling and multistage hydraulic fracturing. The limited success of these technologies and in particular the failure cases of casing pipes during this process is more than in conventional oil and gas wells. This is partly attributed to limited material options from API class, characteristics of long lateral sections in horizontal wells and induced stresses during hydraulic fracturing which results in slip displacement of the structural pipe and its failure. Depending on the stress regime in an area and the operational efficiency of the process, the casing pipe failure can lead to complete loss of access into well resulting in huge financial loss.

This research meticulously itemised objectives to investigate these factors causing casing buckling and to proffer step solutions to increase the success rate of shale gas horizontal well stimulation and prevent casing buckling failure in future wells during the design phase. Critical and strategic review of the literature provided the

understanding of the state of the art and the identification of the casing grades that are popular in developing shale gas wells. These are P110 and Q125 API grades. Also, based on the review of the literature from many case histories reported in the literature on casing lateral buckling from around the world reveals the main causes of casing buckling to included shear loads, fracture slip, thermal loads and operational aspect of the hydraulic fracturing. Besides, the review established the casing failure mix by grades and found P110 casing grade to have the highest failure owing to its application challenging wells is presented in chapter 2. The review found that there are few studies on casing material selection and engineering for shale gas wells application. Also, the literature survey reveals a gap in the literature on combining material selection and machine learning to study structural casing. Based on the literature review conducted in that chapter (chapter 2) and the findings therein – there is the need to shift from limited conventional design approach to the new method that encapsulates material selection, FEA blended with Machine learning to resolve the unconventional challenge posed by shale gas wells.

Results obtained in chapter 3 shows that performance of different materials for shale wells casings under the 3 different scenarios investigated. In the scenario where buckling is caused by external load reveal SM125 casing grade to have the highest performance. While scenario 2 consider induced stress and corrosion found stainless steel austenitic AISI 304 as the overall best material for the casing application. Lastly, scenario 3 found carbon steel AISI 1025 annealed for application in brittle shales with long term service temperature. Additionally, multicriteria decision making methods of TOPSIS, AHP and the new non weighted method rank these materials shortlisted from CES Granta selector accordingly. It was found that

TOPSIS and non- weighted method are similar and strongly correlated for the 10 shortlisted materials analysed. On the other hand, the AHP is inversely correlated to TOPSIS and non- weighted method based on data analysis as per the ranking. Furthermore, the new non- weighted reduced the subjectivity of the selection and ranking as there is no weight assignment in this method.

The research implemented in chapter 4 using finite element modelling (FEM) and exploratory data analysis established the structural responses and correlations between ranking and stress, displacement and safety factor of the 10 shortlisted materials based on AHP, TOPSIS and non-weighted methods. Furthermore, matrix concatenation of stress and safety factor give the strength distribution for these methods (TOPSIS, AHP and non-weighted method) is presented in chapter 4. Findings in this chapter shows that stainless steel (BS145) outperform the P110 and Q125 casing grade based structural analysis. In conclusion, it was found that combining MCDM and FEM is effective for casing material selection and to ensure efficient performance in shale gas wells.

In chapter 5 it was found that temperature reduces the time taken to reach critical conditions on the casing based on simulation and analysis implemented. For example, when the temperature is increased to 450°F from the initial 68°F, critical time reduced from 21 to 17 hours - which represent 19% reduction keeping other parameters constant. Overall, increase in temperature and differential creep load leads to increased stresses and displacements in the casing. The findings in this chapter provides new fundamental insight on the time dependent viscoelastic property of the rock (creep) and thermal stress complexities during stimulation and helps to quantify effect of critical parameters on the production casing.

Chapter 6 prediction and optimisation on casing structural responses for total deformation and von Mises recorded 0.7655mm and 229MPa after the 30 hours of combined loading respectively. This represents over 89% reduction in total deformation and 87% reduction in von Mises compared to initial simulation results. Therefore, adopting to this procedure in casing design for shale gas wells will drastically reduce the potentials of casing buckling as established in this study. Also, data mining using Lunar and Quasar provided major insights into the casing health status and enabled the real time parametric investigation of the casing stress as a function of time. The KNN algorithm prediction gives a metric accuracy of 42.72% based on Rsquared for $k=3$. The algorithm presents variable significance to casing buckling phenomena with slip displacement and casing geometry (inner and outer diameters) accounting for the larger proportions.

The study key findings are:

- Literature review showed that there is complete lack of usage of alternative viable materials from other sources/industries to develop oil and gas wells from the traditional API and propriety grades. Material selection carried out using ANSYS Granta Selector found many alternative viable options for casing material that can sufficiently meet the requirement of shale gas wells. An example of these alternative options that outperform P110 casing Grade is BS 145.
- Also, this research found a new method of reducing the subjectivity of the multicriteria decision making methods (MCDM) which assigns weight to

criteria. This new method unbiasedly gauge alternatives based on ratios and distance.

- Against the general notion of cemented casing is restricted to movement; it was found that a 4000mm long, fully cemented casing cannot withstand a 14 mm displacement during fracturing and buckling of such casing can occur at low shear stresses of 10–15 MPa.
- Thermal loading alone account for 19% reduction in the time taken to buckle the casing. In contrast, combined loading of rock slip and temperature effect on the casing is found to increase casing transverse displacement by 62.09% and von Mises stress to increase by six folds from the initial values.
- It is found that using simulation data, data driven modelling can effectively predict von Mises stress and sensitivities of both dependent and independent variables in casing design for shale gas wells application and similar studies.
- Implementation of new research capability of *ODYSEE* & *AI* specialist skills for prediction and optimisation of casing for shale gas well opened up new improve way of casing design and optimisation.

7.2 Recommendations for future work

Based on the findings and understandings established in this study on casing buckling and deformation phenomena; these recommendations are made:

1. The casing buckling in unconventional shale gas well is unique in every situation and circumstance even in the same well. As such, there is no universal or generalised solution that meet this varied casing failure/ deformation phenomena. However, from findings in this research revealed that there a

limited available casing material (API & non-API), therefore rejigging the material properties for increase performance and possibly manufacturing new - non-API material for shale gas well casing application can lead to discovery of new materials that can potentially prevent casing buckling under a particular scenario.

2. The industry standard software such as stress check and wild cat are unable to predict casing-cement-rock structural response as one entity. Based on this, all the analysis is carried out through finite element analysis (FEA) which is time consuming. It will be interesting to develop a tool not that is capable of predicting of casing- cement and rock formation as one entity quicker than the conventional approach.
3. While this study investigates main factors causing the casing buckling during shale gas hydraulic fracturing based on good drilling and cementing practice. Meaning that both hole, cement and casing are regular concentric circles throughout this research. Further studies should investigate tortuous wellbores and non- concentric cement sheath to study casing buckling phenomena. In addition, while the study investigates with brittle cement, potentials of a new rubberised cement based on the study of Huang et al. (2020) on rubberise cement established that; the rubberise cement absorb micro expansion and shrinkage, which reduces the brittleness of the concrete and improves its deformation performance is a recommended area of further studies.
4. The finite element modelling conducted in these studies for prediction of casing structural responses is time consuming. However, aggregating shale gas

stimulation data ranging from casing pipe material properties to design, installation, operation and final evaluation using micro seismic data, and both the cement and reservoir formation data can provide means of designing a machine learning model for the prediction of the casing responses in a timely manner in the future.

5. The application of machine learning and artificial intelligence has proven to be a useful tool in this study, especially, in keeping the stress at a desired level (e.g., 650MPa) in the casing, however, future works will look into applying findings in this study in real shale gas wells to explore its efficacies.
6. The test rig proposed in appendix 'A' is a means of validating some of the numerical simulation. Experimenting actual fracturing of the rock will be quite challenging in laboratory. However, a safe way of investigating this process in the laboratory will definitely be of interest to both researchers and unconventional operators.

References

- AASEN, J.A. and POLLARD, M., 2003. Casing Design–Review of Design Methodology.
- ABOU-SAYED, A.S. and ZAKI, K.S., 2005. A mechanistic model for formation damage and fracture propagation during water injection. *SPE European Formation Damage Conference*. Society of Petroleum Engineers.
- ABDIDEH, M. and KHAH, S.H., 2018. Analytical and numerical study of casing collapse in Iranian oil field. *Geotechnical and Geological Engineering*, 36(3), pp. 1723-1734.
- AL-ENEZI, B., AL-MUFAREJ, M., ASHQAR, A. and NAVIA, A., 2017. First Successful Openhole Lateral Multistage Acid Frac in a Complex Unconventional Carbonate Reservoir North Kuwait. *SPE Abu Dhabi International Petroleum Exhibition & Conference*. Society of Petroleum Engineers.
- ALLWOOD, J.M. et al., 2011. Material efficiency: A white paper. *Resources, Conservation and Recycling*, 55(3), pp. 362-381
- ANDERSSON, S., 2011. Wear simulation with a focus on mild wear in rolling and sliding contacts. *International Symposium on Friction, Wear and Wear Protection 2008. Aachen, Germany. 9-11 April 2008*. pp. 1-19.
- AMERICAN PETROLEUM INSTITUTE (API), 2006. API SPEC 5CT: 2006. *Specification for Casing and Tubing*. 8th ed. Washington, DC: API.
- ASHBY, M. et al., 2018. The CES EduPack Materials Science and Engineering Package.

AWE, S., ERINLE, A., AKINFOLARIN, A., IBRAHIM, T., OBANYA, P. and ROES, V., 2015. Safeguarding Pressure Integrity of Surface Well Control Equipment: A Review of Fastlock Drilling Adapter and Blow Out Preventer Connection Failure in High Pressure Well. *SPE Nigeria Annual International Conference and Exhibition*. Society of Petroleum Engineers.

Bachu, S. 2017, "Analysis of gas leakage occurrence along wells in Alberta, Canada, from a GHG perspective–Gas migration outside well casing", *International journal of greenhouse gas control*, vol. 61, pp. 146-154.

BAI, Y. and BAI, Q., 2005. *Subsea pipelines and risers*. Elsevier.

BAI, Y. and BAI, Q., 2018. *Subsea engineering handbook*. Gulf Professional Publishing.

BAO, X. and EATON, D.W., 2016. Fault activation by hydraulic fracturing in western Canada. *Science*, 354(6318), pp. 1406-1409.

Bartlett, M. & Cussens, J. 2017, "Integer linear programming for the Bayesian network structure learning problem", *Artificial Intelligence*, vol. 244, pp. 258-271.

BASTOLA, A., WANG, J., MIRZAEI-SISAN, A. and NJUGUNA, J., 2014. Predicting hydrostatic collapse of pipes using finite element analysis. *ASME 2014 33rd International Conference on Ocean, Offshore and Arctic Engineering*. American Society of Mechanical Engineers Digital Collection.

BEST, B., 1986. Casing wear caused by tooljoint hardfacing. *SPE drilling engineering*, 1(01), pp. 62-70.

- Benesty, J., Chen, J., Huang, Y. and Cohen, I., 2009. Pearson correlation coefficient. In *Noise reduction in speech processing* (pp. 1-4). Springer, Berlin, Heidelberg.
- BEUGELSDIJK, L., DE PATER, C. and SATO, K., 2000. Experimental hydraulic fracture propagation in a multi-fractured medium. *SPE Asia Pacific conference on integrated modelling for asset management*. Society of Petroleum Engineers.
- BRANTLEY, S.L. et al., 2014. Water resource impacts during unconventional shale gas development: The Pennsylvania experience. *International Journal of Coal Geology*, 126, pp. 140-156.
- BRAY, J.D. et al., 1994. Earthquake fault rupture propagation through soil. *Journal of Geotechnical Engineering*, 120(3), pp. 543-561.
- BRECHAN, B., SANGESLAND, S. and DALE, S., 2018. NTNU, and Naaden, C. and Borgersen, K. Halliburton (2018)." Well Integrity-next developments. Paper SPE/IADC-189403-MS Middle East Drilling Technology Conference.
- BUSAHMIN, B. et al., 2017. Review on hole cleaning for horizontal wells. *ARPN J.Eng.Appl.Sci*, 12(16), pp. 4697-4708.
- BYROM, T.G., 2014. *Casing and liners for drilling and completion: design and application*. Elsevier.
- CARPENTER, C., 2019. Data Mining Effective for Casing-Failure Prediction and Prevention. *Journal of Petroleum Technology*, 71(07), pp. 55-56.
- CARSLAW, H. and JAEGER, J., 1959. *Conduction of heat in solids*, Clarendon.

ÇALIŞKAN, H. et al., 2013. Material selection for the tool holder working under hard milling conditions using different multi criteria decision making methods. *Materials & Design*, 45, pp. 473-479.

CECCARELLI, T.U., ALBINO, E.H., WATSON, G.M. and DEFFIEUX, D., 2009. Deepwater completion designs: a review of current best practices. *Asia Pacific Oil and Gas Conference & Exhibition*. Society of Petroleum Engineers.

CHEN, V., LIN, V. and CHEATHAM, J., 1989. An analysis of tubing and casing buckling in horizontal wells. *Offshore Technology Conference*. Offshore Technology Conference.

CHEN, Y., YU, J. and KHAN, S., 2013. The spatial framework for weight sensitivity analysis in AHP-based multi-criteria decision making. *Environmental modelling & software*, 48, pp. 129-140.

CHEN, Z., SHI, L. and XIANG, D., 2017. Mechanism of casing deformation in the Changning–Weiyuan national shale gas demonstration area and countermeasures. *Natural Gas Industry B*, 4(1), pp. 1-6.

CHEN, Y.C., Lin, Y.H. and Cheatham, J.B., 1990. Tubing and casing buckling in horizontal wells (includes associated papers 21257 and 21308). *Journal of Petroleum Technology*, 42(02), pp.140-191.

CHEN, Z., Zhu, W. and Di, Q., 2018. Elasticity solution for the casing under linear crustal stress. *Engineering Failure Analysis*, 84, pp.185-195.

CHIPPERFIELD, S.T. et al., 2007. ShEaR DiLaTioN DiagNoSTiCS—a NEW aPPRoach foR EvaLuaTiNg TighT gaS STiMuLaTioN TREaTMENTS. *The APPEA Journal*, 47(1), pp. 221-238.

CIRIMELLO, P. et al., 2018. Oil well drill bit failure during pull out: Redesign to reduce its consequences. *Engineering Failure Analysis*, 83, pp. 75-87

CORRÊA, J.R. et al., 2020. Structural integrity assessment of a 5CT P110 steel riser pipe according to BS 7910: 2013 standard. *International Journal of Pressure Vessels and Piping*, 188, pp. 104206

CRAIG, B.D. and SMITH, L., 2011. Corrosion Resistant Alloys (CRAs) in the oil and gas industry. *Nickel Institute Technical Series*, 1, pp. 0073.

CSISZÁR, O., CSISZÁR, G. and DOMBI, J., 2020. How to implement MCDM tools and continuous logic into neural computation?: Towards better interpretability of neural networks. *Knowledge-Based Systems*, 210, pp. 106530.

Cussens, J., Järvisalo, M., Korhonen, J.H. & Bartlett, M. 2017, "Bayesian network structure learning with integer programming: Polytopes, facets and complexity", *Journal of Artificial Intelligence Research*, vol. 58, pp. 185-229.

DEEKSHATULU, B. and CHANDRA, P., 2013. Classification of heart disease using k-nearest neighbor and genetic algorithm. *Procedia technology*, 10, pp. 85-94.

DANESHY, A., VALKO, P. and NORMAN, L., 1998. Well Stimulation. Chapter 17 In: *Petroleum Well Construction. Edited by M.Economides.Wiley*, , pp. 506

DAVIES, R.J. et al., 2012. Hydraulic fractures: How far can they go? *Marine and Petroleum Geology*, 37(1), pp. 1-6

DAWSON, R., 1984. Drill pipe buckling in inclined holes. *Journal of Petroleum Technology*, 36(10), pp. 1,734-1,738.

DAWSON, W., SPAIN, D., RASHDI, K.A., SAADI, S.A., GANGOPADHYAY, A., MCTEAGUE, M. and BUSAFI, B.A., 2018. Right Data, Right Place, Right Time: The Evolution of a Data Acquisition Strategy for a Tight Gas Development in the Sultanate of Oman. *Abu Dhabi International Petroleum Exhibition & Conference*. Society of Petroleum Engineers.

Donoho, D.L. 2000, "High-dimensional data analysis: The curses and blessings of dimensionality", AMS math challenges lecture, vol. 1, no. 2000, pp. 32.

Drucker, D.C. and Prager, W., 1952. Soil mechanics and plastic analysis or limit design. *Quarterly of applied mathematics*, 10(2), pp.157-165.

Duda, R.O., Hart, P.E. & Stork, D.G. 2012, Pattern classification, John Wiley & Sons.

DUSSEAULT, M.B., MAURY, V., SANFILIPPO, F. and SANTARELLI, F.J., 2004. Drilling around salt: risks, stresses, and uncertainties. *Gulf Rocks 2004, the 6th North America Rock Mechanics Symposium (NARMS)*. American Rock Mechanics Association.

EDITION, F. and ASHBY, M.F., 2011. MATERIAL SELECTION IN MECHANICAL DESIGN.

EKASARI, N. and MARBUN, B., 2015. Integrated Analysis of Optimizing Casing Materials Selection of Geothermal Well by Using a Model for Calculating Corrosion Rates. *World Geothermal Congress. Melbourne, Australia*.

- ENSS, G.C. and PLATZ, R., 2016. Evaluation of uncertainty in experimental active buckling control of a slender beam-column with disturbance forces using Weibull analysis. *Mechanical Systems and Signal Processing*, 79, pp. 123-131.
- EMOVON, I. and OGHENENYEROVWHO, O.S., 2020. Application of MCDM method in material selection for optimal design: A review. *Results in Materials*, 7, pp. 100115.
- FANG, J., WANG, Y. and GAO, D., 2015. On the collapse resistance of multilayer cemented casing in directional well under anisotropic formation. *Journal of Natural Gas Science and Engineering*, 26, pp. 409-418.
- Fan, G., Guo, Y., Zheng, J. & Hong, W. 2019, "Application of the weighted k-nearest neighbor algorithm for short-term load forecasting", *Energies*, vol. 12, no. 5, pp. 916.
- FAZEKAS, B. and GODA, T.J., 2020. New numerical stress solutions to calibrate hyper-visco-pseudo-elastic material models effectively. *Materials & Design*, 194, pp. 108861
- FENG, S., ZHOU, H. and DONG, H., 2019. Using deep neural network with small dataset to predict material defects. *Materials & Design*, 162, pp. 300-310.
- FENG, Y. and GRAY, K., 2017. Parameters controlling pressure and fracture behaviours in field injectivity tests: A numerical investigation using coupled flow and geomechanics model. *Computers and Geotechnics*, 87, pp. 49-61.
- FERLA, A., LAVROV, A. and FJÆR, E., 2009. Finite-element analysis of thermal-induced stresses around a cased injection well. *Journal of Physics: Conference Series*. IOP Publishing. pp. 012051.

FERRO, P. and BONOLLO, F., 2019. Materials selection in a critical raw materials perspective. *Materials & Design*, 177, pp. 107848.

FISCHER, A. and BOBZIN, K., 2009. *Friction, wear and wear protection*. John Wiley & Sons.

FURUI, K. et al., 2010. A comprehensive modeling analysis of borehole stability and production-liner deformation for inclined/horizontal wells completed in a highly compacting chalk formation. *SPE Drilling & Completion*, 25(04), pp. 530-543.

FURUI, K. et al., 2012. A Comprehensive Model of High-Rate Matrix-Acid Stimulation for Long Horizontal Wells in Carbonate Reservoirs: Part II--Wellbore/Reservoir Coupled-Flow Modeling and Field Application. *SPE Journal*, 17(01), pp. 280-291

GAO, L. and HSU, C.T., 1998. Fatigue of concrete under uniaxial compression cyclic loading. *Materials Journal*, 95(5), pp. 575-581.

GOROKHOVA, L., PARRY, A.J. and FLAMANT, N.C., 2014. Comparing soft-string and stiff-string methods used to compute casing centralization. *SPE Drilling & Completion*, 29(01), pp. 106-114.

GOUVEIA, L. et al., 2020. Probabilistic assessment of API casing strength in serviceability limit state. *Journal of Petroleum Exploration and Production Technology*, 10(5), pp. 2089-2104

GUO, X. et al., 2019. Numerical simulation of casing deformation during volume fracturing of horizontal shale gas wells. *Journal of Petroleum Science and Engineering*, 172, pp. 731-742.

GUO, Y., BLANFORD, M. and CANDELLA, J., 2015. Evaluating the Risk of Casing Failure Caused by High-Density Perforation: A 3D Finite-Element-Method Study of Compaction-Induced Casing Deformation in a Deepwater Reservoir, Gulf of Mexico. *SPE Drilling & Completion*, 30(02), pp. 141-151.

GUO, X. et al., 2018. Shale experiment and numerical investigation of casing deformation during volume fracturing. *Arabian Journal of Geosciences*, 11(22), pp. 1-7.

HAGHSHENAS, A., HESS, J. and CUTHBERT, A., 2017. Stress analysis of tubular failures during hydraulic fracturing: cases and lessons learned. *SPE Hydraulic Fracturing Technology Conference and Exhibition*. Society of Petroleum Engineers.

HAN, L. et al., 2018. Strain-Based Casing Design for Cyclic-Steam-Stimulation Wells. *SPE Production & Operations*, 33(02), pp. 409-418.

HAUSLER, R.H., KRISHNAMURTHY, R., GOMEZ, J. and KUSINSKI, G., 2017. Methodology for materials selection basis of design, and equipment testing criteria. *Offshore Technology Conference*. Offshore Technology Conference.

HAY, M.G. and BELCZEWSKI, D., 2003. Development of Recommended Practices for Completing and Producing Critical Sour Gas Wells-Material Requirements. *CORROSION 2003*. OnePetro.

HE, S., ZENG, B., YANG, X., WEI, G., LIU, W. and LIU, T., 2014. Comprehensive Analysis the Casing Deformation in Shale Gas Reservoir Modification by Seismic and Microseismic Technology. *AAPG Annual Convention and Exhibition*.

HEARN, E.J., 1997. *Mechanics of Materials 2: The mechanics of elastic and plastic deformation of solids and structural materials*. Elsevier.

HEATHMAN, J.F. and BECK, F.E., 2006. Finite element analysis couples casing and cement designs for HTHP wells in East Texas. *IADC/SPE Drilling Conference*. Society of Petroleum Engineers.

HOSSAIN, M. and AMRO, M., 2010. Drilling and completion challenges and remedies of CO₂ injected wells with emphasis to mitigate well integrity issues. *SPE Asia Pacific Oil and Gas Conference and Exhibition*. Society of Petroleum Engineers.

HUANG, W. and GAO, D., 2015. A theoretical study of the critical external pressure for casing collapse. *Journal of Natural Gas Science and Engineering*, 27, pp. 290-297.

HUANG, W., GAO, D. and LIU, Y., 2016. A study of tubular string buckling in vertical wells. *International Journal of Mechanical Sciences*, 118, pp. 231-253.

HU, C., AI, C., TAO, F., WANG, F. and YAN, M., 2016. Optimization of well completion method and casing design parameters to delay casing impairment caused by formation slippage. *SPE/IADC Middle East drilling technology conference and exhibition*. Society of Petroleum Engineers.

JALALI, H.H. et al., 2016. Experimental and finite element study of the reverse faulting effects on buried continuous steel gas pipelines. *Soil Dynamics and Earthquake Engineering*, 86, pp. 1-14.

JACOBS, T., 2020. An Unconventional Challenge Can Casing Failures During Hydraulic Fracturing Be Stopped? *Journal of Petroleum Technology*, 72(01), pp. 26-32

JELLISON, M.J. and BROCK, J.N., 1998. The impact of compression forces on casing string designs and connectors. *IADC/SPE Asia Pacific Drilling Technology*. Society of Petroleum Engineers.

JAEGER, J.C., COOK, N.G. and ZIMMERMAN, R., 2009. *Fundamentals of rock mechanics*. John Wiley & Sons.

JINAN, Z., YINLONG, W., CHI, A., JINDAN, Y. and FUPING, F., 2012. Abhesion Mechanics Model of Horizontal Well Cement-Formation Interface. *International Conference on Information Computing and Applications*. Springer. pp. 709-716.

JONES, S.L., KESNER, K.E., O'ROURKE, T.D., STEWART, H.E., ABDOUN, T. and O'ROURKE, M.J., 2004. Large-displacement Facility for Testing Highly Ductile Lifeline Systems. *Proc. of the Third UJNR Workshop on Soil-Structure Interaction*. pp. 1-18.

KABIR, G., SADIQ, R. and TEFAMARIAM, S., 2014. A review of multi-criteria decision-making methods for infrastructure management. *Structure and infrastructure engineering*, 10(9), pp. 1176-1210

KALDAL, G.S. et al., 2015. Structural modeling of the casings in high temperature geothermal wells. *Geothermics*, 55, pp. 126-137.

KAYVANTASH, K. 2015-2019, "ODYSSEE: Optimal Decision Support System for Engineering and Expertise", a ML/ROM based AI software platform for real-time predictions and optimization.

KING, G.E. and KING, D.E., 2013. Environmental Risk Arising From Well-Construction Failure--Differences Between Barrier and Well Failure, and Estimates of Failure Frequency Across Common Well Types, Locations, and Well Age. *SPE Production & Operations*, 28(04), pp. 323-344

KIRAN, R. et al., 2017. Identification and evaluation of well integrity and causes of failure of well integrity barriers (A review). *Journal of Natural Gas Science and Engineering*, 45, pp. 511-526.

KLEMENTICH, E.F. and JELLISON, M.J., 1986. A service-life model for casing strings. *SPE Drilling Engineering*, 1(02), pp. 141-152.

KUANHAI, D. et al., 2017. Experimental study the collapse failure mechanism of cemented casing under non-uniform load. *Engineering Failure Analysis*, 73, pp. 1-10.

KUMAR, R. and RAY, A., 2014. Selection of material for optimal design using multi-criteria decision making. *Procedia materials science*, 6, pp. 590-596.

KYLLINGSTAD, Å., 1995. Buckling of tubular strings in curved wells. *Journal of Petroleum Science and Engineering*, 12(3), pp. 209-218.

LAVROV, A., TODOROVIC, J. and TORSÆTER, M., 2015. Numerical study of tensile thermal stresses in a casing-cement-rock system with heterogeneities. *49th US Rock Mechanics/Geomechanics Symposium*. American Rock Mechanics Association.

LI, Y. et al., 2019. Mechanism of casing failure during hydraulic fracturing: Lessons learned from a tight-oil reservoir in China. *Engineering Failure Analysis*, 98, pp. 58-71.

LI, H. et al., 2020. A novel hybrid MCDM model for machine tool selection using fuzzy DEMATEL, entropy weighting and later defuzzification VIKOR. *Applied Soft Computing*, 91, pp. 106207.

LI, H., DENG, J., LIU, W., LI, Y. and LIN, S., 2017. Research on Casing Deformation Failure Mechanism During Volume Fracturing for Tight Oil Reservoir of Horizontal Wells. *51st US Rock Mechanics/Geomechanics Symposium*. American Rock Mechanics Association.

LI, J. et al., 2012. The effect of fracture-face matrix damage on productivity of fractures with infinite and finite conductivities in shale-gas reservoirs. *SPE Drilling & Completion*, 27(03), pp. 348-354.

LI, L. et al., 2012. Numerical simulation of 3D hydraulic fracturing based on an improved flow-stress-damage model and a parallel FEM technique. *Rock Mechanics and Rock Engineering*, 45(5), pp. 801-818

LI, X., FENG, Y. and GRAY, K., 2018. A hydro-mechanical sand erosion model for sand production simulation. *Journal of Petroleum Science and Engineering*, 166, pp. 208-224.

LI, C. and SAMUEL, R., 2016. Casing integrity: modeling strength degradation. *IADC/SPE Drilling Conference and Exhibition*. Society of Petroleum Engineers.

- LI, Z., 2008. Casing cementing with half warm-up for thermal recovery wells. *Journal of Petroleum Science and Engineering*, 61(2-4), pp. 94-98.
- LIAN, Z. et al., 2015. A study on casing deformation failure during multi-stage hydraulic fracturing for the stimulated reservoir volume of horizontal shale wells. *Journal of Natural Gas Science and Engineering*, 23, pp. 538-546.
- LIANG, E. et al., 2013. Analysis on collapse strength of casing wear. *Chinese Journal of Mechanical Engineering*, 26(3), pp. 613-619.
- LIANG, X. et al., 2017. Staged fracturing of horizontal shale gas wells with temporary plugging by sand filling. *Natural Gas Industry B*, 4(2), pp. 134-140
- LIHONG, H., JIANJUN, W., HANG, W., CHANGYI, Q., YAORONG, F., BIN, X., XUELU, Z. and ZHIHUA, T., 2013. Strain based design and material selection technology for thermal well casing. *International Petroleum Technology Conference*. OnePetro.
- LIN, T. et al., 2016. Evaluation of casing integrity defects considering wear and corrosion–Application to casing design. *Journal of Natural Gas Science and Engineering*, 29, pp. 440-452.
- LIAO, T.W., 2015. Two interval type 2 fuzzy TOPSIS material selection methods. *Materials & Design*, 88, pp. 1088-1099.
- LIU, G., ZHAO, H. and MA, F., 2016. Study of horizontal casing failure caused by fault deformation and movement. *Journal of Engineering Geology*, 24(S1), pp. 1019-1026.
- LIU, L., FENG, C. and LI, R.Z., 2020. Applications of Nickel-Based Alloy for Oil Country Tubular Goods. *Materials Science Forum*. Trans Tech Publ. pp. 604-609.

- LIU, M. et al., 2016. Effect of microstructure and crystallography on sulfide stress cracking in API-5CT-C110 casing steel. *Materials Science and Engineering: A*, 671, pp. 244-253.
- LIU, R. et al., 2015. Extremely-low-cycle fatigue behaviors of Cu and Cu–Al alloys: Damage mechanisms and life prediction. *Acta Materialia*, 83, pp. 341-356.
- LIU, Y. et al., 2017. Numerical modeling of gas flow in deformed well casing for the prediction of local resistance coefficients pertinent to longwall mining and its engineering evaluation. *Environmental Earth Sciences*, 76(20), pp. 686.
- LIU, W., YU, B. and DENG, J., 2017. Analytical method for evaluating stress field in casing-cement-formation system of oil/gas wells. *Applied Mathematics and Mechanics*, 38(9), pp. 1273-1294.
- LOPEZ-ALMANSA, F., Castro-Medina, J.C. and Oller, S., 2012. A numerical model of the structural behavior of buckling-restrained braces. *Engineering Structures*, 41, pp.108-117.
- LUBINSKI, A., 1950. A study of the buckling of rotary drilling strings. *Drilling and Production Practice*. American Petroleum Institute.
- MAINGUY, M. and INNES, R., 2018. Explaining Sustained" A"-Annulus Pressure in Major North Sea High-Pressure/High-Temperature Fields. *SPE Drilling & Completion*.
- MAO, L., CAI, M. and WANG, G., 2018. Effect of rotation speed on the abrasive--erosive--corrosive wear of steel pipes against steel casings used in drilling for petroleum. Available online 4 June 2018.

MARBUN, B. et al., 2020. Casing setting depth and design of production well in water-dominated geothermal system with 330° C reservoir temperature. *Energy Reports*, 6, pp. 582-593.

MARYA, M., 2020. A Comparison of the Pitting and Crevice Corrosion of Directional Drilling Alloys With Oilfield Production Alloys. *NACE International Corrosion Conference Proceedings*. NACE International. pp. 1-15.

MATSUMOTO, K. et al., 2018. Study of Oil Country Tubular Goods Casing and Liner Wear Mechanism on Corrosion-Resistant Alloys. *SPE Drilling & Completion*, 33(01), pp. 41-49

MENAND, S., BJORSET, A. and MACRESY, L., 2011. A New Buckling Model Successfully Validated with Full-Scale Buckling Tests. *AADE 2011 National Technical Conference & Exhibition*. pp. 3p.

MELVIN. F. KANNINEN and POPELAR, C.H., 1985. *Advanced fracture mechanics*. Oxford University Press.

MILLET, C., EVIN, H., DEFFO, M. and NÉEL, G., 2020. Development of High Strength Grade and Cost Effective Super Martensitic Stainless-Steel Solution for High CO₂/H₂S Environment. *CORROSION 2020*. OnePetro.

MITCHELL, R.F. and MISKA, S.Z., 2006. Helical buckling of pipe with connectors and torque. *SPE Drilling & Completion*, 21(02), pp. 108-115.

MITCHELL, S. et al., 2011. Comparing the Results of a Full-Scale Buckling-Test Program to Actual Well Data: New Semiempirical Buckling Model and Methods of Reducing Buckling Effects. *SPE Drilling & Completion*, 26(04), pp. 578-596.

MITCHELL, R.F., ZWARICH, N.R., HUNT, H.L., MCSPADDEN, A.R., TREVISAN, R. and GOODMAN, M.A., 2019. Dynamic Stress Analysis of Critical and Cyclic Loads for Production Casing in Horizontal Shale Wells. *SPE/IADC International Drilling Conference and Exhibition*. Society of Petroleum Engineers.

MOHAMMED, A.I. et al., 2019. *Casing structural integrity and failure modes in a range of well types - A review*. *Journal of natural gas science and engineering*

MOHAMMED, A.I. et al., 2020. Prediction of casing critical buckling during shale gas hydraulic fracturing. *Journal of petroleum science and engineering*, 185, pp. 106655

MUNSON, D.E., 2004. MD constitutive model parameters defined for gulf coast salt domes and structures. *Gulf Rocks 2004, the 6th North America Rock Mechanics Symposium (NARMS)*. American Rock Mechanics Association.

NOSHI, C.I. and SCHUBERT, J.J., 2018. The Role of Machine Learning in Drilling Operations; A Review. *SPE/AAPG Eastern Regional Meeting*. Society of Petroleum Engineers.

NOSHI, C., NOYNAERT, S. and SCHUBERT, J., 2019. Data Mining Approaches for Casing Failure Prediction and Prevention. *International Petroleum Technology Conference*. International Petroleum Technology Conference.

NOSHI, C., NOYNAERT, S. and SCHUBERT, J., 2018. Casing Failure Using Machine Learning Algorithms: Five Case Studies. *SPE Thermal Well Integrity and Design Symposium*. Society of Petroleum Engineers.

OXFORD, W.F., J., 1967. Tubular Goods -Service Conditions and Performance. /5/1/. Society of Petroleum Engineers.

PENG, S., FU, J. and ZHANG, J., 2007. Borehole casing failure analysis in unconsolidated formations: A case study. *Journal of Petroleum Science and Engineering*, 59(3-4), pp. 226-238.

PRASATH, V. et al., 2017. Distance and Similarity Measures Effect on the Performance of K-Nearest Neighbor Classifier--A Review. *arXiv preprint arXiv:1708.04321*.

QI, Y., ZHANG, Z. and ZHANG, C., 2020. Comparison of Stress Corrosion Cracking Behavior of Fe13Cr5Ni-and Fe17Cr5. 5Ni-Based High Chromium Stainless Steels in HTHP CO₂ Environments. *CORROSION 2020*. NACE International.

RAO, R.V., 2007. *Decision making in the manufacturing environment: using graph theory and fuzzy multiple attribute decision making methods*. Springer Science & Business Media.

RODRIGUEZ-PRADA, H., 1990. Improved calculation of casing strains and stresses in a steam injector well simulator. *SPE Latin America Petroleum Engineering Conference*. Society of Petroleum Engineers.

RUBIO-ALIAGA, A. et al., 2021. MCDM-based multidimensional approach for selection of optimal groundwater pumping systems: Design and case example. *Renewable Energy*, 163, pp. 213-224.

SALEHI, S. et al., 2009. Casing collapse risk assessment and depth prediction with a neural network system approach. *Journal of Petroleum Science and Engineering*, 69(1-2), pp. 156-162.

SATHUVALLI, U.B., KRISHNA, S. and SURYANARAYANA, P., 2019. The mechanical response of concentric cemented casings exposed to arbitrary transverse external geomechanical and salt loads. *SPE/IADC International Drilling Conference and Exhibition*. Society of Petroleum Engineers.

SATHUVALLI, U.B. and SURYANARAYANA, P., 2016. Structural-casing/soil interaction effects on wellhead motion. *SPE Drilling & Completion*, 31(04), pp. 273-285.

SCHUPP, J., BYRNE, B., EACOTT, N., MARTIN, C., OLIPHANT, J., MACONOCHIE, A. and CATHIE, D., 2006. Pipeline unburial behaviour in loose sand. *International Conference on Offshore Mechanics and Arctic Engineering*. pp. 297-308.

SHEN, X., SHEN, G. and STANDIFIRD, W., 2016. Numerical Estimation of Upper Bound of Injection Pressure Window with Casing Integrity under Hydraulic Fracturing. *50th US Rock Mechanics/Geomechanics Symposium*. American Rock Mechanics Association.

SHEN, Z. and BECK, F.E., 2012. Intermediate casing collapse induced by casing wear in high-temperature and high-pressure wells. *SPE International Production and Operations Conference & Exhibition*. Society of Petroleum Engineers.

SMITHSON, T., 2016. *HPHT wells*. [online] London: Schlumberger. Available from: https://www.slb.com/-/media/Files/resources/oilfield_review/defining_series/Defining-

[HPHT.pdf?la=en&hash=3FF8F894C76522C77D31DAF3B136B24371E7CCDC](#) [Accessed February/20 2018]

TALEBI, R. et al., 2014. Application of soft computing approaches for modeling saturation pressure of reservoir oils. *Journal of Natural Gas Science and Engineering*, 20, pp. 8-15.

TAN, L., GAO, D. and ZHOU, J., 2018. A prediction model of casing wear in extended-reach drilling with buckled drillstring. *Journal of Applied Mechanics*, 85(2), pp. 021001.

TANG, Y. et al., 2013. Practice and understanding on multiple crack volume fracturing in open hole horizontal well section of Zone Su53. *Oil Drill Prod Technol*, 35, pp. 63-67.

THEODORIDIS, S., 2015. *Machine learning: a Bayesian and optimization perspective*. Academic press.

TURON, A. et al., 2006. A damage model for the simulation of delamination in advanced composites under variable-mode loading. *Mechanics of Materials*, 38(11), pp. 1072-1089

VUDOVICH, A., CHIN, L. and MORGAN, D., 1988. Casing deformation in Ekofisk. *Offshore Technology Conference*. Offshore Technology Conference.

WANG, H. et al., 2014. Advances of technology study of stimulated reservoir volume in an unconventional reservoir. *Spec Oil Gas Reserv.2014b*, 21(2), pp. 8-15

- WANG, H. and SAMUEL, R., 2016. 3D geomechanical modeling of salt-creep behavior on wellbore casing for presalt reservoirs. *SPE Drilling & Completion*, 31(04), pp. 261-272
- WANG, J. et al., 2019. Study of technical specifications for non-API 140 casing in ultra-deep well. *Engineering Failure Analysis*, 97, pp. 115-127.
- WANG, P., ZHU, Q. and BU, X., 2011. Finite element analysis on casing failure based on ADINA. *Systems Engineering Procedia*, 1, pp. 42-47.
- WANG, Q. et al., 2014. Natural gas from shale formation—the evolution, evidences and challenges of shale gas revolution in United States. *Renewable and Sustainable Energy Reviews*, 30, pp. 1-28
- WANG, Q., ZHANG, L. and HU, J., 2018. Real-time risk assessment of casing-failure incidents in a whole fracturing process. *Process Safety and Environmental Protection*, 120, pp. 206-214.
- WILSON, A., 2018. Risk-Based Statistical Approach To Predict Casing Leaks. *Journal of Petroleum Technology*, 70(06), pp. 71-72.
- WU, J. and KNAUSS, M.E., 2006. Casing temperature and stress analysis in steam-injection wells. *International Oil & Gas Conference and Exhibition in China*. Society of Petroleum Engineers.
- XI, Y. et al., 2019. Mechanisms and influence of casing shear deformation near the casing shoe, based on MFC surveys during multistage fracturing in shale gas wells in Canada. *Energies*, 12(3), pp. 372

XI, Y. et al., 2017. Numerical investigation for different casing deformation reasons in Weiyuan-Changning shale gas field during multistage hydraulic fracturing. *Journal of Petroleum Science and Engineering*,

XI, Y., LI, J., YU, Y., LI, Z. and MEI, B., 2017. Coupling Effect of Transient Temperature-Pressure on Casing String During Volume Fracturing in Shale Gas Wells. *Chinese Materials Conference*. Springer. pp. 985-1000 Yang

XING, Y., ZHANG, G., LIN, Q., BU, X., DA, Y. and QI, Y., 2017. Subcritical fracture process of sandstone with AE energy analysis. *51st US Rock Mechanics/Geomechanics Symposium*. American Rock Mechanics Association.

YAN, W. et al., 2017. Investigation of casing deformation during hydraulic fracturing in high geo-stress shale gas play. *Journal of Petroleum Science and Engineering*, 150, pp. 22-29.

YANG, S. et al., 2018. Mechanical performance of casing in in-situ combustion thermal recovery. *Journal of Petroleum Science and Engineering*, 168, pp. 32-38

YAN, Y. et al., 2019. A study on the influence of double ellipsoidal pitting corrosion on the collapsing strength of the casing. *Engineering Failure Analysis*, 100, pp. 11-24.

YIN, F. et al., 2017. Mechanical behavior of casing crossing slip formation in waterflooding oilfields. *Journal of Petroleum Science and Engineering*.

YIN, F. et al., 2018. Mechanical behavior of casing crossing slip formation in waterflooding oilfields. *Journal of Petroleum Science and Engineering*, 167, pp. 796-802

YIN, F. and GAO, D., 2015. Prediction of sustained production casing pressure and casing design for shale gas horizontal wells. *Journal of Natural Gas Science and Engineering*, 25, pp. 159-165

YIN, F. et al., 2018. Quantifying the induced fracture slip and casing deformation in hydraulically fracturing shale gas wells. *Journal of Natural Gas Science and Engineering*, 60, pp. 103-111 Magill

YU, B., HARDY, M. and ZHAO, H., 2017. Laboratory Testing of Casing-Cement Interface and Multi-Scale Modeling of Casing Integrity Within Salt. *51st US Rock Mechanics/Geomechanics Symposium*. American Rock Mechanics Association.

YU, H. et al., 2016. Experimental and numerical study on casing wear in a directional well under in situ stress for oil and gas drilling. *Journal of Natural Gas Science and Engineering*, 35, pp. 986-996.

YU, H., DAHI TALEGHANI, A., LIAN, Z. and LIN, T., 2019. Impact of Asymmetric Stimulated Rock Volume on Casing Deformation in Multi-Stage Fracturing; A Case Study. *SPE Annual Technical Conference and Exhibition*. Society of Petroleum Engineers.

YU, H., TALEGHANI, A.D. and LIAN, Z., 2019. Impact of the dogleg geometry on displacement efficiency during cementing; an integrated modelling approach. *Journal of Petroleum Science and Engineering*, 173, pp. 588-600.

YUAN, B. et al., 2016. Special issue: Formation damage during enhanced gas and liquid recovery. *Journal of Natural Gas Science and Engineering*, (36), pp. 1051-1054

ZENG, J., GAO, D., WANG, Y., FANG, J. and LIU, K., 2018. Research on the Effect of Casing Deformation on Sustained Casing Pressure. *52nd US Rock Mechanics/Geomechanics Symposium*. American Rock Mechanics Association.

ZHANG, Q. et al., 2016. Casing wear analysis helps verify the feasibility of gas drilling in directional wells. *Journal of Natural Gas Science and Engineering*, 35, pp. 291-298.

ZHANG, B. et al., 2017. Development and design of new casing to mitigate trapped annular pressure caused by thermal expansion in oil and gas wells. *Applied Thermal Engineering*, 118, pp. 292-298.

ZHANG, G. et al., 2010. Three-dimensional finite element simulation and parametric study for horizontal well hydraulic fracture. *Journal of Petroleum Science and Engineering*, 72(3-4), pp. 310-317.

ZHAO, C., LI, J., LIU, G., ZHANG, H., WANG, C., REN, K. and ZHANG, X., 2018. The Casing Deformation During Shale Gas Hydraulic Fracturing: Why it is so Serious in Weiyuan-Changning, China? *SPE Trinidad and Tobago Section Energy Resources Conference*. Society of Petroleum Engineers.

ZHAOWEI, C., LIN, S. and DEGUI, X., 2017. Mechanism of casing deformation in the ChangningWeiyuan national shale gas demonstration area and countermeasures.

ZHU, X. and LIU, B., 2018. The reliability-based evaluation of casing collapsing strength and its application in marine gas reservoirs. *Engineering Failure Analysis*, 85, pp. 1-13.

Appendices

Appendix A: Proposed Experimental Rig

A1. Introduction

Experimenting pipes and beams that are buried under the ground can be challenging in the laboratory. This is due to the complex inter-relationship and amongst variables and the limitations on what can be accomplished with such rigs in the laboratory; and as such there are very few detail experimental rigs in the literature.

As stated in chapter 2, buckling is a structural instability owing to applied load(s). Several numerical simulation and analytical mathematical models were developed for the estimation of the buckling under different assumptions and load scenarios. For example, the study of Enss and Platz (2016) developed experimental rig for the investigation of active and passive buckling of slender beam column with rectangular cross section. The experimentation of active and passive buckling is relatively easy – in that the column is axially loaded vertically and strains measure with strain gauges.

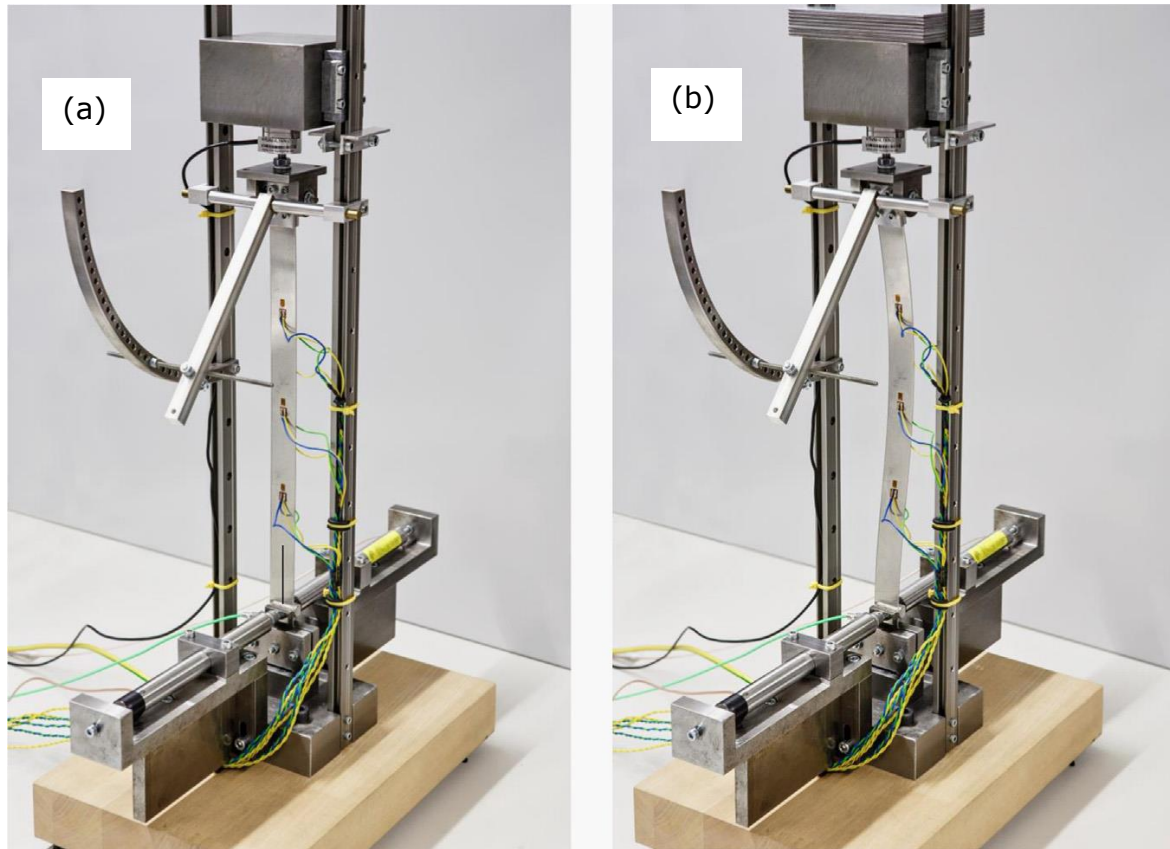


Figure A1 Experimental test setup (a) loaded with subcritical load $F_x \approx 23.5 \text{ N}$, (b) loaded with supercritical load $F_x \approx 31.5 \text{ N}$ and buckled without control (Enss and Platz 2016).

Another study by Schupp et al. (2006) utilised a 975mm X 950mm X 294mm rectangular tank to study pipe and soil response. The aluminium pipe was fixed at both ends so that buckling, or deflection only occur in the vertical plane. Then, a small initial vertical imperfection (approximately 0.5mm deflection) was introduced into the pipe so that buckling would occur upwards (Schupp et al. 2006). An actuating device is utilised to load pipe while axial displacement is measured. A recent study of Jalali et al. (2016) on the effect of reverse faulting in oil and gas pipeline was accomplished using a split box to determine the pipeline responses

closely to field conditions. However, the study pointed out that experimental investigation of the field condition is complex. As such, some simplifying assumptions are inevitable in studies that involves soil rupture and earthquakes (Jalali et al. 2016; Bray et al. 1994; Jones et al. 2004).

However, experimenting the casing pipe buckling deformation phenomena in laboratory is a still a complex big challenge. As such, this chapter made some simplifying assumption to examine the casing pipe based on slip displacement and the compressional load applied from one end while the other end is totally fix in all degree of freedom. The influence of internal fracturing pressure and reservoir/ rock thermal are assumed to 0MPa and the room temperature respectively.

A2 Experimental setup

The full-scale laboratory testing of the casing pipe under slip displacement and compression should enable the determination of field conditions associated with slippage during hydraulic fracturing to be calculated. In addition, it is worthy to mention that both natural and hydraulic fractures during hydraulic fracturing are spatially irregular and randomly distributed to the far field

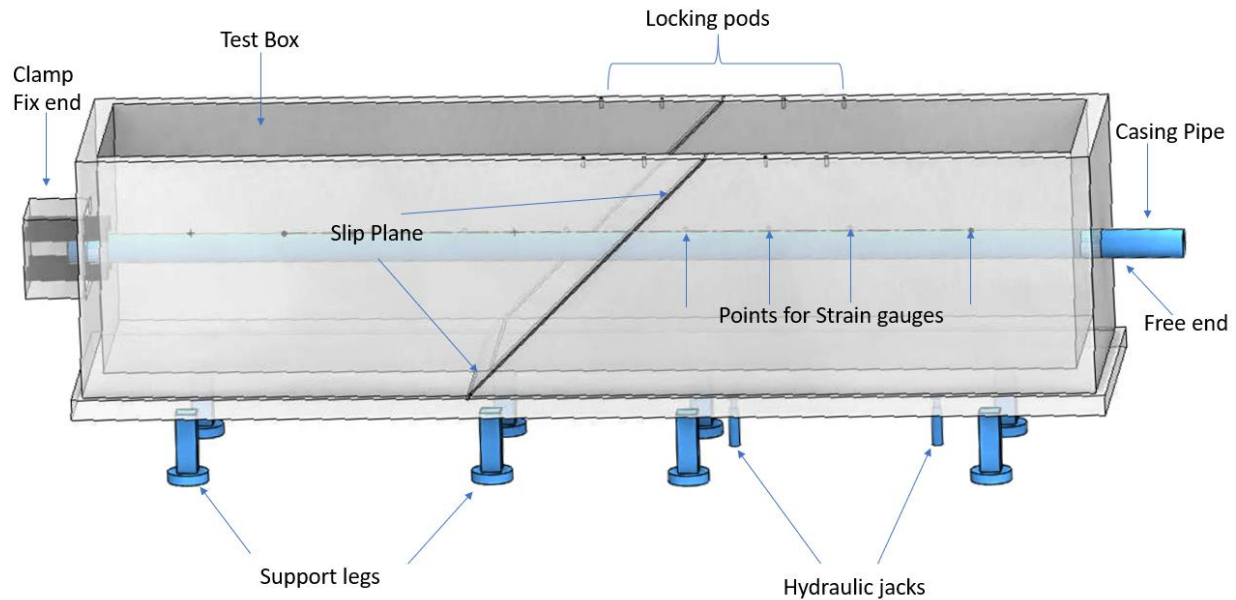


Figure A2 Schematic of the proposed experimental rig.

However, the main goal is quantifying the effect of slip displacement on casing buckling during hydraulic fracturing. Therefore, determining the impact of soil/rock failure due to the applied load on the casing and/or pipeline across a predefined slip plane has been justified by the studies of (Bray et al. 1994; Jones et al. 2004).

A large rectangular box test rig was design for studying the behaviour of buried shale gas casing subjected to slippage (Figure 7.2). The test rig was designed to test a number of 5m long steel casing with one end of the casing clamp while the other end is free depending the test being conducted (slip or compression). The estimated dimensions of the test box are 5.0 X 0.6 X 0.6m (length X width X height) with a slip angle equal to 45° with respect to the vertical plane. The slip plane is constructed in such a way that it divides the box at the centre.

During the compression test, the slip plane is lock so that the applied compressional load become effective on the casing. With one end clamped, the compressional load will be applied on the free end gradually in a small increment until the deflection force overcome the overburden load by soil/rock. Meanwhile, the displacement is being monitored with strain gauges.

If on the other hand, a slip displacement test is being conducted, the free end is left free and the slip plane is made active, essentially dividing the test rig into parts. Gradual slip displacement is applied using hydraulic jacks until the desired slip displacement is achieved. In the same way buckling or deflection of the casing pipe is monitored with strain gauges.

A3 Test materials

Shale rock and clays that are well graded can be used for the experiment or soil with similar characteristics to backfill the box. Based on the study of Jalali et al. (2016) on the effect of reverse faulting on pipeline suggested a water content of about 4.5–5% and compaction to a relative density of about 75%. Therefore, it is suggested that these figures be applied to denotes the rock consolidation and pore water saturation during the experiment.

The steel pipe specimen can API or non-API, but preferably the P110 and Q125 grades of any diameter ranging from 4.5 to 7.0 inches in diameter will be sufficient. However, if availability of these grades becomes a challenge, then non-API with similar specification in terms of yield strength and Poisson's ratio is recommended. In order to ensure accuracy, multiple uni-axial tensile tests can be performed on standard specimens to assess their tensile strengths and for any other studies that required tensile strength.

A4 Instrumentation

To monitor the structural response of the pipe during slippage, the casing pipe should be instrumented with 6 strain gauges in the axial configuration separated 750mm apart. This separation between strain gauges can be modified to suits the test objective (compression and slippage). However, this is chosen to give a very coverage of the 5m length casing. The strain gauges that have the capacity to monitor both stress and strain in three directions at angle of 0°, 45°, 90° is recommended for greater accuracy. The strain gauge (TY120-3CA-10%-X) are chosen of high accuracy and long-term stability as established in the study of (Kuanhai et al.2016) on casing collapse under opposed line load.

A5 Experimental procedure

Once the pipe was instrumented with strain gauges as shown on Figure 7. 2 the box can be filled with clay/shale/ or similar soil/ using a soil bucket. The capacity of box is approximately 8.20m³ of soil was needed for each test to be performed. The soil was placed in 12 layers/lifts, each 108.3mm in thickness and subsequently compacted using a vibratory plate tamper. This is to ensure a very good compaction of the sand as indicated by Jalali et al. (2016).

Appendix B: R CODES

Strength Distribution for TOPSIS, AHP and Non-Weighed Methods

```
```{r}
library(plot3D)

NON WEIGHTED

x<- seq(633,640, by = 0.2)
y<- seq(1.5, 1.8, by = 0.02)
grid<- mesh(x,y)
z<- with(grid, x*y)
par(mfrow = c(2,2))
persp3D(z=z, x=x,y=y)
persp3D(z=z, x=x,y=y, along ="xy",space = 0.3)
contour2D(z,lwd = 1.5, clab = "Strength (MPa)", xlab="von Mises Stress (MPa)",
ylab= "Safety Facator")
image2D(z,lwd = 3, contour = TRUE, clab = "Strength (MPa)", xlab="von Mises
Stress (MPa)", ylab= "Safety Facator")
```

```{r}
AHP
x<- seq(633, 640, by = 0.2)
y<- seq(1.3, 1.7, by = 0.02)
grid<- mesh(x,y)
z<- with(grid, x*y)
par(mfrow = c(2,2))
persp3D(z=z, x=x, y=y)
contour2D(z, lwd =2)
```

```
contour2D(z,lwd = 1.5, clab = "Strength (MPa)", xlab="von Mises Stress (MPa)",
ylab= "Safety Facator")
```

```
image2D(z,lwd = 3, contour = TRUE, clab = "Strength (MPa)", xlab="von Mises
Stress (MPa)", ylab= "Safety Facator")
```

```
TOPSIS
```

```
x<- seq(632, 633, by = 0.2)
```

```
y<- seq(1.4, 1.5, by = 0.02)
```

```
grid<- mesh(x,y)
```

```
z<- with(grid, x*y)
```

```
par(mfrow = c(2,2))
```

```
persp3D(z=z, x=x, y=y)
```

```
contour2D(z, lwd =2)
```

```
contour2D(z,lwd = 1.5, clab = "Strength (MPa)", xlab="von Mises Stress (MPa)",
ylab= "Safety Facator")
```

```
image2D(z,lwd = 3, contour = TRUE, clab = "Strength (MPa)", xlab="von Mises
Stress (MPa)", ylab= "Safety Facator")
```

```
````
```

P110 and Q125 Classification Data

```
```{r}
```

```
set.seed(1)
```

```
library(caret)
```

```
library(pROC)
```

```
library(mlbench)
```

```
library(ggplot2)
```

```
````
```

```
# Read the 125 data
```

```

```{r}
read.csv("C:\\Users\\haske\\Documents\\My R Tutorials\\Q125 Data.csv")
Data125<- read.csv("C:\\Users\\haske\\Documents\\My R Tutorials\\Q125
Data.csv")
Data125
ggplot(Data125,aes(Time, vonMises, fill = Status))+geom_point(shape =21, size =
3)

```

### **Correlation Codes**

```

```{r}
library(plot3D)
library(plotly)
library(rgl)
library(corrplot)
```

#Reading the Data

```{r}
read.csv("C:\\Users\\haske\\Desktop\\MCDM_DATA ANALYSIS\\AHP.csv")
AHP<-read.csv("C:\\Users\\haske\\Desktop\\MCDM_DATA ANALYSIS\\AHP.csv")

View(AHP)

Name<- c("FV535","BS144","BS145","BS143","V150","S33207","AISI
416","Q125","SM125","P110")
AHP<- cbind(AHP,Name)
View(AHP)
AHP<- AHP[,-1]

```

```
View(AHP)
```

```
scatter3D(x=AHP$Mises,y=AHP$SF,z=AHP$Rank, bty = "b2", pch =20, cex =3,  
ticktype = "detailed", clab = "Ranking",xlab= "von Mises Stress",ylab= "Safety  
Factor",zlab="Rank")
```

```
```\n
```

```
Correlation matrix plot for non weighted method
```

```
```\n{r}
```

```
library(corrplot)
```

```
plot(AHP)
```

```
Ahp<- AHP[,-5]
```

```
View(Ahp)
```

```
plot(Ahp)
```

```
cr<-cor(Ahp)
```

```
corrplot(cr)
```

```
corrplot(cr, method = "number")
```

```
```\n
```

```
Codes for non-weighted method
```

```
```\n{r}
```

```
read.csv("C:\\Users\\haske\\Desktop\\MCDM_DATA  
ANALYSIS\\Non_weighted.csv")
```

```
Non_weighted<-read.csv("C:\\Users\\haske\\Desktop\\MCDM_DATA  
ANALYSIS\\Non_weighted.csv")
```

```
View(Non_weighted)
```

```
Name<-c("AISI", "416", "  
V150", "Q125", "SM125", "P110", "BS145", "BS143", "BS144", "S33207", "FV535  
")
```

```

Non_weighted<- cbind(Non_weighted,Name)
View(Non_weighted)
Non_weighted<- Non_weighted[,-1]
View(Non_weighted)
scatter3D(x=Non_weighted$Mises,y=Non_weighted$SF,z=Non_weighted$Rank,
bty = "b2", pch =20, cex =3, ticktype = "detailed", clab = "Ranking",xlab= "von
Mises Stress",ylab= "Safety Factor",zlab="Rank")

```

```

` ``
# correlation matrix for non_wieghted data
`` `{r}
plot(Non_weighted)
non_weighted<- Non_weighted[,-5]
View(non_weighted)
plot(non_weighted)
nw<-cor(non_weighted)
corrplot(nw)
corrplot(nw,method="ellipse")
options(prompt = " ")
options(continue = " ")
options(width=75)
non_weighted <- non_weighted[seq(1, nrow(non_weighted), by = 1),
seq(1, ncol(non_weighted), by = 1)]
par(mfrow = c(10, 4), mar = c(3, 3, 3, 2))
image2D(non_weighted, contour = TRUE)
contour2D(non_weighted, lwd = 2)
image2D(non_weighted, clab = "m")

` ``

```

```

` `

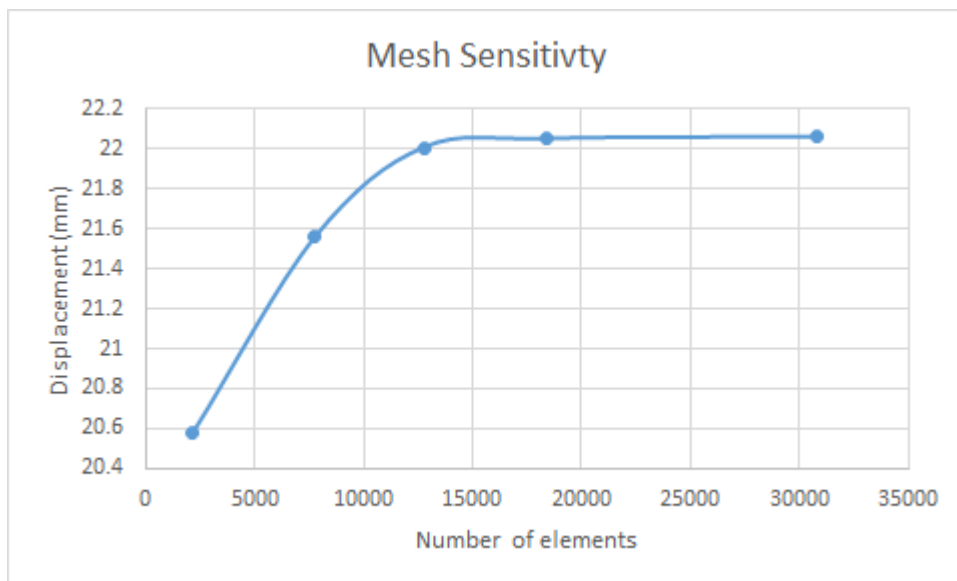
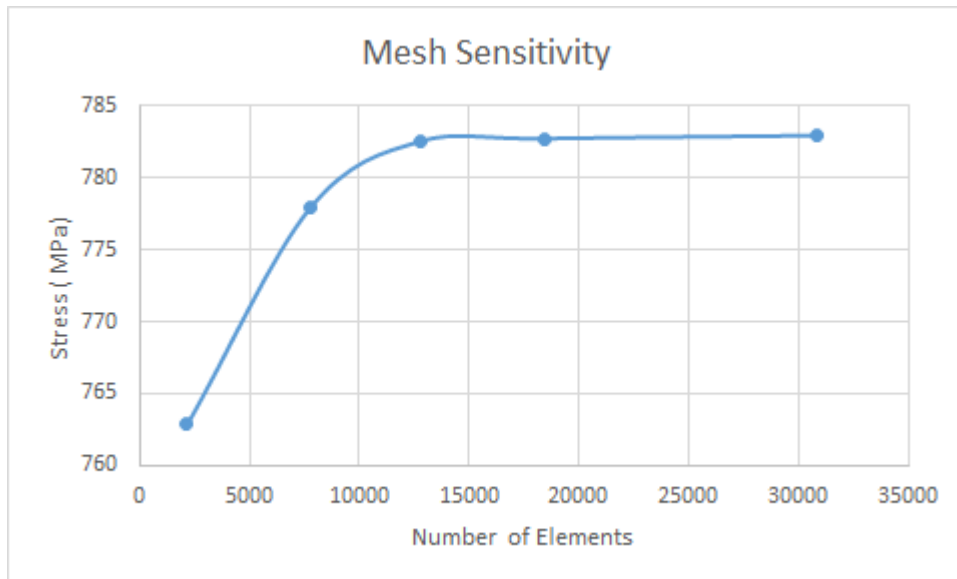
# TOPSIS Correlation
```{r}
read.csv("C:\\Users\\haske\\Desktop\\MCDM_DATA ANALYSIS\\TOPSIS.csv")
TOPSIS<-read.csv("C:\\Users\\haske\\Desktop\\MCDM_DATA
ANALYSIS\\TOPSIS.csv")
Topsis<- TOPSIS[,-1]
View(Topsis)
plot(Topsis)
cr<-cor(Topsis)
corrplot(cr)
corrplot(cr, method = "number")

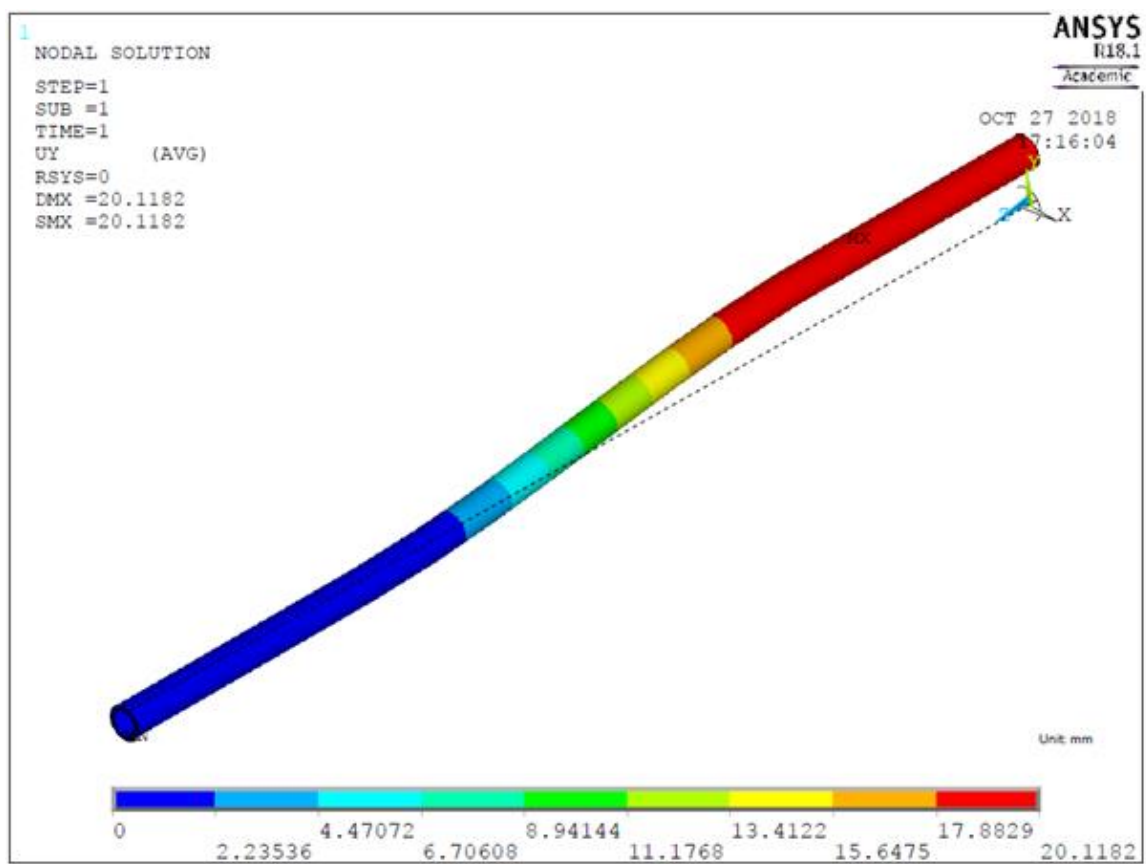
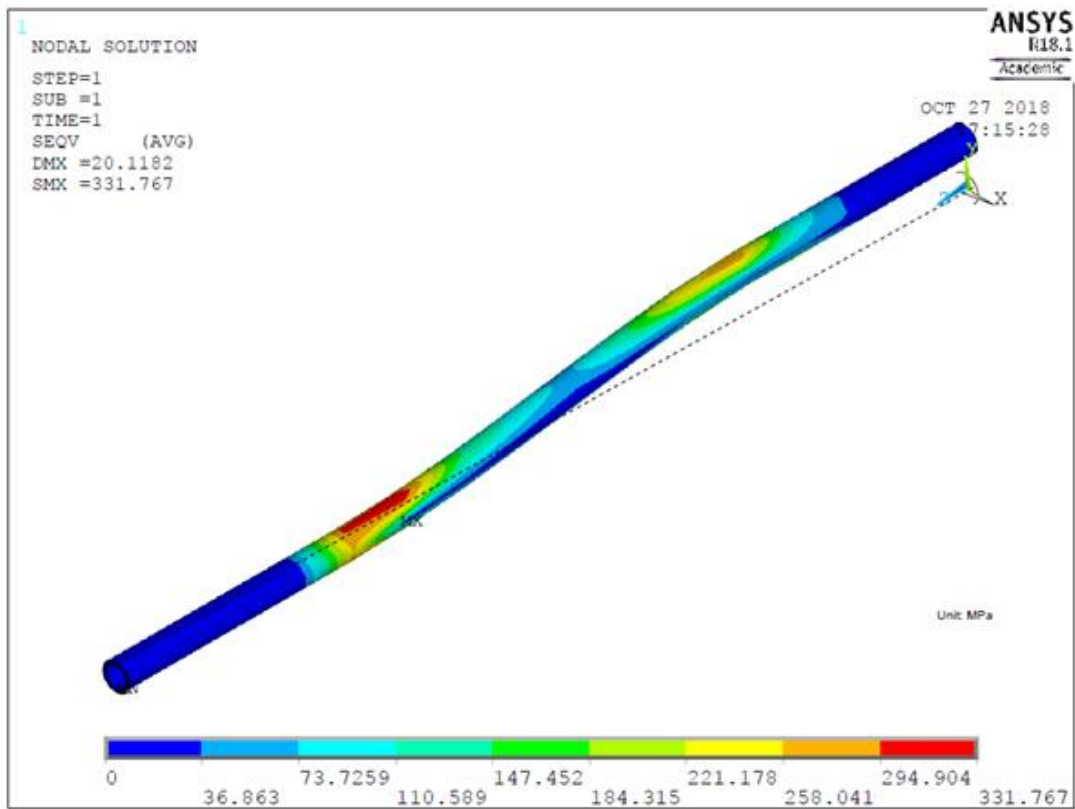
View(TOPSIS)

` ` `

```

## Appendix C: Tables Data and Mesh Sensitivities plots







SlipPlane	InnerDiam	OuterDiam	CementMc	CementRa	ReservoirT	AmbientTe	FracPressu	SlipDisplac	CoeTherrn	CementDic	HoleDiam	vonMises
60	4.5	5.5	7000	0.23	154	22	65	5	8.35E-06	6.013462	6.013462	814.8095
55	5.012	5.5	10000	0.23	130	23	55	5	8.49E-06	6.059151	6.056203	801.2348
45	4.95	5.5	12000	0.23	80	24	50	5	8.63E-06	6.104841	6.098945	791.9366
35	4.892	5.5	13000	0.23	60	25	45	5	8.78E-06	6.150531	6.141687	808.1511
30	4.778	5.5	14000	0.23	160	26	30	5	8.92E-06	6.19622	6.184429	829.7102
25	4.67	5.5	15000	0.23	180	37	35	5	9.06E-06	6.24191	6.227171	786.7387
20	4.548	5.5	20000	0.23	190	28	30	5	9.20E-06	6.287599	6.269913	778.7015
15	4.5	5.5	25000	0.23	200	13	70	5	9.34E-06	6.333289	6.312655	869.6379
10	4.44	5.5	7000	0.23	132	20	75	5	9.48E-06	6.378979	6.355397	770.0376
75	4.376	5.5	10000	0.23	220	21	80	5	9.62E-06	6.424668	6.398139	823.3314
80	4.276	5.5	12000	0.23	250	18	85	5	9.77E-06	6.470358	6.440881	863.1944
85	4.25	5.5	13000	0.23	300	17	90	5	9.91E-06	6.516048	6.483623	831.2539
60	4.09	5.5	15000	0.23	40	10	100	5	1.00E-05	6.561737	6.526365	821.0058
55	4	5.5	20000	0.23	50	8	65	5	8.35E-06	6.013462	6.013462	795.8409
45	3.876	5.5	25000	0.23	350	22	55	5	8.49E-06	6.059151	6.056203	808.0399
35	3.75	5.5	7000	0.23	75	23	50	5	8.63E-06	6.104841	6.098945	606.7452
30	4.56	5	10000	0.23	154	24	45	5	8.78E-06	6.150531	6.141687	787.0572
25	4.494	5	12000	0.23	130	25	30	5	8.92E-06	6.19622	6.184429	795.2308
20	4.408	5	13000	0.23	80	26	35	5	9.06E-06	6.24191	6.227171	765.8648
15	4.276	5	14000	0.23	60	37	30	5	9.20E-06	6.287599	6.269913	778.5267
10	4.184	5	15000	0.23	160	28	70	5	9.34E-06	6.333289	6.312655	787.5533
68	4.126	5	25000	0.23	190	20	80	5	9.48E-06	6.378979	6.355397	817.0946
70	4.044	5	7000	0.23	200	21	85	5	9.62E-06	6.424668	6.398139	861.2783
60	3.88	5	12000	0.23	220	17	95	5	9.77E-06	6.470358	6.440881	823.4541
60	3.876	5	13000	0.23	250	15	100	5	9.91E-06	6.516048	6.483623	847.5587
55	3.75	5	14000	0.23	300	10	65	5	1.00E-05	6.561737	6.526365	818.3431
45	3.626	5	15000	0.23	175	8	55	5	8.35E-06	6.013462	6.013462	797.3358
35	3.5	5	20000	0.23	40	22	50	5	8.49E-06	6.059151	6.056203	717.6292
25	4.052	4.5	7000	0.23	350	24	30	5	8.63E-06	6.104841	6.098945	148.5085
20	4.026	4.5	7000	0.23	75	25	35	5	8.78E-06	6.150531	6.141687	163.372
15	4	4.5	7000	0.23	154	26	30	5	8.92E-06	6.19622	6.184429	131.3217
45	3.5	4.5	7000	0.23	132	15	65	5	9.06E-06	6.24191	6.227171	164.3678
35	3.38	4.5	7000	0.23	220	10	55	5	9.20E-06	6.287599	6.269913	126.866

30	3.24	4.5	7000	0.23	250	8	50	5	9.34E-06	6.333289	6.312655	103.9867
25	5.901	6.625	7000	0.23	300	22	45	5	9.48E-06	6.378979	6.355397	868.3049
20	5.791	6.625	7000	0.23	175	23	30	5	9.62E-06	6.424668	6.398139	891.1658
15	5.675	6.625	7000	0.23	40	24	35	5	9.77E-06	6.470358	6.440881	925.4668
10	5.625	6.625	7000	0.23	50	25	30	5	9.91E-06	6.516048	6.483623	822.6402
75	5.575	6.625	10000	0.23	350	26	70	5	1.00E-05	6.561737	6.526365	1016.534
80	5.501	6.625	12000	0.23	75	37	75	5	8.35E-06	6.013462	6.013462	929.8114
85	5.375	6.625	13000	0.23	154	28	80	5	8.49E-06	6.059151	6.056203	852.0734
60	5.165	6.625	15000	0.23	80	20	90	5	8.63E-06	6.104841	6.098945	869.1116
55	5.125	6.625	20000	0.23	60	21	95	5	8.78E-06	6.150531	6.141687	841.7168
45	5.001	6.625	25000	0.23	160	18	100	5	8.92E-06	6.19622	6.184429	830.9389
35	4.875	6.625	7000	0.23	180	17	65	5	9.06E-06	6.24191	6.227171	815.5761
30	4.375	6.625	10000	0.23	190	15	55	5	9.20E-06	6.287599	6.269913	809.4114
25	6.538	7	12000	0.23	200	10	50	5	9.34E-06	6.333289	6.312655	855.374
20	6.456	7	13000	0.23	132	8	45	5	9.48E-06	6.378979	6.355397	889.6861
15	6.366	7	14000	0.23	220	22	30	5	9.62E-06	6.424668	6.398139	892.2425
10	6.314	7	15000	0.23	250	23	35	5	9.77E-06	6.470358	6.440881	987.2711
60	5.92	7	12000	0.23	350	28	85	5	9.91E-06	6.516048	6.483623	1047.436
60	5.82	7	13000	0.23	75	13	90	5	1.00E-05	6.561737	6.526365	927.04
55	5.75	7	14000	0.23	154	20	95	5	8.35E-06	6.013462	6.013462	910.3682
45	5.72	7	15000	0.23	130	21	100	5	8.49E-06	6.059151	6.056203	835.0788
35	5.66	7	20000	0.23	80	18	65	5	8.63E-06	6.104841	6.098945	831.4221
30	5.626	7	25000	0.23	60	17	55	5	8.78E-06	6.150531	6.141687	845.4258
25	5.54	7	7000	0.23	160	15	50	5	8.92E-06	6.19622	6.184429	829.9135
20	5.5	7	10000	0.23	180	10	45	5	9.06E-06	6.24191	6.227171	819.1021
15	5.376	7	12000	0.23	190	8	30	5	9.20E-06	6.287599	6.269913	838.7945
10	5.25	7	13000	0.23	200	22	35	5	9.34E-06	6.333289	6.312655	801.281
60	4.5	5.5	7000	0.23	175	37	85	5	9.48E-06	6.378979	6.355397	823.4114
55	4.5	5.5	10000	0.23	40	28	90	5	9.62E-06	6.424668	6.398139	807.2794
45	4.5	5.5	12000	0.23	50	13	95	5	9.77E-06	6.470358	6.440881	791.7762
35	4.5	5.5	13000	0.23	350	20	100	5	9.91E-06	6.516048	6.483623	788.0087
30	4.5	5.5	14000	0.23	75	21	65	5	1.00E-05	6.561737	6.526365	781.1307
25	4.5	5.5	15000	0.23	154	18	55	5	8.35E-06	6.013462	6.013462	772.0412
20	4.5	5.5	20000	0.23	154	17	50	5	8.49E-06	6.059151	6.056203	768.2292

15	4.5	5.5	25000	0.23	154	15	45	5	8.63E-06	6.104841	6.098945	833.7088
10	4.5	5.5	7000	0.23	154	10	30	5	8.78E-06	6.150531	6.141687	768.4812
60	4.5	5.5	7000	0.23	100	22	65	5	8.92E-06	6.19622	6.184429	831.822
60	5.012	5.5	7000	0.23	100	22	65	5	9.06E-06	6.24191	6.227171	817.0151
60	4.95	5.5	7000	0.23	100	22	65	5	9.20E-06	6.287599	6.269913	813.0945
60	4.892	5.5	7000	0.23	100	22	65	5	9.34E-06	6.333289	6.312655	812.5038
60	4.778	5.5	7000	0.23	100	22	65	5	9.48E-06	6.378979	6.355397	848.7729
60	4.67	5.5	7000	0.23	100	22	65	5	9.62E-06	6.424668	6.398139	862.011
60	4.548	5.5	7000	0.23	100	22	65	5	9.77E-06	6.470358	6.440881	874.0431
60	4.44	5.5	7000	0.23	100	22	65	5	9.91E-06	6.516048	6.483623	839.2536
60	4.376	5.5	7000	0.23	100	22	65	5	1.00E-05	6.561737	6.526365	842.4199
60	4.276	5.5	7000	0.23	100	22	65	5	8.35E-06	6.013462	6.013462	829.4397
60	4.25	5.5	7000	0.23	100	22	65	5	8.49E-06	6.059151	6.056203	820.1093
60	4.126	5.5	7000	0.23	100	22	65	5	8.63E-06	6.104841	6.098945	833.0607
60	4.09	5.5	7000	0.23	100	22	65	5	8.78E-06	6.150531	6.141687	833.1185
60	4	5.5	7000	0.23	100	22	65	5	8.92E-06	6.19622	6.184429	823.92
60	3.876	5.5	7000	0.23	100	22	65	5	9.06E-06	6.24191	6.227171	802.7028
60	3.75	5.5	7000	0.23	100	22	65	5	9.20E-06	6.287599	6.269913	781.2988
60	4.56	5	7000	0.23	100	22	65	5	9.34E-06	6.333289	6.312655	816.9388
60	4.494	5	7000	0.23	100	22	65	5	9.48E-06	6.378979	6.355397	813.9966
60	4.408	5	7000	0.23	100	22	65	5	9.62E-06	6.424668	6.398139	839.542
60	4.276	5	7000	0.23	100	22	65	5	9.77E-06	6.470358	6.440881	878.1192
60	4.184	5	7000	0.23	100	22	65	5	9.91E-06	6.516048	6.483623	907.614
60	4.156	5	7000	0.23	100	22	65	5	1.00E-05	6.561737	6.526365	913.8172
60	4.126	5	7000	0.23	100	22	65	5	8.35E-06	6.013462	6.013462	918.0945
60	4.044	5	7000	0.23	100	22	65	5	8.49E-06	6.059151	6.056203	921.0724
60	4	5	7000	0.23	100	22	65	5	8.63E-06	6.104841	6.098945	831.3337
60	3.88	5	7000	0.23	100	22	65	5	8.78E-06	6.150531	6.141687	839.5177
60	3.876	5	7000	0.23	100	22	65	5	8.92E-06	6.19622	6.184429	839.393
60	3.75	5	7000	0.23	100	22	65	5	9.06E-06	6.24191	6.227171	849.3281
60	3.626	5	7000	0.23	100	22	65	5	9.20E-06	6.287599	6.269913	835.8784
60	3.5	5	7000	0.23	100	22	65	5	9.34E-06	6.333289	6.312655	822.9353
60	3.75	4.5	7000	0.23	100	22	65	5	9.48E-06	6.378979	6.355397	188.4913
60	3.74	4.5	7000	0.23	100	22	65	5	9.62E-06	6.424668	6.398139	185.9876

60	3.696	4.5	7000	0.23	100	22	65	5	9.77E-06	6.470358	6.440881	175.8155
60	3.64	4.5	7000	0.23	100	22	65	5	9.91E-06	6.516048	6.483623	163.8578
60	3.5	4.5	7000	0.23	100	22	65	5	1.00E-05	6.561737	6.526365	164.3678
60	3.38	4.5	7000	0.23	100	22	65	5	8.35E-06	6.013462	6.013462	149.9358
60	3.24	4.5	7000	0.23	100	22	65	5	8.49E-06	6.059151	6.056203	135.1862
60	5.901	6.625	7000	0.23	100	22	65	5	8.63E-06	6.104841	6.098945	941.1209
60	5.791	6.625	7000	0.23	100	22	65	5	8.78E-06	6.150531	6.141687	929.4424
60	5.675	6.625	7000	0.23	100	22	65	5	8.92E-06	6.19622	6.184429	924.8495
60	5.625	6.625	7000	0.23	100	22	65	5	9.06E-06	6.24191	6.227171	903.656
60	5.575	6.625	7000	0.23	100	22	65	5	9.20E-06	6.287599	6.269913	927.5746
60	5.501	6.625	7000	0.23	100	22	65	5	9.34E-06	6.333289	6.312655	905.4004
60	5.375	6.625	7000	0.23	100	22	65	5	9.48E-06	6.378979	6.355397	886.0023
60	5.251	6.625	7000	0.23	100	22	65	5	9.62E-06	6.424668	6.398139	894.4225
60	5.165	6.625	7000	0.23	100	22	65	5	9.77E-06	6.470358	6.440881	882.0845
60	5.125	6.625	7000	0.23	100	22	65	5	9.91E-06	6.516048	6.483623	878.627
60	5.001	6.625	7000	0.23	100	22	65	5	1.00E-05	6.561737	6.526365	887.6202
60	4.875	6.625	7000	0.23	100	22	65	5	8.35E-06	6.013462	6.013462	873.8576
60	4.375	6.625	7000	0.23	100	22	65	5	8.49E-06	6.059151	6.056203	846.9042
60	6.538	7	7000	0.23	100	22	65	5	8.63E-06	6.104841	6.098945	850.6652
60	6.456	7	7000	0.23	100	22	65	5	8.78E-06	6.150531	6.141687	738.2074
60	6.366	7	7000	0.23	100	22	65	5	8.92E-06	6.19622	6.184429	889.9032
60	6.314	7	7000	0.23	100	22	65	5	9.06E-06	6.24191	6.227171	981.6801
60	6.276	7	7000	0.23	100	22	65	5	9.20E-06	6.287599	6.269913	977.3114
60	6.184	7	7000	0.23	100	22	65	5	9.34E-06	6.333289	6.312655	896.8059
60	6.094	7	7000	0.23	100	22	65	5	9.48E-06	6.378979	6.355397	912.2247
60	6.004	7	7000	0.23	100	22	65	5	9.62E-06	6.424668	6.398139	980.5539
60	5.92	7	7000	0.23	100	22	65	5	9.77E-06	6.470358	6.440881	947.8701
60	5.82	7	7000	0.23	100	22	65	5	9.91E-06	6.516048	6.483623	954.3078
60	5.75	7	7000	0.23	100	22	65	5	1.00E-05	6.561737	6.526365	932.8932
60	5.72	7	7000	0.23	100	22	65	5	8.35E-06	6.013462	6.013462	930.7121
60	5.66	7	7000	0.23	100	22	65	5	8.49E-06	6.059151	6.056203	919.0262
60	5.626	7	7000	0.23	100	22	65	5	8.63E-06	6.104841	6.098945	935.3559
60	5.54	7	7000	0.23	100	22	65	5	8.78E-06	6.150531	6.141687	878.6255
60	5.5	7	7000	0.23	100	22	65	5	8.92E-06	6.19622	6.184429	875.3224

60	5.376	7	7000	0.23	100	22	65	5	9.06E-06	6.24191	6.227171	885.2971
60	5.25	7	7000	0.23	100	22	65	5	9.20E-06	6.287599	6.269913	861.0864
60	5.126	7	7000	0.23	100	22	65	5	9.34E-06	6.333289	6.312655	895.6908
60	5	7	7000	0.23	100	22	65	5	9.48E-06	6.378979	6.355397	876.1595
60	4.5	5.5	7000	0.23	154	22	65	0	9.62E-06	6.424668	6.398139	392.9701
55	5.012	5.5	10000	0.3	130	23	55	0	9.77E-06	6.470358	6.440881	440.9712
45	4.95	5.5	12000	0.4	80	24	50	0	9.91E-06	6.516048	6.483623	271.4923
35	4.892	5.5	13000	0.49	60	25	45	0	1.00E-05	6.561737	6.526365	203.7543
30	4.778	5.5	14000	0.18	160	26	30	0	8.35E-06	6.013462	6.013462	276.4988
25	4.67	5.5	15000	0.23	180	37	35	0	8.49E-06	6.059151	6.056203	254.6188
20	4.548	5.5	20000	0.3	190	28	30	0	8.63E-06	6.104841	6.098945	222.5982
15	4.5	5.5	25000	0.4	200	13	70	0	8.78E-06	6.150531	6.141687	349.8393
10	4.44	5.5	7000	0.49	132	20	75	0	8.92E-06	6.19622	6.184429	239.0421
75	4.376	5.5	10000	0.18	220	21	80	0	9.06E-06	6.24191	6.227171	763.7071
80	4.276	5.5	12000	0.23	250	18	85	0	9.20E-06	6.287599	6.269913	799.7067
85	4.25	5.5	13000	0.3	300	17	90	0	9.34E-06	6.333289	6.312655	946.0791
88	4.126	5.5	14000	0.4	175	15	95	0	9.48E-06	6.378979	6.355397	873.3138
60	4.09	5.5	15000	0.49	40	10	100	0	9.62E-06	6.424668	6.398139	248.8397
55	4	5.5	20000	0.18	50	8	65	0	9.77E-06	6.470358	6.440881	154.4891
45	3.876	5.5	25000	0.23	350	22	55	0	9.91E-06	6.516048	6.483623	587.4477
35	3.75	5.5	7000	0.3	75	23	50	0	1.00E-05	6.561737	6.526365	109.9795
30	4.56	5	10000	0.4	154	24	45	0	8.35E-06	6.013462	6.013462	411.308
25	4.494	5	12000	0.49	130	25	30	0	8.49E-06	6.059151	6.056203	265.5534
20	4.408	5	13000	0.18	80	26	35	0	8.63E-06	6.104841	6.098945	160.0772
15	4.276	5	14000	0.23	60	37	30	0	8.78E-06	6.150531	6.141687	104.041
10	4.184	5	15000	0.23	160	28	70	0	8.92E-06	6.19622	6.184429	224.0318
68	4.126	5	25000	0.3	190	20	80	0	9.06E-06	6.24191	6.227171	749.2273
88	4	5	10000	0.49	132	18	90	0	9.20E-06	6.287599	6.269913	808.6751
60	3.88	5	12000	0.18	220	17	95	0	9.34E-06	6.333289	6.312655	607.9103
60	3.876	5	13000	0.23	250	15	100	0	9.48E-06	6.378979	6.355397	698.6409
55	3.75	5	14000	0.3	300	10	65	0	9.62E-06	6.424668	6.398139	675.0481
45	3.626	5	15000	0.4	175	8	55	0	9.77E-06	6.470358	6.440881	317.7299
35	3.5	5	20000	0.49	40	22	50	0	9.91E-06	6.516048	6.483623	103.275
30	4.09	4.5	25000	0.18	50	23	45	0	1.00E-05	6.561737	6.526365	271.6791

25	4.052	4.5	7000	0.23	350	24	30	0	8.35E-06	6.013462	6.013462	165.0672
20	4.026	4.5	6800	0.3	75	25	35	0	8.49E-06	6.059151	6.056203	181.4333
15	4	4.5	30000	0.4	154	26	30	0	8.63E-06	6.104841	6.098945	145.7844
66	3.75	4.5	28000	0.49	160	20	85	0	8.78E-06	6.150531	6.141687	268.3587
32	3.74	4.5	24000	0.18	180	21	90	0	8.92E-06	6.19622	6.184429	280.0113
60	3.696	4.5	23000	0.23	190	18	95	0	9.06E-06	6.24191	6.227171	275.078
55	3.64	4.5	7000	0.3	200	17	100	0	9.20E-06	6.287599	6.269913	271.2154
45	3.5	4.5	65000	0.4	132	15	65	0	9.34E-06	6.333289	6.312655	177.7123
35	3.38	4.5	7000	0.49	220	10	55	0	9.48E-06	6.378979	6.355397	136.6895
30	3.24	4.5	30000	0.18	250	8	50	0	9.62E-06	6.424668	6.398139	111.6836
25	5.901	6.625	16500	0.23	300	22	45	0	9.77E-06	6.470358	6.440881	788.0037
20	5.791	6.625	14500	0.3	175	23	30	0	9.91E-06	6.516048	6.483623	455.6704
15	5.675	6.625	26000	0.4	40	24	35	0	1.00E-05	6.561737	6.526365	122.8904
10	5.625	6.625	8000	0.49	50	25	30	0	8.35E-06	6.013462	6.013462	112.1611
75	5.575	6.625	10000	0.18	350	26	70	0	8.49E-06	6.059151	6.056203	842.6012
80	5.501	6.625	12000	0.23	75	37	75	0	8.63E-06	6.104841	6.098945	337.1269
85	5.375	6.625	13000	0.3	154	28	80	0	8.78E-06	6.150531	6.141687	749.1017
88	5.251	6.625	14000	0.4	130	13	85	0	8.92E-06	6.19622	6.184429	998.451
60	5.165	6.625	15000	0.49	80	20	90	0	9.06E-06	6.24191	6.227171	328.243
55	5.125	6.625	20000	0.18	60	21	95	0	9.20E-06	6.287599	6.269913	265.535
45	5.001	6.625	25000	0.23	160	18	100	0	9.34E-06	6.333289	6.312655	512.3143
35	4.875	6.625	7000	0.3	180	17	65	0	9.48E-06	6.378979	6.355397	457.676
30	4.375	6.625	10000	0.4	190	15	55	0	9.62E-06	6.424668	6.398139	405.9929
25	6.538	7	12000	0.49	200	10	50	0	9.77E-06	6.470358	6.440881	837.6767
20	6.456	7	13000	0.18	132	8	45	0	9.91E-06	6.516048	6.483623	501.8079
15	6.366	7	14000	0.23	220	22	30	0	1.00E-05	6.561737	6.526365	525.182
10	6.314	7	15000	0.3	250	23	35	0	8.35E-06	6.013462	6.013462	408.4752
60	5.92	7	12000	0.23	350	28	85	0	8.49E-06	6.059151	6.056203	841.3947
60	5.82	7	13000	0.3	75	13	90	0	8.63E-06	6.104841	6.098945	377.4833
55	5.75	7	14000	0.4	154	20	95	0	8.78E-06	6.150531	6.141687	585.1333
45	5.72	7	15000	0.49	130	21	100	0	8.92E-06	6.19622	6.184429	474.3731
35	5.66	7	20000	0.18	80	18	65	0	9.06E-06	6.24191	6.227171	261.2736
30	5.626	7	25000	0.23	60	17	55	0	9.20E-06	6.287599	6.269913	177.8155
25	5.54	7	7000	0.23	160	15	50	0	9.34E-06	6.333289	6.312655	375.0993

20	5.5	7	10000	0.3	180	10	45	0	9.48E-06	6.378979	6.355397	357.3148
15	5.376	7	12000	0.4	190	8	30	0	9.62E-06	6.424668	6.398139	278.3855
10	5.25	7	13000	0.49	200	22	35	0	9.77E-06	6.470358	6.440881	188.0391
75	5.126	7	14000	0.18	132	23	30	0	9.91E-06	6.516048	6.483623	737.7136
60	4.5	5.5	7000	0.49	175	37	85	0	1.00E-05	6.561737	6.526365	449.6503
55	4.5	5.5	10000	0.18	40	28	90	0	8.35E-06	6.013462	6.013462	296.3905
45	4.5	5.5	12000	0.23	50	13	95	0	8.49E-06	6.059151	6.056203	313.464
35	4.5	5.5	13000	0.23	350	20	100	0	8.63E-06	6.104841	6.098945	694.4362
30	4.5	5.5	14000	0.3	75	21	65	0	8.78E-06	6.150531	6.141687	214.1241
25	4.5	5.5	15000	0.4	154	18	55	0	8.92E-06	6.19622	6.184429	258.9852
20	4.5	5.5	20000	0.49	154	17	50	0	9.06E-06	6.24191	6.227171	226.8168
15	4.5	5.5	25000	0.18	154	15	45	0	9.20E-06	6.287599	6.269913	256.8088
10	4.5	5.5	7000	0.23	154	10	30	0	9.34E-06	6.333289	6.312655	117.2057
75	4.5	5.5	10000	0.23	154	8	35	0	9.48E-06	6.378979	6.355397	559.112
80	4.5	5.5	12000	0.3	154	22	30	0	9.62E-06	6.424668	6.398139	451.9
60	4.5	5.5	7000	0.23	154	22	65	5	9.77E-06	6.470358	6.440881	828.6409
55	5.012	5.5	10000	0.23	130	23	55	5	9.91E-06	6.516048	6.483623	791.6186
45	4.95	5.5	12000	0.23	80	24	50	5	1.00E-05	6.561737	6.526365	817.5918
35	4.892	5.5	13000	0.23	60	25	45	5	8.35E-06	6.013462	6.013462	784.6176
30	4.778	5.5	14000	0.23	160	26	30	5	8.49E-06	6.059151	6.056203	795.187
25	4.67	5.5	15000	0.23	180	37	35	5	8.63E-06	6.104841	6.098945	778.8092
20	4.548	5.5	20000	0.23	190	28	30	5	8.78E-06	6.150531	6.141687	778.0486
15	4.5	5.5	25000	0.23	200	13	70	5	8.92E-06	6.19622	6.184429	785.4307
10	4.44	5.5	7000	0.23	132	20	75	5	9.06E-06	6.24191	6.227171	657.1136
75	4.376	5.5	10000	0.23	220	21	80	5	9.20E-06	6.287599	6.269913	817.7298
80	4.276	5.5	12000	0.23	250	18	85	5	9.34E-06	6.333289	6.312655	868.4878
85	4.25	5.5	13000	0.3	300	17	90	5	9.48E-06	6.378979	6.355397	887.9419
60	4.09	5.5	15000	0.49	40	10	100	5	9.62E-06	6.424668	6.398139	801.9983
55	4	5.5	20000	0.18	50	8	65	5	9.77E-06	6.470358	6.440881	800.3211
45	3.876	5.5	25000	0.23	350	22	55	5	9.91E-06	6.516048	6.483623	798.8273
35	3.75	5.5	7000	0.3	75	23	50	5	1.00E-05	6.561737	6.526365	518.9031
30	4.56	5	10000	0.4	154	24	45	5	8.35E-06	6.013462	6.013462	811.9507
25	4.494	5	12000	0.49	130	25	30	5	8.49E-06	6.059151	6.056203	784.9071
20	4.408	5	13000	0.18	80	26	35	5	8.63E-06	6.104841	6.098945	777.7069

15	4.276	5	14000	0.23	60	37	30	5	8.78E-06	6.150531	6.141687	753.7292
10	4.184	5	15000	0.3	160	28	70	5	8.92E-06	6.19622	6.184429	784.4431
68	4.126	5	25000	0.4	190	20	80	5	9.06E-06	6.24191	6.227171	828.8934
70	4.044	5	7000	0.49	200	21	85	5	9.20E-06	6.287599	6.269913	843.827
60	3.88	5	12000	0.23	220	17	95	5	9.34E-06	6.333289	6.312655	839.2704
60	3.876	5	13000	0.3	250	15	100	5	9.48E-06	6.378979	6.355397	824.3188
55	3.75	5	14000	0.4	300	10	65	5	9.62E-06	6.424668	6.398139	826.2357
45	3.626	5	15000	0.49	175	8	55	5	9.77E-06	6.470358	6.440881	790.9806
35	3.5	5	20000	0.18	40	22	50	5	9.91E-06	6.516048	6.483623	611.0393
25	4.052	4.5	7000	0.23	350	24	30	5	1.00E-05	6.561737	6.526365	132.0026
20	4.026	4.5	7000	0.23	75	25	35	5	8.35E-06	6.013462	6.013462	145.2136
15	4	4.5	7000	0.23	154	26	30	5	8.49E-06	6.059151	6.056203	116.7225
45	3.5	4.5	7000	0.23	132	15	65	5	8.63E-06	6.104841	6.098945	146.1018
35	3.38	4.5	7000	0.23	220	10	55	5	8.78E-06	6.150531	6.141687	112.7682
30	3.24	4.5	7000	0.23	250	8	50	5	8.92E-06	6.19622	6.184429	92.43173
25	5.901	6.625	7000	0.3	300	22	45	5	9.06E-06	6.24191	6.227171	854.58
20	5.791	6.625	7000	0.4	175	23	30	5	9.20E-06	6.287599	6.269913	945.8384
15	5.675	6.625	7000	0.49	40	24	35	5	9.34E-06	6.333289	6.312655	818.4499
10	5.625	6.625	7000	0.18	50	25	30	5	9.48E-06	6.378979	6.355397	791.6701
75	5.575	6.625	10000	0.23	350	26	70	5	9.62E-06	6.424668	6.398139	981.2802
80	5.501	6.625	12000	0.3	75	37	75	5	9.77E-06	6.470358	6.440881	950.8716
85	5.375	6.625	13000	0.4	154	28	80	5	9.91E-06	6.516048	6.483623	882.1501
60	5.165	6.625	15000	0.18	80	20	90	5	1.00E-05	6.561737	6.526365	845.6114
55	5.125	6.625	20000	0.23	60	21	95	5	8.35E-06	6.013462	6.013462	818.3039
45	5.001	6.625	25000	0.3	160	18	100	5	8.49E-06	6.059151	6.056203	810.5658
35	4.875	6.625	7000	0.4	180	17	65	5	8.63E-06	6.104841	6.098945	798.4463
30	4.375	6.625	10000	0.49	190	15	55	5	8.78E-06	6.150531	6.141687	834.8242
25	6.538	7	12000	0.18	200	10	50	5	8.92E-06	6.19622	6.184429	886.1425
20	6.456	7	13000	0.23	132	8	45	5	9.06E-06	6.24191	6.227171	899.2326
15	6.366	7	14000	0.3	220	22	30	5	9.20E-06	6.287599	6.269913	927.3425
10	6.314	7	15000	0.4	250	23	35	5	9.34E-06	6.333289	6.312655	940.115
80	6.184	7	25000	0.18	175	25	70	5	9.48E-06	6.378979	6.355397	877.8915
85	6.094	7	7000	0.23	40	26	75	5	9.62E-06	6.424668	6.398139	888.1612
-15	4.5	5.5	7000	0.23	120	22	65	0	9.77E-06	6.470358	6.440881	468.0072



-45	4.95	5.5	10000	0.3	154	23	65	0	9.91E-06	6.516048	6.483623	991.7359
-35	4.892	5.5	12000	0.4	130	24	55	0	1.00E-05	6.561737	6.526365	722.4153
-30	4.778	5.5	13000	0.49	80	25	50	0	8.35E-06	6.013462	6.013462	415.493
-25	4.67	5.5	14000	0.18	60	26	45	0	8.49E-06	6.059151	6.056203	441.6867
-20	4.548	5.5	15000	0.23	160	37	30	0	8.63E-06	6.104841	6.098945	272.875
-15	4.5	5.5	20000	0.3	180	28	35	0	8.78E-06	6.150531	6.141687	382.7768
-10	4.44	5.5	25000	0.4	190	13	30	0	8.92E-06	6.19622	6.184429	341.1777
-60	4.09	5.5	14000	0.23	300	15	90	0	9.06E-06	6.24191	6.227171	831.6709
-38	4	5.5	15000	0.3	175	10	95	0	9.20E-06	6.287599	6.269913	483.2127
-45	3.876	5.5	20000	0.4	40	8	100	0	9.34E-06	6.333289	6.312655	547.1289
-35	3.75	5.5	25000	0.23	50	22	65	0	9.48E-06	6.378979	6.355397	296.0537
-30	4.56	5.5	7000	0.3	350	23	55	0	9.62E-06	6.424668	6.398139	700.1054
-25	4.494	5.5	10000	0.4	75	24	50	0	9.77E-06	6.470358	6.440881	339.2785
-14.161	4.670605	5.410555	7344.952	0.232261	108.8963	21.70921	60.5481	0	9.91E-06	6.516048	6.483623	497.9869
-14.5365	4.718423	5.962237	7169.618	0.217205	112.2239	20.21654	67.61867	0	1.00E-05	6.561737	6.526365	429.0747
-13.5788	4.6486	5.452349	6575.443	0.214974	122.9473	21.73557	67.12855	0	8.35E-06	6.013462	6.013462	505.4425
-14.0907	4.724264	5.709653	6353.844	0.212735	128.0064	20.80181	62.72179	0	8.49E-06	6.059151	6.056203	416.1864
-15.1811	4.329311	5.276766	7018.042	0.247481	109.5219	22.32403	65.65898	0	8.63E-06	6.104841	6.098945	420.2197
-15.4681	4.607177	5.765078	7440.326	0.241863	115.4619	22.99944	69.59275	0	8.78E-06	6.150531	6.141687	545.8233
-13.7587	4.445404	5.586154	7274.386	0.208523	128.9013	23.8853	71.02802	0	8.92E-06	6.19622	6.184429	396.5757
-15.7673	4.834941	5.38566	6658.241	0.221146	115.2449	21.89397	58.66767	0	9.06E-06	6.24191	6.227171	573.2023
-16.0865	4.827896	5.529911	7559.397	0.230843	122.478	19.95176	62.31731	0	9.20E-06	6.287599	6.269913	478.8553
-16.4014	4.897291	5.004207	7119.396	0.226856	131.9024	21.15141	70.71445	0	9.34E-06	6.333289	6.312655	335.9578
-15.0494	4.745843	5.922435	7319.459	0.219925	113.0302	22.8642	68.14573	0	9.48E-06	6.378979	6.355397	398.3286
-14.9414	4.155335	5.493766	7240.001	0.223159	112.3343	22.67342	68.20375	0	9.62E-06	6.424668	6.398139	348.4012
-16.0033	4.11449	5.474864	6470.962	0.228134	121.2224	22.40992	63.08602	0	9.77E-06	6.470358	6.440881	371.9907
-15.2498	4.281092	5.032806	7132.522	0.239495	129.1415	19.80945	67.31285	0	9.91E-06	6.516048	6.483623	508.7504
-14.008	4.246317	5.561556	7670.895	0.242431	124.1473	21.37593	64.78398	0	1.00E-05	6.561737	6.526365	399.9557
-16.29	4.875965	5.971821	6958.367	0.229493	131.3554	23.09308	63.78142	0	8.35E-06	6.013462	6.013462	474.7781
-14.7303	4.204518	5.655517	6501.334	0.250021	130.1193	21.55917	66.13017	0	8.49E-06	6.059151	6.056203	375.5349
-16.4725	4.489922	5.60593	6882.145	0.223867	111.0628	23.71386	66.43828	0	8.63E-06	6.104841	6.098945	421.5427
-16.1451	4.437181	5.779702	6432.454	0.238079	111.4547	20.56375	71.29395	0	8.78E-06	6.150531	6.141687	380.6626
-14.2438	4.541361	5.808354	6731.369	0.235141	127.6566	23.81345	64.14888	0	8.92E-06	6.19622	6.184429	394.4004
-13.8822	4.913227	5.258521	6601.111	0.251747	118.4452	22.10371	59.98127	0	9.06E-06	6.24191	6.227171	745.449

-15.831	4.376424	5.183938	7498.926	0.218019	120.7419	20.46263	65.29978	0	9.20E-06	6.287599	6.269913	482.1284
-13.7259	4.480333	5.213521	7530.184	0.245321	116.8276	21.2509	69.20053	0	9.34E-06	6.333289	6.312655	507.9653
-15.6332	4.272728	5.867839	7641.885	0.216192	119.7099	23.43786	64.46946	0	9.48E-06	6.378979	6.355397	340.3467
-15.3263	4.584918	5.902762	7087.743	0.248919	119.0141	20.08118	61.57527	0	9.62E-06	6.424668	6.398139	395.1116
-14.9763	4.307162	5.16889	6933.925	0.25238	126.0976	24.15821	60.19846	0	9.77E-06	6.470358	6.440881	467.3193
-14.6083	4.357427	5.3498	7387.852	0.234005	121.8059	23.23894	69.15711	0	9.91E-06	6.516048	6.483623	459.6573
-16.2465	4.218715	5.314038	7451.264	0.2132	127.0345	20.25517	59.34858	0	1.00E-05	6.561737	6.526365	403.2678
-14.8778	4.561675	5.128876	6392.778	0.235834	116.1451	22.19198	69.92821	0	8.35E-06	6.013462	6.013462	613.5901
-14.7658	4.69511	5.846124	6664.452	0.228344	114.6628	20.87362	58.98311	0	8.49E-06	6.059151	6.056203	437.9818
-14.4338	4.797892	6.025873	6817.805	0.246958	130.7328	21.45202	70.46913	0	8.63E-06	6.104841	6.098945	424.6978
-15.6932	4.417327	5.050548	6300.595	0.24015	113.9445	22.83072	68.70252	0	8.78E-06	6.150531	6.141687	522.7954
-13.5713	4.055571	5.336883	6707.169	0.210838	125.6518	20.94232	61.46352	0	8.92E-06	6.19622	6.184429	386.7139
-14.2804	4.092659	5.631758	6770.752	0.209669	117.3905	20.70077	66.68097	0	9.06E-06	6.24191	6.227171	356.5297
-14.676	4.907441	5.894132	7167.065	0.225429	128.6625	21.4706	61.19259	0	9.20E-06	6.287599	6.269913	596.1873
-14.1632	4.648791	6.040766	7213.731	0.245413	116.4264	20.70932	65.36494	0	9.34E-06	6.333289	6.312655	366.5175
-15.0611	4.052019	5.779647	6545.978	0.235194	119.6509	23.37684	61.85562	0	9.48E-06	6.378979	6.355397	320.0577
-15.1397	4.377993	5.611811	6784.433	0.242479	111.9686	20.96237	63.47523	0	9.62E-06	6.424668	6.398139	399.6037
-15.8083	4.513281	5.55018	7321.879	0.228698	120.2118	23.88172	63.05464	0	9.77E-06	6.470358	6.440881	493.0395
-13.9884	4.134073	5.723954	7445.585	0.215769	127.3268	22.6082	64.77719	0	9.91E-06	6.516048	6.483623	372.9027
-13.6881	4.094821	5.84954	7040.586	0.236788	111.278	22.71718	70.8588	0	1.00E-05	6.561737	6.526365	313.2265
-15.9323	4.267967	5.388049	7531.996	0.210175	126.5015	22.26432	69.09125	0	8.35E-06	6.013462	6.013462	416.0515
-16.132	4.176415	5.080992	7579.286	0.24018	117.1275	21.59289	67.57458	0	8.49E-06	6.059151	6.056203	449.9925
-14.9154	4.582323	5.984805	7070.368	0.210865	114.4016	21.90204	69.75205	0	8.63E-06	6.104841	6.098945	416.0515
-16.4247	4.57967	5.985448	6317.799	0.227701	109.0983	21.70921	64.19257	0	8.78E-06	6.150531	6.141687	874.4655
-15.0874	4.226425	5.954015	6784.587	0.218874	130.1599	20.21654	70.85417	0	8.92E-06	6.19622	6.184429	923.1357
-14.4818	4.306318	5.420674	6317.799	0.248625	110.6592	21.73557	68.60738	0	9.06E-06	6.24191	6.227171	110.7386
-15.7569	4.087613	5.276436	6784.587	0.232927	123.5498	20.80181	58.81538	0	9.20E-06	6.287599	6.269913	95.99903
-15.1574	4.112053	6.006028	6317.799	0.246466	116.7531	22.32403	59.78665	0	9.34E-06	6.333289	6.312655	1002.453
-13.5947	4.174708	5.083681	6784.587	0.239747	112.3369	22.99944	71.17021	0	9.48E-06	6.378979	6.355397	132.5356
-14.9453	4.490207	5.576419	6317.799	0.247928	116.5488	23.8853	60.44091	0	9.62E-06	6.424668	6.398139	882.505
-15.5019	4.722372	5.627984	6317.799	0.221453	120.314	21.89397	61.86172	0	9.77E-06	6.470358	6.440881	131.1073
-13.769	4.403402	5.151845	6784.587	0.233972	114.7493	19.95176	59.45374	0	9.91E-06	6.516048	6.483623	672.4644
-15.0124	4.914246	5.845928	6317.799	0.228928	125.5324	21.15141	63.64292	0	1.00E-05	6.561737	6.526365	152.3978
-13.9535	4.595992	5.768731	6317.799	0.210506	126.5143	22.8642	60.64661	0	8.35E-06	6.013462	6.013462	855.1068

-16.3532	4.542333	5.500516	6784.587	0.245249	127.7203	22.67342	63.36249	0	8.49E-06	6.059151	6.056203	133.3927
-15.3777	4.793492	5.880919	6317.799	0.249912	127.2482	22.40992	67.78652	0	8.63E-06	6.104841	6.098945	719.5787
-15.6125	4.663094	5.541599	6784.587	0.216566	118.6835	19.80945	64.1009	0	8.78E-06	6.150531	6.141687	694.7539
-16.2316	4.902133	5.098844	6317.799	0.208329	117.6246	21.37593	70.37153	0	8.92E-06	6.19622	6.184429	677.7836
-14.8059	4.273607	5.670213	6784.587	0.242673	114.9506	23.09308	69.01081	0	9.06E-06	6.24191	6.227171	948.8209
-15.3206	4.43305	5.930635	6317.799	0.235401	111.8582	21.55917	62.77882	0	9.20E-06	6.287599	6.269913	92.19522
-13.9972	4.682733	5.449548	6784.587	0.237667	124.821	23.71386	68.47595	0	9.34E-06	6.333289	6.312655	635.7723
-15.9897	4.528769	5.543805	6317.799	0.215614	113.2865	20.56375	66.41469	0	9.48E-06	6.378979	6.355397	921.0861
-16.0853	4.938521	5.472789	6317.799	0.251308	129.8424	23.81345	61.46532	0	9.62E-06	6.424668	6.398139	186.9289
-14.2944	4.477892	5.75523	6784.587	0.223208	118.0803	22.10371	65.60929	0	9.77E-06	6.470358	6.440881	954.1826
-15.908	4.385832	5.818272	6317.799	0.251978	111.2429	20.46263	69.33052	0	9.91E-06	6.516048	6.483623	906.4705
-13.8363	4.296935	5.395669	6317.799	0.24429	126.2785	21.2509	61.58156	0	1.00E-05	6.561737	6.526365	114.8262
-15.217	4.336058	5.8644	6784.587	0.207342	123.0683	23.43786	59.1189	0	8.35E-06	6.013462	6.013462	767.3167
-14.0797	4.85609	5.701655	6317.799	0.241998	128.613	20.08118	66.71818	0	8.49E-06	6.059151	6.056203	631.395
-14.2164	4.135565	6.0436	6317.799	0.211695	121.8727	24.15821	67.97286	0	8.63E-06	6.104841	6.098945	1052.928
-15.8726	4.162214	5.371143	6784.587	0.225882	119.4666	23.23894	69.70293	0	8.78E-06	6.150531	6.141687	849.3857
-14.6107	4.370108	5.178595	6317.799	0.230457	115.3877	20.25517	64.72782	0	8.92E-06	6.19622	6.184429	108.0143
-14.1886	4.746172	5.036723	6317.799	0.234928	113.7559	22.19198	65.85602	0	9.06E-06	6.24191	6.227171	1081.147
-16.3186	4.065845	4.999642	6784.587	0.2376	124.2108	20.87362	67.29933	0	9.20E-06	6.287599	6.269913	108.4133
-15.6922	4.609919	5.296269	6317.799	0.21467	122.3305	21.45202	65.29553	0	9.34E-06	6.333289	6.312655	157.0845
-14.8375	4.210135	5.133502	6317.799	0.211787	119.8702	22.83072	60.00191	0	9.48E-06	6.378979	6.355397	129.2259
-13.526	4.44396	5.737466	6784.587	0.220247	130.8512	20.94232	70.67879	0	9.62E-06	6.424668	6.398139	915.9152
-13.6588	4.627111	5.325513	6317.799	0.218323	109.3299	20.70077	60.89652	0	9.77E-06	6.470358	6.440881	662.7559
-15.4017	4.771498	5.97568	6317.799	0.23577	120.6279	21.4706	64.47324	0	9.91E-06	6.516048	6.483623	882.0502
-13.863	4.241904	5.577772	6784.587	0.231594	117.8773	20.70932	61.0431	0	1.00E-05	6.561737	6.526365	95.33615
-13.584	4.396088	5.868965	6317.799	0.247885	128.1354	23.37684	71.07361	0	8.35E-06	6.013462	6.013462	887.2271
-15.8729	4.109324	5.348323	6784.587	0.241892	111.8324	20.96237	67.15061	0	8.49E-06	6.059151	6.056203	94.06361
-15.9145	4.534102	5.107008	6317.799	0.216507	124.8382	23.88172	71.23203	0	8.63E-06	6.104841	6.098945	798.4336
-15.7895	4.668487	5.996155	6317.799	0.251694	126.2099	22.6082	63.91775	0	8.78E-06	6.150531	6.141687	863.0103
-16.2985	4.484563	5.258082	6784.587	0.237022	115.451	22.71718	64.74879	0	8.92E-06	6.19622	6.184429	610.2013
-14.5484	4.57123	5.775771	6317.799	0.226882	114.1882	22.26432	63.65618	0	9.06E-06	6.24191	6.227171	829.0224
-14.9992	4.268101	5.410414	6317.799	0.240505	112.7169	21.59289	62.5963	0	9.20E-06	6.287599	6.269913	108.4046
25.24038	4.054327	4.952644	6516.827	0.207928	150.7212	10.16827	30.33654	-5.48678	8.29E-06	5.96887	5.96887	219.1688
28.18156	4.101695	4.976557	8266.827	0.272261	180.7212	15.16827	36.70017	-5.27524	8.31E-06	6.01456	6.011612	223.1875

31.12274	4.149064	5.00047	7391.827	0.336595	210.7212	20.16827	43.06381	-5.0637	8.32E-06	6.06025	6.054354	270.2656
34.06391	4.196432	5.024383	9141.827	0.229372	240.7212	25.16827	49.42745	-4.85216	8.34E-06	6.105939	6.097096	320.9033
37.00509	4.243801	5.048296	6954.327	0.293706	270.7212	30.16827	55.79108	-4.64063	8.36E-06	6.151629	6.139838	374.4366
39.94627	4.291169	5.072209	8704.327	0.358039	156.7212	35.16827	62.15472	-4.42909	8.38E-06	6.197318	6.18258	431.8119
42.88744	4.338537	5.096122	7829.327	0.250817	186.7212	40.16827	68.51836	-4.21755	8.40E-06	6.243008	6.225322	493.9113
48.7698	4.433274	5.143949	6735.577	0.379483	246.7212	15.88255	81.24563	-3.79447	8.43E-06	6.334387	6.310806	928.4626
51.71097	4.480643	5.167862	8485.577	0.215076	276.7212	20.88255	87.60927	-3.58293	8.45E-06	6.380077	6.353548	951.1768
54.65215	4.528011	5.191775	7610.577	0.279409	162.7212	25.88255	93.9729	-3.37139	8.47E-06	6.425767	6.39629	905.6108
57.59333	4.57538	5.215688	9360.577	0.343743	192.7212	30.88255	30.91505	-3.15986	8.48E-06	6.471456	6.439031	878.4738
60.5345	4.622748	5.239601	7173.077	0.23652	222.7212	35.88255	37.27869	-2.94832	8.50E-06	6.517146	6.481773	907.8661
63.47568	4.670116	5.263514	8923.077	0.300854	252.7212	40.88255	43.64232	-5.47051	8.52E-06	6.562836	6.524515	1002.627
66.41686	4.717485	5.287427	8048.077	0.365187	282.7212	11.59684	50.00596	-5.25897	8.54E-06	6.608525	6.567257	1056.45
69.35803	4.764853	5.311134	9798.077	0.257965	168.7212	16.59684	56.3696	-5.04743	8.55E-06	6.654215	6.609999	1014.022
72.29921	4.812222	5.335253	6626.202	0.322298	198.7212	21.59684	62.73323	-4.83589	8.57E-06	6.699905	6.652741	1017.816
25.4134	4.85959	5.359166	8376.202	0.386632	228.7212	26.59684	69.09687	-4.62435	8.59E-06	6.745594	6.695483	855.8431
28.35457	4.906959	5.383079	7501.202	0.222224	258.7212	31.59684	75.46051	-4.41281	8.61E-06	6.791284	6.738225	861.7556
31.29575	4.05682	5.406992	9251.202	0.286558	288.7212	36.59684	81.82414	-4.20128	8.63E-06	6.836974	6.780967	858.6516
34.23692	4.104188	5.430905	7063.702	0.350891	174.7212	41.59684	88.18778	-3.98974	8.64E-06	6.882663	6.823709	828.0235
37.1781	4.151557	5.454818	8813.702	0.243669	204.7212	12.31113	94.55141	-3.7782	8.66E-06	6.928353	6.866451	847.827
40.11928	4.198925	5.478731	7938.702	0.308002	234.7212	17.31113	31.49356	-3.56666	8.68E-06	6.974043	6.909193	845.9536
43.06045	4.246294	4.953684	9688.702	0.372335	264.7212	22.31113	37.8572	-3.35512	8.70E-06	7.019732	6.951935	847.175
46.00163	4.293662	4.977597	6844.952	0.265113	294.7212	27.31113	44.22084	-3.14358	8.71E-06	7.065422	6.994677	865.9056
48.94281	4.341031	5.00151	8594.952	0.329446	151.9212	32.31113	50.58447	-2.93205	8.73E-06	7.111112	7.037419	823.6643
51.88398	4.388399	5.025423	7719.952	0.39378	181.9212	37.31113	56.94811	-5.45423	8.75E-06	7.156801	7.080161	905.343
54.82516	4.435767	5.049336	9469.952	0.210311	211.9212	42.31113	63.31175	-5.2427	8.77E-06	7.202491	7.122902	913.2423
57.76634	4.483136	5.073249	7282.452	0.274644	241.9212	13.02541	69.67538	-5.03116	8.78E-06	7.248181	7.165644	939.6973
66.58987	4.625241	5.144988	9907.452	0.296088	187.9212	28.02541	88.76629	-4.39654	8.84E-06	6.061825	5.970249	608.4145
69.53104	4.672609	5.168901	6571.514	0.360422	217.9212	33.02541	95.12993	-4.185	8.86E-06	6.107515	6.012991	969.7842
72.47222	4.719978	5.192814	8321.514	0.253199	247.9212	38.02541	32.07208	-3.97347	8.87E-06	6.153204	6.055733	810.5824
25.58641	4.767346	5.216727	7446.514	0.317533	277.9212	43.02541	38.43571	-3.76193	8.89E-06	6.198894	6.098475	1009.332
28.52758	4.814715	5.24064	9196.514	0.381866	163.9212	13.7397	44.79935	-3.55039	8.91E-06	6.244584	6.141217	983.2837
31.46876	4.862083	5.264553	7009.014	0.217459	193.9212	18.7397	51.16298	-3.33885	8.93E-06	6.290273	6.183959	1012.67
34.40993	4.909452	5.288467	8759.014	0.281792	223.9212	23.7397	57.52662	-3.12731	8.94E-06	6.335963	6.226701	1012.626
37.35111	4.059313	5.31238	7884.014	0.346125	253.9212	28.7397	63.89026	-2.91577	8.96E-06	6.381653	6.269443	937.3694

40.29229	4.106681	5.336293	9634.014	0.238903	283.9212	33.7397	70.25389	-5.43796	8.98E-06	6.427342	6.312184	1033.828
43.23346	4.15405	5.360206	6790.264	0.303237	169.9212	38.7397	76.61753	-5.22642	9.00E-06	6.473032	6.354926	906.6733
46.17464	4.201418	5.384119	8540.264	0.36757	199.9212	43.7397	82.98117	-5.01489	9.01E-06	6.518722	6.397668	909.0168
49.11582	4.248787	5.408032	7665.264	0.260348	229.9212	14.45398	89.3448	-4.80335	9.03E-06	6.564411	6.44041	941.9192
52.05699	4.296155	5.431945	9415.264	0.324681	259.9212	19.45398	95.70844	-4.59181	9.05E-06	6.610101	6.483152	945.4133
54.99817	4.343524	5.455858	7227.764	0.389014	289.9212	24.45398	32.65059	-4.38027	9.07E-06	6.655791	6.525894	955.4228
57.93935	4.390892	5.479771	8977.764	0.224607	175.9212	29.45398	39.01422	-4.16873	9.09E-06	6.70148	6.568636	898.7221
60.88052	4.43826	4.954724	8102.764	0.28894	205.9212	34.45398	45.37786	-3.95719	9.10E-06	6.74717	6.611378	941.5713
63.8217	4.485629	4.978637	9852.764	0.353274	235.9212	39.45398	51.7415	-3.74565	9.12E-06	6.792859	6.65412	941.7216
66.76288	4.532997	5.00255	6680.889	0.246051	265.9212	44.45398	58.10513	-3.53412	9.14E-06	6.838549	6.696862	958.2595
69.70405	4.580366	5.026463	8430.889	0.310385	295.9212	10.27031	64.46877	-3.32258	9.16E-06	6.884239	6.739604	971.4423
72.64523	4.627734	5.050376	7555.889	0.374718	153.1212	15.27031	70.83241	-3.11104	9.17E-06	6.929928	6.782346	923.7425
25.75942	4.675103	5.074289	9305.889	0.267496	183.1212	20.27031	77.19604	-2.8995	9.19E-06	6.975618	6.825088	852.216
28.70059	4.722471	5.098202	7118.389	0.331829	213.1212	25.27031	83.55968	-5.42169	9.21E-06	7.021308	6.86783	942.9631
31.64177	4.769839	5.122115	8868.389	0.396162	243.1212	30.27031	89.92332	-5.21015	9.23E-06	7.066997	6.910572	901.3436
34.58295	4.817208	5.146028	7993.389	0.212693	273.1212	35.27031	96.28695	-4.99861	9.24E-06	7.112687	6.953313	1077.837
37.52412	4.864576	5.169941	9743.389	0.277027	159.1212	40.27031	33.2291	-4.78707	9.26E-06	7.158377	6.996055	845.1082
40.4653	4.911945	5.193854	6899.639	0.34136	189.1212	10.9846	39.59274	-4.57554	9.28E-06	7.204066	7.038797	873.2734
43.40647	4.061806	5.217767	8649.639	0.234138	219.1212	15.9846	45.95637	-4.364	9.30E-06	7.249756	7.081539	858.9714
46.34765	4.109175	5.24168	7774.639	0.298471	249.1212	20.9846	52.32001	-4.15246	9.32E-06	5.972021	7.124281	323.5231
58.11236	4.298648	5.337332	8212.139	0.384249	225.1212	40.9846	77.77455	-3.30631	9.39E-06	6.15478	5.971628	1135.442
61.05353	4.346017	5.361245	9962.139	0.219841	255.1212	11.69888	84.13819	-3.09477	9.40E-06	6.200469	6.01437	1163.351
63.99471	4.393385	5.385158	6544.171	0.284175	285.1212	16.69888	90.50183	-2.88323	9.42E-06	6.246159	6.057112	1271.503
66.93589	4.440754	5.409071	8294.171	0.348508	171.1212	21.69888	96.86546	-5.40542	9.44E-06	6.291849	6.099854	1235.879
69.87706	4.488122	5.432984	7419.171	0.241286	201.1212	26.69888	33.80761	-5.19388	9.46E-06	6.337538	6.142595	1454.965
72.81824	4.53549	5.456898	9169.171	0.305619	231.1212	31.69888	40.17125	-4.98234	9.47E-06	6.383228	6.185337	1430.368
25.93243	4.582859	5.480811	6981.671	0.369953	261.1212	36.69888	46.53489	-4.7708	9.49E-06	6.428918	6.228079	998.9912
34.75596	4.724964	5.003589	9606.671	0.391397	207.1212	17.41317	65.62579	-4.13619	9.55E-06	6.565987	6.356305	941.5666
37.69713	4.772332	5.027502	6762.921	0.22699	237.1212	22.41317	71.98943	-3.92465	9.56E-06	6.611676	6.399047	1201.806
40.63831	4.819701	5.051415	8512.921	0.291323	267.1212	27.41317	78.35307	-3.71311	9.58E-06	6.657366	6.441789	1094.238
43.57948	4.867069	5.075329	7637.921	0.355656	297.1212	32.41317	84.7167	-3.50157	9.60E-06	6.703056	6.484531	1055.672
46.52066	4.914438	5.099242	9387.921	0.248434	154.3212	37.41317	91.08034	-3.29003	9.62E-06	6.748745	6.527273	871.1303
49.46184	4.064299	5.123155	7200.421	0.312767	184.3212	42.41317	97.44398	-3.07849	9.63E-06	6.794435	6.570015	841.5801
52.40301	4.111668	5.147068	8950.421	0.377101	214.3212	13.12745	34.38613	-2.86696	9.65E-06	6.840125	6.612757	855.6825

55.34419	4.159036	5.170981	8075.421	0.269879	244.3212	18.12745	40.74976	-5.38915	9.67E-06	6.885814	6.655499	946.0639
58.28537	4.206404	5.194894	9825.421	0.334212	274.3212	23.12745	47.1134	-5.17761	9.69E-06	6.931504	6.698241	945.5661
61.22654	4.253773	5.218807	6653.546	0.398545	160.3212	28.12745	53.47703	-4.96607	9.70E-06	6.977194	6.740983	939.3044
64.16772	4.301141	5.24272	8403.546	0.208722	190.3212	33.12745	59.84067	-4.75453	9.72E-06	7.022883	6.783725	937.4282
67.1089	4.34851	5.266633	7528.546	0.273055	220.3212	38.12745	66.20431	-4.54299	9.74E-06	7.068573	6.826466	941.2003
70.05007	4.395878	5.290546	9278.546	0.337389	250.3212	43.12745	72.56794	-4.33145	9.76E-06	7.114263	6.869208	940.3319
72.99125	4.443247	5.314459	7091.046	0.230167	280.3212	13.84174	78.93158	-4.11991	9.78E-06	7.159952	6.91195	1012.321
26.10544	4.490615	5.338372	8841.046	0.2945	166.3212	18.84174	85.29522	-3.90838	9.79E-06	7.205642	6.954692	814.1499
29.04661	4.537983	5.362285	7966.046	0.358833	196.3212	23.84174	91.65885	-3.69684	9.81E-06	7.251332	6.997434	823.5887
34.92897	4.63272	5.410111	6872.296	0.315944	256.3212	33.84174	34.96464	-3.27376	9.85E-06	6.019286	7.082918	273.9981
37.87014	4.680089	5.434024	8622.296	0.380278	286.3212	38.84174	41.32827	-3.06222	9.86E-06	6.064976	7.12566	339.6848
40.81132	4.727457	5.457937	7747.296	0.21587	172.3212	43.84174	47.69191	-2.85068	9.88E-06	6.110666	7.168402	387.1181
43.7525	4.774826	5.48185	9497.296	0.280204	202.3212	14.55602	54.05555	-5.37287	9.90E-06	6.156355	7.211144	461.9484
55.5172	4.066792	5.028542	9934.796	0.365981	178.3212	34.55602	79.51009	-4.52672	9.97E-06	6.339114	6.05849	533.1621
58.45838	4.114161	5.052455	6598.858	0.258759	208.3212	39.55602	85.87373	-4.31518	9.99E-06	6.384804	6.101232	592.3158
61.39955	4.161529	5.076368	8348.858	0.323092	238.3212	44.55602	92.23736	-4.10364	1.00E-05	6.430493	6.143974	922.1115
64.34073	4.208898	5.100281	7473.858	0.387426	268.3212	10.37235	98.601	-3.8921	1.00E-05	6.476183	6.186716	988.6543
67.28191	4.256266	5.124194	9223.858	0.223018	298.3212	15.37235	35.54315	-3.68057	1.00E-05	6.521873	6.229458	984.1133
70.22308	4.303634	5.148107	7036.358	0.287352	155.5212	20.37235	41.90679	-3.46903	1.01E-05	6.567562	6.2722	939.8187
73.16426	4.351003	5.17202	8786.358	0.351685	185.5212	25.37235	48.27042	-3.25749	1.01E-05	6.613252	6.314942	944.6159
26.27845	4.398371	5.195933	7911.358	0.244463	215.5212	30.37235	54.63406	-3.04595	1.01E-05	6.658942	6.357684	816.3553
29.21962	4.44574	5.219846	9661.358	0.308796	245.5212	35.37235	60.9977	-2.83441	1.01E-05	6.704631	6.400426	815.4938
31.09663	4.220722	5.108991	6575.405	0.360422	209.7854	10.76259	95.04101	-5.24686	8.80E-06	5.979251	6.008405	1056.53
25.93243	4.133369	4.997692	6983.921	0.369953	189.8584	36.69888	47.25367	-4.88945	9.48E-06	6.33763	6.228079	292.237
31.09663	4.77673	5.339522	6575.405	0.373191	209.7854	29.32744	94.45598	-3.44726	9.86E-06	5.979251	6.008405	999.7384
26.6984	4.405799	5.460109	6714.777	0.394364	155.8833	28.12745	92.21402	-4.9996	8.86E-06	7.257783	6.757088	831.7068
26.00005	4.139674	5.039443	6694.159	0.236829	155.7151	28.32212	36.57184	-5.37798	8.89E-06	6.324788	6.355633	285.5126
29.04661	4.399673	5.361205	6670.437	0.357698	196.3212	23.8471	91.73465	-3.69684	9.81E-06	7.2297	6.736547	829.3301
26.00005	4.14004	5.039443	6695.279	0.232648	155.8826	28.32212	34.74631	-5.38748	8.89E-06	6.324788	6.371739	271.3409
40.4653	4.911945	5.193854	6944.378	0.322414	198.8418	11.35022	36.2375	-4.6175	8.58E-06	7.213515	6.813316	870.0826
27.92241	4.537983	5.362286	6722.872	0.358833	196.3212	23.84174	91.49654	-3.69684	9.81E-06	7.251256	6.695122	616.8841
26.00005	4.14004	5.039443	6656.552	0.225594	160.3995	24.13069	34.36269	-5.38904	8.89E-06	6.324788	6.333871	268.3447
46.91523	4.078762	5.360183	7192.5	0.355876	196.188	24.71084	97.48619	-3.24851	9.52E-06	7.247145	6.611216	541.884
28.70987	4.911945	5.335938	7209.305	0.322414	191.3092	42.89887	39.56319	-4.58929	9.57E-06	7.261364	6.518473	501.3489

58.34578	4.581221	5.486385	7286.311	0.356827	194.4194	42.72647	91.51994	-3.12396	9.58E-06	7.258799	6.518415	717.2635
26.6984	4.405433	5.460109	6713.657	0.398545	155.7158	28.12745	94.03954	-4.9901	8.86E-06	7.257783	6.740983	620.4305
29.04661	4.633349	5.360687	7893.743	0.358833	196.3212	23.8471	91.65885	-3.69684	9.81E-06	7.2297	6.736547	823.9513
40.40555	4.898119	5.198423	6922.121	0.285112	191.0021	10.9846	36.2375	-4.57495	8.45E-06	7.203675	6.443828	619.7402
29.04661	4.537983	5.362285	7449.346	0.352921	193.7947	23.84174	97.73886	-3.68367	8.46E-06	7.266432	6.814838	818.9864
29.04661	4.537983	5.362285	6679.438	0.239088	194.9164	23.84174	91.65885	-5.43097	8.46E-06	7.251333	6.476473	613.79
49.82148	4.89789	5.317991	8960.826	0.357706	196.2703	24.36524	97.04827	-3.16534	9.92E-06	7.264205	6.941327	904.2191
29.21832	4.538335	5.372244	7272.964	0.239867	194.4263	24.20753	96.79525	-3.69684	9.82E-06	7.264182	6.522563	642.4676
49.26147	4.537983	5.362706	7543.719	0.358833	196.4045	23.84174	97.34622	-3.09801	9.82E-06	7.264079	6.725318	653.4795
26.6984	4.639109	5.459591	7936.963	0.39968	155.7158	28.12745	93.96375	-4.9901	8.86E-06	7.257783	6.740983	641.8259
29.04661	4.537983	5.362697	7534.453	0.358833	196.293	23.84174	96.85112	-3.69684	9.82E-06	7.264182	6.725318	650.1685
26.17306	4.537983	5.052723	7534.877	0.358833	196.3212	23.84174	34.7935	-3.69684	8.77E-06	7.251256	6.695122	368.1695
29.04661	4.633349	5.361113	7848.029	0.358833	196.3212	23.84694	91.65885	-3.69684	9.81E-06	7.2297	6.736547	823.9781
29.06831	4.520153	5.360687	7893.743	0.358833	196.2936	23.84197	92.06842	-3.69303	9.81E-06	7.230537	6.7253	608.0024
33.83478	4.554776	5.37046	6735.82	0.225571	243.6647	24.1556	98.41565	-5.38915	9.81E-06	7.251561	6.655499	671.2032
34.90444	4.078255	5.369175	7188.186	0.35797	195.851	42.41317	98.39447	-3.2452	9.63E-06	7.258813	6.306299	932.2174
33.83478	4.554776	5.37046	6690.825	0.232625	239.1477	28.34704	98.79928	-5.38758	9.81E-06	7.251561	6.693366	672.9114
40.4653	4.911945	5.193854	7943.773	0.322414	198.8418	23.87439	36.2375	-4.58929	8.58E-06	7.26792	6.813316	862.2947
49.26147	4.537983	5.362705	7543.719	0.358833	196.404	23.84174	97.40209	-3.09801	9.82E-06	7.264079	6.725318	653.824
33.83478	4.554776	5.37046	6652.097	0.225571	243.6647	24.1556	98.41565	-5.38915	9.81E-06	7.251561	6.655499	671.1381
49.34921	4.502376	5.363112	7529.641	0.358861	196.2703	24.36524	97.40209	-3.16534	9.82E-06	7.264205	6.725318	634.7561
34.87476	4.078255	5.348931	7200.421	0.35797	195.851	42.41317	97.44398	-3.12773	9.63E-06	7.258855	6.306299	936.1263
49.12366	4.537949	5.362705	7529.641	0.358858	196.2934	23.84174	97.40209	-3.19425	9.82E-06	7.264205	6.725318	653.8432
33.83478	4.554776	5.37046	6655.371	0.225571	243.6647	24.1556	98.41565	-5.38915	9.81E-06	7.25133	6.655499	671.0827
34.79851	4.078255	5.348931	7200.421	0.35797	195.851	42.41317	97.44398	-3.12773	9.57E-06	7.258855	6.306299	936.496
55.84931	4.564998	5.486875	6652.097	0.281145	193.3828	24.14784	36.6367	-5.38456	9.01E-06	7.239876	6.461443	1379.747
29.04661	4.537983	5.362285	7172.006	0.239088	193.7947	23.84174	91.65885	-3.68367	8.46E-06	7.251332	6.478227	612.5794
55.84931	4.564998	5.486875	6652.097	0.341935	243.7402	24.14784	98.61773	-5.38456	8.94E-06	7.239876	6.655499	817.269
29.04661	4.617902	5.360687	7893.743	0.358833	196.3212	23.8471	97.45928	-3.69684	9.82E-06	7.2297	6.736547	824.0219
41.16146	4.405799	5.460109	6714.777	0.393836	191.6747	27.55702	92.21402	-4.9996	8.92E-06	7.257783	6.754868	612.3343
28.73768	4.078255	5.348931	7200.421	0.35797	195.851	22.97013	96.70026	-3.69816	9.63E-06	7.258848	6.306299	945.5445
29.04661	4.537983	5.360666	7534.453	0.358833	196.2934	23.84187	96.79525	-3.69684	9.81E-06	7.228896	6.725493	651.5313
71.13159	4.526507	5.325039	7501.998	0.375794	196.558	38.7397	45.01115	-3.1888	9.89E-06	7.233718	6.688995	320.9003
54.05815	4.537983	5.362705	7534.847	0.379286	196.3212	23.84174	94.58635	-3.69684	9.82E-06	7.264151	6.722754	635.8198

34.51422	4.917099	5.357618	6953.899	0.360862	221.8387	41.6954	76.42393	-3.14437	9.72E-06	7.243164	6.343818	1029.757
49.80518	4.912534	5.00151	8890.654	0.329446	219.7655	32.31113	50.58447	-2.96434	8.94E-06	7.204828	6.91876	902.2662
33.85707	4.537983	5.362705	7166.772	0.245001	196.2934	23.84174	91.32208	-3.69684	9.82E-06	7.249051	6.439957	612.4202
54.05815	4.537983	5.362705	7534.877	0.379286	196.3212	23.84174	94.87941	-3.69684	9.82E-06	7.264151	6.722754	637.7332
55.80754	4.547149	5.37046	6739.094	0.225571	243.6647	40.83269	98.41201	-3.30328	9.81E-06	7.259358	6.655499	663.5783
27.16635	4.078255	5.348931	7200.421	0.357393	195.851	42.41317	97.44398	-4.97511	9.57E-06	7.257781	6.306299	995.8208
36.91338	4.393919	5.348931	8917.098	0.35797	195.851	25.73608	97.44762	-5.37274	9.63E-06	7.250826	6.556089	688.6983
29.04661	4.537983	5.362275	7172.006	0.239088	193.8219	23.84174	91.93953	-3.68367	8.49E-06	7.251332	6.481809	614.46



